Rui Estêvão Silva de Jesus Moreira

SECOND GENERATION BIOREFINERIES
A CONTRIBUTION TO THE SYNGAS AND LIGNIN PLATFORMS

October 2020

Rui Estêvão Silva de Jesus Moreira

SECOND GENERATION BIOREFINERIES

A CONTRIBUTION TO THE SYNGAS AND LIGNIN PLATFORMS

PhD Thesis in Chemical Engineering supervised by Professor António Alberto Torres Garcia Portugal and Professor José Luis Sánchez Cebrián and submitted to the Department of Chemical Engineering of the Faculty of Sciences and Technology of the University of Coimbra

October 2020

To my parents

Acknowledgments:

Above all and everything I am infinitely thankful to my parents and brother. "*They are the reason I am, they are all my reasons.*" (by John Nash, 1994, Stockholm, Sweden).

I would like to express my gratitude:

➤ To my Supervisor António Portugal (PhD Associate Professor) and to my Co-supervisor José Luis Sánchez (PhD Professor) for their friendship, infinite patience and hard work even in the most difficult times.

➤ To Fernando Bimbela (PhD Professor) for the friendship and keen advices in many crucial moments of this Thesis.

➤ To Alfonso Cornejo (PhD Professor) for the friendship and keen advices.

➤ To Jesús Araúzo (Full Professor) for the friendship, motivation and example of someone who does never give up.

➤ To the following members of the Universidade de Coimbra (UC, Portugal) mentioned here by alphabetical order: Abel Ferreira (PhD Professor), Beatriz Banaco (MsC Researcher), Cátia Mendes (PhD Student), Dora Pontinha (Post-Doc Researcher), Graça Carvalho (PhD Professor), José Santos (Lab Assistant), Luis Santos (Accountant), Manuel Leitão da Silva (Lab Assistant), Maria João Travassos (Chemical Engineer and Qualified Lab Technician) and Olga Terreiros (from Academic Services).

➤ To the following members of the Universidad de Zaragoza (UNIZAR, Spain), mentioned here by alphabetical order: Alberto Gonzalo (PhD Professor), Javier Ábrego (PhD Professor), José Antonio Mateo (Lab Technician), Noemí Gil-Lalaguna (Post-Doc Researcher) and Olga Marín (Lab Technician).

➤ To the following members of the Universidad Publica de Navarra (UPNA, Spain), mentioned here by alphabetical order: Guillermo Cruz (PhD Student), Karina Hablich (PhD Student), Luis Gandía (Full Professor), Maia Espinal (Post-Doc Researcher), Santiago Reinoso (PhD Professor) and Victor Martínez-Merino (Full Professor).

➤ To following members of the Instituto de Carboquímica (ICB) de Zaragoza, mentioned here by alphabetical order: Elba Ochoa (PhD Student), Esther Frecha (PhD Student), Isabel Suelves (PhD Head Researcher), José Luis Pinilla (PhD Researcher) and Daniel Torres (PhD Researcher).

➢ To all of the people that did not intervened directly with my PhD Thesis, but contributed in one way or another for the equilibrium I needed to accomplish this life goal.

Resumo

O objectivo principal foi contribuir para o desenvolvimento das plataformas de gás de síntese e lignina, uma vez que o gás de síntese pode ser convertido em compostos quimicamente idênticos aos derivados do petróleo, enquanto a lignina poderá ser usada como fonte de novos compostos aromáticos para as indústrias do futuro. A produção de gás de síntese foi estudada por duas estratégias diferentes: (1) por gasificação do carvão vegetal e (2) por reformação oxidativa do glicerol. A produção de novos produtos aromáticos a partir da lignina foi estudada por (1) fraccionamento da madeira de pinheiro, seguido por (2) despolimerização da lignina obtida e, finalmente, (3) o *upgrading* do principal produto de despolimerização da lignina (guaiacol).

O carvão vegetal foi gasificado com o objectivo de produzir gás de síntese usando ar, oxigénio puro e misturas de oxigénio/vapor como agentes de gasificação. Os efeitos da razão de equivalência (ER) e da razão vapor/carbono (S/C) na conversão da fracção de carbono do carvão vegetal, no rendimento a gás produto, no rendimento a gás de síntese, no poder calorífico e composição do gás produto e na eficiência energética aparente (AEE) também foram estudados. Os testes de gasificação foram realizados numa unidade laboratorial de leito fluidizado a 900 ºC usando γ-Al_2O_3 como leito. Os maiores rendimentos de gás de síntese e a maior AEE foram alcançados usando uma S/C=0,625 g/g e uma ER=0,3. O menor teor de alcatrão do gás produto foi obtido usando uma S/C=0,5 g/g e uma ER=0,3.

A produção de gás de síntese foi estudada por reformação oxidativa de glicerol. Os resultados obtidos usando diferentes leitos de enchimento (SiO_2, SiC e γ-Al_2O_3) foram comparados com os resultados obtidos usando um catalisador de Co/Al disperso em cada um dos daqueles leitos. Os efeitos do material do leito de enchimento, da temperatura de activação (750-850 ºC) e da temperatura de reacção (550-750 ºC) na conversão e produção de gás foram estudados, bem como a reutilização do catalisador. Os melhores resultados em termos de produção total de gás, produção de H_2 e razão de gás de síntese foram obtidos usando um leito γ-Al_2O_3. O uso de sílica como leito em testes catalíticos permitiu maior produção de hidrogénio e o aumento da razão de gás de síntese. A menor temperatura testada permitiu a maior produção de hidrogénio e a mais alta razão de gás de síntese. Após a regeneração e subsequente activação, o catalisador recuperou sua estrutura original e actividade inicial.

Madeira de pinheiro bravo (PPW) foi fraccionada por duas vias diferentes: (1) um sistema em duas etapas por soda etanol organosolv (SEOS) seguido por precipitação de lignina

(LP) e (2) um procedimento em três etapas englobando auto-hidrólise (AH) seguido por SEOS e LP. No fraccionamento em duas etapas foi estudado o efeito da fracção mássica de etanol no licor de cozimento (15-55 wt.%) na pureza das pastas e ligninas obtidas. No sistema de três etapas foram avaliados os efeitos da temperatura de AH (160-180 ºC) e do tempo de reacção (30 e 60 min) na remoção de hemiceluloses. Em seguida, foram estudados os efeitos da temperatura AH (175 e 180 ºC) e da concentração de etanol (15-35 wt.%) na pureza das pastas e das ligninas obtidas. No fraccionamento em dois passos, até 81 wt.% da celulose e 66 wt.% da lignina foram respectivamente recuperados nas pastas e nos precipitados. No fraccionamento em três etapas, até 17 wt.% da biomassa de PPW original foi recuperada nos licores de AH, as pastas apresentaram teores de hemicelulose e lignina tão baixos quanto 3 wt.% e 5 wt.%, enquanto os produtos LP apresentaram teores de lignina até 98 wt.%.

A despolimerização da lignina produzida por fraccionamento em três etapas foi estudada usando catalisadores de Ni e Cu por impregnação em zeólita ZSM-5 e hidrotalcita. Foram também usados catalisadores comerciais (Pd/C, Ru/C e Pt/Al_2O_3) e um catalisador de Mo_2C sintetizado por carborredução. Todos os catalisadores foram testados a 200-250 ºC e 20 bar de H_2 (pressão inicial). Destes, o catalisador de Ru/C permitiu obter maior rendimento e foi seleccionado para estudos posteriores. Foi tentado um procedimento de despolimerização em duas etapas, englobando a despolimerização catalisada por base (a 220 e 250 ºC) seguida de hidrogenólise com o catalisador Ru/C (a 250 ºC). O rendimento máximo de monómeros foi alcançado com Ru/C a 250 ºC por 30 min, e os principais produtos foram guaiacóis.

A hidrodesoxigenação (HDO) de guaiacol foi estudada com um catalisador de Mo_2C suportado em nanofibras de carbono (CNF). Foram estudados os efeitos da temperatura (300 e 350 ºC), da pressão inicial de H_2 (20 e 30 bar) e do tempo de reacção (2 e 4 h) na conversão do guaiacol e no rendimento dos produtos. A maior conversão de guaiacol foi alcançada após 4 h de reacção a 350 ºC e 20 bar de H_2. Quando a pressão foi aumentada a conversão do guaiacol aumentou após 2 h de reacção a 350 ºC. A análise de XRD do catalisador usado não revelou mudanças significativas na estrutura em comparação com o catalisador fresco. Os principais produtos da reacção foram cresóis, xilenóis e catecóis.

Palavras chave: gás de síntese, gasificação, fraccionamento de biomassa lenhocelulósica, lenhina, hidrodesoxigenação

Abstract

The main objective was to contribute to the development of the syngas and lignin platforms, because syngas can be converted to chemical commodities identical to those nowadays derived from petroleum, while lignin is expected to be a source of new aromatic commodities for the industries of the future. The production of syngas was studied by two different strategies: (1) by the gasification of commercial charcoal and (2) by the oxidative steam reforming of glycerol. The production of new aromatic commodities from lignin was studied by (1) the fractionation of pinewood, followed by (2) the depolymerization of the obtained lignin and finally (3) the upgrading of a major product of lignin depolymerization (guaiacol).

The commercial charcoal was gasified using air, oxygen, oxygen/steam mixtures. The effects of the equivalence ratio (ER) and steam to carbon ratio (S/C) on carbon conversion, producer gas yield, syngas yield, gas heating value and apparent energy efficiency (AEE) were also investigated. The gasification experiments were performed in a laboratory-scale fluidized bed rig at 900 ºC using γ-Al_2O_3 as bed material. The highest syngas yield and AEE were reached using a S/C=0.625 g/g and an ER=0.3. The lowest producer gas tar content was achieved using an ER=0.3 and a S/C=0.5 g/g.

The syngas production was also investigated via oxidative steam reforming of glycerol. Results obtained using different (bulk) bed materials (SiO_2, SiC and γ-Al_2O_3) were compared against those achieved over a Co/Al catalyst dispersed in each of those bed fillers. The effects of each filler bed material, activation temperature (750-850 ºC) and reaction temperature (550-750 ºC) on conversion, gas production and syngas ratio were investigated, as well as the catalyst reuse. The best overall results in terms of total gas production, H_2 production and syngas ratio were obtained with γ-Al_2O_3 in non-catalyzed experiments. The use of silica as bed filler in catalytic experiments allowed for the highest hydrogen production and syngas ratio. The lowest tested temperature allowed for the highest hydrogen production and H_2/CO ratio. Upon regeneration and subsequent activation, the catalyst recovered its original structure and initial activity.

In what concerns the lignin platform, *Pinus pinaster* wood (PPW) was fractionated by two different routes: (1) a two-step system by soda ethanol organosolv (SEOS) followed by lignin precipitation (LP) and (2) a three-step procedure encompassing autohydrolysis (AH) followed by SEOS and LP. In the two-step route, the effect of the ethanol concentration (15-55 wt.%) on pulps and lignins purities was studied. In the three-step system, the effects of AH temperature (160-180 ºC) and reaction time (30 and 60 min) on

hemicelluloses removal were evaluated. Then the effects of the AH temperature (175 and 180 ºC) and the ethanol concentration (15-35 wt.%) on the purities of SEOS products were considered. Up to 81 wt.% of the cellulose and 66 wt.% of the lignin initially present in PPW were recovered in pulps and precipitates (respectively) by the two-step route. When the three-step fractionation was applied, up to 17 wt.% of the original biomass was recovered in the AH liquors, and pulps having hemicellulose and lignin contents as low as 3 wt.% and 5 wt.% (respectively) were obtained, simultaneously with LP products having lignin contents up to 98 wt.%.

The depolymerization of the lignin produced by three-stage fractionation in was attempted using Ni and Cu catalysts supported on ZSM-5 zeolite and hydrotalcite. Commercial catalysts (Pd/C, Ru/C and Pt/Al$_2$O$_3$) and a Mo$_2$C catalyst synthesized by carboreduction were also used. All the catalysts were tested at 200-250 ºC and 20 bar of H$_2$ (initial pressure). Of those, Ru/C allowed to obtain the highest yield (3.5 wt.%) results and was selected for further studies. A two-step procedure was attempted, encompassing the first the base catalyzed depolymerization (at 220 and 250 ºC) followed by hydrogenolysis over Ru/C catalyst. The maximum monomer yield was achieved over Ru/C at 250 ºC for 30 min, and the major products were guaiacols.

The hydrodeoxygenation (HDO) of guaiacol was studied using a molybdenum carbide (Mo$_2$C) catalyst supported on commercial carbon nanofibers (CNF). The effects of temperature (300 and 350 ºC), initial pressure of H$_2$ (20 and 30 bar) and reaction time (2 and 4 h) on the conversion of guaiacol and product yields were studied. The highest guaiacol conversion was achieved upon 4 h of reaction at 350 ºC. When the pressure was increased the conversion of guaiacol increased. The XRD analysis of spent catalysts did not reveal any significant changes as compared to the fresh catalyst. The major reaction products were cresols, xylenols and catechols.

Keywords: syngas, gasification, lignocellulosic biomass fractionation, lignin, hydrodeoxygenation

Sumário

A investigação desenvolvida para esta Tese de Doutoramento foi dedicada ao conceito de produção de *commodities* em biorrefinarias de que possam ser utilizadas como matérias-primas para a indústria química. O objectivo principal foi contribuir para o desenvolvimento das plataformas de gás de síntese e lignina, uma vez que o gás de síntese pode ser convertido em compostos quimicamente idênticos aos derivados do petróleo, enquanto a lignina poderá ser usada como fonte de novos compostos aromáticos para as indústrias do futuro. A produção de gás de síntese foi estudada por duas estratégias diferentes: (1) por gasificação do carvão vegetal e (2) por reformação oxidativa (*oxidative steam reforming*) do glicerol. A produção de novos produtos aromáticos a partir da lignina foi estudada por (1) fraccionamento da madeira de pinheiro (*Pinus pinaster*), seguido por (2) despolimerização da lignina obtida e, finalmente, (3) o *upgrading* de um dos produtos de despolimerização da lignina (guaiacol). Nos parágrafos seguintes é feita uma breve descrição do trabalho realizado e das principais conclusões.

1. Gasificação de carvão vegetal. Carvão vegetal comercial foi gasificado com o objectivo de produzir gás de síntese usando ar, oxigénio puro e misturas de oxigénio/vapor como agentes de gasificação. Os efeitos da razão de equivalência (ER) e da razão vapor/carbono (S/C) na conversão da fracção de carbono do carvão vegetal, no rendimento a gás produto, no rendimento a gás de síntese, no poder calorífico e composição do gás produto e na eficiência energética aparente (AEE) do processo foram também estudados. Os testes de gasificação foram realizados numa unidade laboratorial de leito fluidizado a 900 ºC e pressão atmosférica, usando γ-Al_2O_3 como leito. Os resultados mostraram que, ao usar o mesmo ER, a composição do gás produto obtido pela gasificação com ar foi comparável à obtida com oxigénio puro (em base livre de N_2). A fracção de carbono convertida a gás melhorou quando o ER foi aumentado de 0,25 para 0,35, bem como quando a relação S/C foi aumentada até 0,625. O maior rendimento de gás produto (1,31 Nm^3/kg de carvão) e a conversão máxima de carbono (66,5% em massa) foram alcançados usando uma ER=0,35 e uma S/C=0,625 g/g, enquanto a maior concentração de H_2 (35 vol.%) foi alcançada usando um ER = 0,25 e uma S/C = 0,625 g/g. O maior rendimento de H_2 (0,412 Nm^3/kg de carvão), o maior rendimento de gás de síntese (0,8 Nm^3/kg de carvão) e a maior AEE (33,4%) foram alcançados usando uma S/C=0,625 g/g e um ER=0,3 (oxigénio puro). O menor teor de alcatrão do gás produto (290 mg/Nm^3) foi conseguido usando um ER=0,3 e uma S/C=0,5. De uma forma geral, pode concluir-se que a produção de gás de

síntese a partir da gasificação do carvão vegetal a partir de misturas O_2/vapor tem potencial para constituir um meio de produção de gás de síntese renovável. Este estudo resultou na publicação de um artigo de revisto por pares (*R. Moreira, R. Vaz, A. Portugal, N. Gil-Lalaguna, J. Sánchez, F. Bimbela, Gasification of Charcoal in Air, Oxygen, and Steam Mixtures over a γ-Al₂O₃ Fluidized Bed, Energy & Fuels 32 (2017) 407-415*), e num artigo de revisão (*R. Moreira, N. Gil-Lalaguna, F.Bimbela, J. L. Sánchez, António Portugal, Clean syngas production by gasification of lignocellulosic charcoal: state of the art and future prospects, submitted in 10-07-2020*).

2. <u>Reformação oxidativa do glicerol.</u> Outra via investigada para a produção de gás de síntese foi reformação oxidativa (*oxidative steam reforming*) de soluções aquosas de glicerol (S/C=4 e 6 vol.% O_2 em N_2). Os resultados obtidos usando diferentes materiais/leitos de dispersão/enchimento (SiO_2, SiC e γ-Al_2O_3) foram comparados com os resultados obtidos usando um catalisador de aluminato de cobalto (Co/Al) preparado por coprecipitação disperso em cada um dos desses leitos de enchimentos. Os efeitos do material no leito de enchimento, da temperatura de activação (750 ºC, 800 ºC e 850 ºC) e da temperatura de reacção (550 ºC, 650 ºC e 750 ºC) na conversão e produção de gás foram estudados, bem como a reutilização do catalisador (a 750 ºC) de forma a avaliar seu desempenho após a regeneração. Níveis substanciais de conversão de glicerol (>83%) foram obtidos a 750 ºC sem o catalisador. Os principais produtos gasosos foram H_2, CO, CO_2 e CH_4, e os melhores resultados em termos de produção total de gás, produção de H_2 e razão de gás de síntese foram obtidos usando um leito γ-Al_2O_3 (266 mg/g de alimentação, 31 mg/g de glicerol H_2/CO=0,94, respectivamente). Comparado com os testes em que o catalisador não foi disperso no leito de enchimento, o uso do catalisador não resultou num aumento significativo na conversão de carbono em gás, mas a distribuição dos produtos gasosos foi significativamente afectada, evidenciando o papel exercido pelo catalisador. O uso de sílica como leito de enchimento em testes catalíticos permitiu maior produção de hidrogénio e o aumento da razão de gás de síntese (63 mg H_2/g glicerol e H_2/CO=2,53) em comparação com alumina (54 mg H_2/g glicerol, H_2/CO=2,15) e carboneto de silício (39 mg H_2/g glicerol, H_2/CO=1,08). O aumento das temperaturas de reacção ou de activação não melhorou o desempenho do catalisador, a conversão de glicerol ou a produção de gás. Em qualquer caso, todos os leitos de enchimentos permitiram obter conversões de carbono em gases superiores a 91% nos testes catalíticos. A formação de gás durante a reformação catalítica do glicerol conduzida

diminuiu com o aumento da temperatura (a 550, 650 e 750 ºC). Por outro lado, a conversão de carbono em gás aumentou ligeiramente com o aumento da temperatura. A menor temperatura testada (550 ºC) permitiu a maior produção de hidrogénio (90 mg H_2/g glicerol) e a mais alta razão de gás de síntese (H_2/CO=15,3) atribuída à maior estabilidade do catalisador. O catalisador Co/Al pôde ser usado com eficácia durante 20 horas em quatro ciclos consecutivos de reacção/regeneração a 750 ºC. A desactivação do catalisador por encapsulamento de carbono causou mudanças drásticas na estrutura do catalisador, que evoluiu para uma configuração "núcleo-casca" quando desactivada. Após a regeneração e subsequente activação, o catalisador recuperou sua estrutura original e actividade inicial. Os resultados deste estudo foram publicados num artigo revisto por pares (*R. Moreira, A. Moral, F. Bimbela, A. Portugal, A. Ferreira, J. Sánchez, L. Gandía, Syngas production via catalytic oxidative steam reforming of glycerol using a Co/Al coprecipitated catalyst and different bed fillers, Fuel Processing Technology 189 (2019) 120–133*) e num artigo de revisão (*R. Moreira, F. Bimbela, L. M. Gandía, A. Ferreira, J. L. Sánchez, A. Portugal, Oxidative steam reforming of glycerol. A review, submitted in 13-09-2020*).

3. Fraccionamento da madeira. Madeira de pinheiro bravo (PPW) foi fraccionada por duas vias diferentes: (1) um sistema em duas etapas por soda etanol organosolv (SEOS) seguido por precipitação de lignina (LP) e (2) um procedimento em três etapas englobando auto-hidrólise (AH) seguido por SEOS e LP. No fraccionamento em duas etapas foi estudado o efeito da fracção mássica de etanol no licor de cozimento (15, 25, 35, 45 e 55 % em massa) na pureza das pastas e ligninas obtidas. No sistema de três etapas foram avaliados os efeitos da temperatura de AH (160, 170, 175 e 180 ºC) e do tempo de reacção (30 e 60 min) na remoção de hemiceluloses. Em seguida, foram estudados os efeitos da temperatura AH (175 e 180 ºC) e da concentração de etanol (15, 25 e 35% em massa) na pureza das pastas e das ligninas obtidas. A temperatura da reacção do SEOS (170 ºC) e o tempo (90 min) foram mantidos constantes em todos os testes de SEOS. No caso do fraccionamento em duas etapas, foram obtidas pastas com teores de lignina e hemicelulose na ordem de 6 e 15% (em massa), respectivamente, bem como precipitados com teores de lignina de até 94% (em massa). Por esta via de fraccionamento, até 81% da massa de celulose e 66% (em massa) da lignina inicialmente presentes no PPW foram respectivamente recuperados nas pastas e nos precipitados. No fraccionamento de três etapas, até 17% (em massa) da biomassa de PPW original foi recuperada nos licores de

AH. As pastas obtidas por esta via apresentaram teores de hemicelulose tão baixos quanto 3% (em massa) e teores de lignina tão baixos quanto 5% (em massa), enquanto os produtos LP apresentaram teores de lignina até 98% (em massa). Os resultados evidenciaram o potencial do fraccionamento em três etapas para uma bioeconomia baseada em biorrefinarias. Os resultados obtidos neste estudo resultaram na publicação de um artigo revisto por pares (*R. Moreira, C. Mendes, M. Banaco, M. Carvalho, A. Portugal, New insights in the fractionation of Pinus pinaster wood: sequential autohydrolysis, soda ethanol organosolv and acidic precipitation, Industrial Crops & Products 152 (2020) 112499*).

4. Despolimerização de lignina. A despolimerização da lignina produzida nas condições experimentais (AH a 175 ºC seguida de SEOS com 35% de etanol) que permitiram obter o maior rendimento (75% em massa) foi tentada usando várias estratégias catalíticas. Vários catalisadores foram preparados por impregnação por umidade incipiente de Ni e Cu sobre zeólita ZSM-5 e hidrotalcita. Um catalisador Mo_2C suportado em carvão activado também foi preparado por carboredução. Catalisadores comerciais Ru/C e Pd/Al_2O_3 também foram usados. Todos os catalisadores foram testados a 200-250 ºC e 20 bar de H_2 (pressão inicial). Destes, o catalisador de Ru/C permitiu obter maior rendimento (3,5% em massa) e foi seleccionado para estudos posteriores. Com o objectivo de aumentar o rendimento de monómeros, foi tentado um procedimento de despolimerização em duas etapas, englobando na primeira a despolimerização catalisada por NaOH (a 220 e 250 ºC) seguida de hidrogenólise com o catalisador Ru/C (a 250 ºC). O rendimento máximo de monómeros (7,3% em massa) foi alcançado com Ru/C a 250 ºC por 30 min, correspondendo a reduções globais nas massas moleculares médias (Mw) e número (Mn) de 3005 e 2296 g/mol para 818 e 468 g/mol, respectivamente. respectivamente. Uma possível explicação para os resultados obtidos pode estar relacionada com o processo de extracção utilizado para obtenção da lignina (AH seguido de SEOS), que aparentemente terá resultado num material altamente condensado e não reactivo. Possivelmente, condições de reacção mais severas (temperatura e pressão) poderiam eventualmente ser usadas para melhorar os rendimentos a monómeros, o que poderá ser explorado em trabalhos futuros. Os resultados desta investigação foram publicados num artigo colaborativo revisto por pares, no qual o candidato a doutorado apenas participou como co-autor (*A. Cornejo, F. Bimbela, R. Moreira, K. Hablich, Í. García-Yoldi, M. Maisterra, A. Portugal, V. Martínez-Merino, L.M. Gandía, Production*

of Aromatic Compounds by Catalytic Depolymerization of Technical and Downstream Biorefinery Lignins, Biomolecules 10-9 (2020) 1338), pelo que não está incluído no quadro desta Tese.

5. <u>*Upgrading* de Guaiacol</u>. Um catalisador de carbeto de molibdénio (Mo$_2$C) suportado em nanofibras de carbono comerciais (CNF) foi sintetizado e testado na hidrodesoxigenação (HDO) de guaiacol. Foram estudados os efeitos da temperatura (300 e 350 ºC), da pressão inicial de H$_2$ (20 e 30 bar) e do tempo de reacção (2 e 4 h) na conversão do guaiacol e no rendimento dos produtos de reacção. O uso de condições operacionais mais severas durante a HDO do guaiacol deu lugar a uma diversificação das vias de reacção e consequentemente nos rendimentos dos produtos. A maior conversão de guaiacol (79% em massa) foi alcançada após 4 h de reacção a 350 ºC e 20 bar de H$_2$ (pressão inicial). Quando a pressão foi aumentada (de 20 para 30 bar de H$_2$) a conversão do guaiacol aumentou (de 51% para 59%) após 2 h de reacção a 350 ºC. Foi observada corrosão do suporte carbonáceo (*etching*), possivelmente relacionada com formação dos carbonetos de molibdénio durante a carborredução em atmosfera de hidrogénio. O catalisador Mo$_2$C/CNF apresentou bastante maior selectividade para produtos de demetoxilação do que para produtos de desidroxilação. A análise de XRD do catalisador usado não revelou mudanças significativas na estrutura em comparação com o catalisador fresco. Os principais produtos da reacção foram fenol e fenóis substituídos (cresóis, xilenóis e catecóis), indicando que a abordagem escolhida merece uma investigação mais aprofundada por forma a melhorar a conversão do guaiacol naqueles compostos químicos valiosos. Os resultados deste estudo resultaram na publicação de um artigo revisto por pares (*R. Moreira, E. Ochoa, J. Pinilla, A. Portugal, I. Suelves, Liquid-Phase Hydrodeoxygenation of Guaiacol over Mo$_2$C Supported on Commercial CNF. Effects of Operating Conditions on Conversion and Product Selectivity, Catalysts 127 (2018) 127*).

Summary

The research carried out for this Doctoral Thesis was devoted to the concept of obtaining commodities in biorefineries that could be used as feedstock for the chemical industry. The main objective was to contribute to the development of the syngas and lignin platforms, because syngas can be converted to chemical commodities identical to those nowadays derived from petroleum, while lignin is expected to be a source of new aromatic commodities for the industries of the future. The production of syngas was studied by two different strategies: (1) by the gasification of commercial charcoal and (2) by the oxidative steam reforming of glycerol. The production of new aromatic commodities from lignin was studied by (1) the fractionation of pinewood, followed by (2) the depolymerization of the obtained lignin and finally (3) the upgrading of the major of the product of lignin depolymerization (guaiacol). In the following paragraphs, a short description of the work carried out and the main findings are summarized.

1. Charcoal gasification. Commercial charcoal was gasified using air, oxygen, oxygen/steam mixtures aiming to produce syngas. The effects of the equivalence ratio (ER) and steam to carbon ratio (S/C) on carbon conversion, producer gas yield, syngas yield, gas heating value and composition as well as on the apparent energy efficiency (AEE) of the process were also investigated. The gasification experiments were performed in a laboratory-scale fluidized bed rig working at 900 ºC and atmospheric pressure, using γ-Al_2O_3 as bed material. The results showed that, on a N_2-free basis, the composition of the producer gas obtained by gasification with air and pure oxygen was comparable when using the same ER. Furthermore, the carbon fraction converted into gas improved when ER was increased from 0.25 up to 0.35, as well as when the S/C ratio was increased up to 0.625. The highest producer gas yield (1.31 Nm^3/kg of charcoal) and the maximum carbon conversion (66.5 wt.%) were achieved using an ER=0.35 and a S/C=0.625 g/g, while the highest H_2 concentration (35 vol.%) was achieved using an ER=0.25 and a S/C=0.625 g/g. The highest H_2 yield (0.412 Nm^3/kg of charcoal), the highest syngas yield (0.8 Nm^3/kg charcoal) and the highest AEE (33.4%) were reached using a S/C=0.625 g/g and an ER=0.3 (pure oxygen). The lowest producer gas tar content (290 mg/Nm^3) was achieved using an ER=0.3 and a S/C=0.5 g/g. Overall, it was concluded that syngas production from charcoal gasification using O_2/steam mixtures has potential for producing renewable syngas. This investigation resulted in the publication of a peer review paper (R. Moreira, R. Vaz, A. Portugal, N. Gil-Lalaguna, J. Sánchez, F.

Bimbela, Gasification of Charcoal in Air, Oxygen, and Steam Mixtures over a γ-Al$_2$O$_3$ Fluidized Bed, Energy & Fuels 32 (2017) 407-415) and a review paper (R. Moreira, N. Gil-Lalaguna, F.Bimbela, J. L. Sánchez, António Portugal, Clean syngas production by gasification of lignocellulosic charcoal: state of the art and future prospects, submitted in 10-07-2020).

2. Glycerol oxidative steam reforming. Another route for syngas production was investigated via oxidative steam reforming of glycerol aqueous solutions (S/C=4 and 6 vol.% O$_2$ in N$_2$). Results obtained using different (bulk) bed materials (SiO$_2$, SiC and γ-Al$_2$O$_3$) were compared with results achieved while using a cobalt aluminate (Co/Al) catalyst prepared by coprecipitation dispersed in each of those same bed fillers. The effects of each filler bed material, activation temperature (750, 800 and 850 ºC) and reaction temperature (550, 650 and 750 ºC) on conversion, gas production and syngas ratio were investigated, as well as the catalyst reuse (at 750 ºC) to assess its performance after regeneration. High glycerol conversion levels (above 83%) were attained at 750 ºC without the catalyst. The main gaseous products were H$_2$, CO, CO$_2$ and CH$_4$. While using those bulk materials, the best overall results in terms of total gas production, H$_2$ production and syngas ratio were obtained with γ-Al$_2$O$_3$ (266 mg/g feed, 31 mg/g of glycerol H$_2$/CO=0.94, respectively). When compared to the runs in which the catalyst was not dispersed in the bed filler, the use of the catalyst did not result in a significant increase in carbon conversion to gas, but the product gas distribution was significantly affected, thus evidencing the role exerted by the catalyst. The use of silica sand as bed filler in catalytic experiments allowed for the highest hydrogen production and syngas ratio (63 mg H$_2$/g glycerol and H$_2$/CO=2.53) as compared to alumina (54 mg H$_2$/g glycerol, H$_2$/CO=2.15) and silicon carbide (39 mg H$_2$/g glycerol, H$_2$/CO=1.08). Higher activation temperatures did not improve the catalyst performance, the glycerol conversion or gas production. In any case, all bed fillers allowed to achieve a carbon conversion to gases higher than 91% in catalytic experiments. The overall gas formation during 4 h time on stream in the catalytic oxidative steam reforming of glycerol decreased with the temperature increase. Conversely, the carbon conversion to gas increased slightly with the temperature increase. The lowest tested temperature (550 ºC) allowed for the highest hydrogen production (90 mg H$_2$/g glycerol) and H$_2$/CO ratio (15.3) due to the better stability of the catalyst. The Co/Al catalyst could be effectively used during 20 h on stream at 750 ºC in four consecutive reaction/regeneration cycles. Catalyst deactivation

by encapsulating carbon caused drastic changes in the catalyst structure, which evolved into a core-shell configuration when deactivated. Upon regeneration and subsequent activation, the catalyst recovered its original structure and initial activity. This investigation resulted in the publication of a peer reviewed paper (R. Moreira, A. Moral, F. Bimbela, A. Portugal, A. Ferreira, J.L. Sánchez, L. Gandía, Syngas production via catalytic oxidative steam reforming of glycerol using a Co/Al coprecipitated catalyst and different bed fillers, Fuel Processing Technology 189 (2019) 120–133) and a review paper (R. Moreira, F. Bimbela, L. M. Gandía, A. Ferreira, J. L. Sánchez, A. Portugal, Oxidative steam reforming of glycerol. A review, submitted in 13-9-2020)

3. Wood fractionation. Pinus pinaster wood (PPW) was fractionated by two different routes: (1) a two-step system by soda ethanol organosolv (SEOS) followed by lignin precipitation (LP) and (2) a three-step procedure encompassing autohydrolysis (AH) followed by SEOS and LP. In the two-step route, the effect of the ethanol mass fraction in the cooking liquor (15, 25, 35, 45 and 55 wt.%) on pulps and lignins purities was studied. In the three-step system, the effects of AH temperature (160, 170, 175 and 180 ºC) and reaction time (30 and 60 min) on hemicelluloses removal were evaluated. Then the effects of the AH temperature (175 and 180 ºC) and the ethanol concentration (15, 25 and 35 wt.%) on SEOS derived pulps and lignins purities were considered. The SEOS reaction temperature (170 ºC) and time (90 min) were kept constant in all SEOS experiments. In the case of the two-step approach, pulps with lignin and hemicellulose contents as low as 6 and 15 wt.% (respectively), as well as precipitates having lignin contents up to 94 wt.% were obtained. Up to 81 wt.% of the cellulose and 66 wt.% of the lignin initially present in PPW were recovered in pulps and precipitates (respectively) by this fractionation pathway. When the three-step fractionation was applied, up to 17 wt.% of the original biomass was recovered in the AH liquors. Pulps having hemicellulose contents as low as 3 wt.% and lignin contents as low as 5 wt.% were produced by sequential AH and SEOS, while LP products presented lignin contents higher than 98 wt.%. The results show the potential of the three-step fractionation towards a biorefinery-based bioeconomy. This investigation resulted in the publication of a peer reviewed paper (R. Moreira, C. Mendes, M. Banaco, M. Carvalho, A. Portugal, New insights in the fractionation of Pinus pinaster wood: sequential autohydrolysis, soda ethanol organosolv and acidic precipitation, Industrial Crops & Products 152 (2020) 112499).

4. Lignin depolymerization. The depolymerization of the lignin produced by AH at 175 ºC followed by SEOS with 35% ethanol experimental conditions that allowed to obtain the highest yield, i.e., ca. 75 wt.%) was attempted. Several catalysts were prepared by incipient wetness impregnation of Ni and Cu on ZSM-5 zeolite and hydrotalcite. A Mo_2C catalyst supported on activated carbon was also prepared by carboreduction. Commercial Ru/C and Pd/Al_2O_3 catalysts were also used. All the catalysts were tested at 200-250 ºC and 20 bar of H_2 (initial pressure). Of those, Ru/C allowed to obtain the highest yield (3.5 wt.%) results and was selected for further studies. Aiming to increase the monomer yield, a two-step procedure was attempted, encompassing the first the base catalyzed depolymerization (at 220 and 250 ºC) followed by hydrogenolysis over Ru/C catalyst. The maximum monomer yield (7.3 wt.%) was achieved over Ru/C at 250 ºC for 30 min, corresponding to overall reductions in the average (M_w) and number (M_n) molecular masses from 3005 and 2296 g/mol to 818 and 468 g/mol, respectively. A possible explanation for such results may have been related with the extraction process used to obtain the lignin used in this work (AH followed by SEOS), which seems to have resulted in a highly condensed non-reactive lignin material. It was anticipated that harsher conditions (temperature and pressure) could eventually be used to improve the monomers yields, which can be addressed in future works. The results of this investigation were used in a collaborative peer reviewed paper in which the PhD candidate only participated as a coauthor (A. Cornejo, F. Bimbela, R. Moreira, K. Hablich, Í. García-Yoldi, M. Maisterra, A. Portugal, V. Martínez-Merino, L.M. Gandía, Production of Aromatic Compounds by Catalytic Depolymerization of Technical and Downstream Biorefinery Lignins, Biomolecules 10-9 (2020) 1338), and thus it is not included in the frame of this Thesis.

5. Guaiacol upgrading. A molybdenum carbide (Mo_2C) catalyst supported on commercial carbon nanofibers (CNF) was synthetized and tested in the hydrodeoxygenation (HDO) of guaiacol. The effects of temperature (300 and 350 ºC), initial pressure of H_2 (20 and 30 bar) and reaction time (2 and 4 h) on the conversion of guaiacol and product yields were studied. The use of more severe operating conditions during the HDO of guaiacol caused a diversification in the reaction pathways and consequently in the product yields. The highest guaiacol conversion (79 wt.%) was achieved upon 4h of reaction at 350 ºC and 20 bar of H_2 (initial pressure). When the pressure was increased (from 20 to 30 bar of H_2) the conversion of guaiacol increased (from 51% to 59%). Etching of carbonaceous materials involving molybdenum was observed, which was possibly related with the

formation of molybdenum carbides by carburization in hydrogen atmosphere. The Mo$_2$C/CNF catalyst showed higher selectivity for demethoxylation products than to dehydroxylation products. The XRD analysis of spent catalysts did not reveal any significant changes as compared to the fresh catalyst. The main reaction products were phenol (0.2-28.1 wt.%), cresols (0.2-11.9 wt.%), xylenols (0-5.0 wt.%) and catechols (0-2.1 wt.%), meaning that the chosen approach deserves further investigation in order to improve the conversion of guaiacol into those valuable chemicals. This investigation resulted in the publication of a peer reviewed paper (R. Moreira, E. Ochoa, J. Pinilla, A. Portugal, I. Suelves, Liquid-Phase Hydrodeoxygenation of Guaiacol over Mo$_2$C Supported on Commercial CNF. Effects of Operating Conditions on Conversion and Product Selectivity, Catalysts 127 (2018) 127).

Glossary

AC – activated carbon

AEE – apparent energy efficiency

AH – autohydrolysis

AHL – autohydrolysis liquors

AHS – autohydrolysis solids

AHS175 – autohydrolysis solids produced by AH at 175 ºC for 30 min

AHS180 – autohydrolysis solids produced by AH at 180 ºC for 30 min

AL – aliphatic fraction

APR – aqueous phase reforming

AR – aromatic fraction

ASAE – Alkali-Sulfite-Antraquinone-Ethanol

ATR – autothermal reforming

ATR-FTIR - attenuated total reflectance Fourier-transform infrared spectroscopy

BCD – base catalyzed depolymerization

BET – Brunauer-Emmett-Teller

B:S – biomass to solvent mass ratio

C-C – carbon-carbon bonds

CNF – carbon nanofibers

CNT – carbon nanotube

C-O-C – ether bonds

D – delignification

DOSY – diffusion-ordered spectroscopy

DP – degree of polymerization

DTG - differential thermal analysis

EA – elemental analysis

EDS – energy dispersive X-ray spectroscopy

ER – equivalence ratio

EtOH – ethanol

LP – lignin precipitation

FBR – fluidized bed reactor

FID – flame ionization detector

FT – Fischer-Tropsch synthesis

GC – gas chromatography

GHG – greenhouse gas

H_2/CO – hydrogen to carbon monoxide molar ratio or syngas ratio

HDO – hydrodeoxygenation

HDM – hydrodemetallization

HDN – hydrodenitrogenation

HDS – hydrodesulphurization

HHV – high heating value

HPLC – High performance liquid chromatography

HY – hydrogenation

HYD – hydrogenolysis

#K – kappa number

LHV – low heating value

MS – mass spectroscopy

MTE – methanol-to-ethylene

MTG – methanol-to-gasoline

MTO – methanol-to-olefins

MTE – methanol-to-ethylene

MTP – methanol-to-propylene

M_{Al1} – molecular mass of the aliphatic fraction 1 determined by DOSY

M_{Al2} – molecular mass of the aliphatic fraction 2 determined by DOSY

M_{AR} – molecular mass of the aromatic fraction determined by DOSY

M_n – number average molecular mass

M_w – weight average molecular mass

NMR – nuclear magnetic resonance

OS – organosolv

OSR – oxidative steam reforming

PPW – *Pinus pinaster* wood

PW – pulp washing

RID – Refractive index detector

S/C – steam to carbon ratio

scEtOH – supercritical ethanol

SEC – size exclusion chromatography

SEOS – soda ethanol organosolv

SR – steam reforming

STEM – scanning transmission electron microscopy

TCD – thermal conductive detector

TGA – thermogravimetric analysis

TEM – transmission electron microscopy

TPD – temperature programmed desorption

TPR – temperature programmed reduction

TPO – temperature programed oxidation

WGSR – water gas shift reaction

X – conversion (%)

X_G – conversion of glycerol (%)

XRD – X-ray diffraction

Table of contents

Figures:

Tables:

1. Introduction

The growth of world population (expected to grow 40% from 7 billion in 2012 to 10 billion in 2050) and the industrial development of emergent countries is leading to an increase in the world consumption of energy and natural resources [1]. The world faces unprecedented (and possibly) irreversible changes on Earth's climate, and loss in biodiversity is threatening the stability of the living systems on which humans depend on, both often associated to greenhouse gas (GHG) emissions originated on the burning of fossil fuels (petroleum, coal and natural gas) [1]. Petroleum is the primary raw material of the organic chemical industry, and long term sustainable alternatives are needed [2]. Oil has been a large volume continuous source of hydrocarbons that have been converted (by rearrangement, polymerization and functionalization) into a panoply of valuable chemicals and fuels [2]. The increasing difficulty in the exploitation of petroleum reserves and political instability in many oil-producing countries have caused a significant rise of oil derived commodities during the last decades.

To reduce GHG emissions and mitigate global warming, the European Union (EU) established mandatory reduction targets and the incorporation of biofuels (10% by 2020) in transportation fuels, this way reducing the dependence on fossil resources. The agriculture and the industry sectors answered to this challenge by producing unprecedented amounts of raw materials for first-generation biofuels (essentially bioethanol and biodiesel). However, the massive cultivation of raw materials (such as sugarcane, corn, soybean and palm) to produce first-generation biofuels led to competition for land use between food and energy crops, increase in food prices and significant environmental pollution.

On the other hand, the chemical industry is nowadays concerned with the long term and affordable availability of raw materials, and cost of energy and waste disposal have increased at rates greater than the prices of their associated products [2].

Solutions for such complex and inter-connected challenges require innovative approaches in order to strategically achieve fast, concerted and sustainable changes in resource usage and economy paradigm [1,3]. Thus, sustainable development has been defined as the "*development that meets the needs of the present without compromising the ability of future generations to meet their own needs*" [4]. Said in another way, the world should change from a "linear economy" to a more "circular economy", in which the value of products, materials and resources are maintained in the economy for as long as possible, nothing should be lost and ultimately everything should feed a new cycle [5,6]. In this

context, bioeconomy is the renewable segment of the circular economy [7]. The bioeconomy comprises the production of renewable resources, as well as the conservation of these resources and derived wastes into added-value products, such as food, feed, bioproducts and bioenergy [1].

In a certain perspective, biomass is the nature's method of harvesting carbon and storing solar energy in the form of organic matter (chemical energy) [8]. The use of solar energy and carbon in the form of biomass is compatible with the human time scale, because biomass can be used after a few months of solar energy harvesting (as in the cases of grasses and manures) or years (as in the case of trees). The use of biomass chemical energy can repeat itself indefinitely as long as the environmental conditions are within the favorable ranges for biomass to grow. As result, biomass is considered a renewable resource that can be used for energy and material applications in a bioeconomy perspective.

The Directive 2009/28/CE [9] defines biomass as "*the biodegradable fraction of products, waste and residues from biological origin from agriculture (including vegetal and animal substances), forestry and related industries including fisheries and aquaculture, as well as the biodegradable fraction of industrial and municipal waste.*" In a broad sense, biomass can be defined as all the organic matter derived from biological processes (living or wastes) [8]. It includes organic materials derived from agriculture activities (such as bagasse, corn stalks and cobs, straws, pruning wastes), cattle breeding (such as poultry and hog wastes), forest exploitation (such as wood, bark, timber slash and mill scrap), industrial manufacture (such as sawdust, black liquor, nutshells and seed hulls), urban lifestyle (such as food waste, sewage sludge, yard clippings and waste paper) and energy crops (such as poplar, willow, switch grass, sugarcane, corn, soybean and rapeseed) [8].

As biomass is the organic materials originated from plants and animals, it is generally constituted by cellulose, hemicellulose, lignin, lipids, proteins, sugars and starches, and the proportion of each component vary depending on biomass origin [10,11]. Biomass can only be considered as renewable if the resources used in its production are compensated by those obtained from its use. Using the carbon cycle and plants as an example, the biomass is only a renewable resource if the CO_2 emitted during its use is compensated by the carbon stock accumulated during plant growth [10]. If CO_2 emissions caused by biomass production are not compensated during the natural growth of plants,

then the so produced biomass is not and should not be considered as a renewable resource [10].

In 2017, Fantini [8] studied the availability and potential of primary biomass for the production of energy. The author concluded that, in spite the energy content of the annual total production (terrestrial and maritime) of biomass (ca. 57 million TEP) is higher than the energy yearly consumed from oil (ca. 13 million TEP), there are other factors that should be taken into account which in practice invalidate the idea that biomass can complety replace the use of oil [8]. This was in agreement the study of Barber [12] who concluded that the overall efficiency of biomass formation is not enough to replace fossil fuels on a global scale. Some of the reasons pointed out by Fantini [8] include: (1) the agriculture is mostly orientated to food and feed production; (2) significant terrestrial land areas are devoted to ecosystem protection and conservation; (3) substantial terrestrial areas are remote and difficult to access in other to be used for the cultivation of energy crops; (4) the use of biomass as an energy and biofuel source is more difficult and expensive than fossil resources; (5) many technologies devoted to the collection and conversion of biomass into fuels and energy are less developed than those used for fossil resources transformation; and (6) a worldwide cultivation of energy crops would require significant land areas, causing an inherent competition of land use between food/feed production and energy crops. The land use issue has already been somehow observed in massive production of raw materials for first generation biofuels (bioethanol and biodiesel), causing deforestation and change of endogenous cultures by energetic crops (such as sugarcane, corn, soybean and palm). However, lignocellulosic crops can be grown in lands that are not suitable for agriculture [13]

The studies of Fantini [8] and Barber [12] showed that it is not possible to use biomass to completely substitute fossil fuels. On the other hand, non-energy applications account for approximately 16% of oil products [14]. Therefore, biomass could be more effectively used in the production of higher added-value products (such as polymers and chemicals), and only low value byproducts and residues should be used in energy applications (biofuels, electricity and heat). This reasoning seems to be supported by the literature review of Zakzeski et al. [15], who reported that biomass production in Europe could fully supply the raw materials nowadays required by the chemical industry. Moreover, the life-cycles of polymers and materials are usually longer than the life-cycle of fuels, meaning that GHG are retained for longer periods in those materials (possibly for years or even decades) than by immediately burning biomass (in the production of heat and

electricity) or derived biofuels. In such context, biorefineries emerge as a technological solution to address the increasing needs for chemicals and materials. In fact, the European Commission has already addressed this issue by stating that: *"Biorefineries should adopt a cascading approach to the use of their inputs, favoring highest value added and resource efficient products, such as bio-based products and industrial materials, over bioenergy. The principle of cascading use is based on single or multiple material uses followed by energy use through burning at the end of life of the material, including taking into account the greenhouse gas emissions (GHG) mitigation potential. Byproducts and wastes from one production process are used to feed into other production processes or for energy. Biorefineries can thus contribute to the principles of a «zero-waste society»."* [1]

Likewise, the production of oxygenated chemicals from biomass may present significant advantages as compared to the production of biofuels [16]. First, chemicals have higher economic value than fuels, and may allow economic viability of biorefineries at moderate (10-30 kton/year) or even at small (1 kton/year) scales [16]. Second, chemicals require less deoxygenation of biomass materials as compared to extensive deoxygenation needed for biofuels [16]. Third, platform chemicals derived from biomass already have the functionalities of the parental material (such as alcohol, aldehyde, carboxylic, ether, carboxyl groups and unsaturated bonds) [16].

The International Energy Agency (IEA) defined a biorefinery as *"the sustainable processing of biomass into a spectrum of marketable products (food, feed, materials and chemicals) and energy (fuels, power and/or heat)"* [14]. In other words, a biorefinery may be defined as a plant or a cluster of integrated facilities dedicated to the conversion of biomass into marketable products, in a similar approach as nowadays refineries transform petroleum into fuels and chemicals. The IEA adopted a classification system of biorefineries based on four main features, namely, platforms, products, feedstock and processes [17]. The platforms are the chemical intermediates from which the final products are derived, and are the most prominent feature in this classification system [14,17,18]. Ten platforms are used in this classification method: C5 sugars, C6 sugars, oils, biogas, syngas, hydrogen, organic juices, pyrolytic liquid, lignin and electricity and heat [17]. Products are divided in energy products (biodiesel, bioethanol, biomethane, synthetic biofuels, and electricity and heat) and material products (food, animal feed, fertilizer, glycerin, biomaterials, chemicals and building blocks, polymers and resins, and biohydrogen) [14,17,18]. Feedstock are divided in dedicated crops (oil crops, sugar crops,

starch crops, lignocellulosic crops, grasses, and marine biomass) and residues (lignocellulosic residues, oil based residues, organic residues and others) [14,17,18]. Processes are divided in thermochemical (combustion, gasification, hydrothermal treatment, pyrolysis, supercritical), biochemical (fermentation, anaerobic digestion, aerobic conversion, and enzymatic processes), chemical (catalytic processes, pulping, esterification, hydrogenation, hydrolysis, methanation, steam reforming, water electrolysis, and water gas shift) and mechanical/physical (extraction, fiber separation, mechanical fractionation, pressing/disruption, pretreatment, and separation) [14,17,18].

As above mentioned, platform chemicals are meant to be used as substrate for the production of numerous value-added products [18]. Oxygenates derived from biomass can be divided into two main classes: chemicals that are identical to those produced from petroleum cuts (such as tetrahydrofuran or 1,4-butanediol), and new chemicals that are not currently produced from oil (such as α-methylene-γ-valerolactone or 2,5-furandicarboxylic acid) [16]. There is an apparent advantage for the first route, because they benefit from an already established market, however, they have to compete against commodity prices practiced by the current petroleum industry [16]. On the other hand, the production of oxygenates from oil presents considerable technical challenges, while new biomass derived chemicals obtained from non-edible biomass may have interesting properties for the production of new chemicals, solvents and polymers [16]. Moreover, biochemicals are appealing to end users concerned with environment (green products) and they have less carbon footprint [16]. Although new biochemicals might compete in price (1,000-5,000 $/ton) with petroleum derived products if produced at large scale, presently they do not benefit from an established market, and their acceptance by the industry may take time [16]. Therefore, the purpose of this Doctoral thesis was to prepare a contribution to the syngas and lignin platforms. In the syngas platform the gasification of charcoal and the oxidative steam reforming of glycerol were studied. In the field of lignin platform, the fractionation of pinewood biomass was performed by autohydrolysis followed by soda ethanol organosolv and acidic precipitation of lignin. This fractionation procedure had the purpose of obtaining two high purity carbohydrate fractions that could be further processed by thermochemical or biochemical routes in various applications, as well as a high purity lignin that could be used in the production of aromatic compounds for the industry. The hemicelluloses and pulps obtained from the fractionation procedure were used by other researchers in parallel studies aiming the production of ethanol and other chemicals, the reason by which they are not addressed in this thesis. The

depolymerization of the lignin precipitate that presented the highest yield during the fractionation of pinewood was attempted using different catalytic strategies. Then, the upgrading of a model monomer of pinewood lignin (guaiacol) was studied by partial hydrodeoxygenation. The last two chapters of the thesis are dedicated to the discussion of results and to the presentation of the major conclusions.

2. Objectives

The main objective of this Doctoral Thesis was to prepare a contribution for the development of the syngas and lignin platforms, having as background concept the Biorefinery as the future route to obtain feedstock for the chemical industry.

The components of syngas, hydrogen and carbon monoxide, are necessary for hydrogenation, hydroformylation, hydrogenolysis and carbonylation reactions. Therefore, the purpose of researching in this platform was to study different ways for obtaining gas streams having potential to be converted into commodities or building blocks for the chemical industry, such as hydrocarbons (ex. Fischer-Tropsch and Methanol-to-Gasoline processes) or alcohols (ex. methanol and ethanol), which in turn could be further transformed into an almost infinite panoply of commercial materials and products. As so, in the syngas platform the gasification of charcoal and the oxidative steam reforming of glycerol were studied. Commercial charcoal was gasified using air, oxygen and oxygen/steam mixtures aiming to produce renewable syngas. The effects of the equivalence ratio (0.25-0.35) and steam-to-carbon ratio (0.5-0.75) on carbon conversion, producer gas yield, gas composition, heating value (HHV) and apparent energy efficiency (AEE) of the process were studied. The gasification experiments were performed in a laboratory-scale fluidized bed rig working at 900 ºC and atmospheric pressure, using γ-Al_2O_3 as bed material. Then, syngas production was investigated via oxidative steam reforming of concentrated glycerol aqueous solutions (Steam-to-Carbon molar ratio of 4 and 6 vol.% O_2 in N_2). The results obtained using different (bulk) bed materials (SiO_2, SiC and γ-Al_2O_3) were compared with results achieved while using a cobalt aluminate catalyst prepared by coprecipitation dispersed in each of those same bed fillers. The effects on conversion and gas production of the bed filler, activation temperature (750-850 ºC) and reaction temperature (550-750 ºC) were studied, as well as the catalyst reuse (at 750 ºC) to assess its performance after regeneration.

On the other hand, lignocellulosic biomass is expected to be sustainably transformed (refined) into an array of materials and chemicals in biorefineries in a close future. Nowadays, most industries that process lignocellulosic biomass only use the carbohydrate fraction (C5 and C6 biorefinery platforms), while lignin is usually burned to produce energy and steam. Around 70 million tons of lignin are annually produced by the paper industry alone but less than 1-2 wt.% are converted to chemicals, meaning that the

remaining the other 98-99 wt.% are underexploited in terms of chemical valorization. It should be borne in mind that lignin is the only natural resource of aromatic structure, this way having potential for replacing many chemicals that are nowadays produced from petroleum. However, the efficient separation of lignocellulosic biomass into high purity fractions that could be used as feedstock for the chemical industry is still a challenging topic. The conversion of lignin to chemicals depends on the interplay of the three major biorefinery operations, namely, (i) the fractionation of lignocellulosic biomass, (ii) depolymerization of lignin and (iii) the upgrading to desired chemicals. As so, in the field of the lignin platform, the fractionation of pinewood biomass was performed with the purpose of obtaining two high purity carbohydrate fractions that could be further processed by thermochemical or biochemical routes in various applications, as well as a high purity lignin that could be used in the production of aromatic compounds. The depolymerization of an experimentally produced lignin was attempted, as well as the upgrading of a model compound (guaiacol) of the depolymerization products of softwood lignins. In more detail, Pinus pinaster wood (PPW) was fractionated by two different routes: (1) a two-step system by soda ethanol organosolv (SEOS) followed by lignin precipitation (LP) and (2) a three-step procedure encompassing autohydrolysis (AH) followed by SEOS and LP. In the two-step route, the effect of ethanol mass fraction in the cooking liquor (15-55 wt.%) on pulp and lignin purities was studied. In the three-step system, the effects of AH temperature (160-180 ºC) and reaction time (30-60 min) on hemicelluloses removal (at constant biomass to solvent mass ratio B:S=1:8) were evaluated. Then the effects of AH temperature (175-180 ºC) and ethanol concentration (15-35 wt.%) on SEOS derived pulps and lignins purities were considered. The SEOS reaction temperature (170 ºC) and time (90 min) were kept constant in all SEOS experiments. The depolymerization of the lignin obtained by autohydrolysis (175 ºC and 30 min) followed by soda ethanol organosolv (30 wt.% NaOH, 35 wt.% ethanol, B:S=1:8, 170 ºC for 90 min) and acidic precipitation (12 M H_2SO_4 dropwise until pH=5) was attempted using different hydrothermal strategies and catalysts. Then, a molybdenum carbide (Mo_2C) catalyst supported on commercial carbon nanofibers (CNF) was synthetized and tested in the hydrodeoxygenation (HDO) of guaiacol. The effects of temperature (300-350 ºC) and initial pressure of H_2 (20-30 bar) and reaction time (2-4 h) on the conversion of guaiacol and product yields were studied. PPW fractionation, lignin depolymerization and guaiacol hydrodeoxygenation were all performed in batch autoclave reactors.

3. Background

Due to the variety of the technologies addressed in this document, a nonsystematic literature review regarding each process investigated in this thesis was prepared, only encompassing the major aspects of each technology.

3.1. Gasification of charcoal

During the last decades, huge efforts have been put on replacing fossil raw materials by renewable ones. In this context, lignocellulosic biomass has been pointed out as an important raw material for the production of fuels and chemicals [19].

Using thermochemical processes, lignocellulosic biomass can be converted into bio-oils through fast pyrolysis [20–23] and hydrothermal liquefaction [24–27]. These bio-oils can then be upgraded into hydrocarbons by hydrodeoxygenation [20,28–31], or converted into syngas (H_2+CO) using gasification technologies [32,33]. Syngas can also be obtained by direct gasification of lignocellulosic biomass [34–37], and converted into hydrocarbons by the commercial Fischer-Tropsch synthesis [3,38,39] upon conditioning through water gas shift reaction (WGSR) [40–43]. Alternatively, the production of hydrocarbons from syngas can be accomplished by commercial methanol routes such as methanol-to-gasoline (MTG), methanol-to-olefins (MTO), methanol-to-ethylene (MTE), methanol-to-propylene (MTP) [44–46].

Requirements for postprocessing of producer gas depend on its final application [11,47,48]. One of the main problems of biomass gasification is tar contamination of the produced gas [49]. For instance, the tar limits of a gas stream used to feed boilers (no tar limit) or electrical generator engines (50-100 mg/Nm^3) are much different from those to feed gas turbines (0.05-5 mg/Nm^3), fuel cells (<1 mg/Nm^3) or catalytic processes for the production of chemicals and fuels, such as methanol (<0.1 mg/Nm^3) or FT (<1 mg/Nm^3) [47–49].

In order to produce a cleaner gas stream by gasification, there are two kinds of methods: primary and secondary [11,49]. Primary methods consist of modifications inside the gasification reactor to reduce tar formation by modifying the gasification conditions, such as temperature, pressure, gasifying medium, residence time and equivalence ratio, or using catalysts located inside the reactor (such as catalytic bed materials in fluidized systems) [11,48,49]. Dolomite, alumina, olivine, alkali, ferrous oxides and nickel catalysts have been reported as efficient and cheap in tar reduction [11,48,50–55]. Another primary strategy is the use of different gasification reactors, since fluidized bed

systems can produce gas streams with low (300 mg/Nm^3) tar contents and entrained-flow reactors can produce gases with negligible (1 mg/Nm^3) tar contents [48,49]. Secondary methods are applied after the gasification reactor [11,49]. These processes can be conducted using traditional mechanical dry (such as cyclones, rotating particle separators, baffle filters, ceramic filters, electrostatic precipitators and bag filters) and wet (such as spray towers, packed bed scrubbers, venturi scrubbers, wet electrostatic precipitators and wet cyclones) methods [11,47,49]. Dry systems have been mainly developed for particle removal and in most cases they are not effective or economically sustainable for tar removal [11,48,49]. Thermal cracking of tars can be achieved at temperatures in the range of 1100-1300 ºC, with lower temperatures requiring longer residence times for effective cracking [48,49,56]. However thermal cracking can only be applied to reactions systems with high temperature zones, and is not attractive for large scale systems due to economic and operative reasons [56]. Catalytic tar cracking methods are preferred to destroy tars taking advantage of the high temperatures of the exiting syngas [11,47,49]. Non-metallic catalysts such as dolomite, alumina, olivine and zeolite are reported as efficient and cheap in tar reduction [11,48,50]. Metallic catalysts (such as Ni, Ni-Co, Ni-Fe and Ni-Mo) as well as more expensive noble metal (such as Ru, Pt, Pd and Rh) supported catalysts (on alumina, iron oxides, magnesium oxides, silica and zeolites, for instance) have been reported as effective [48,49]. Despite those methods can achieve tar removal efficiencies up to 100%, catalysts deactivate upon time on stream and therefore need to be regenerated [48,49]. To date, several gasification approaches have been proposed by different authors, including the use of dual bed concepts [57], staged gasification of lignocellulosic raw materials [58] and staged conditioning of the producer gas using inexpensive bulk materials and tar reforming catalysts sequentially downstream from the gasifier [59].

A possible strategy to reduce tar contamination in the producer gas is to pretreat the gasification feedstock. Lignocellulosic biomass can be devolatilized by slow pyrolysis (or carbonization) in order to maximize charcoal production, and the so produced biochar can be then gasified [60,61]. Due to the much lower chemical complexity of charcoals when compared to lignocellulosic biomass, syngas with lower cleaning requirements (less contaminant content) can theoretically be produced from its gasification or steam reforming [61–64]. The use of slow pyrolysis charcoals as gasification feedstock present other advantages over lignocellulosic raw materials. Small particles are needed for gasification processes, especially in large scale ones (fluidized and entrained flow systems). Such grinding processes are expensive and energy intensive (ca. 50 kWh/ton)

[65]. On the other hand, slow pyrolysis can be performed autothermally with almost no biomass pretreatment, and the so derived charcoals are highly brittle and easy to grind therefore needing low energy inputs [60,66]. Moreover, the charcoals produced by carbonization of lignocellulosic biomass conserve ca. 50% of the energy of the original feedstock [61,67].

In spite of the extensive application of gasification technologies to virtually all organic materials, the available scientific literature regarding gasification of charcoal has been mainly focused on TGA/DTG analysis [63,68] and TGA-like experimental setups [69,70]. Fewer studies can be found regarding charcoal gasification in fixed bed reactors [71–73], where experimental conditions are often substantially different from the ones present in real fluidized bed reactors (FBR). A small number of works have been published on charcoal gasification using FBR in batch regime [74,75], and only one work was found regarding steam gasification of lignocellulosic pyrolysis char in FBR under continuous regime [76].

The reacting gases (gasifying agents or gasification mediums) usually employed in biomass gasification are air, oxygen, CO_2, steam or their mixtures [77]. Steam gasification of biomass is usually used to produce hydrogen-rich syngas without nitrogen dilution [77,78]. However, several drawbacks derived from the highly endothermic nature of steam gasification reactions may compromise the economic viability of the process [3]. Despite of being less efficient because of N_2-dilution, air is the most common and generally preferred gasifying agent in biomass gasification technologies. It is the cheapest gasification agent and its use benefits from its readily availability and easy feeding without requiring sophisticated equipment. To avoid N_2-dilution, pure oxygen can be used instead of air, while mixtures of oxygen and steam may enhance the performance of gasification processes under autothermal conditions by increasing the hydrogen content of the produced gas stream [77,79].

In a previous work [80], silica sand was compared with alumina as bed material. The results showed that γ-Al_2O_3 improved the charcoal gasification by reducing the amount of contaminant gases (other than H_2, CO and CO_2), as well as the tar content in the outlet stream. These effects were attributed to the improvements in heat transfer (as alumina has a higher heat transfer coefficient than silica sand), and to the catalytic effect of alumina in cracking bigger gas molecules, as reported in earlier works [50]. However, gasification of charcoal with oxygen as well as with oxygen/steam mixtures was not explored in that previous work [80]. Moreover, the experimental setup could not provide enough heat to

maintain the temperature at 900 ºC when steam was fed to the reactor (to promote the production of hydrogen). To overcome such drawbacks, a new experimental work was performed in a more powerful laboratory setup, which is presented in this Doctoral Thesis.

3.2. Oxidative steam reforming of glycerol

The European Union (EU) legislation demands that at least 10% of biofuels should be mixed in transportation diesel by 2020. Of those, 7% can be fulfilled by first generation biodiesel (produced from virgin vegetable oil), 2.5% can be attained by biodiesel produced from waste vegetable oil and animal grease, and 0.5% should be met by advanced biofuels [9,81–83]. Those advanced (second generation) fuels are expected to be obtained by thermochemical processes, such as gasification followed by the Fischer-Tropsch process. Thermochemical biofuels may also be obtained by fast pyrolysis or hydrothermal liquefaction of biomass followed by HDO, provided that renewable hydrogen is available for the upgrading of the raw bio-oils. An alternative to fulfill the advanced fuels quota in diesel by 2020 is the production of biodiesel from microalgae (third generation biofuel). This would mean that the whole biofuels target for diesel engines could eventually be fully attained by biodiesel derived from different raw materials, namely, virgin vegetable oils (7%), waste vegetable oils and animal grease (2.5%) and microalgae oils (0.5%).

The diesel consumption in the EU was 283 million of tons in 2015 [84]. Assuming that such consumption remains stable until 2020, according to the numbers detailed above no less than 28.3 million of tons of biofuels should be produced to satisfy the EU legislation by 2020. Roughly, 100 kg of glycerol ($C_3H_8O_3$) are obtained per each ton of biodiesel produced from triglycerides. If the whole biofuels quota in diesel were fulfilled by biodiesel, this would imply an amount of byproduct glycerol corresponding to 1 wt.% of the whole diesel used in transportation, *i.e.*, 2.83 million of tons of glycerol just within the EU. The large-scale implementation of economically viable applications for glycerin valorization may pose an interesting technological challenge. Hence, new sustainable uses must be found for this byproduct.

The production of hydrogen from glycerol via steam reforming has been widely studied and extensive reviews dealing with this topic can be found elsewhere [85–89]. Theoretically, 7 mol of renewable hydrogen can be obtained from 1 mol of glycerin by steam reforming (Reaction 1), which can be considered as combination of two reactions,

namely, glycerol pyrolysis (Reaction 2) and Water-Gas Shift (WGSR) equilibrium reaction (Reaction 3). However, steam reforming is a highly energy intensive process due to the strong endothermicity of the reaction, as well as to the significant energy requirements necessary to vaporize water (ΔH^o_{vap}=41 kJ/mol) and then heat it up to the reaction temperatures ($C_{p,steam}$=37.47 J/mol·°C at 100 °C), typically in the range of 550-750 °C [90].

$$C_3H_8O_3 + 3\ H_2O \rightarrow 3\ CO_2 + 7\ H_2,\ \Delta H^o_{298}=+128\ \text{kJ/mol} \qquad\qquad \text{(R.1)}$$

$$C_3H_8O_3 \rightarrow 3\ CO + 4\ H_2\ \Delta H^o_{298}= +251\ \text{kJ/mol} \qquad\qquad \text{(R.2)}$$

$$CO + H_2O \leftrightarrow CO_2 + H_2,\ \Delta H^o_{298}= -41\ \text{kJ/mol} \qquad\qquad \text{(R.3)}$$
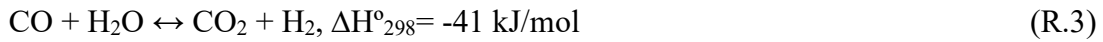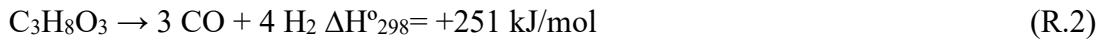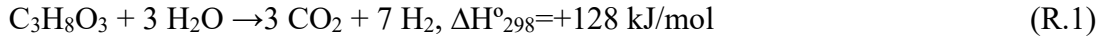
A strategy to overcome these drawbacks is to feed a small amount of oxygen for the promotion of the partial oxidation of the glycerol (Reaction 4), following combined oxidative reforming ("oxy-reforming") strategies that have proven to be beneficial with Rh-based catalysts [91–93] in terms of catalyst stability and selectivity to syngas. The simultaneous occurrence of all three reactions (pyrolysis, WGSR and combustion) is defined in the literature as oxidative steam reforming (Reaction 5), and by a careful selection of the operating conditions, operation in autothermal regime could theoretically be achieved, thus avoiding the need for external energy inputs once the steady-state conditions have been reached. Therefore, by oxidative steam reforming 5.5 mol of H_2 can be theoretically obtained from 1 mol of glycerol, while producing the necessary heat for the process [94–96].

$$C_3H_8O_3 + 7/2\ O_2 \rightarrow 3\ CO_2 + 4\ H_2O,\ \Delta H^o_{298}= -1,565\ \text{kJ/mol} \qquad\qquad \text{(R.4)}$$

$$C_3H_8O_3 + 3/2\ H_2O + ¾\ O_2 \rightarrow 3\ CO_2 + 11/2\ H_2,\ \Delta H^o_{298}= -240\ \text{kJ/mol} \qquad\qquad \text{(R.5)}$$
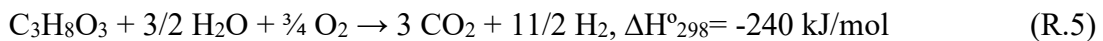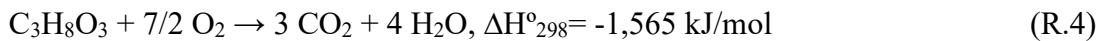
Besides, feeding a small amount of oxygen during glycerol reforming reduces coke deposition on the catalysts, thus increasing their stability while allowing for longer time-on-stream operation [92,95,97,98]. However, oxygen addition must be carefully controlled to avoid reoxidation of the active phase which results in the loss of catalytic activity. This is particularly important in the case of reforming catalysts based in

transition metals like cobalt and nickel. These active phases have been widely researched owing to their competitive cost and performance [99,100] compared to the noble-metal based counterparts like Ru or Pt [91,100], which generally offer an excellent catalytic performance though at a much higher economic cost and limited resources availability [101].

In this context, Co-based catalysts can be a suitable option for the oxidative steam reforming of glycerin. It is well known that Co reoxidation is easier than Ni [102], which could *a priori* hinders the development of oxidative steam reforming using Co catalysts. However, as evidenced in a recently published work, very promising results have been obtained with Co catalysts in the partial oxidation of methane, in spite of operating under much higher oxidizing conditions than those of oxidative steam reforming [92].

Several Co-based catalysts have been used in steam reforming of glycerol. Simpler formulations include Co supported on CeO_2 [96], γ-Al_2O_3 [103–105], and ZrO_2 [106], as well as in bimetallic catalysts associated with Ni [107,108]. A major drawback of transition metal based catalysts in the steam reforming of glycerin is the deactivation by carbon deposition [103–105,109]. In order to improve the stability of Co catalysts, more complex formulations have also been tested, such as CeZrCo and CeZrCo fluorite type oxides [109–112], Co and Co-Ce supported on Ca hydroxyapatite [113] and LaCo or LaCeCo perovskite type oxides [99,114]. An alternative approach to increase the stability of Co catalysts was also attempted by including promoters such as Ru and Na in oxidative steam reforming of glycerol in ethanol solutions [115].

Contrary to steam reforming of glycerol, the oxidative reforming of glycerol has been considerably less studied. A possible reason may be related with the fact that most of the research on glycerol gasification was devoted to the production of hydrogen from glycerin. However, hydrogen will be most likely obtained in the future by water electrolysis associated with electrical power supplied by renewable energies, such as photovoltaic, wind and geothermal energies. For instance, it is possible to produce 1.41 GWh/ha·year of electricity by solar power (considering 12 h daylight, 20% solar panel efficiency, 161 W/m^2 mean incident solar energy), which through water electrolysis (considering 90% electrolyzer efficiency) can be converted into 32.2 tons/ha·year of hydrogen [116]. The current production cost of photovoltaic electricity is 0.05 €/kWh, which is expected to decrease to 0.03 €/kWh by 2020-2025 and 0.01 €/kWh by 2030-2040 [116]. Such prices would allow for corresponding electricity costs spent in hydrogen production of 2.2, 1.3 and 0.4 €/kg H_2, respectively [116]. Considering the capital

(CAPEX) and operational (OPEX) expenditures, the total hydrogen production cost is expected to go below 1 €/kg by 2030-2040 [116]. This means that the production of renewable hydrogen at affordable prices could be accomplished by other routes while sparing biomass for higher added-value applications. On the other hand, most of the materials and chemicals used in a daily basis need a carbon source for their production. The production of syngas is needed for Fischer Tropsch synthesis and methanol to hydrocarbon processes, as well as for hydroformylations and carbonylation reactions still needs to be addressed. As so, in this Doctoral thesis, the oxidative steam reforming of glycerin was studied aiming the production of syngas, as later presented.

3.3. Pinewood fractionation

As previously mentioned, the production of chemicals and fuels from lignocellulosic biomass has been pursued by the scientific community under the concepts of green, sustainable and circular economy [117]. Lignocellulosic biomass and its main polymers (cellulose, hemicelluloses and lignin) are expected to be sustainably transformed (refined) into a panoply of materials and chemicals in biorefineries, resembling petroleum refining in nowadays oil industry [14,118]. Chemical routes for the transformation of biomass carbohydrates (C5 and C6 biorefinery platforms) into chemicals have been extensively addressed in the literature [14,119]. Hemicellulose derived oligomers and monomers can be used in food, prebiotics, textile, paper, explosives, cosmetic, petroleum and mining industries [118,120,121]. Cellulose can be used in building materials, paper products, linen and rayon for clothes (viscose), or as nitrocellulose for explosives, cellulose acetate for films (cellophane), excipients for pharmaceuticals, or sorbents to eliminate pollutants from water [122,123]. On the other hand, lignin could be used in the production of antioxidants, fuel additives, polyurethane foams, phenol-formaldehyde resins and added-value chemicals (such as vanillin and syringaldehyde for the pharmaceutical industry), as well as for substituting aromatics derived from petroleum [124–127]. However, an efficient fractionation system is needed to transform lignocellulosic biomass into biorefinery feedstock for C5, C6, and lignin platforms (Figure 1).
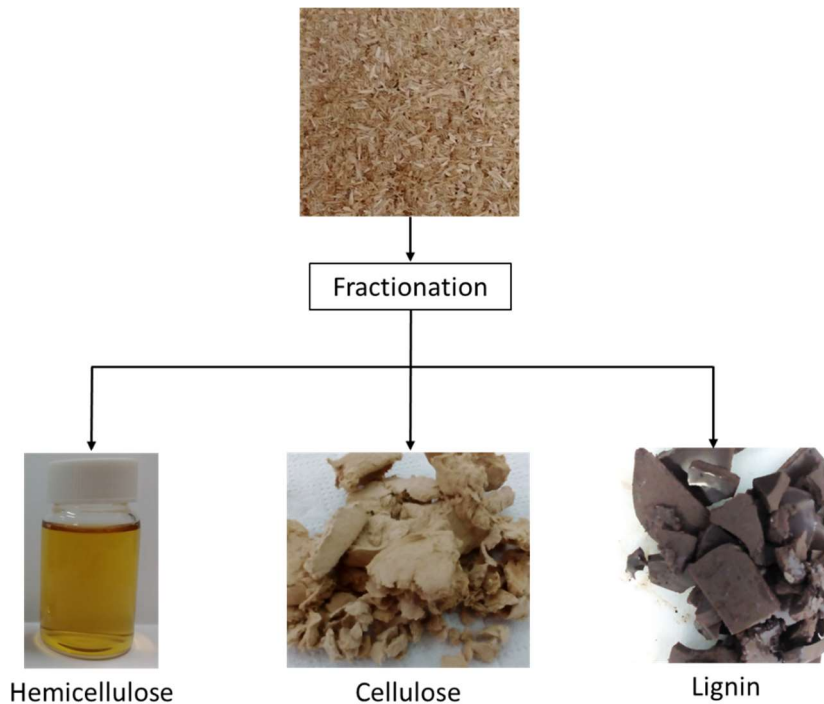
Figure 1 – Hemicellulose, cellulose and lignin fractions obtained from lignocellulosic biomass.

Autohydrolysis (AH) has been suggested as a route for the separation of the hemicellulose fraction from lignocellulosic biomass, leaving a solid mainly constituted by cellulose and lignin [128,129]. It does not require corrosive chemicals or expensive reactor materials and avoids generation of neutralization salts [118]. In this hydrothermal process, compressed hot water (150-240 ºC) is used as solvent [129]. AH is initially catalyzed by hydronium ions generated *in situ* by autoionization of water, and then by hydronium ions generated by autoionization of acetic acid [129]. Acetic acid is formed by deacetylation of hemicelluloses, while furfural and 5-hydroxymethylfurfural (HMF) are produced by dehydration of pentoses and hexoses, respectively [130].

Pine wood has been processed by autohydrolysis, sometimes preceded by aqueous extraction to remove the biomass extractives, and has been reported that no significant hemicellulose removal occurs during the aqueous extraction [131–134]. During autohydrolysis, cellulose is not significantly affected because only a small fraction of the initial anhydroglucose present in wood polysaccharides is converted into glucose oligomeric saccharides [131,132]. The increment in autohydrolysis harshness (temperature and time) results in the decrease of liquor pH and the increased formation of hemicellulose degradation products [133,134]. Interestingly, none of the above

reviewed works reported the application of a delignification/pulping process to the autohydrolysis derived solids.

Pulping processes have been designed to fractionate wood to comply with the pulp and paper industry specifications (such as fiber length and strength), so they are usually targeted to separate cellulose (as solid product) from lignin, which is dissolved in the liquor along with almost half of hemicelluloses [135]. Conventional pulping technologies (such as kraft, sulfite and soda processes) have been used at industrial scale for more than a century in the production of pulps, using inorganic chemicals dissolved in water as reaction medium. In organosolv pulping, organic solvents such as alcohols [136] and organic acids [137] are usually used mixed with water. Organic solvents are reported to enhance lignin solubility and prevent lignin precipitation [138]. In the case of alcohols, ethanol is considered a green solvent because it can be sustainably produced by fermentation of sugars derived from lignocellulosic biomass itself [139].

Ethanol organosolv (EOS) has been mainly studied as autocatalyzed [140] or acid catalyzed [136] process, while base catalyzed has been less exploited [139]. Although ethanol/water mixtures have been reported to be quite effective in pulping hardwoods and herbaceous lignocelluloses, catalysts are needed to accomplish the delignification of softwoods (such as *Pinus pinaster*) [141,142]. In the last decade, works on EOS have been mainly devoted to the preparation of lignocellulosic biomass for enzymatic saccharification and fermentation of derived sugars into second-generation bioethanol. As a consequence of their higher activity in the depolymerization/degradation of cellulose, acid catalysts have been preferred because similar digestibility of the organosolv solid product can be achieved under milder operating conditions, as compared to autocatalyzed or base catalyzed organosolv [139]. Under alkaline conditions, the hydrolysis of glycosidic bonds occurs at a lower rate than delignification, when compared to acidic conditions [143]. Acid catalyzed organosolv has been reported to be ineffective in the removal of lignin from softwoods, producing pretreated solids with high lignin contents [143–146]. Moreover, the production of carbohydrate degradation products is high and the solid yield decreases when the catalyst load is increased [143,146]. In contrast, higher delignification has been achieved when base catalyzed organosolv is applied on softwoods, and lignin removal increases with the alkali charge applied [143,144]. Such results seem to indicate that alkali catalysts should be used in organosolv of softwoods to produce pulps with low lignin contents which can be used as feedstock for the C5 and C6 biorefinery platforms.

Soda ethanol organosolv (SEOS) delignification has been successfully applied to non-woody biomass such as cotton stalks [147] and jute [141], and SEOS delignification kinetics was studied using giant reed biomass [148], all these works devoted to the paper industry. Nevertheless, if the output of a biorefinery is targeted to be a raw material for the chemical industry, purity specifications of organosolv products may differ from those needed for paper making [141] or bioethanol production [139]. In this context, the chemical behavior of the organosolv derived fractions (such as swelling, reactivity, solubility and filtration properties) may be more important than mechanical and optical specifications usually pursued in the pulp and paper industry [141,149], or biodigestibility desired in the case of bioethanol production [139]. In alkaline processes, lignin can be separated from the black liquors by precipitation with acids, while in acidic processes it can be precipitated by antisolvent method [125,150]. Curiously, lignin was not recovered from the pulping liquor in the above reviewed works, neither the separation of hemicelluloses before the SEOS was attempted.

In fact, only a few works were found in literature encompassing the fractionation of lignocellulosic biomass using autohydrolysis followed by organosolv [128,140,151–153]. For instance, the sequential autohydrolysis followed by acid catalyzed organosolv (1 wt.% H_2SO_4) of pinewood has been reported to achieve 60 wt.% hemicellulose removal in the AH step. However, the acidic organosolv pulp contained 26 wt.% lignin, corresponding to a global delignification as low as 50 wt.% [153]. During the literature review performed for this Doctoral Thesis, no published works were found involving the fractionation of *Pinus pinaster* wood (PPW) by autohydrolysis (AH) followed by soda ethanol organosolv (SEOS) and lignin precipitation (LP) to separate the main three biomass components. Moreover, it was not possible to find in literature a comparison between the fractionation of PPW (or other softwoods) by AH followed by SEOS against direct SEOS of the original softwood. In this Doctoral Thesis, these issues were addressed, and the results are presented later in this document.

3.4. Depolymerization of lignin

Lignocellulosic biomass contains 20-30 wt.% of lignin, which represents about 40% of its energetic content [15,154]. Nowadays industries that process lignocellulosic biomass only use the carbohydrate fraction (cellulose and hemicelluloses), while lignin is usually combusted to provide energy and steam for the plant [155,156]. For instance, about 355 L ethanol/ton dry biomass can be produced in a biochemical biorefinery, and only 40%

of the inherent lignin is needed to provide energy for the unit, meaning that the remaining 60% could be used in the production chemicals and fuels [157]. Moreover, around 70 million tons of lignin are annually produced by the paper industry but less than 1-2 wt.% (mainly derived from sulfite process) are converted to lignosulfonates, while the other 98-99 wt.% are combusted for energy and steam [15,156,158]. The price of industrial lignin was evaluated to be lower than $50/dry ton [155]. Considering the conversion of 20% of the lignin extracted from a lignocellulosic biomass having 25 wt.% lignin content to products having an economic value of $2/kg, a revenue of $100/ton of feedstock could be generated (which is higher than the price of the original biomass itself) [155].

It comes out from the above that lignin is an abundant low-cost renewable resource that is still underexploited in terms of added-value applications, however, in order to use lignin as feedstock for the production of chemicals and fuels several obstacles still need to be overcome [155]. These problems are mostly related to the lignin structure, as well as to lignin extraction, depolymerization and product upgrading methods [155].

Lignin is a natural aromatic tridimensional biopolymer found in large quantities in plant cell walls, whose composition depends on plant type (herbaceous, hardwood or softwood) plant species, and part of the plant (leaves, stems or roots) [15,156,159]. It is synthetized in plants by a complex biochemical pathway that is still not completely understood. Lignin synthesis involves the production of three aromatic alcohols (namely, p-coumaryl, coniferyl and sinapyl alcohols, Figure 2) derived from L-phenylalanine, which are then incorporated in plant cell walls by enzymatic radical polymerization in the form of phenylpropanoid subunits having different degrees of methoxy substitutions, namely, 4-hydroxyphenyl (H), guaiacyl (G) and syringyl (S) subunits [156–158,160].
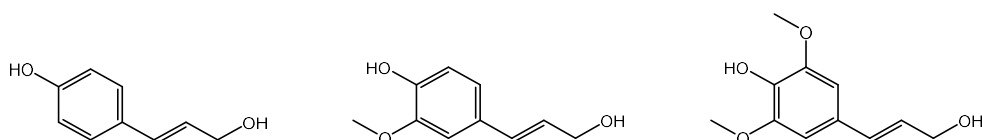
Figure 2 - Monolignols: p-coumaryl (left), coniferyl (center) and sinapyl (right) alcohols.

These phenylpropanoid subunits are randomly polymerized originating three-dimensional polymers of amorphous structures, linked by C-O-C (such as β-O-4, α-O-4, and 4-O-5) and C-C bonds (such as 5-5, β-β, β-5 and β-1) [155,156]. The proportions of the subunits (H/G/S) in lignocellulosic biomass are 0:5/95:100/0:1 in softwoods, 0:4/25:50/46:75 in hardwoods and 2:6/38:68:/28:60 in herbaceous plants [15,156,159].

Softwood lignin (such as that obtained from *Pinus pinaster* wood) has a more condensed structure than hardwood lignin, because G subunits have one less methoxy group (in comparison with S subunits) which stearic facilitates the formation of additional C-C bonds (such as 5-5 and β-5) [15,156,159]. It should be noted that the bonding network between lignin monomers basically determines the lignin reactivity [15,156,159]. A bidimensional schematic of a possible structure of softwood lignin is presented in Figure 3, which illustrates the complexity of the chemical bonding between subunits.
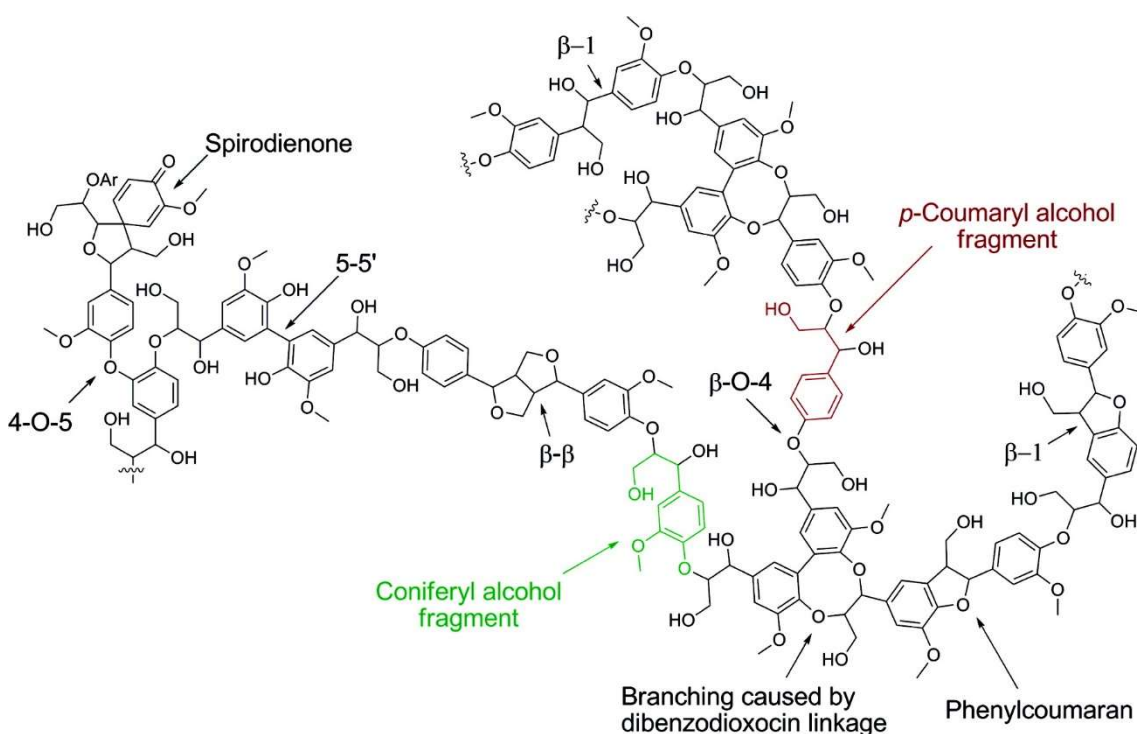
Figure 3 – Softwood lignin structure. Reprinted with permission from reference [15].

Other subunits have been identified in lignin, such as ferulic acid, ferulates (which form bonds between lignin and hemicelluloses), coniferyl aldehyde, sinapyl aldehyde, 5-hydroxyconiferyl alcohol, acetylated monolignols and p-coumarate moieties [159]. Lignin has several functional groups (such as hydroxyl, benzyl, methoxy, carboxyl and ether) that confers it an amphiphilic nature (simultaneously having hydrophilic and hydrophobic properties) [158]. Of those functionalities, hydroxyl and methoxy groups are of utmost importance in lignin depolymerization and product upgrading. The hydroxyl groups content (both aliphatic and phenolic) influence the solubility of lignin, while methoxy groups are very stable and difficult to disrupt, so high temperatures (ca. 250 ºC) and pressures (*ca.* 50 bar) are usually needed [158].

Lignins isolated by soda, kraft, sulfite and organosolv pulping processes are usually referred to in the literature as technical lignins [158,161]. Of those, organosolv lignin is generally considered to present great potential for valorization because of their high purity (in terms of carbohydrates and sulfur content) [158,161].

The depolymerization of lignin usually results in a pool of numerous different products which separation by conventional methods is very challenging or not possible in practice. Moreover, the products of lignin depolymerization usually are very reactive and prone to uncontrollable reactions, including condensation and repolymerization [155]. Lignin has low solubility in water due to its medium polarity, which significantly increases in alkaline mediums owing to deprotonation of hydroxyl groups [162].

The isolated lignin structure, reaction solvents, catalysts and reaction conditions considerably interfere in the outcome of the depolymerization reactions [15,162]. Alkali participate in lignin depolymerization by cleavage of ether bonds, leading to fragments that are rather solubilized in the reaction medium or participate in repolymerization reactions [162]. On the other hand, acidic conditions do not necessarily stimulate solubilization, but promote depolymerization by cleavage of ether bonds leading to very reactive fragments that can repolymerize into condensed forms [162]. Oxidative depolymerization mostly occurs by cleavage of C-C bonds while keeping aromaticity in reaction products, or aromatic rings are disrupted originating aliphatic carboxylic acids. However, the aromatic structures derived from C-C cleavage are not stable in oxidative conditions and can undergo further transformation into aliphatic products [162]. Differently, reductive depolymerization conditions can be achieved by using H_2 or H_2-donor solvents in combination with a catalyst. Reductive conditions do not promote the cleavage of C-C bonds in lignin structure, but strongly diminishes the possibility of repolymerization by yielding more stable deoxygenated products via the cleavage of ether bonds and the partial removal of hydroxyl groups [162].

The reductive depolymerization methods of lignin can be subdivided in four major methods: mild hydroprocessing (usually at 130-320 ºC, 10-100 bar of H_2, solvent and metal or base catalyst), harsh hydroprocessing (usually at 320-450 ºC, 35-100 bar of H_2 and catalyst with or without solvent), bifunctional hydroprocessing (at 150-320 ºC, 20-70 bar of H_2, solvent and bifunctional catalysts containing both acid and metal sites), and liquid-phase reforming (usually at 150-400 ºC, H_2-donor solvent and catalyst) [159,162]. Differently from harsh hydroprocessing, mild conditions enable the preservation of methoxy groups [162]. Common organic solvents are methanol, ethanol, propanol,

butanol, dioxane and tetrahydrofuran (THF) [162]. In the context of green chemistry, ethanol and methanol have become popular solvents due to high heat transfer and solubility [163]. Both of these alcohols can act as H_2 donors, and specifically ethanol can also act as a capping agent and formaldehyde scavenger, this way inhibiting repolymerization reactions [163]. Noble metal (Pd, Pt, Rh and Ru) supported on carbons or alumina, base metal (Raney Ni, Ni/TiN, Cu/PMO, $Cu_2Cr_2O_5$, $CoMoO_x$, WP/C) and bimetallic catalysts (NiAu and NiRu nanoparticles) have been reported in literature on the depolymerization of lignin under mild conditions, sometimes conjugated with inorganic additives (such as H_3PO_4, HCl, NaOH, KOH, Na_2CO_3) [162]. However, most studies report a monomer yields below 20 wt.% [162].

The products of lignin depolymerization reactions consist of mixtures monomeric phenols and poly-(hydroxy)aromatic ethers. Possible applications of depolymerization products strongly depend on their molecular masses. Therefore, one of the lignins obtained upon the fractionation of PPW was depolymerized using different catalytic strategies, and the molecular masses of raw materials and reaction products were determined by SEC and DOSY and compared in this Doctoral Thesis, as presented latter.

3.5. Upgrading of guaiacol

As previously mentioned, the depolymerization of lignin typically results in a pool of different products which separation by conventional methods is extremely challenging or close to impossible [162]. The monomers obtained from lignin depolymerization usually require transformation into useful products, which are generally named as upgrading processes [162]. The depolymerization monomers typically resemble their parent monolignol precursors, meaning that they usually consist of a phenolic core having up to two methoxy groups and a *para*-propyl sidechain [162]. Upgrading processes can be generally divided in two major groups: (i) those that affect the phenolic core and its degree of substitution (such as partial or total deoxygenation through the removal of methoxy groups by hydrodeoxygenation) and (ii) those that change the structure of the side chain (such as oxidation into carboxylic acids) [162].

Hydrodeoxygenation (HDO) is a catalytic upgrading process undertaken in a wide range of pressures (20-300 bar) and temperatures (150-450 ºC), where hydrogen is used to remove oxygen from lignin monomers [28]. High pressures are used to ensure adequate solubility of hydrogen in the reaction media, this way increasing its availability in the vicinity of the catalyst particles and consequently accelerating the reaction rate [28].

Conventional hydrotreating and hydrogenation catalysts have been tested in HDO, as well as novel ones based on alkaline, alkaline-earth, transition and noble metals supported in carbon or metal oxides. However, those catalysts suffer from irreversible deactivation caused mainly by coking, active phase loss and water poisoning [20,28,164].

Metal carbides, nitrides and phosphides have been also attempted. Of those, carbides have recently received increased attention as their properties resemble those of noble metal catalysts, the reason why they are sometimes named as pseudo precious metals [159]. Carburization confers electron densities to the parent metals similar to those of noble metals, and the higher the carbon content, the higher the noble metal-like behavior of the obtained materials [165–168]. Molybdenum carbide (Mo_2C) is an excellent catalyst for hydrogenation and hydrogenolysis of hydrocarbons [29,167]. There are three catalytically relevant molybdenum carbide phases, namely, cubic (δ-Mo_2C), hexagonal (α-Mo_2C) and orthorhombic (β-Mo_2C), following the notation convention defined by the Joint Committee on Power Diffraction Standards. Density functional theory (DFT) studies revealed that the β-Mo_2C phase has the strongest metallic and ionic character [169,170]. It is particularly suitable as heterogeneous catalyst in reactions where electron transfer is needed from the catalyst to adsorbed reactants, characteristic of bond breaking reactions [169,170]. These studies show that molybdenum carbides present an interesting potential as catalyst material for HDO [167].

Metal based catalysts have been usually supported on metal oxides and zeolites, which are sometimes pointed out as the cause for catalyst deactivation [20,28,165]. Within the universe of carbon supports, carbon nanofibers (CNFs) and carbon nanotubes (CNTs) have been less exploited as catalyst supports in HDO of oxygenated organics [171]. CNFs and CNTs present high mechanical resistance, high electrical conductivity, high thermal stability, high capacity for hydrogen adsorption even at high temperatures, and a morphology that allows for the rapid access of reactants and evacuation of products from catalytic active sites [172–175]. Moreover, acid and alkali treatments can be used to enhance the hydrophilicity by creating oxygen functionalities over the carbonaceous materials, and facilitating the dispersion of metals over the CNFs with water solutions [172,173,176]. These properties of CNFs and CNTs attracted the interest of the catalysis community working on HDO of lignin monomers [171,177,178]. Supported molybdenum carbides can be synthetized by carbothermal reduction [179,180]. By this process, the Mo_2C phase is formed by using carbonaceous supports as carbon source under a hydrogen atmosphere.

Guaiacol (2-methoxyphenol) is a lignin depolymerization product and suitable lignin model compound for the evaluation of HDO catalysts, since it incorporates two different oxygen groups commonly present in lignin derived compounds (OH and OCH_3), and it resembles both the conyferyl alcohol and the guaiacyl subunits in softwood (and hardwood) lignin structure [15,28,164,181].

So far, HDO research has almost exclusively targeted the full deoxygenation of lignin derived monomers into fuel grade liquids [162]. A new area of research is the conversion of depolymerization monomers into pure chemicals such (substituted) phenols, which preserve OH functionality and therefore can be used for instance as intermediates for the synthesis of various polymer building blocks [162,182]. Cresols and xylenols can be used as solvents and well as in the production of disinfectants, textile auxiliaries, polymers, ore flotation chemicals and formaldehyde resins, while catechol can be used in the production of pesticides and as precursor of perfumes and drugs [183,184]. Phenol is large scale derivative of petroleum refining which is extensively used in the production of plastics, polymers, herbicides, cosmetics and pharmaceuticals [185]. Phenol market is around 8 million tons/year and its price is ca. $1,500/ton, translating into 12 billion US dollars/year, which is expected to grow at 3.9% per year over the next 10 years [155]. Therefore, in this Doctoral Thesis, the HDO of guaiacol over Mo_2C/CNF catalyst was studied with the aim of maintaining the hydroxy functionality in the derived products, as present latter on this document.

4. Methodology

4.1 Methodology used in the study of the gasification of charcoal

4.1.1 Raw materials and chemicals

Commercial charcoal (Ibecosol, Madrid) produced from hardwood biomass meeting the EN 1860-2 quality standard was purchased in a local supplier. The raw material was grinded and sieved to obtain a particle size distribution of 250-500 μm, which was used as feed in all the experiments. High purity alumina (Puralox, Sasol Germany GmbH) having a mean particle diameter of 237 μm was selected as reaction bed for the gasification experiments. The γ-Al$_2$O$_3$ was activated by *ex situ* calcination at 750 ºC for 3 hours and kept in a desiccator before its use as fluidization bed material. Alumina bulk density was ca. 1000 g/L and charcoal density was *ca.* 380 g/L. Major characteristics of the alumina were BET surface area 142 m^2/g, mesopore average diameter 10.5 nm, and mesopore volume (BJH analysis) 0.42 m^3/g [50]. Synthetic air (>99%), O$_2$ (>99%) and N$_2$ (>99%) were used for the gasification experiments. High purity commercial gases (>99.9 %) were supplied by Air Liquide Spain: H$_2$, N$_2$, O$_2$, He and Ar, as well as the standard gas mixture (N$_2$, H$_2$, CO$_2$, CO, CH$_4$, C$_2$H$_6$, C$_2$H$_4$ and C$_2$H$_2$) used for calibration of the gas chromatograph.

4.1.2. Characterization of raw materials and products

The charcoal used as raw material was characterized by elemental analysis (C, H, N and S contents, and O content determined by difference) using an elemental analyzer (LecoTruSpec® Micro). Proximate analysis (moisture, ash and volatile matter contents) were determined according to the European standards: UNE-EN 14775:2013 (ash content), UNE-EN 32002:1995 (moisture) and UNE-EN 1774-1:2011 (volatile matter). The energy content of the raw material was determined by measuring the higher heating value (HHV) using a C2000-basic IKA-calorimeter. The ash composition of the charcoal was determined by atomic absorption spectroscopy (AAS) regarding the following elements: Al, Ba, Ca, Co, Cr, Cu, Fe, K, Li, Mg, Mn, Na, Ni, Si, Ti and Zn. The surface area of the charcoal was also determined by Brunauer-Emmett-Teller (BET) method using N$_2$ adsorption measurements at -196 ºC (Micromeritics ASAP 2020 Surface Area and Porosity Analyzer Software V3.00). The pore size distribution was analyzed by means of the Barrett-Joiner-Halenda (BJH) method.

The producer gas and the condensates were chemically characterized. The producer gas was analyzed online for H_2, N_2, CO, CO_2, CH_4, C_2H_4, C_2H_6, C_2H_2 and H_2S by gas chromatography (Agilent M3000 series MicroGC, model G2801A). The chromatographic separation of CO_2, C_2H_4, C_2H_6, C_2H_2 and H_2S was performed using a capillary column (Plot U), while the separation of H_2, N_2, CH_4 and CO was performed in a molecular sieve column (MolSieve 5A), each connected to a thermal conductivity detector (TCD). The gas was automatically sampled by the chromatographic system at ambient temperature ($\simeq 20$ ºC) every 3 minutes. The analysis conditions were the following: pressure and temperature in both columns: 1.5 bar-g and 60 ºC, injector temperature: 100 ºC, 30 s of sampling time, 0.1 s of injection time. The total organic carbon (TOC) content of the liquids collected in the condensation system (condensates) was determined using a total organic carbon analyzer (TOC-L CSH/CSN Shimadzu).

4.1.3. Gasification experiments

The gasification experiments were performed in a laboratory-scale (<1 kg/h) experimental setup operating at 900 ºC and atmospheric pressure. The equivalence ratio (ER) and steam-to-carbon mass ratio (S/C) set in all the experiments are presented in Table 1.

Table 1 – Equivalence ratio (ER) and steam-to-carbon mass ratio (S/C) used in the charcoal gasification experiments (all using γ-Al_2O_3 bed).

	Cond. 1	Cond. 2	Cond. 3	Cond. 4	Cond. 5	Cond. 6	Cond. 7
Gasification medium	Air	O_2	O_2 steam	O_2 steam	O_2 steam	O_2 steam	O_2 steam
ER	0.3	0.3	0.3	0.3	0.3	0.25	0.35
S/C (g/g)	0.0	0.0	0.5	0.625	0.75	0.625	0.625

The layout of the experimental setup is presented in Figure 4 and its detailed description can be found elsewhere [78,79]. The dimensions of the fluidized bed gasifier and the location of the thermopars are presented in Figure 5.

Figure 4 – Schematic diagram of the laboratory-scale fluidized bed setup used in the charcoal gasification tests.

Figure 5 - Details of the fluidized be gasifier (T_p – thermopar).

Succinctly, the gasification rig encompassed a solid feeding system (a hopper combined with a screw feeder), a fluidized bed reactor (internal diameter of 40 mm in the bed zone and 70 mm in the freeboard) heated by an electric furnace (9 kW), a gas particulate removal system (a gas cyclone followed by a glass fiber hot filter, both heated at 450 ºC), a condensation system composed by two ice-cooled condensers, followed by a cotton filter for aerosols collection and a gas volumetric meter. The minimum fluidization velocity of alumina was 1.03 cm/s and the high of the bed was ≃12 cm.

The screw feeder hopper was filled with a known amount of raw material. Prior to each experiment, the screw-feeder was calibrated to feed 120 g/h of charcoal. After assembling and connecting all the rig components, 150 g of pre-activated γ-Al_2O_3 were loaded over the bottom distribution plate of the gasifier, after which the reactor was hermetically closed and heated up to the set point temperature (900 ºC) under a nitrogen flow. Before initiating an experiment, the nitrogen flow was substituted by the fluidizing/gasifying gas mixture (air, O_2 and steam). During the reaction time (90 minutes), the reactor temperature and pressure, as well as the gas volumetric flow and gas composition were registered. At the end of each experiment, the mass of produced of solids and liquids were gravimetrically determined to close the mass balances. In all experiments the mass balance closure was >91%.

4.1.4. Calculations

The carbon conversion (C) into each gasification product (gas, liquid or solid), the lower heating value of the product gas (LHV_{gas}), the apparent energy efficiency (AEE), the yield to any gas product (in Nm^3/kg char) and the yield to tar (in mg/g char fed) were calculated using Equations 1-5, as follows:

$$C = \frac{m_{C,i}}{m_{C,feed}} \times 100 \tag{Eq.1}$$

$$LHV_{gas=} \sum x_i \times LHV_i \tag{Eq.2}$$

$$AEE = \frac{Vol_{gas} \times LHV_{gas}}{m_{charcoal} \times LHV_{charcoal}} \times 100 \tag{Eq.3}$$

$$Yield_{gas,i} = \frac{vol_{i,}}{m_{charcoal}} \qquad (Eq.4)$$

$$Yield_{tar} = \frac{TOC \times CV}{m_{charcoal}} \qquad (Eq.5)$$

Where $m_{C,i}$ is the mass of carbon contained in each of the gasification product: gas, solid and liquid ($m_{C,liquid}$ was calculated by multiplying the TOC by the condensate volume), $m_{C,feed}$ is the mass of carbon fed as charcoal, x_i is the volume fraction of component i in the producer gas, LHV_i is the lower heating value of component i in the producer gas, vol_{gas} is the volume of producer gas (measured at standard temperature and pressure), LHV_{gas} is the lower heating value of the producer gas, $LHV_{charcoal}$ is the lower heating value of the charcoal (calculated from the HHV as suggested by Basu [186]), $m_{charcoal}$ is the mass of charcoal fed to the gasifier, vol_i is the volume of the gas component i (measured at standard conditions) and CV is the volume of condensate collected at the condensation system.

The experimental error has been calculated as the 95% confidence interval from three replicates for each experimental data, whereas propagation of independent errors has been assumed to estimate the error of calculated parameters.

4.2. Methodology used in the study of the oxidative reforming of glycerol

4.2.1. Chemicals

Pure glycerol (99.9%, Panreac) was used for preparing the aqueous solutions used as feed. The chemical precursors used in the catalyst preparation were cobalt nitrate hexahydrate ($Co(NO_3)_2 \cdot 6H_2O$, >98%) and aluminum nitrate nonahydrate ($Al(NO_3)_3 \cdot 9H_2O$, >98% purity), all supplied by Panreac, while ammonium hydroxide (NH_4OH, 20-30%, Merck) was used as precipitating agent. High purity alumina (γ-Al_2O_3) (Puralox, Sasol Germany GmbH) was subjected to *ex situ* calcination at 750ºC for 3 h. After calcination, the material was sieved to have particle size distributions in the 200-300 µm range and kept in a desiccator before its use as bed material. Further details on the alumina characterization can be found elsewhere [50]. Washed silica sea sand (SiO_2) and silicon carbide (or carborundum, SiC) were supplied by Sigma-Aldrich and sieved to have particle size distributions in the 200-300 µm range, being readily used right after without

any further pretreatments. High purity commercial gases (>99.9 %) were supplied by Air Liquide Spain: H_2, N_2, O_2, He and Ar, as well as the standard gas mixture (N_2, H_2, CO_2, CO, CH_4, C_2H_6, C_2H_4 and C_2H_2) used for calibration of the gas chromatograph.

4.2.2. Catalyst synthesis and characterization

The detailed methodology regarding the catalyst synthesis was described elsewhere [187]. Succinctly, the Co/Al catalyst was prepared by co-precipitation of the correspondent nitrates, aiming to obtain a spinel structure upon calcination of the hydrated precursor. Aqueous solutions of $Co(NO_3)_2 \cdot 6H_2O$ and $Al(NO_3)_3 \cdot 9H_2O$ were prepared with adequate concentrations. The catalyst was formulated and prepared to have a theoretical excess of 10% of Co in addition to the stoichiometric amount of Co needed to obtain cobalt aluminate spinel, $CoAl_2O_4$, (nominal Co content equal to 40 wt.%). Precipitation was achieved by adding a NH_4OH solution until the required pH ($\simeq 7.7$) was reached. Afterwards, the precipitate was aged for 36 h at room temperature in N_2 atmosphere and washed with deionized water. Finally, the wet precursor was oven dried at 105 ºC for 12 h and calcined at 750 ºC for 6 h under air flow.

The Co/Al catalyst in powder form was characterized by different techniques, including N_2 adsorption-desorption, temperature-programmed reduction (TPR), X-ray diffraction (XRD), transmission electron microscopy (both in the conventional TEM mode and in the scanning mode, STEM) combined with energy dispersive X-ray spectroscopy (EDS) and CO pulse chemisorption. The N_2 adsorption-desorption isotherms were determined in a Micromeritics Gemini V 2380 surface area and pore size analyzer, using static volumetric measurements at -196 ºC, with previous preconditioning of the samples at 200 ºC during 2 h under N_2 gas flow. The surface area of the different samples was determined using the Brunauer-Emmett-Teller (BET) method, and the pore size distribution was calculated using the Barrett-Joyner-Halenda (BJH) method. TPR analyses were carried out using a Micromeritics AUTOCHEM II 2920 equipped with a TCD detector. The sample was reduced using 75 N mL/min of H_2 diluted in Ar (5 vol.% H_2) from room temperature through 950ºC under a 5 ºC/min temperature ramp. A Micromeritics AUTOCHEM II 2920 was used in the CO chemisorption analyses, which were conducted using a dynamic method. Pulse CO chemisorption analyses were done at 35 ºC under a diluted CO flow (10% of CO in He) until saturation of the sample was achieved. Prior to the chemisorption step, the catalyst had been reduced *in situ* at the same reduction conditions used in the catalytic tests (see below), followed by a descent of the temperature

to 35 ºC under a pure He flow (50 NmL/min). The XRD analyses were done using a Rigaku D/Max-B System diffractometer. A copper anode was employed, choosing the wavelength corresponding to copper (λ=0.15418 nm) by means of a graphite monochromator. The measurements were completed in the range of 2θ angles between 20 and 80º (scan step size of 0.05º). The microscopy works (TEM/STEM-EDS) were conducted using a Tecnai F30 microscope.

4.2.3. Oxidative steam reforming tests

The experimental installation used in the catalytic tests was a Microactivity Reference v3.0 developed and commercialized by PID Eng&Tech (Spain), and has been previously described in detail elsewhere [32,188]. Succinctly, it consists of a fixed-bed tubular quartz reactor with 9 mm inner diameter, heated by an electric furnace. In this setup, which operates at atmospheric pressure, liquids are fed into the reactor by means of a high-performance liquid chromatography (HPLC) pump, while gases (H_2, N_2, and O_2) are fed through three different mass controllers. The products flow through a Peltier condenser for the removal of condensable components, and the gas stream containing permanent gases is analyzed online by a gas chromatograph (Agilent Micro GC 3000 series). To calculate the overall values, data obtained in the gas analyses were integrated as function of time, meaning that Table 6-Table 9 should be analyzed with caution since data can be affected by deactivation, which could lead to misleading interpretation. To overcome such difficulty, evolution over time of relevant data is presented in Figure 17-Figure 23. The effects on conversion and yield of the reaction bed material (SiO_2, SiC and γ-Al_2O_3) with and without the catalyst, activation temperature (750 ºC, 800 ºC and 850 ºC), and reaction temperature (550 ºC, 650 ºC and 750 ºC) were studied in different sets of experiments. A series of oxidative steam reforming experiments without the catalyst was carried out using each of the three bed materials as reaction beds without de Co/Al catalyst. These experiments were performed at a reaction temperature of 750 ºC and a reaction time of 4 h.

To study the effect of the Co/Al coprecipitated catalyst on the oxidative reforming of glycerol, the catalyst was diluted in each of the three bed (or filler) materials. In these experiments, 39 mg of catalyst were dispersed in 900 mg of filler material (SiO_2, SiC or γ-Al_2O_3), and deposited on a plug of glass wool. The effect of catalyst activation temperature was studied using SiO_2 as bed material. For that, the catalyst was activated at 750 ºC, 800 ºC and 850 ºC for 2 h before the experiments. The effect of reaction

temperature was studied at 550 ºC, 650 ºC and 750 ºC, using an activation temperature of 850 ºC for 2 h.

In all the experiments carried out, pure glycerol was diluted in high-purity deionized water and fed to the reactor as a 30 wt.% solution (12:1 glycerol to steam molar ratio or 4:1 steam to carbon ratio) at a flow rate of 35 µL/min. A catalyst mass-to-glycerol flow rate ratio of 3.5 g catalyst·min/g glycerol was kept constant in all catalytic experiments. Prior to the reaction, the catalyst was activated *in situ* for 2 h in 80 NmL/min of pure hydrogen at the desired temperature. Then, the flow of hydrogen was substituted by a 35 NmL/min flow of nitrogen and the temperature of the reaction was adjusted. After the reactor was stabilized at the reaction temperature, the experiments were initiated by feeding the glycerol aqueous solution, while adjusting the N_2 flow to 25 NmL/min while co-feeding 10 NmL/min of synthetic air, thus attaining a 6 vol.% concentration of O_2 (O/C=0.5) in the feed. The reaction time in all experiments was 4 h. The results presented in this work are the average of at least three replicated experiments performed under the same operating conditions.

Catalyst regeneration and reuse was also studied at the harshest conditions tested (reaction temperature of 750 ºC). In regeneration experiments, between each reforming reaction the catalytic bed was subjected to reoxidation at 750 ºC. During the reoxidation stage, the liquid feed was suspended while maintaining the same flow of the 6 vol.% O_2 in N_2 gas mixture used in the previous stage, until only nitrogen and oxygen were detected by gas chromatography. Then, the catalyst was reactivated again under H_2 flow following the same reduction conditions already detailed, and the reaction was performed as above mentioned.

4.3. Methodology used in the study of the fractionation of pinewood

4.3.1. Raw materials and chemicals

Pinus pinaster wood (PPW) chips were kindly supplied by Europac (Portugal). The chemical reactants used were: sulfuric acid (H_2SO_4, >95% PA, Fisher; 72%, Chem-Lab), sodium hydroxide (NaOH, Extra Pure, SLR Pellets, Fischer), calcium carbonate ($CaCO_3$, >99%, ACS reagent, Acros Organics 99%), ethanol (C_2H_5OH, >99.8%, Fischer), potassium permanganate ($KMnO_4$, 0.02 M, Chem-Lab), sodium thiosulfate ($Na_2S_2O_3\cdot5H_2O$, 0.1 M, Chem-Lab), potassium iodide (KI, >99.5%, Fluka), cupri-

ethylenediamine (CED, Panreac), starch (>95%, Riedel-de Haën), D(+)-glucose ($C_6H_{12}O_6$, >99%, Riedel-de-Haën), D(+)-mannose ($C_6H_{12}O_6$, >99%, Riedel-de-Haën), L(+)-arabinose ($C_5H_{10}O_5$, >99%, Riedel-de-Haën), D(+)-cellobiose ($C_{12}H_{22}O_{11}$, 98%, Acros Organics), D(+)-glucuronic acid (>98%, Acros Organics), D(+)-galacturonic acid ($C_6H_{10}O_7.H_2O$, 99%, Fluka), acetic acid ($C_2H_4O_2$, >99.8%, Fluka), formic acid (CH_2O_2, >98%, Panreac), furfural ($C_5H_4O_2$, >99%, Merck) and 5-hydroxymethylfurfural ($C_6H_6O_3$, >99%, Acros Organics).

4.3.2. Wood fractionation

PPW was fractionated using two different routes, namely, a two-step and a three-step procedure, as shown in Figure 6.
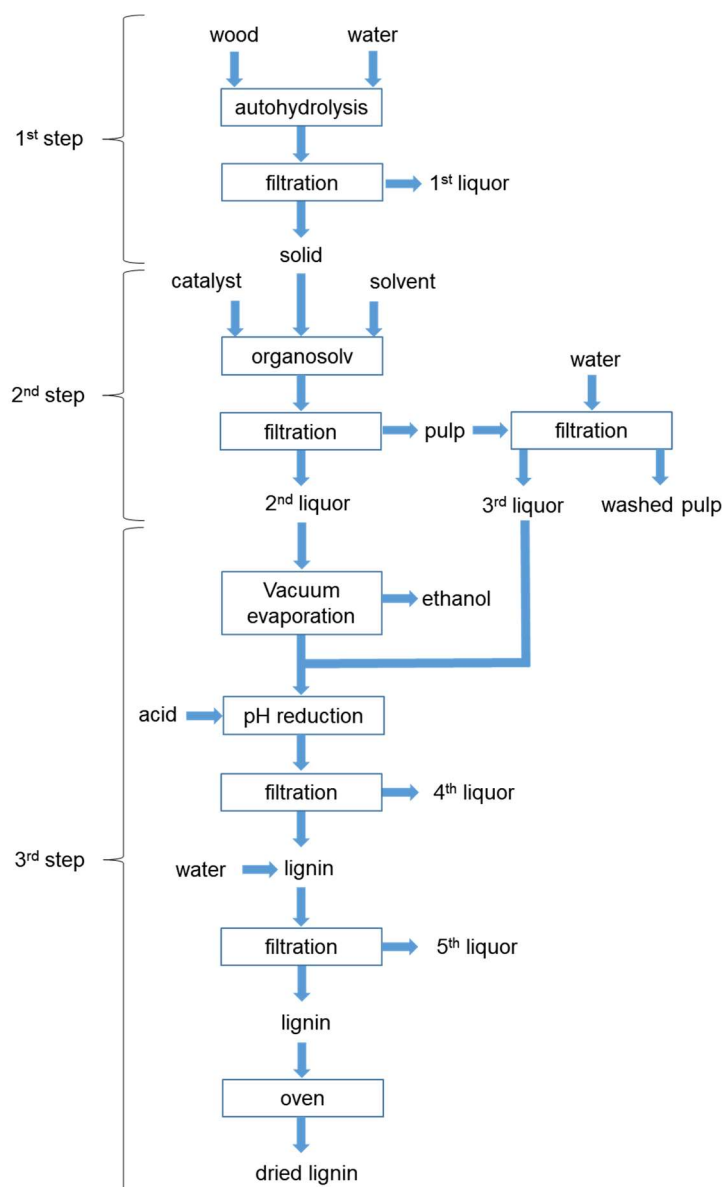
Figure 6 – Flowsheet of the fractionation process.

Prior to fractionation, as received PPW chips were air-dried and grounded in a Retsch Cutting Mill SM 100 with a sieve of square holes of 4 mm. In the three-step procedure (1st, 2nd and 3rd step in Figure 6), PPW fractionation was performed in three sequential stages, namely autohydrolysis (AH), soda ethanol organosolv (SEOS) and lignin precipitation (LP). In the two-step system (2nd and 3rd steps in Figure 6), PPW was directly fed to the reactor for organosolv cooking without previous AH, meaning that the fractionation system consisted in only two stages: SEOS and LP. Both AH and SEOS experiments were performed in a 1 L autoclave reactor (Parr Instruments), agitated by a double six-blade propeller, using a biomass to solvent ratio (B:S) of 1:8 (kg/kg). The results presented in this work are mean values of at least two replicates (three in most cases) from which standard deviation were calculated (±values)

4.3.2.1. Autohydrolysis (AH)

Autohydrolysis experiments were performed using 60 g of dry biomass and 480 mL of distilled water. The autoclave reactor was heated to the desired temperature and the reaction was left to occur for 30 or 60 min. At the end of the reaction time, the reactor was cooled to 20 ºC, and its whole content was vacuum filtered using a paper filter (11 μm pore size, Fioroni), to separate the solid fraction from the liquid (1st liquor in Figure 6). The effects of reaction temperature (160, 170, 175 and 180 ºC) and reaction time (30 or 60 min) were studied on the yield and chemical composition of the obtained solids and liquors.

4.3.2.2. Soda ethanol organosolv (SEOS)

In the two-step procedure (direct SEOS followed by LP, 2nd and 3rd steps in Figure 6), experiments were initiated by feeding 60 g of dry biomass to the autoclave reactor. The effect of ethanol concentration in the cooking solvent (15, 25, 35, 45 and 55 wt.%) on the yield and the chemical composition of the obtained pulps was studied. A 30 wt.% NaOH load (on wood basis) was used as catalyst. After each reaction, the whole reactor content was vacuum filtered (11 μm pore size, Fioroni) to separate the solid fraction (pulp) from the black liquid (2nd liquor in Figure 6). The pulp washing (PW) was performed using 1 kg distillated water at 40 ºC and the derived liquid (3rd liquor in Figure 6) was collected. In the case of the three-step procedure (AH followed by SEOS and LP), the filtration residue from autohydrolysis (solid retained on the filter) was used instead of raw PPW

biomass, while maintaining the counterpart reaction conditions. In this case, the effects of AH reaction temperature (175 and 180 ºC) and ethanol concentration in cooking solvents (15, 25 and 35 wt.%) on the yield and the chemical composition of the derived pulps were studied.

4.3.2.3. Lignin precipitation (LP)

LP was performed using appropriate laboratory glassware and a pH meter. The 2nd and 3rd liquors (in Figure 6) resulting from the SEOS and PW were combined and acidified dropwise to pH 5 ±0.1 using a 12 M H_2SO_4 solution. The acidified mixture was vacuum filtered using a fiberglass filter (2.7 μm pore size, Fioroni). Then, the filtration residue was resuspended in 1 kg of distilled water and vacuum filtered to remove soluble salts and acid residues. Then, lignin was oven dried at 40 ºC before use. The effect of pretreatment conditions (SEOS or AH+SEOS) on yield and chemical composition of the obtained precipitates was studied.

4.3.3. Chemical characterization

PPW, autohydrolysis solids, pulps and precipitates were characterized in terms of cellulose, hemicelluloses, lignin and ash contents, as proposed by the NREL protocols [189,190]. Succinctly, 300 mg of material (oven dried at 40 ºC) were hydrolyzed in a 72% H_2SO_4 (12 M) solution for 60 min at 30 ºC. Then hydrolysates were diluted to obtain a 4% H_2SO_4 solution, autoclaved at 121 ºC for 60 min and left to naturally cool down to room temperature (18 ºC ±3 ºC). The autoclaved solutions were vacuum filtered using weighted filtering crucibles to gravimetrically determine the acid insoluble lignin (AIL), after washing the insoluble material. Aliquots of the primary filtrates were adequately diluted and used in determination of acid soluble lignin (ASL) by measuring the solutions absorbances at 205 nm in a UV-VIS spectrometer (Beckman DU 650). For sugar and degradation products analysis by high performance liquid chromatography (HPLC), 15 mL of the same filtrate were neutralized to $5 \leq pH \leq 6$ using $CaCO_3$ and filtered using a nylon syringe filter (0.2 μm pore size, Clarify), before injection in the HLPC equipment (Knauer). The operating conditions in all HPLC analyses were: injection volume of 20 μL, Rezex ROA-Organic acid column at 40 ºC with the respective guard column, mobile phase flowrate of 0.6 mL/min and refractive index (RI) detector at room temperature. The mobile phase used was ultrasonicated H_2SO_4 0.005 N solution was filtered using a membrane filter (0.2 μm pore size, Fioroni). Autohydrolysis liquors were characterized

by HPLC after hydrolysis of liquor aliquots with 4 wt.% H_2SO_4 at 121 ºC for 60 min, and then following the same procedure used for the solid fractions, as described above. The moisture and ash contents were determined gravimetrically after drying at 105 ºC overnight and calcination at 525 ºC for 10 h.

The kappa number (#K) of the obtained pulps was determined according to Tappi T236 Standard with some modifications of the procedure [191]. The pre-weighed pulp was introduced into a 400 mL beaker and 150 mL of distilled water was added. The beaker was kept in a thermostatic bath set at 25ºC to disintegrate the pulp with a mechanical stirrer. Then, 20 mL of 0.01 M $KMnO_4$ and 20 mL of 2 M H_2SO_4 solutions were pipetted into a 100 mL beaker, subsequently heated to 25 ºC and added to the disintegrated pulp suspension. In this moment, the timer was turned on and after 10 min, 10 mL of 1 M KI was added. Then, the iodine produced was titrated with 0.05 M $Na_2S_2O_3$.

The intrinsic viscosity (η) of the pulps was determined following the ISO 5351 standard [192], in which cellulose pulp is dissolved in a CED solution and its time of efflux is measured through a capillary tube at a known pulp mass concentration at 25 ºC. The intrinsic viscosity of a pulp solution gives an approximation of the degree of degradation (or depolymerization) of the cellulose. The degree of polymerization (DP) and molecular weight (M_w) of cellulose were calculated through their correlation with the pulp intrinsic viscosity as suggested by Wang et al. [193].

Precipitated lignins were also characterized by elemental analysis (EA) and attenuated total reflectance Fourier-transform infrared spectroscopy (ATR-FTIR). EA was performed for quantification of C, H, N and S contents, while O content was calculated by difference (LecoTruSpec Micro). Higher heating value (HHV) of raw materials and precipitated lignins were calculated from respective elemental compositions based on DIN 51900 [194]. ATR-FTIR was performed in a Perkin Elmer FT-IR/FIR spectrometer, and the spectra were recorded between 4000 cm^{-1} and 400 cm^{-1} with a 4 cm^{-1} resolution and 32 scans.

Delignification (D) was calculated as follows:

$$D(\%) = \left(1 - \frac{L_f}{L_i}\right) \times 100$$ (Eq.6)

Where L_i is the initial lignin content and L_f is the final lignin content of the product stream (AH solids and pulps) in dry wood basis.

In the autohydrolysis literature, authors usually express their results regarding liquid products (AH liquors) in mass/volume concentration (g/L). However, this approach presents the disadvantage that the results depend on the B:S ratio used in AH experiments. Another issue is that AH solids produced at different temperatures may retain different amounts of water, due to different porosities and hydrophilic/hydrophobic properties. Because authors frequently do not report the volume of liquid that was actually recovered, the concentration of each compound may induce to interpretational misunderstandings about yields, which are important for the evaluation of the results. In order to avoid such drawbacks, the results are presented in dry basis as mass yields (kg of products/100 kg of PPW) or as mass concentrations (wt.%) of hemicellulose, cellulose and lignin of each product stream (liquors, pulps and precipitates).

4.4. Methodology used in the study of lignin depolymerization

4.4.1. Chemicals

Acids and bases: hydrochloric acid (HCl) and sodium hydroxide (NaOH) were purchased to Fischer. Solvents: ethanol absolute (C_2H_5OH, >99%), methanol (CH_3OH, >99%), ethyl acetate ($C_4H_8O_2$, >99%), dimethylformamide (C_3H_7NO, >99%), tetrahydrofuran (THF C_4H_8O, HPLC grade) and deuterated dimethylsulfoxide (d6-DMSO C_2D_6OS for NMR) were purchased to Fischer. Metal precursors: nickel nitrate hexahydrate ($Ni(NO_3)_2 \cdot 6H_2O$, >99%), copper nitrate hexahydrate ($Cu(NO_3)_2 \cdot 6H_2O$, >98%) were purchased to Acros; ammonium heptamolybdate tetrahydrated (($NH_4)_3Mo_7O_{24} \cdot 4H_2O$, >98%) was purchased to Alfa Aesar. Catalyst supports: Socony Mobil-5 (ZSM5) zeolites (Si/Al=80:1, 50:1 and 20:1) were purchased to Alfa Aesar; hydrotalcite (HTC Mg/Al=3:1) was purchased to Sigma-Aldrich. Activated carbon was purchased to Panreac. Commercial catalysts: Pt/Al_2O_3 (5 wt.%) was purchased to Sigma-Aldrich; Pd/C (10 wt.%) and Ru/C (5 wt.%) were purchased to Alfa Aesar. Gases: H_2 (>99%), N_2 (>99%), He (>99%), synthetic air (>99%) and 0.5 vol.% O_2 in Ar (>99%) were purchased from Nippon Gases Spain. Internal standard: bromobenzene (C_6H_5Br) was purchased to Sigma-Aldrich.

4.4.2. Lignin preparation

Lignin was obtained by fractionation of *Pinus pinaster* wood (PPW) through autohydrolysis (AH) and soda alkaline organosolv (SEOS), followed by lignin precipitation (LP) as above described (*vide* 4.3.2. Wood fractionation). Succinctly, AH was performed in a 1L autoclave reactor (Parr) at 175 °C for 30 min. At the end of the reaction time the reactor was cooled to 20 °C, and the content was vacuum filtered to separate the solid fraction from the liquid. The AH filtration residue (solid retained on the filter) was processed by SEOS at 170 °C for 90 min using a NaOH load of 30 wt.% (on wood basis), a B:S=1:8 and 35 wt.% ethanol in water (as reaction solvent). After each reaction, the whole reactor content was vacuum filtered (11 μm pore size filter, Fioroni), with the purpose of separating the solid fraction (pulp) from the black liquid. The pulp washing (PW) was performed using 1 kg distillated water at 40 °C and the derived liquid was collected. Both liquors (from the SEOS and PW) were mixed and acidified dropwise to pH=5 using a 12 M H_2SO_4 solution. Then, the acidified mixture was vacuum filtered (2.7 μm pore size, Fiorini). The filtration residue was resuspended in 1 kg of distilled water and vacuum filtered again, for removing soluble salts and acid residues.

4.4.3. Catalyst synthesis

All catalysts supported in HTC and ZSM5 were synthetized by incipient wetness impregnation with $Ni(NO_3)_2 \cdot 6H_2O$ or $Cu(NO_3)_2 \cdot 6H_2O)$ to obtain a metal content of 5 wt.%. Bimetallic catalyst were also prepared by incipient wetness impregnation with $Ni(NO_3)_2 \cdot 6H_2O$ and $Cu(NO_3)_2 \cdot 6H_2O)$ to obtain a metal content of 2.5 wt.% of Ni and 2.5 wt.% of Cu. Prior to impregnation, HTC was calcinated at 450 for 16 h as suggested by Kruger et al. [195], while ZSM5 zeolites were washed with deionized water until pH=7, dried at 105 °C overnight and calcinated at 400 °C for 4 h. Activated carbon (AC) was used as received. After impregnation, ZSM5 and HTC supported catalysts were dried overnight at 105 °C, reduced at 400 °C for 4 h in a 75 NmL/min H_2 flow, and passivated for 90 min in 50 NmL/min flow of 1 vol.% O_2 in Ar. Two catalysts supported on activated carbon were carboreduced as described elsewhere [183,196]. Succinctly, AC was impregnated in three steps with aqueous solutions of $(NH_4)_3Mo_7O_{24} \cdot 4H_2O$ to achieve 15 and 30 wt.% Mo content. Between each step the precursors were oven dried at 105 °C for 1 hour between each impregnation step. The dried impregnated precursors were heated at 5 °C/min up to 450 °C, then up to 750 °C at 1 °C/min, and the carboreduction reaction was

left to occur for 2 h, always under a H_2 flow of 100 NmL/min. Then the reactor was cooled to 20 ºC with a 50 NmL/min flow of He and passivated for 12 h with 100 NmL/min flow of 0.5 vol.% O_2 in Ar. All commercial catalysts were used as received.

4.4.4. Homogenous depolymerization reactions

Homogenous base catalyzed depolymerization (BDC) reactions were undertaken by trying to resemble the original SEOS black liquor, and avoid the formation of char [197]. In other words, the lignin was resuspended in a 35 wt.% ethanol in water solution having NaOH load of 30 wt.% (on wood basis) and a B:S=1:8. The mixture (lignin, NaOH and solvent) was heated up to 220 ºC or 250 ºC in a 100 mL autoclave (Autoclave Engineers) for 1 h. At the end of the reaction, the whole reactor content was cooled to 20 ºC and the reaction mixture was vacuum filtered. The filtrate was vacuum evaporated (at 40 ºC and 80 mbar) to remove the ethanol. Liquid-liquid extraction with ethyl acetate was used to separate the organic fraction. After slow evaporation of the solvent (at 40 ºC and 80 mbar), the dried product was weighted (until constant weight) to gravimetrically estimate the yields according to Equation 7.

$$Y_{BCD}(\%) = \frac{DP_{out}}{L_{in}} \times 100 \qquad \qquad \text{(Eq.7)}$$

where Y_{BCD} is the yield of BCD, L_{in} is the mass of lignin fed to reactor, DP is the mass of depolymerization product determined gravimetrically as above mentioned. Since no solid residue was detected after filtration of the reactor content, complete conversion of lignin into depolymerization products was assumed. 1 mL of the organic layer was separated and passed through a syringe filter (0.45 μm pore size) for GC-FID and GC-MS analysis, while the remaining product was concentrated upon slow evaporation of the solvent (at 40 ºC and 80 mbar) to be used in heterogeneous depolymerization experiments.

4.4.5. Heterogenous depolymerization reactions

Heterogeneous depolymerization of lignin was performed in a 100 mL high-pressure batch reactor (Autoclave Engineers) at 200-250 ºC for 30-240 min. The reactor was fed with 20 bar of H_2 (initial pressure), 0.5 g of catalyst, 0.25 g of lignin (or a BCD product) and 50 mL of absolute ethanol. At the end of the reaction, the reactor was cooled to 20 ºC, the whole content was vacuum filtered, and the residue was washed with 50 mL of

absolute ethanol. Both liquids (filtrate and washing) were combined, and vacuum evaporated at 40 ºC and 80 mbar to remove the ethanol. The evaporation residue was acidified to pH 1-2 dropwise with 1M chloridric acid. The organic phase was separated in a decantation funnel, passed through a syringe filter of 0.45 μm pore size before GC-FID and GC-MS analysis.

4.4.6. Characterization of reaction products

GC-FID was performed in an Agilent 6890 chromatograph equipped with a HP-5MS capillary column using He as the carrier gas. The program started at 50 ºC and the temperature was increased at 10 ºC/min, holding at 120 ºC for 5 min, at 280 ºC for 8 min, and at 300 ºC for 2 min. The response factors of 27 standard compounds were calibrated using bromobenzene as internal standard. The identity of the monomeric phenols was confirmed by GC-MS (Shimadzu GC2010 equipped with Shimadzu QP-2010 detector) using the same analysis conditions as in GC-FID. Weight yield (wt.%) is referred to the weight of known monomers in the actual amount of lignin in the starting solid

SEC measurements were made using a HPLC (Agilent 1100) apparatus equipped with a RID, using a HR-5 column coupled with a HR-1 Styragel column (Waters) at 30 ºC as stationary phase, THF as mobile phase at 1 mL/min flow and an injection volume of 25 μL was used. 5 mg of lignin or reaction mixture was dried in a vacuum desiccator at 50 ºC overnight and then solubilized in a 1 vol.% solution of methanol in THF. Weight (M_w) and number (M_n) average molecular masses were calculated using to calibration curves of polystyrene standard.

NMR was performed at 27 ºC using a Bruker Ascend III spectrometer equipped with a PABBO 5 probe and were processed using Bruker Topspin 3.2 software. Samples were prepared at 1% (w/v) in DMSO-*d6*. ^{1}H experiments were run using the *zg30* pulse program at 16 scans. Two-dimensional ^{1}H-^{13}C correlation was carried out using HSQC that run *hsqcetgpsi2* pulse program in an echo-antiecho acquisition mode. DOSY experiments were made in DMSO-*d6* at 27 ºC and at fixed low concentrations of 1% (w/v). DOSY analyses were processed using TOPSPIN 3.2 software from Bruker. Molecular masses determined by DOSY were calculated using calibration curves of polystyrene standards. ^{31}P measures were made using a proton-decoupled experiment. Derivatization prior to ^{31}P measurements was carried out following the protocol described by Pu et al. [198].

The calibrations needed for SEC and NMR analysis were carried out by the DSEO research group (*Diseño, Síntesis Evaluación y Optimización de Nuevas Sustancias de Interés*) at the Department of Sciences of the Public University of Navarre (Spain), and detailed procedures can be found elsewhere [199,200].

4.5. Methodology used in the study of the hydrodeoxygenation of guaiacol

4.5.1. Chemicals

Commercial carbon nanofibers (PR-24 XT-PS, Pyrograf) were used as catalyst support material, while ammonium heptamolybdate tetrahydrated ((NH_4)$_3Mo_7O_{24}·4H_2O$, >98%, Sigma Aldrich) was used as metal precursor. Guaiacol ($C_7H_8O_2$, >99%, Sigma Aldrich) was used as model compound of softwood lignin, and n-decane ($C_{10}H_{22}$, >99%, Sigma Aldrich) was used as reaction solvent. N_2 (99%, Air Liquid) was used for purging the reactor and H_2 (>99%, Air Liquid) was used as reactant. Ethanol (C_2H_5OH, >99.8%, Sigma Aldrich) was used as solvent for rinsing the catalyst after its separation from the reaction products, while nitric acid (HNO_3, >90%, Sigma Aldrich) was used in CNF pretreatment.

4.5.2. Catalyst synthesis and characterization

The as received commercial carbon nanofibers (CNF) were functionalized with HNO_3 to create surface oxygen groups with the purpose of facilitating the metal dispersion on the CNF surface, as detailed in previous works [201,202]. Succinctly, the CNF were treated for 2 hours in diluted boiling HNO_3 using the following proportions: 2 g CNF / 50 mL HNO_3 / 150 mL distilled water. The so pretreated nanofibers were separated by vacuum filtration from the diluted acid using a fiberglass filter (0.2 μm pore size, Whatman), rinsed with distilled water until the filtrate has reached pH=7, and oven dried at 105 ºC for 12 hours.

The catalyst was prepared by incipient wetness impregnation followed by carbothermal reduction. The pretreated CNF were impregnated with an ammonium heptamolybdate hexahydrate solution in one step and oven dried at 105 ºC for 12 hours. The so prepared catalyst precursor was carboreduced in flowing hydrogen (100 NmL/min) using a heating rate of 10 ºC/min up to 750 ºC and maintained at this set point temperature for 2 h. Then,

the catalyst was cooled down to room temperature 50 NmL/min flow of N_2 and passivated with a 50 NmL/min flow of 1 vol.% O_2 in N_2 for 2 hours.

Phase composition, structure of supports and fresh catalyst were determined by X-Ray Diffraction (XRD), in a PANalytical diffractometer equipped with a Ni-filtered Cu Kα radiation and a secondary graphite monochromator, using a θ-2θ configuration. Bulk morphology was studied by Transmission Electron Microscopy (TEM) using a Jeol 2011 microscope with a LaB_6 gun operating at 200 kV and coupled to Energy-Dispersive X-Ray Spectroscopy (EDS). Crystallite size was determined by XRD and TEM. The textural properties were measured by N_2 adsorption at -196 °C in a Micromeritics Tristar apparatus. Specific surface area and pore volume were calculated by applying the BET method to the N_2 adsorption isotherm and the pore size distribution was calculated by the Barrett-Joyner-Halenda (BJH) method based on desorption branch of the isotherm. Temperature Programmed Desorption (TPD) was performed to evaluate the CO and CO_2 eluted from pretreated (CNF) in an AutoChem II 2920 apparatus under constant flow (50 NmL/min) of Ar and using a heating rate of 10 °C/min up to 1000 °C. The eluted gas was analyzed by mass spectroscopy (MS). The total amount of CO and CO_2 released was calculated by integrating the area under the concentration versus volume curve. The oxygen content was determined from the amount of CO and CO_2 released.

4.5.3. Catalytic testing and product characterization

The effects of temperature (300-350 °C), initial H_2 pressure (20-30 bar), reaction time (2-4 hours) on the conversion of guaiacol and product yields were studied. The catalytic tests were performed in a 100 mL high pressure batch reactor (Autoclave Engineers). Prior to each run, the autoclave reactor was loaded with 1.2 mL (3 wt.%) of guaiacol in 40 mL of n-decane (97 wt.%), and 0.2 g of catalyst. Before each experiment, the reactor was purged with N_2 and then with H_2. Next, the reactor was loaded with 20 bar (or 30 bar) of H_2 and heated to the reaction temperature, while stirring at 300 rpm (to minimize reaction during heating). Once the reaction temperature has been reached the stirring was increased to 1000 rpm and the reaction time counting was initiated. The reaction was stopped by decreasing the stirring to 300 rpm and cooling the reactor with compressed air until room temperature was achieved. Blank experiments both with and without CNF were performed to distinguish eventual catalytic effect of the bare CNF support from the effect of reaction temperature on conversion of guaiacol and yields to HDO products. Five tests were performed using the same experimental conditions to assess repeatability of results

(standard deviations: 5.1% for conversion and 6.2% for yields). Guaiacol conversion of (X) and product yields (Y) were calculated using Equations 8-9 as follows.

$$X(\%) = \frac{m_i - m_f}{m_i} \times 100 \qquad\qquad (Eq.8)$$

$$Y(\%) = \frac{m_{pi}}{m_i} \times 100 \qquad\qquad (Eq.9)$$

Where m_i is the initial mass of guaiacol, m_f is the final mass of guaiacol in the reaction products and m_{pi} is the mass of product i.

After each experiment, the catalyst was separated by gravity filtration from the reaction products using a fiberglass filter (0.2 μm pore size, Whatman). The so recovered catalyst was rinsed with 50 mL pure ethanol. The characterization of reaction products was performed using a gas chromatograph (CLARUS 580, Perkin Elmer) equipped with a 30 m long and 250 μm diameter Elite-5 column. The sample was injected employing a split ratio of 19/1 at 275 ºC and measured by a flame ionization detector (FID) at 330 ºC. He was employed as a carried gas, 40 ºC was set as initial temperature, ramped to 275 ºC by 5 ºC/min, further ramped to 330 ºC by 15 ºC/min and held at it for 5 min to ensure the complete elution of all compounds present in the sample. Reaction products were identified in a Varian CP 3800 GC coupled with a Varian Saturn 2200 mass spectrometer (MS) by comparison with the spectrum found in the instrument library. The GC-MS was fitted with the same column as the GC-FID and operated using the same temperature program.

5. General discussion

5.1. Gasification of charcoal

5.1.1. Characterization of the charcoal

The characterization of the charcoal used in the gasification study is presented in Table 2. The elemental, proximate and calorimetric analyses of the charcoal used in this work were within the ranges reported in literature [203], which were obtained from fast pyrolysis (at 500 ºC and atmospheric pressure) of *Acacia dealbata* and *Pterospartum tridentatum*.

Table 2 – Elemental analysis, proximate analysis, ash metal content, surface area and heating value of the commercial charcoal (ND=not detected; * determined by difference).

Proximate analysis (wt. %, as received)	
Moisture	3.6 ± 0.1
Ash	4.2 ± 0.5
Volatiles	19.0 ± 0.3
Fixed carbon*	73.2 ± 0.6
Ultimate analysis (dry and ash free)	
C (wt.%)	80.0 ± 0.4
H (wt.%)	3.1 ± 0.1
N (wt.%)	1.8 ± 0.1
S (wt.%)	0.02 ± 0.00
O* (wt.%)	15.2 ± 0.4
Ash metal contents (mg/kg)	
Al	ND
Ba	ND
Ca	59637
Cr	37
Cu	19
Fe	86
K	2468
Li	5
Mg	315
Mn	28
Na	477
Ni	ND
Si	18
Zn	12
Surface area (m^2/g)	49.5
LHV (MJ/kg)	30.2 ± 0.5

Amutio et al. [204] prepared chars from pinewood sawdust through fast pyrolysis at 400 ºC, 450 ºC, 500 ºC and 600 ºC for which surface areas of 1.9 m^2/g, 2.2 m^2/g, 16.2 m^2/g and 73.2 m^2/g were reported, respectively. In their work, the increase in the surface area

was attributed to a decrease in the average pore diameter caused by an increase in the pyrolysis operating temperature [204]. Therefore, the surface area of the charcoal used in this work (49.5 m^2/g) was roughly on average between the bio-chars produced by fast pyrolysis at 500 ºC and 600 ºC. The analysis of the pore size distribution revealed that the porous structure of the biochar mainly consisted of micropores having diameters lower than 2 nm. Amutio et al. [204] also reported that the char produced by fast pyrolysis at 500 ºC had a LHV (30.4 MJ/kg) and a fixed carbon content (73.6 wt.%), similar to those of the charcoal used here (29.7 MJ/kg and 73.2 wt.%, respectively).

Moreover, the composition of the charcoal used in this work was also similar to that used by He et al. [205] while working on charcoal gasification. In their case, the charcoal was produced at 500 ºC and atmospheric by fast pyrolysis of lignocellulosic biomass. The LHV of the so-produced char (28.4 MJ/kg) was similar to the commercial charcoal used in this work, and the major differences were the N and ash contents (which mainly depend on the nature of the original biomass). Moreover, the proximate analyses were almost identical in terms of volatile and fixed carbon contents [205].

Regarding the mineral content, the main ash components of the charcoal used in the present work were Ca and K, followed by Na and Mg, meaning that alkali and alkaline earth metals (AAEM) were the major components of the charcoal ash. Low concentrations of transition metals were detected, and surprisingly, the Si content was very low (usually an important metalloid in lignocellulosic biomass), while the Ca content was very high [23,62,63]. The catalytic effect of AAEM in the gasification of lignocellulosic charcoals was studied by several authors [62,64,206,207]. Generally, they concluded that the highest catalytic effect was caused by potassium, while calcium exerted the lowest catalytic effect on char gasification, which was the main AAEM detected in the charcoal used in this work.

5.1.2. Gasification of the charcoal with air and pure oxygen

Aiming to address the limitations found in a previous work [80], and to get deeper insight the effect of replacing air by oxygen in the gasification of charcoal, both oxidants were tested using a constant ER=0.3 (S/C=0). Table 3 shows the results of those experiments.

Table 3 – Results of the preliminary charcoal gasification experiments using air or pure oxygen as gasifying agents. ND=not detected

Parameter	Air	Oxygen
Carbon conversion into gas (wt.%)	49.2 ±0.7	51.9 ±0.8
Gas yield (Nm^3/kg charcoal)	2.5 ±0.2	0.9 ±0.1
LHV$_{gas}$ (MJ/Nm^3)	2.5 ±0.1	7.5 ±0.1
AEE (%)	20.5 ±0.6	21.5 ±0.3
Gas composition		
H$_2$ (vol.%)	7.2 ±0.6	17.3±0.6
CO (vol.%)	12.0 ±0.2	43.2 ±0.2
CO$_2$ (vol.%)	14.7 ±0.1	38.5 ±0.1
CH$_4$ (vol.%)	0.6 ±0.0	0.5 ±0.0
C$_2$H$_4$ (vol.%)	ND	ND
C$_2$H$_4$ (vol.%)	ND	ND
C$_2$H$_2$ (vol.%)	ND	ND
H$_2$S (vol.%)	0.0 ±0.0	0.0 ±0.0
N$_2$ (vol.%)	65.5 ±0.6	0.5 ±0.6
H$_2$/CO	0.6 ±0.1	0.4 ±0.0
CO/CO$_2$	0.8 ±0.0	1.1 ±0.0
Gas yields (NL/kg of charcoal)		
H$_2$	179 ±2	151 ±5
CO	298 ±4	375 ±4
CO$_2$	365 ±4	335 ±3
CH$_4$	15 ±0.7	5 ±0.2

The results show that the carbon distribution among the reaction products was similar when using both gases as gasifying agents. The charcoal conversion was slightly higher when oxygen was used as gasifying agent. As expected, the overall producer gas yield was much higher when air was used as oxidant, but the gas heating value was much higher when oxygen was used as gasifying agent resulting in a slightly higher AAE.

The H$_2$S volumetric concentration in the producer gas was <0.01 vol.% for air gasification and <0.02 vol.% for pure oxygen gasification, which can mainly be related to N$_2$-dilution. Moreover, the tar mass yield (related to the amount of charcoal fed to the gasifier) was higher in air gasification (0.79 mg/g char) as compared to oxygen gasification (0.38 mg/g char). However, the volume concentration of tar was lower in air gasification (317 mg/Nm^3) as compared to oxygen gasification (436 mg/Nm^3). Such results were attributed

to the dilution effect caused by the N_2 partial pressure when air was used as gasifying agent.

The hydrogen to carbon monoxide molar ratio (H_2/CO) was lower while the carbon monoxide to carbon dioxide molar ratio (CO/CO_2) was higher in oxygen gasification as compared to air gasification. These results indicated that the WGSR was more effective when air was used as oxidant. Because N_2 is an inert gas it does not interfere in the WGSR equilibrium (Le Chatelier principle), so these results were attributed to the endothermal reverse Boudouard reaction (Reaction 6) favored by the higher residence time of produced gases in oxygen gasification as compared to air gasification, which seems to be corroborated by the higher yield of CO and the lower CO_2 yield in the case of oxygen gasification (Table 3).

$$CO_2 + C \leftrightarrow 2\ CO, \Delta H^{o}_{298}=172\ kJ/mol \hspace{4cm} (R.6)$$

The contents of syngas components (H_2+CO) in the producer gas were much higher when pure oxygen was used as gasifying agent. However, on a N_2-free dry basis, the producer gas composition from air gasification was: 20.9 vol.% of H_2, 34.7 vol.% of CO, 42.5 vol.% of CO_2 and 1.7 vol.% of CH_4, and the gas production was 0.86 Nm^3/kg. Such data compares with 17.3 vol.%, 43.2 vol.%, 38.5 vol.%, 0.5 vol.% and 0.87 0.86 Nm^3/kg obtained from oxygen gasification.

The yields of H_2, CH_4 and CO_2 were lower when oxygen was used as compared to air, while CO production was much higher. These differences in the yields might be attributed to the lower residence time of gases during air gasification caused by the additional flow of N_2 introduced in the reactor. Hence, a higher residence time of the gases within the reactor during oxygen gasification seems to promote the consumption of H_2, CH_4 and CO_2 and the formation of CO.

Due to the fact that, as previously reported [80], the experimental setup could not provide enough heat to maintain the rig at 900 ºC while feeding mixtures of air and steam, further experimental work was performed by using mixtures of pure oxygen and steam.

5.1.3. Influence of the steam-to-carbon ratio (S/C)

To study the effect of the steam-to-carbon ratio, the charcoal gasification was carried out by varying it in the range of 0-0.75 g/g, while keeping the ER constant (at 0.30). Figure 7 shows the influence of S/C ratio on the distribution of the charcoal carbon fraction among gas (a) and the carbon recovered in solids (non-converted) (c) products (ER=0.3).
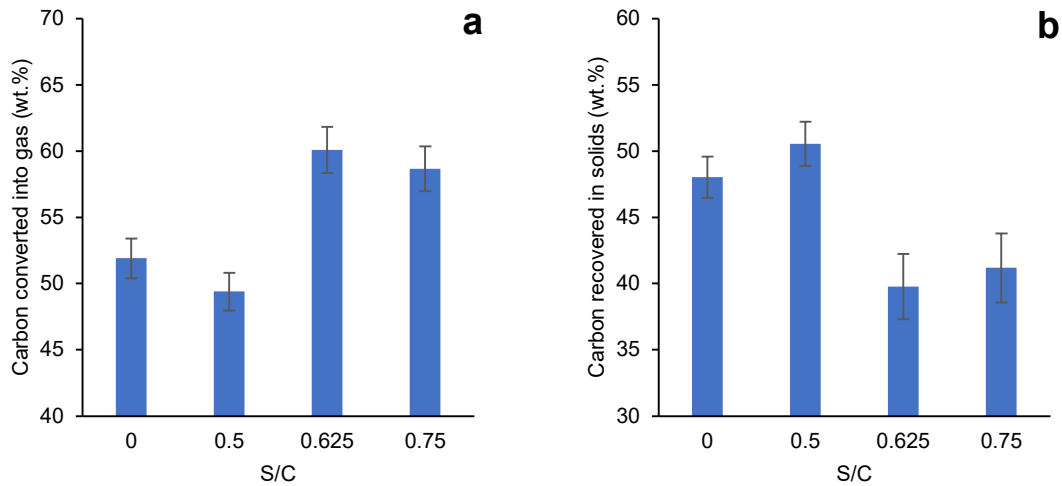
Figure 7 – Influence of S/C ratio on the distribution of charcoal carbon fraction among gas (a) and solid (b) products (ER=0.3).

The fraction of the charcoal carbon converted into gas slightly decreased when the S/C ratio was increased from 0 to 0.5 g/g (Figure 7a). Such results may have been caused by the flowrate increase of the gasifying mixture when steam was fed to the gasifier, resulting in a reduction of the residence time of the gases within the reactor. Additionally, the most reactive gas (oxygen) was diluted with a less reactive gas (steam), so the contact time between oxygen and the charcoal decreased when the S/C ratio was increased from 0 to 0.5 g/g. However, when the S/C was further increased from 0.5 to 0.625 g/g, the carbon fraction converted into gas improved but did not vary much upon increasing the S/C to 0.75 g/g. These results indicated that the intensification of turbulence caused by the increase in the superficial gas velocity (due to the increasing the flow of gas feeding) enhanced the gasification kinetics by improving the contact between the charcoal and the gasifying mixture (O_2 and steam), prompting an increase in the carbon conversion into gas (when S/C=0.625 g/g) [208]. However, a point seems to have been reached beyond wherein the residence time of both feeds (gas and solid) was so small that it hindered the gasification kinetics by reducing the contact time within the reactor (when S/C=0.75).

Accordingly, the producer gas and syngas yields (Figure 8) increased as the S/C ratio was augmented up to 0.625 g/g, after which they both decreased upon further increases of the S/C ratio (up to 0.75 g/g). The changes in volumetric yields of the main gas products are presented in Figure 9.
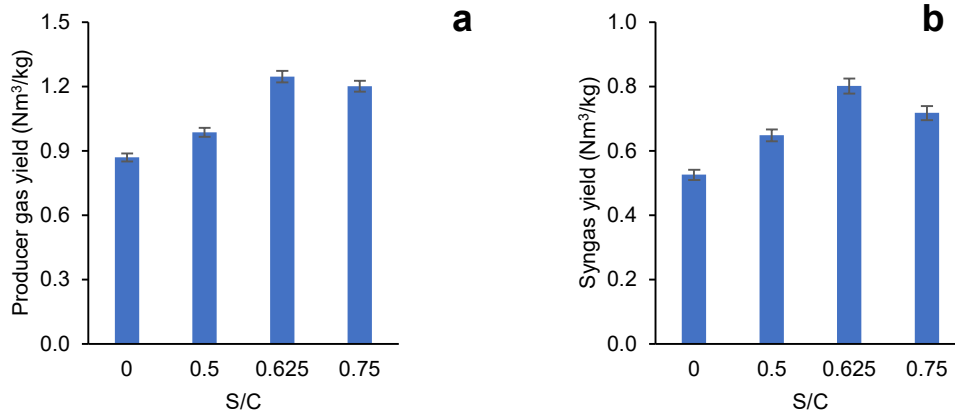
Figure 8 – Influence of S/C ratio on producer gas (a) and syngas (b) yields (ER=0.3).
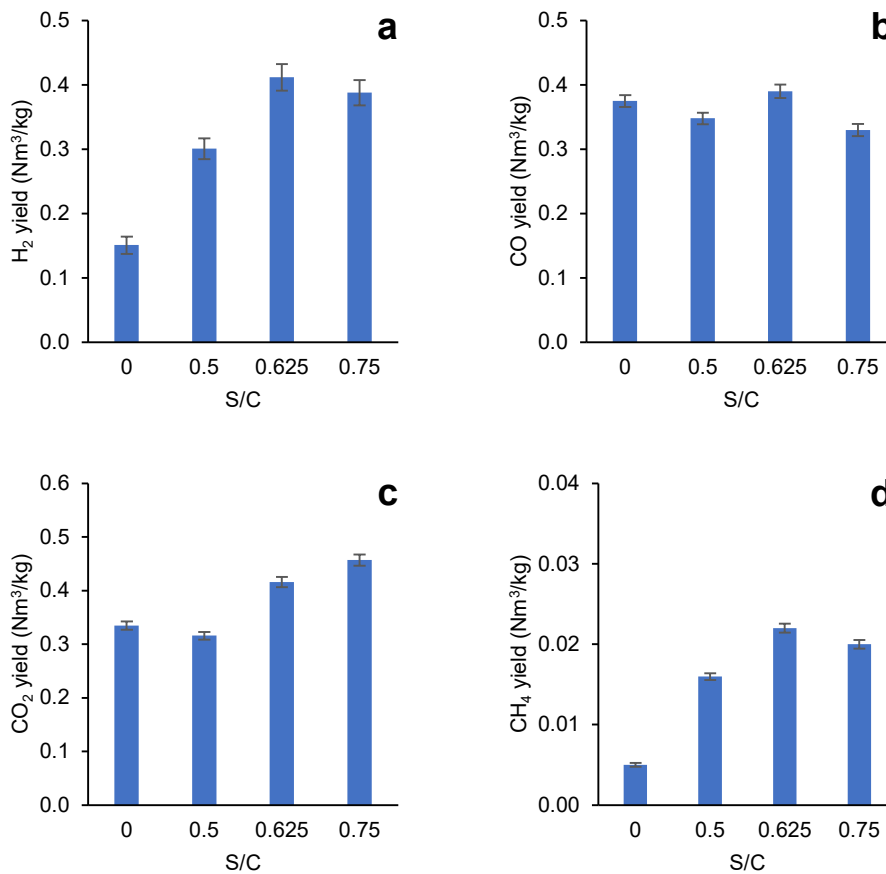
Figure 9 – Influence of S/C ratio on gas yields of H_2 (a), CO (b), CO_2 (c) and CH_4 (d) (ER=0.3).

The yields of H_2, CO_2 and CH_4 globally increased when the S/C ratio was increased up to 0.625, while the yield of CO did not show a clear trend for the same experimental conditions. On the other hand, when the S/C was increased from 0.625 up to 0.75, the yields of H_2, CO and CH_4 decreased, while the yield of CO_2 increased. In the experiments performed for studying the effect of the S/C, the H_2S volumetric concentration in the producer gas was always <0.02 vol.%. The H_2/CO (from 0.4 to 1.2) increased while the CO/CO_2 (from 1.1 to 0.7) declined with the increase in S/C, evidencing the effect of the WGSR.

The mass tar yields decreased (from 0.38 mg/g char to 0.29 mg/g char) when steam was introduced (S/C from 0 to 0.5 g/g), possibly due to the slightly lower carbon conversion to gas. When the feed of steam was further increased (from 0.5 to S/C to 0.75 g/g.), the tar production also increased (to 0.85 mg/g char and then to 0.99 mg/g char). The volumetric tar yields followed the same pattern (486 mg/Nm^3, 290 mg/Nm^3, 685 mg/Nm^3 and 819 mg/Nm^3, respectively). These results seem to show that tar production increased consistently with the increase in the S/C ratio. Apparently, the results are in contradiction with the literature [186], since it is widely accepted that the increase in the S/C ratio has been suggested as a primary method for reducing tar production in the gasification of lignocellulosic material. However, the explanation for these results seems to be related with the higher amount of unreacted steam when the S/C ratio was increased. Similar effects were previously reported by other authors while studying the air steam gasification of charcoal in cyclone furnace gasifiers [205], as well as during steam gasification of char in fixed-bed reactors [73]. He et al. [205] used several mixtures of air and steam as gasification agent, different ER (0.25-0.41 with a S/C=0.35) and different S/C ratio (0.25-0.55 with an ER=0.36). They concluded that the introduction of steam improved the gas quality, but excessive steam (>0.44 while using an ER of 0.36) hindered the char conversion and the gas quality. Yan et al. [73] performed the steam gasification of biomass char in a fixed-bed reactor, using a steam flow rate of 0–0.357 g/min/g of biomass char at 600-850 ºC. Their results showed that the introduction of the steam improved the carbon conversion efficiency when the steam flow rate was increased from 0 to 0.165 g/min/g biomass char, but then dropped when the steam flow rate was further increased.

The LHV (Figure 10a) of the producer gas slightly increased when steam was introduced in charcoal gasification up to S/C=0.5 g/g, and then dropped when the S/C ratio was increased above 0.625 g/g, reflecting the changes in the composition of the produced gas.

The AEE increased with the S/C ratio in a similar way as the producer gas and syngas yields, meaning that a maximum AEE was observed when S/C=0.625 g/g (Figure 10b). These results indicated that the decrease in the producer gas heating value was overpassed by the increase in the gas yield when varying the S/C ratio from 0 to 0.625 g/g. The lowest LHV of the producer gas corresponded to the experiments where the concentration of CO_2 (which does not contribute to the heating value) was higher, namely, the experiments performed with no steam and with S/C=0.75 g/g.
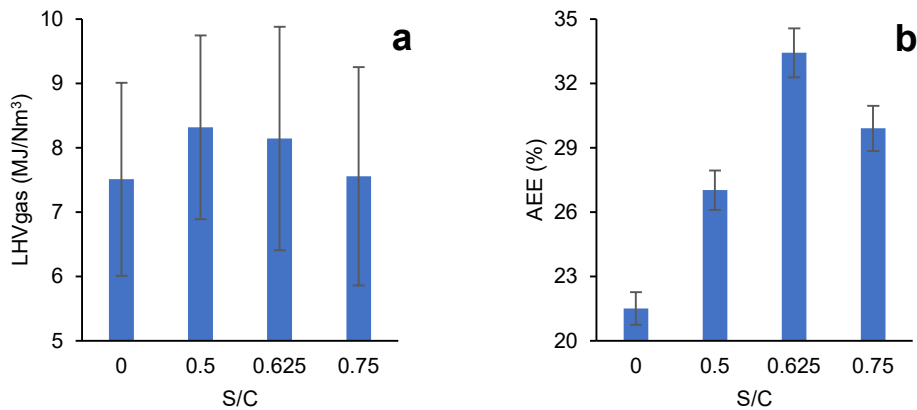
Figure 10 – Influence of S/C ratio on producer gas LHV (a) and apparent energy efficiency (b) (ER=0.3).

Due to the fact that a S/C ratio of 0.625 g/g allowed to achieve the highest producer gas yield, as well as the highest energetic efficiency and the highest H_2 and CO yields compared to the other experiments performed to study the effect of the S/C ratio, and due to the fact that the calorific value of the produced gas was also the second highest, the S/C=0.625 g/g was kept constant in the following experiments undertaken to study the ER effect on the gasification performance.

5.1.4. Influence of the equivalence ratio (ER)

To study the effect of the ER, the charcoal was gasified by varying that ratio between 0.25 and 0.35, while maintaining constant the S/C=0.625 g/g. Figure 11 shows that the charcoal carbon fraction converted into gas improved when the ER was increased from 0.25 to 0.35.

b

51
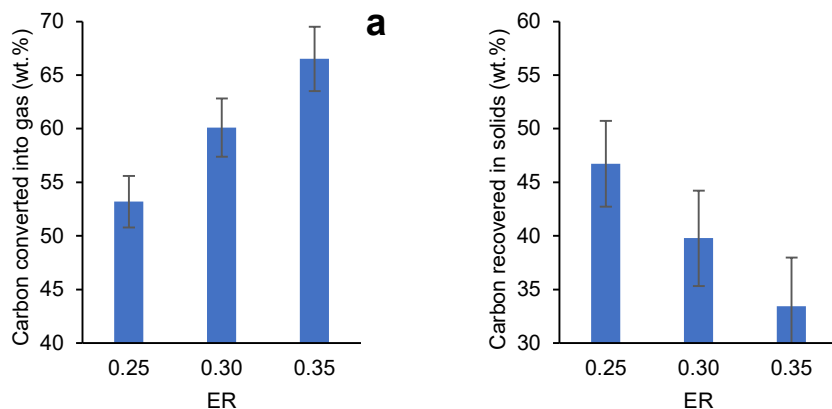
Figure 11 – Influence of ER ratio on the distribution of charcoal carbon fraction among gas (a) and solid (b) products (S/C=0.625 g/g).

The mass tar yields increased when the ER was increased from 0.25 to 0.3 (from 0.51 mg/g to 0.85 mg/g), and then decreased when the ER was increased to 0.35 (from 0.85 mg/g to 0.56 mg/g). Accordingly, the corresponding volumetric tar yields were: 483 mg/Nm^3, 685 mg/Nm^3 and 425 mg/Nm^3 (respectively).

The produced gas yield showed a consistent tendency to increase when the ER was increased, but the syngas yields slightly decreased when the ER was higher than 0.3 (Figure 12).
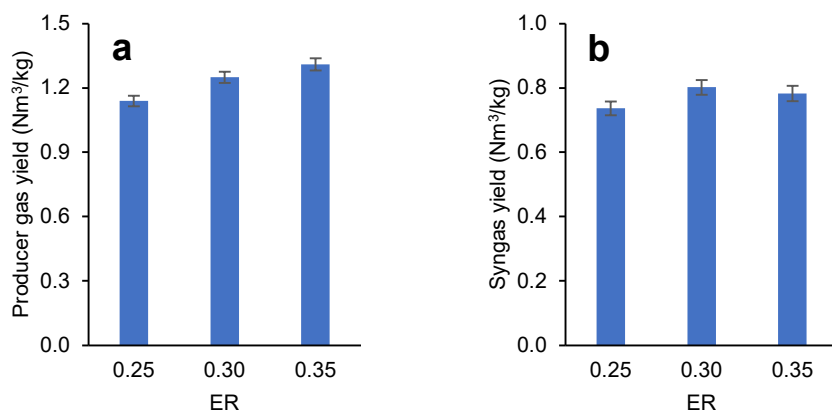
Figure 12 – Influence of ER on producer gas (a) and syngas (b) yields (S/C=0.625).

In terms of individual gas production (Figure 13), the volumetric yields of CO and CO_2 increased when the ER was augmented from 0.25 to 0.3, while non-significant changes were found for the H_2 yields.
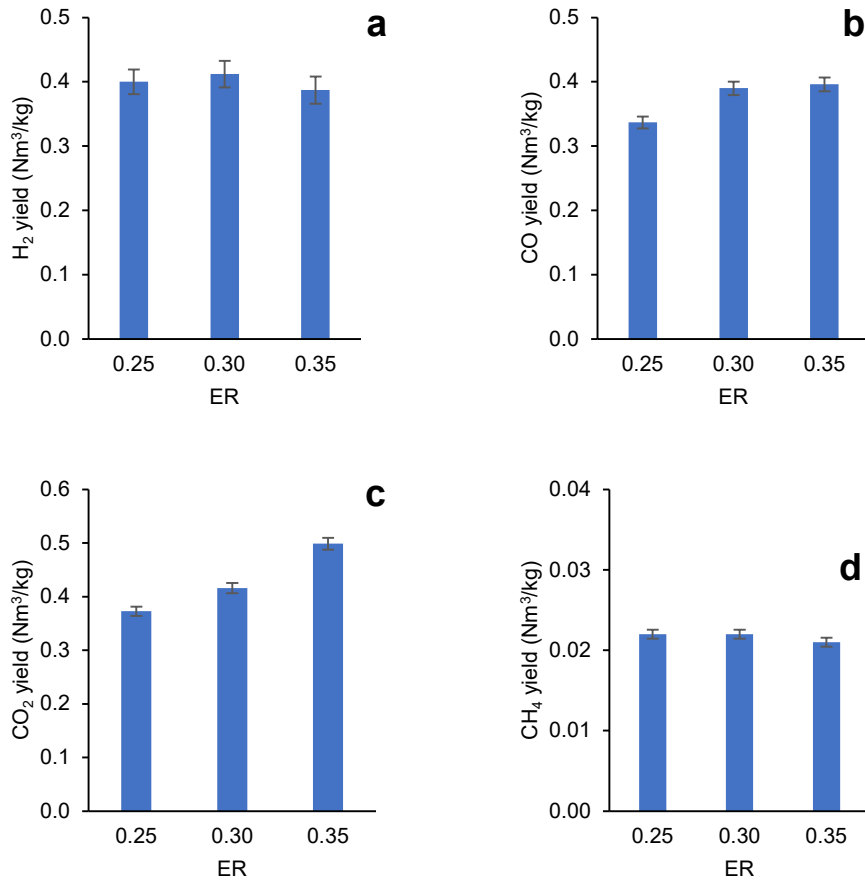
Figure 13 – Influence of ER on gas yields of H_2 (a), CO (b), CO_2 (c) and CH_4 (d) (S/C=0.625 g/g).

However, when the ER was increased from 0.3 to 0.35, the yield of H_2 decreased while the yield of CO_2 increased, while the yield of CO remained almost constant. Both the H_2/CO (from 1.2 to 1.0) and CO/CO_2 (from 1.0 to 0.8) ratios declined with the increase in ER, possibly caused by combustion of CO and H_2 and explaining why the syngas yield decreased for ER=0.35. The yield of CH_4 presented only slight variations when the ER was increased from 0.25 to 0.35. These results seem to be related with the complexity of the gasification process, in that the weight of each individual chemical reaction changes as a function of the availability of oxygen and steam within the reactor. This helps to understand the observed drop in the producer gas heating value when the ER was increased from 0.30 to 0.35 (Figure 14). The LHV of the gas dropped as more reacting gas (oxygen) was fed to the gasifier (Figure 14a). On the other hand, the AEE of the process (Figure 14b) improved when the ER was increased from 0.25 up to 0.3.
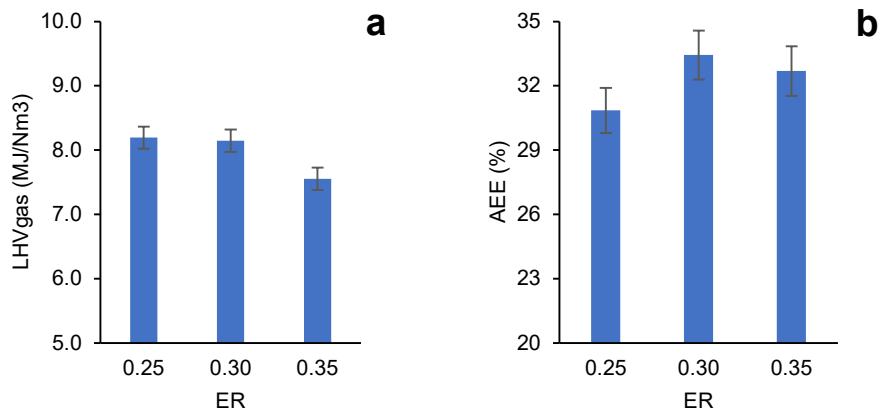
Figure 14 – Influence of ER on the producer gas LHV (a) and apparent energy efficiency (b) (S/C=0.625 g/g).

Other authors [205] working in air-steam gasification of fast pyrolysis char in a furnace reactor achieved higher carbon conversions into gas (95%) when using a S/C=0.65 g/g and an ER=0.36. However, because they used air instead of pure oxygen in the gasifying mixture, the LHV of the gas (2.46 MJ/m^3) and the H_2 yield (0.069 Nm^3/kg char), as well as the H_2/CO ratio (0.14), where much lower than those attained in this work (LHV of 7.55 MJ/Nm^3, H_2 yield of 387 Nm^3/kg char, and H_2/CO ratio of 0.98, respectively).

5.1.5. Overall considerations

As previously mentioned, the requirements for postprocessing of the producer gas depend on its final application (tar limits: electrical generator engine 50-100 mg/Nm^3, gas turbines 0.05-5 mg/Nm^3, fuel cells <1 mg/Nm^3, methanol synthesis <0.1 mg/Nm^3 and Fischer-Tropsch <1 mg/Nm^3) [47–49]. None of the product gas streams obtained in this work fulfilled such limits, however, it should be noted that the tar concentrations above reported were measured in the liquids collected as condensates, meaning that these tars were removed from the produced gas stream upon cooling in ice condensers, not in the gas itself.

Direct comparisons based on literature are somehow difficult due to the different ways of reporting operational conditions and experimental results of each work. For the sake of completeness, an effort was made in this work to at least undertake global comparisons. For that, the results obtained in this work and those found in literature regarding the gasification of lignocellulosic charcoals in continuous systems is presented in Table 4.

Table 4 – Summary of reaction conditions and main results reported in literature of charcoal gasification performed in continuous reactors.

T (ºC)	Air/(N₂)	O₂	H₂O	CO₂	Reactor	X (%)	HHV$_{GAS}$ (MJ/Nm³)	Y$_{GAS}$/(Flow)	Y$_{H2}$	Y$_{CO}$	H₂/CO	H₂ (%)	CO (%)	Refs.
900-1200	-	-	0.25-3 bar	0.25-3 bar	Drop tube furnace	88.2-97.9	-	-	-	-	-	-	-	[98]
1100-1200	100 vol.%	-	-	-	Downdraft	-	6-6.5	(50 Nm³/h)	-	-	-	24.9-26.9	42.6-44.3	[209]
1100-1200	100 vol.%	-	-	-	Downdraft	-	-	-	-	-	-	27	15.3	[210]
1100-1200	-	21-25 vol.%	-	75-79 vol.%	Downdraft	-	-	-	-	-	-	20.6-24.0	18.6-26.9	[210]
890	-	-	-	100 vol.%	Entrained flow	73.5-87.2	-	-	-	-	-	-	-	[211]
779-987	ER=0.25-0.41	-	S/C=0.2-0.7	-	Cyclone furnace	51.9-95.2	2.46-3.36	2.2-3.9 mol/kg	2.0-19.3 mol/kg	-	0.09-0.57	6-12	17-22	[205]
1000	(59 vol.%)	3 vol.%,	30 vol.%,	8 vol.%,	Downdraft tubular fixed bed	>90	3.347	(292.4 g/min)	(3.8 g/min)	(32.9 g/min)	-	15.9	9.8	[212]
979-1235	ER=0.25	-	-	-	Spouted bed	70.4-99.7	3.35–4.25	2.48-3.74 Nm³/kg	-	-	-	10.8-13.5	12.8-19.8	[213]
750-900	-	-	S/C=1-4	-	Fluidized bed	49.3-90.4	-	-	42.1-83.3 mol/kg char	12-17 mol/kg char	3.64-5.57	54.3-56.4	9.7-15.0	[76]
846-873	4.1-6.1 NL/min	-	550 g/h	-	Fluidized bed	-	-	-	-	-	-	-	-	[61]
900	ER=0.3	ER=0.25-0.35	S/C=0-0.75	-	Fluidized bed	49-66.5	2.5-8.3	0.87-2.48 Nm³/kg char; 38.84-110.71 mol/kg char	0.170-0.412 Nm³/kg char; 7.59-18.39 mol/kg char	0.298-0.396 Nm³/kg char; 13.30-17.68 mol/kg char	0.4-1.2	7.2-35.0	12.0-43.2	This work

The gas H_2 yields (0.170-0.412 Nm^3/kg char or 7.59-21.43 mol H_2/kg char) were in the same range of those reported by He et al. [205], but inferior to those reported by Ma et al. [76]. On the other hand the yields of CO in this work (0.298-0.396 Nm^3/kg char or 10.64-14.00 mol CO/kg char) were similar to those reported by Ma et al. [76]. The yield of gas produced by air gasification in this work were also comparable to those achieved by He et al. [205] and by Salam et al. [213]. The charcoal conversions achieved in this work were globally lower than those reported in several works, but on the other hand the heating value of the gas produced by oxygen gasification was higher than those reported in the literature. The reason for that was attributed to the higher reaction temperatures used in the experiments, as well as to different reactor configurations.

5.2. Oxidative steam reforming of glycerol

5.2.1. Catalyst characterization

The Co/Al catalyst prepared for the oxidative steam reforming of glycerin had a surface area of 94 m^2/g, a pore volume of 0.17 cm^3/g and an average pore size of around 10 nm. Figure 15 shows the TPR profile of the Co/Al catalyst.
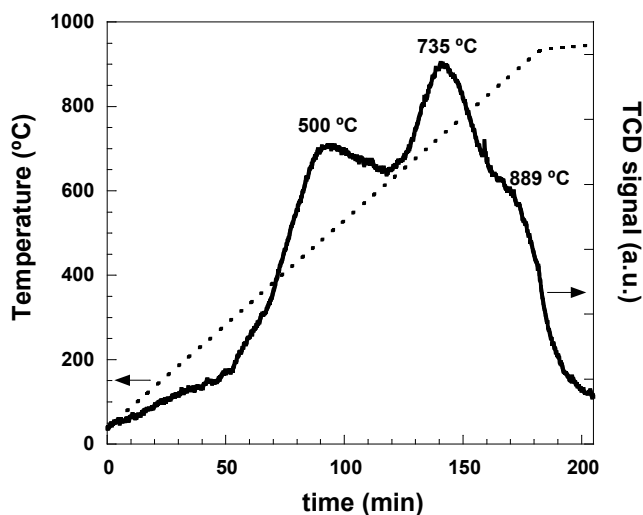
Figure 15 - TPR profile of the Co/Al catalyst.

Three distinct reduction regions can be observed, characterized by two major reduction peaks and a shoulder peak at relatively high temperature. The main peaks had their maxima at 500 ºC and 735 ºC, respectively, whilst the shoulder peak was observed at approximately 889 ºC. These results could be due to the existence of various Co oxide species presenting different degrees of interaction with the support. Anyhow, the relatively high values of the maxima of the different peaks are indicative of a high degree of interaction between the Co and the Al species. The first two peaks (at 500 ºC and 735 ºC) could correspond to the reduction in two stages of large particles constituted by Co_3O_4 crystalline species, which would be in a high degree of interaction with the support [214,215]. The shoulder peak (at 889 ºC) could be attributed to the partial reduction of Co-Al spinel [216]. This would be in agreement with the crystalline phases observed in the XRD (Figure 16), in which the crystalline phases corresponding to Co_3O_4 and Co/Al spinel ($CoAl_2O_4$) could be detected. However, as a consequence of the overlapping in the characteristic peaks of the diffraction patterns of these species [216], it is not possible to elucidate the actual crystalline morphology of this type of solids by XRD. It is most likely

that Co_3O_4 and Co/Al spinel ($CoAl_2O_4$ and/or Co_2AlO_4) coexist in the material.
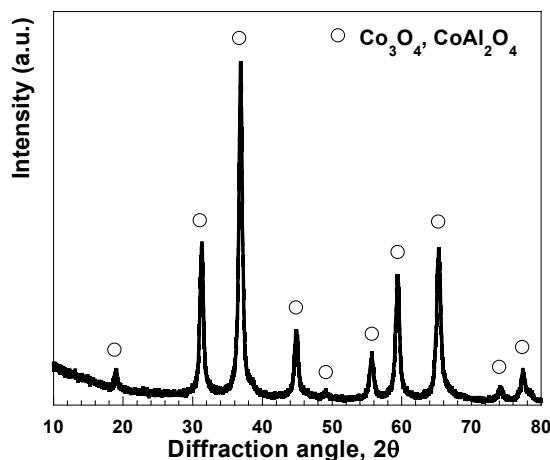
Figure 16 - XRD pattern of the Co/Al catalyst.

Regarding the CO pulse chemisorption analyses, the Co/Al catalyst evidenced a very low degree of Co dispersion (less than 1%), whilst the metallic surface area was equal to 1.3 m^2/g of sample and to 3.0 m^2/g of metal, respectively. These results were somewhat expected, given the usual characteristics and physicochemical properties of this type of bulk catalysts prepared by coprecipitation [188] and the high metal content present in the prepared catalyst.

5.2.2. Oxidative steam reforming of glycerol using different bulk bed filler materials
The results of these experiments are presented in Table 5. The standard deviations were determined from series of three replicate experiments using each material.

The gas production using all three bed materials was consistently steady over 4 h on stream. The highest gas production was observed in the reactions carried out using γ-Al_2O_3, followed by SiC and SiO_2. The carbon conversion to gas was similar in the runs using γ-Al_2O_3 and SiC, both higher than that attained in the SiO_2 runs. The H_2 production was more than two-fold higher in the case of γ-Al_2O_3 than those obtained with the other two bed materials. Conversely, the CO production was much lower using γ-Al_2O_3 when compared with SiO_2 and SiC reaction beds. This could indicate that γ-Al_2O_3 promoted the WGSR more efficiently when compared to the other bed materials. Accordingly, the CO_2 production was more than three-fold higher when using γ-Al_2O_3. Regarding light hydrocarbons, the CH_4 productions were similar in all cases, whilst the productions of

58

C$_2$H$_4$ and C$_2$H$_2$ were lower for γ-Al$_2$O$_3$ in comparison to the other two materials. This could be explained by a higher cracking activity of the alumina bed as compared to the other two bed materials. The higher cracking activity of γ-Al$_2$O$_3$ as compared to SiO$_2$ was expected, in agreement with previous works on charcoal gasification [80,217], as well as on the cracking of tars produced during the co-gasification of sewage sludge and coal [50]. These results corroborate that alumina may be used with good results as bulk material with moderate catalytic activity on the gasification of other biomass materials, including biochar [218]. On the other hand, SiC and SiO$_2$ showed higher dehydration activities since the formation of unsaturated products (C$_2$H$_4$ and C$_2$H$_2$) was somewhat higher over these bed materials.

Table 5 – Results of the runs performed with different bed materials (reaction temperature = 750 ºC, ND = not detected).

Parameter	γ-Al$_2$O$_3$	SiO$_2$	SiC
Total gas production (mg/g feed)	266 ±12	216 ±3	231 ±6
Mass balance closure (wt.%)	98 ±3	95 ±3	98 ±2
Carbon conversion to gas (wt.%)	89 ±4	83.3 ±1	89 ±3
Individual gas productions [a]			
(mg/g glycerol)			
H$_2$	30.6 ±2.2	11.2 ±0.2	12.4 ±0.6
CO	456 ±2	535 ±1	559 ±6
CO$_2$	318 ±10	81 ±6	96 ±10
CH$_4$	60.5 ±5.5	51.9 ±3.5	52.6 ±3.0
C$_2$H$_4$	20.9 ±2.8	37.7 ±2.8	42.2 ±3.9
C$_2$H$_6$	3.3 ±0.6	2.3 ±0.2	3.6 ±0.5
C$_2$H$_2$	ND	1.9 ±0.2	3.8 ±0.9
Gas composition [a]			
(% mol. N$_2$ free)			
H$_2$	35.2 ±0.7	18.0 ±0.2	18.6 ±0.7
CO	37.4 ±0.6	61.0 ±0.5	59.8 ±0.9
CO$_2$	16.7 ±0.5	5.9 ±0.6	6.5 ±0.5
CH$_4$	8.7 ±0.3	10.4 ±0.6	9.8 ±0.4
C$_2$H$_4$	1.7 ±0.2	4.3 ±0.2	4.5 ±0.3
C$_2$H$_6$	0.3 ±0.0	0.2 ±0.2	0.4 ±0.1
C$_2$H$_2$	ND	0.2 ±0.2	0.4 ±0.1

[a] Average values obtained during 4 h of reaction time

5.2.3. Oxidative steam reforming using the Co/Al catalyst dispersed in different bed materials

The overall results from the different runs performed with catalyst dispersed in different reaction bed materials are presented in Table 6 and Figure 17-Figure 19. These results differed notably from those obtained in the experiments carried out using only the filler bed materials (Table 6), demonstrating the positive effect of the Co/Al catalyst on the gasification of glycerin (Figure 17-Figure 19). Globally, the gas productions and carbon conversion to gas were higher when the catalyst was used.

Table 6 – Results of the runs performed with catalyst dispersed in alumina, silica and silicon carbide (activation temperature = 850 ºC, reaction temperature = 750 ºC, ND = not detected, Cat=catalyst).

Parameter	Cat/γ-Al$_2$O$_3$	Cat/SiO$_2$	Cat/SiC
Total gas production (mg/g feed)	315 ±9	333 ±14	288 ±5
Mass balance closure (wt.%)	94 ±2	94 ±2	94 ±1
Carbon conversion to gas (wt.%)	91 ±4	93 ±2	94 ±3
Individual gas productions[a] (mg/g glycerol)			
H$_2$	53.6 ±1.8	63.0 ±7.5	39.4 ±0.4
CO	348 ±35	344 ±62	508 ±20
CO$_2$	586 ±11	655 ±10	339 ±10
CH$_4$	51.0 ±3.9	42.1 ±0.3	50.1 ±3.1
C$_2$H$_4$	6.8 ±2.1	3.8 ±3.2	19.7 ±2.8
C$_2$H$_6$	2.6 ±0.3	2.1 ±0.1	3.7 ±0.5
C$_2$H$_2$	ND	ND	ND
Gas composition[a] (mol.% N$_2$ free)			
H$_2$	47.8 ±1.4	51.1 ±3.1	39.8 ±0.8
CO	22.2 ±1.9	20.2 ±5.0	36.7 ±1.0
CO$_2$	23.8 ±0.9	24.1 ±2.4	15.6 ±0.7
CH$_4$	5.7 ±0.3	4.3 ±0.3	6.3 ±0.3
C$_2$H$_4$	0.4 ±0.1	0.2 ±0.2	1.4 ±0.2
C$_2$H$_6$	0.2 ±0.0	0.1 ±0.0	0.3 ±0.0
C$_2$H$_2$	ND	ND	ND

[a] Average values obtained during 4 h of reaction time
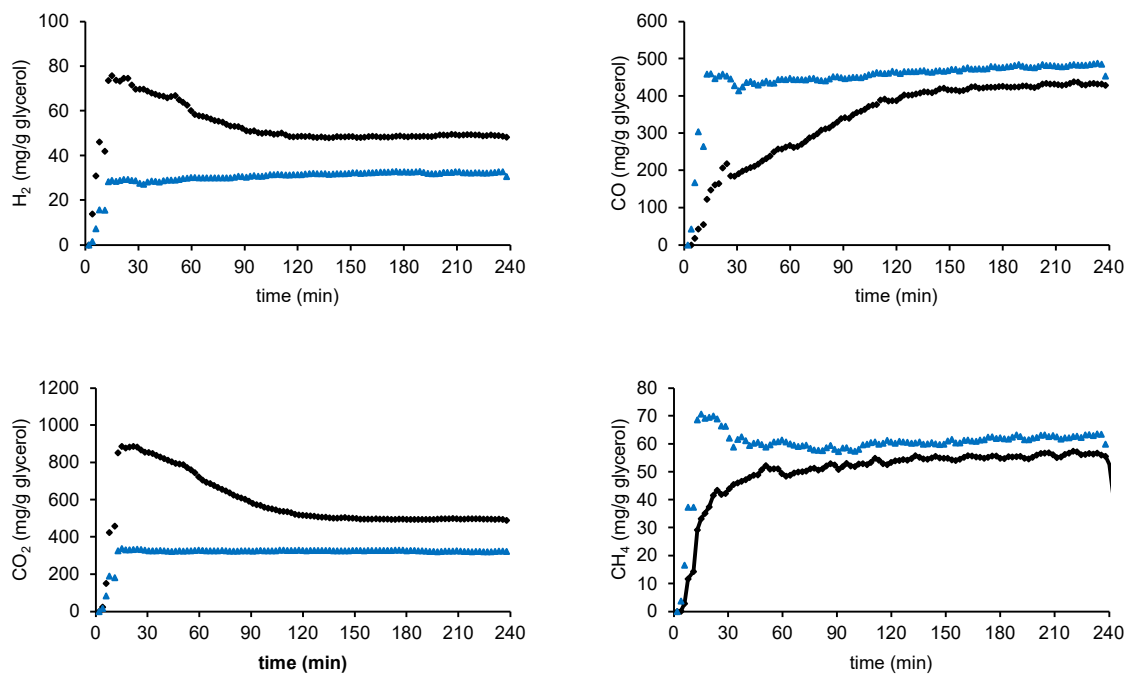
Figure 17 – Comparison of H₂, CO, CO₂ and CH₄ productions obtained between experiments without (blue ▲) and with (black ◆) catalyst using alumina as bed material at 750 ºC.
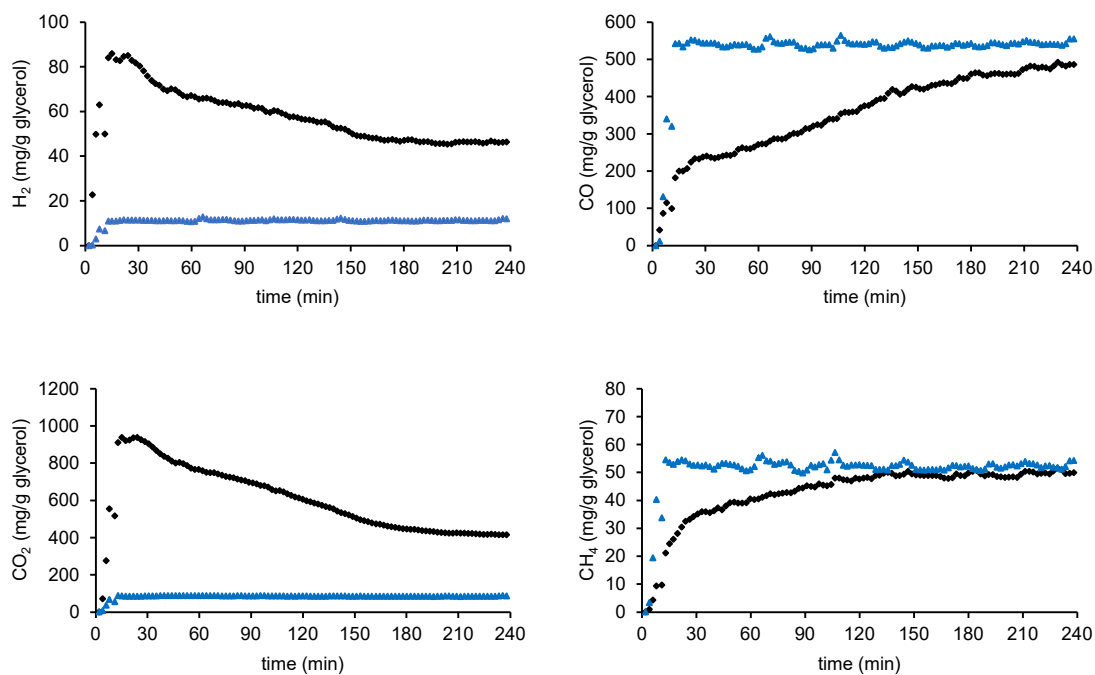
Figure 18 - Comparison of H₂, CO, CO₂ and CH₄ productions obtained between experiments without (blue ▲) and with (black ◆) catalyst using silica as bed material at 750 ºC.
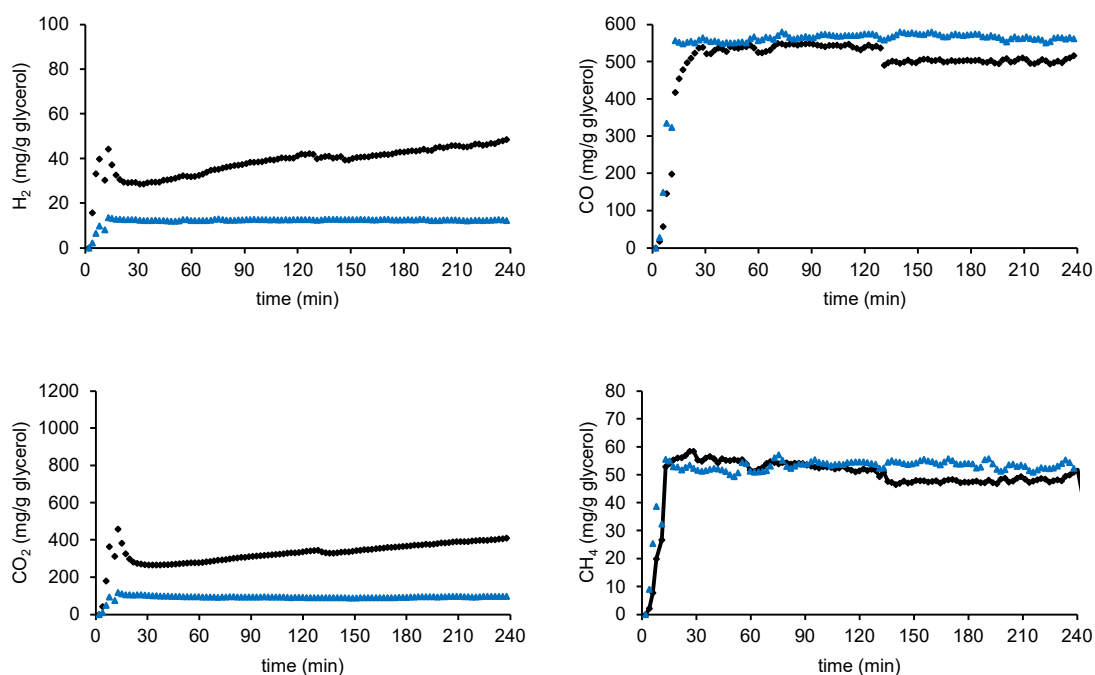
Figure 19 - Comparison of H_2, CO, CO_2 and CH_4 productions obtained between experiments without (blue ▲) and with (black ◆) catalyst using silicon carbide as bed material at 750 ºC.

When alumina was used as bed material (Figure 17, Table 5-Table 6), the increase in H_2 and CO_2 production was ca. 60% higher when the Co/Al catalyst was added. Moreover, CO production was generally much lower in the runs with Co/Al catalyst while in turn the production of CO_2 was much higher. These results could indicate that the higher H_2 production was very likely caused by an increase in activity towards the WGSR exerted by the Co/Al catalyst in contrast to the reforming runs without it. The CH_4 production was slightly lower when the catalyst was used, while the production of C2 hydrocarbons decreased, especially in the case of ethylene, evidencing a higher cracking and subsequent steam reforming activity exhibited by the bed material doped with the Co/Al catalyst in comparison to that of the runs performed without it.

In view of these results and taking into account the remarkable carbon conversion to gas attained using γ-Al_2O_3 alone as bed material, it could be hypothesized that comparable results could be achieved (at 750 ºC and atmospheric pressure) by using a two reactor system, in which the first reaction would occur over an alumina bed followed by a second reactor with a commercial WGSR catalyst bed, in line with similar concept proofs proposed for the steam reforming of other biomass-derived oxygenates [58,219,220].

Such a system would benefit from the fact that γ-Al_2O_3 could be regenerated by oxidation of carbonaceous deposits, while enabling prolonged operation of a commercial WGSR catalyst that can operate without significant deactivation. Furthermore, in the experiments undertaken with pure filler bed materials (*i.e.*, without the Co/Al catalyst), γ-Al_2O_3 kept a steady activity on glycerol conversion to gas over 4-hour experiments.

When silica was used as bed material (Figure 18, Table 5-Table 6), the H_2 production was six-fold higher with the Co/Al catalyst in comparison with the bare SiO_2. The CO production was 56 % higher when the catalyst was added to the bulk material, while the production of CO_2 was eightfold higher, indicating an increase in WGSR activity caused by the catalyst, and in line with the results obtained while using alumina as bed filler.

The productions of H_2 and CO_2 were more than threefold when the catalyst was dispersed in silicon carbide than in their homologous runs without the Co/Al catalyst (Figure 19). Moreover, the profiles of the evolution of both gases along time are very similar, evidencing again the WGSR activity of the Co/Al spinel catalyst used in this work. On the other hand, the productions of CO and CH_4 were similar in both types of experiments (with and without catalyst) using carborundum (SiC).

Comparing the overall results achieved in experiments with the Co/Al catalyst dispersed in all three bulk materials (Table 6), the total gas productions were similar when the catalyst was dispersed in γ-Al_2O_3 and SiO_2, both higher than in the case of SiC. The carbon conversions to gas were similar and independent from the material used as bed filler. Contrary to the results obtained in the runs without catalyst, the mean production of H_2 was higher when SiO_2 was used for dispersing the catalyst, closely followed by the experiments where the Co/Al spinel was diluted in γ-Al_2O_3. On the other hand, the production of CO was much higher when SiC in conjunction with the catalyst, while the CO_2 production observed was the lowest of the three materials. These results could indicate that the Co/Al catalyst activity for WGSR was lower when SiC was used as bed filler as compared to SiO_2 and γ-Al_2O_3. Interestingly, the production of C2 hydrocarbons was higher when the catalyst was combined with SiC, especially in the case of C_2H_4, despite the low productions of this gas in all experiments. This could be related to a potential higher tendency to glycerol thermal cracking and dehydrogenation on SiC as compared to the other bed materials.

From Figure 17-Figure 19, it should be noticed that after 4 h of reaction the productions to H_2 and CO_2 in catalytic runs were always noticeably higher than those achieved over the bare bed materials. Moreover, the productions of CO at the end of the reaction were

lower in the catalytic experiments than those observed in the runs when SiO_2 and γ-Al_2O_3 were used alone, this effect being less evident when the catalyst was dispersed in SiC. These results indicate that after 4 h on stream, the catalyst still presented significant activity for WGSR reaction under the studied conditions. It is also noteworthy the average H_2/CO molar ratios obtained with SiO_2 and γ-Al_2O_3, ranging between 2.0 and 2.5. Such values represent that this syngas could be potentially ideal as raw material in Fischer-Tropsch and methanol-to-hydrocarbon (MTG, MTO, MTE and MTP) processes to produce synthetic fuels and chemicals by Gas-to-Liquid (GTL) technologies [221].

The evolution of H_2, CO, CO_2, and CH_4 productions during the oxidative steam reforming of glycerin with the Co/Al catalyst diluted in all three bed materials is shown in Figure 20.
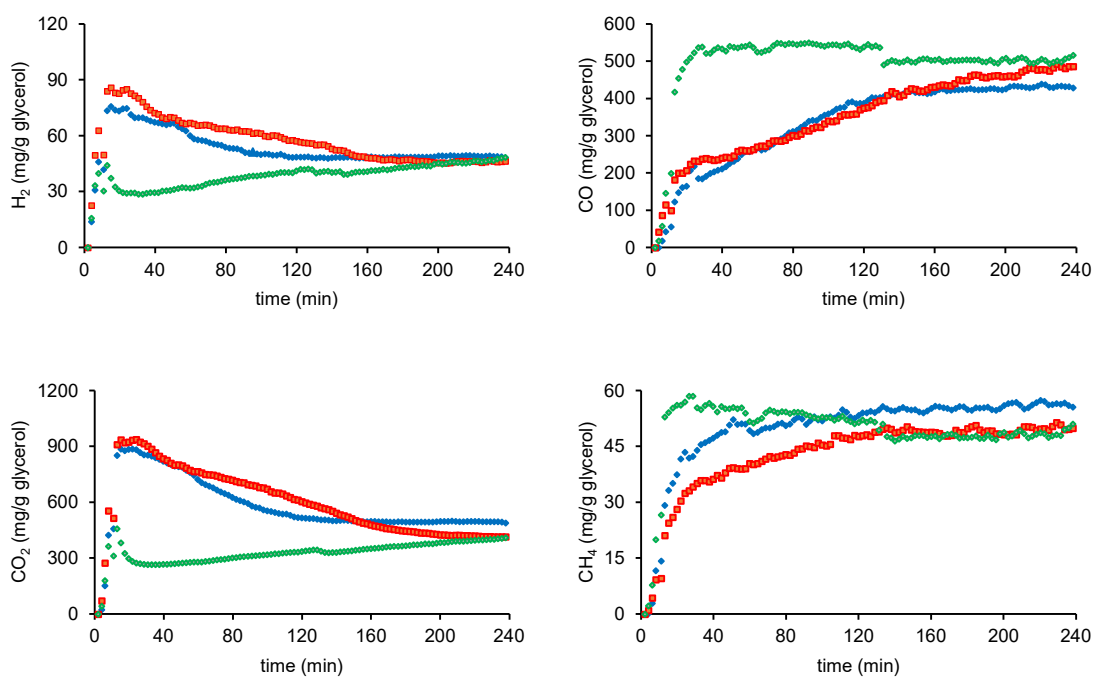
Figure 20 – Evolution of H_2, CO, CO_2 and CH_4 productions over time using the catalyst dispersed in γ-Al_2O_3 (blue ▲), SiO_2 (red ■), SiC (green ◆); (activation temperature = 850 ºC, reaction temperature = 750 ºC).

Generally, the profiles of CO_2 were similar to those of H_2, evidencing their interconnectivity related to the WGSR. In accordance, the production of CO and CH_4 increased along time as the Co/Al spinel catalyst lost its activity. These effects indicated catalyst deactivation caused by the occurrence of carbon deposition of encapsulating

nature on the catalyst surface, in agreement with the STEM images discussed later, as well as with previous studies [222,223]. The production of H_2 gradually decreased over the reaction time when the catalyst was combined with SiO_2 and γ-Al_2O_3. The evolution these profiles were quite similar. The production to CH_4 increased with catalyst deactivation, indicating a decrease in the methane reforming activity (Reaction 7).

$$CH_4 + H_2O \leftrightarrow CO + 3\ H_2\ ,\ \Delta H^{\circ}_{298} = +206\ kJ/mol \qquad\qquad (R.7)$$

The increase in CH_4 production is characteristic of catalyst deactivation by coke deposition, resulting in the production of this hydrocarbon on the deactivated catalyst surface as a consequence of thermal cracking reactions, as previously reported by Bimbela et al. [188] while using similar spinel Ni-based coprecipitated catalysts. Bartholomew [224] described that the encapsulating carbon deposits on the catalyst surface can lead to the formation of CH_4 by the evolution of surface CH_x adsorbed species into coke and ultimately into carbon deposits, but also to an increase of CO in the product gases favored by the reactivity of these carbon deposits via the reverse Boudouard reaction (Reaction 6).

On the other hand, when SiC was used in conjunction with the Co/Al catalyst, the H_2 evolution over time was quite different. In this case, an initial peak of production was observed, followed by a decrease in the H_2 production and a slow recovery up to the initial production peak values. Contrary to the other two materials, the productions of CO and CH_4 decreased with time on stream, likely indicating an increase in the Co/Al catalyst activity towards the WGSR and methane reforming, and probably in connection with the enhanced thermal cracking of glycerol on the SiC particles used as filler, as previously discussed.

From the results above, it was decided that the study of the Co/Al spinel catalyst used in this study should proceed using SiO_2 as filler material. Firstly, because not only this material allowed for higher H_2/CO ratios, but it also allowed for a better distinction between the effect of the catalyst versus the dispersion medium.

5.2.4. Effect of the catalyst activation temperature

To study the effect of the activation temperature on the activity of the Co/Al catalyst, several experiments were conducted under the same operating conditions used in the previous runs (atmospheric pressure, reaction temperature of 750 ºC and reaction time of

4 h). The Co/Al catalyst was diluted in SiO_2 and activated *in situ* prior to the reaction at three different temperatures, namely, 750 ºC, 800 ºC and 750 ºC. The results obtained in those runs are presented in Table 7 and Figure 21.

Table 7 – Effect of the catalyst activation temperature (reaction temperature = 750 ºC, ND = not detected).

Parameter	750 ºC	800 ºC	850 ºC
Total gas production (mg/g feed)	329 ±23	326 ±1	333 ±14
Mass balance closure (wt.%)	95 ±6	94 ±2	94 ±2
Carbon conversion to gas (wt.%)	94 ±1	94 ±2	93 ±2
Individual gas productions [a] (mg/g glycerol)			
H_2	60.6 ±1.1	57.8 ±3.5	63.0 ±7.5
CO	370 ±9	387 ±34	344 ±62
CO_2	613 ±17	590 ±55	655 ±10
CH_4	45.6 ±5.7	45.0 ±4.0	42.1 ±0.4
C_2H_4	5.4 ±3.6	5.1 ±3.9	3.8 ±3.2
C_2H_6	2.5 ±2.2	3.3 ±1.3	2.1 ±0.1
C_2H_2	ND	ND	ND
Gas composition [a] (% mol. N_2 free)			
H_2	49.7 ±4.5	48.8 ±1.5	51.1 ±3.1
CO	22.3 ±7.2	23.4 ±2.5	20.2 ±5.0
CO_2	22.8 ±4.1	22.7 ±1.9	24.1 ±2.4
CH_4	4.8 ±1.0	4.8 ±0.4	4.3 ±0.3
C_2H_4	0.3 ±0.2	0.3 ±0.2	0.2 ±0.2
C_2H_6	0.2 ±0.1	0.2 ±0.7	0.1 ±0.1
C_2H_2	ND	ND	ND

[a] Average values obtained during 4 h of reaction time
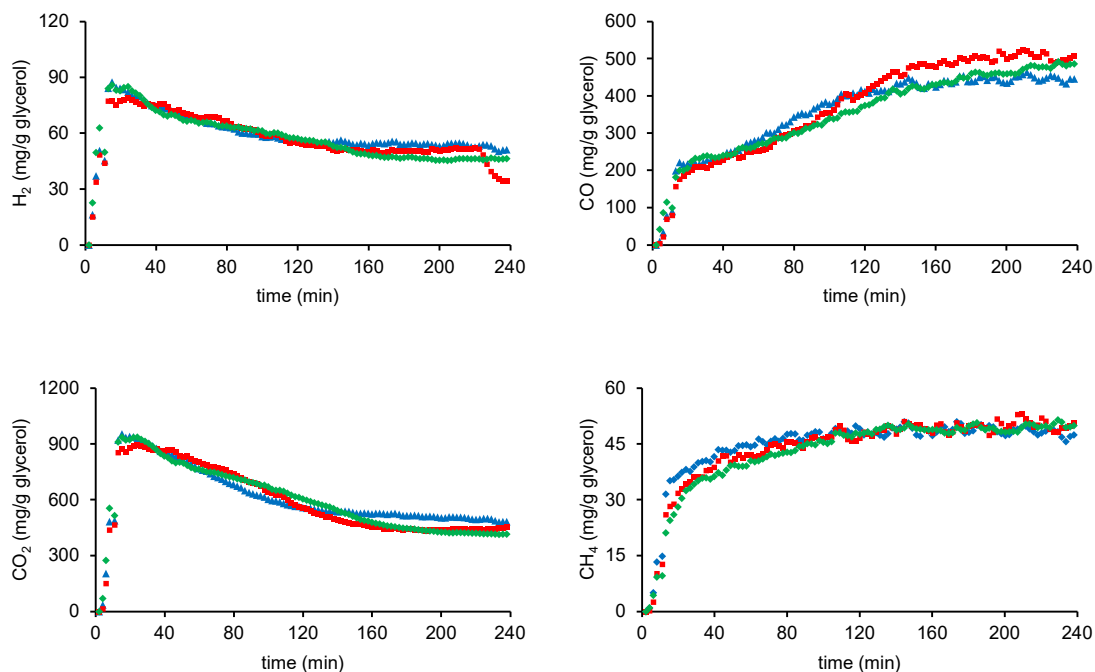
Figure 21 – Evolution of H_2, CO, CO_2 and CH_4 productions over time using the catalyst dispersed in SiO_2. Effect of the catalyst activation temperature: 750 ºC (blue ▲), 800 ºC (red ■) and 850 ºC (green ◆) (reaction temperature =750 ºC).

It could be concluded from Table 7 that the activation temperature had little to no effect on the activity of the catalyst within the tested reduction temperature range. Moreover, the profiles shown in Figure 21 regarding the evolution of H_2, CO, CO_2 and CH_4 productions over time obtained at the three tested temperatures were quite similar and superposed in several points. The differences found in the data obtained at the three reduction temperatures tested fall within the range of the experimental error. Since no significant effects were observed in the range of activation temperatures tested in this work, the following experiments were performed by maintaining the activation at 850 ºC.

5.2.5. Effect of the reaction temperature

To study the effect of the reaction temperature on the performance of the Co/Al spinel catalyst, several experiments were undertaken using the previous mentioned operating conditions (atmospheric pressure, activation temperature of 850 ºC *in situ*, reaction time of 4 h and SiO_2 as bed material). This time, the oxidative reforming of glycerin was undertaken at three different temperatures (550 ºC, 650 ºC and 750 ºC). The results obtained in those runs are presented in Table 8 and Figure 22.

Table 8 – Effect of the reaction temperature (activation temperature = 850 ºC, ND = not detected).

Parameter	550 ºC	650 ºC	750 ºC
Total gas production (mg/g feed)	379 ±10	373 ±26	333 ±14
Mass balance closure (wt.%)	95 ±9	95 ±3	94 ±2
Carbon conversion to gas (wt.%)	88 ±2	91 ±7	93 ±2
Individual gas productions [a] (mg/g glycerol)			
H_2	89.7 ±4.1	82.9 ±1.4	63.0 ±7.5
CO	82.8 ±6	153 ±14	344 ±62
CO_2	1,069 ±24	979 ±62	655 ±10
CH_4	21.0 ±1.2	27.5 ±2.5	42.1 ±0.3
C_2H_4	ND	ND	3.8 ±3.2
C_2H_6	1.4 ±0.2	1.9 ±0.3	2.1 ±0.1
C_2H_2	ND	ND	ND
Gas composition (% mol. N_2 free)			
H_2	61.0 ±0.7	58.5 ±1.3	51.1 ±3.1
CO	4.0 ±0.1	7.7 ±0.7	20.2 ±5.0
CO_2	33.1 ±0.8	31.3 ±1.5	24.1 ±2.4
CH_4	1.8 ±0.0	2.4 ±0.2	4.3 ±0.3
C_2H_4	ND	ND	0.2 ±0.2
C_2H_6	0.1 ±0.0	0.1 ±0.0	0.1 ±0.0
C_2H_2	ND	ND	ND

[a] Average values obtained during 4 h of reaction time

On the one hand, it can be seen in Table 8 that the total gas production decreased when the reaction temperature was increased from 550 ºC up to 750 ºC, which can be a consequence of a faster deactivation of the catalyst at 750 ºC, as discussed later. On the other hand, the carbon conversion to gas showed an increasing tendency with increasing reaction temperatures, though this has to be analyzed cautiously because the analytical uncertainty in these values in Table 8 could lead to the conclusion that the differences found may fall within the range of the experimental error.
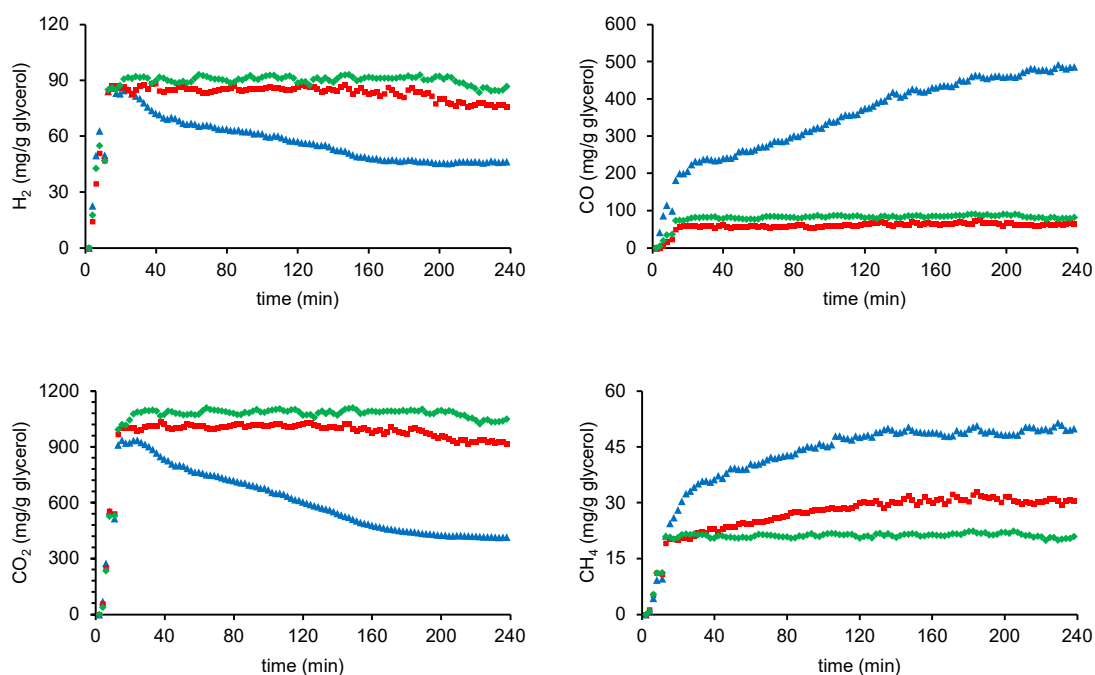
Figure 22 – Evolution of the H_2, CO, CO_2 and CH_4 productions over time. Effect of the reaction temperature: 550 ºC (green ◆), 650 ºC (red ■) and 750 ºC (blue ▲), (activation temperature = 850 ºC).

Anyhow, the H_2 and CO_2 productions dropped when the reaction temperature was increased from 550 ºC up to 750 ºC, while the production of CO steadily doubled with the temperature increase. This tendency could indicate that the WGSR was favored by the lower reaction temperatures, in accordance with thermodynamics principles because the WGSR is an exothermal reaction. The productions of CH_4 and C2 hydrocarbons also dropped with the decrease in the reaction temperature. The decrease in the production of CH_4 as the reaction temperature was lowered indicated that the stability of the catalyst could be maintained more easily at conditions that did not favor catalyst deactivation by carbon deposits, as a result of thermal cracking reactions of the oxygenates [90].

Indeed, in Figure 22 it can be seen that at 750 ºC the productions of H_2 and CO_2 decreased with time, while those of CO and CH_4 increased as a result of the deactivation of the catalyst with the time on stream, possibly due to carbon deposition, as already mentioned. In the case of the reactions undertaken at 650 ºC, the productions to H_2, CO and CO_2 were quite stable most of the time, but the increase in CH_4 with time on stream indicated that deactivation was occurring. Conversely, in the experiments performed at 550 ºC the productions to H_2, CO, CO_2 and CH_4 were stable throughout the experiment duration,

evidencing that the Co/Al catalyst stability could be secured for longer reaction times at these reaction conditions.

5.2.6. Catalyst regeneration and reuse

As previously mentioned, the Co/Al catalyst regeneration and reuse cycles were carried out at 750 ºC following the procedure already detailed in Section 2.3. The results of these experiments are presented in Table 9 and Figure 23.

Table 9 – Study of catalyst regeneration and reuse (activation temperature = 850 ºC, reaction temperature = 750 ºC, ND = not detected).

Parameter	Run1	Run2	Run3	Run4	Run5
Total gas production (mg/g feed)	346	324	335	340	333
Mass balance closure (wt.%)	95.0	98.0	99.8	98.1	98.1
Carbon conversion to gas (wt.%)	93.3	91.2	94.0	92.8	90.4
Individual gas productions [a]					
(mg/g glycerol)					
H_2	67.8	59.0	62.0	65.4	66.9
CO	305	357	365	309	290
CO_2	735	615	640	713	706
CH_4	41.7	42.4	43.4	42.8	44.5
C_2H_4	1.2	2.4	2.6	2.4	1.6
C_2H_6	2.5	2.8	2.5	2.8	2.4
C_2H_2	ND	ND	ND	ND	ND
Gas composition [a]					
(% mol. N_2 free)					
H_2	52.8	50.0	50.4	52.1	53.3
CO	16.9	21.6	21.2	17.6	16.5
CO_2	26.0	23.7	23.7	25.8	25.5
CH_4	4.1	4.5	4.4	4.3	4.4
C_2H_4	0.1	0.2	0.2	0.1	0.1
C_2H_6	0.1	0.2	0.1	0.2	0.1
C_2H_2	ND	ND	ND	ND	ND

[a] Average values obtained during 4 h of reaction time
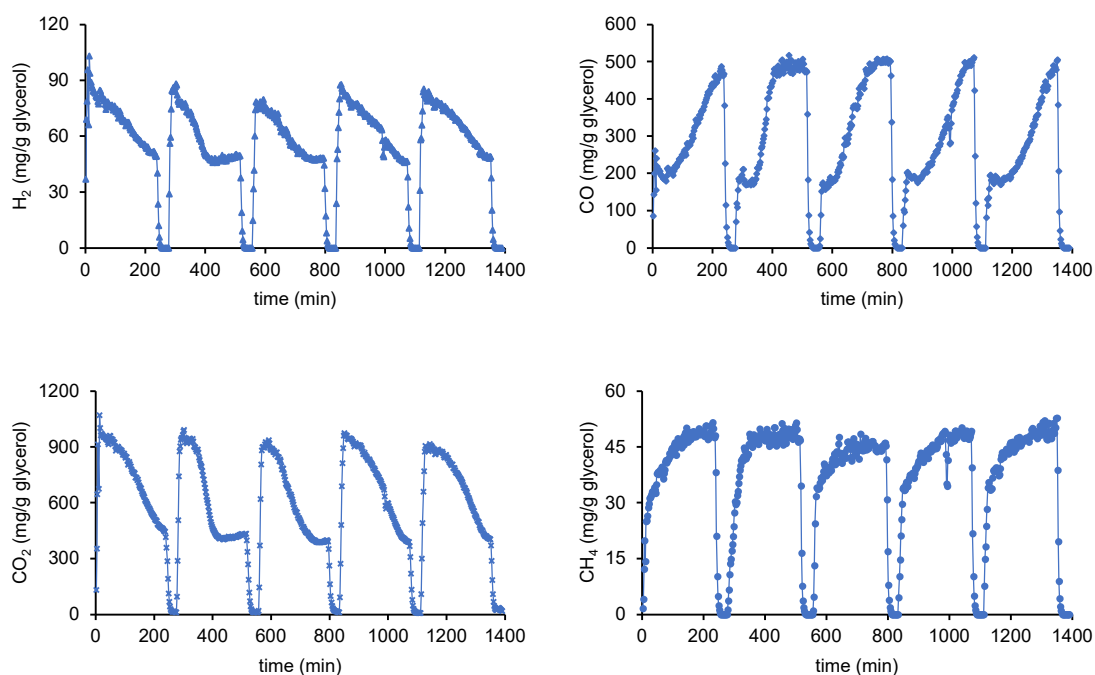
Figure 23 – Evolution of H_2, CO, CO_2 and CH_4 productions over 5 reaction cycles (reaction temperature = 750 ºC, reaction time = 4 h/per each reaction cycle).

Considering the five runs, the mean total gas production was 335 ± 8 mg of producer gas/g of liquid fed, while the carbon conversion to gas was always higher than 90%. The hydrogen production was fairly stable, with a global mean production for runs 1-5 of 64.2 mg H_2/g glycerol, presenting an average variation of roughly 6%. However, the deviations in the productions to CO and CO_2 were slightly higher, showing variations of about 10% and 8%, respectively. In any case, these variations in the productions of H_2, CO and CO_2 indicate slight differences in the catalyst activity in the WGSR, since when the productions of H_2 and CO_2 increased, those of CO decreased accordingly in response. The production of CH_4 was quite stable, presenting a small variation of 2.4%.

In general, the results obtained in the experiments carried out in the study of the catalyst regeneration reuse (Table 9 and Figure 23) were in accordance with those previously observed at 750 ºC (Table 8 and Figure 22) with the Co/Al catalyst dispersed in SiO_2, therefore reinforcing the repeatability and consistency of the results presented in this work.

The data in Table 9 and Figure 23 show that the Co/Al spinel catalyst tested in this study presents great potential to be used in the oxidative steam reforming of glycerin, because not only good conversion and gas productions were attained, but also because the catalyst

could be reused without substantial activity loss after a combined total of 20 h on stream under the most unfavorable conditions (750 ºC).

5.2.7. Study of the Co/Al catalyst by electron microscopy

Figure 24 shows representative electron microscopy images of the fresh catalyst sample subjected to reduction and passivation. The image was taken in STEM mode. Irregular clusters of small (20-40 nm) hexagonal-like particles could be observed. The EDS analysis of the darker regions observed for these particles confirmed the presence of mixed Al and Co oxides, whilst the brighter regions in the STEM images revealed the presence of Co-rich areas at the catalyst surface, though the coexistence of mixed Co and Al oxides could still be detected in those brighter regions.

After its use in a single oxidative steam reforming run at 750 ºC, interesting changes could be observed. Figure 25-Figure 26 show characteristic images of the spent catalyst samples taken both in TEM (light grey background) and STEM (black background) modes, respectively. The presence of carbon deposits of encapsulating nature could be evidenced by TEM. Several layers of graphitic platelets showing characteristic gaps of 0.34 nm between crystallographic graphite planes could be easily observed enclosing the catalyst particles. In many cases, the encapsulating coke covering the catalyst particles had a very clearly defined hexagonal shape conformed over the surface of the catalyst particles. It is worth remarking the utter absence of filamentous carbon in comparison to Ni-based spinel-like steam reforming catalysts [33,188]. But what it is more interesting, after their use in the oxidative steam reforming of glycerol, the catalyst particles evolved into a core-shell like structure in which Co migrated into the core of the particles. This core-shell structure could be verified by physically shifting the position of the sample inside the microscope and taking images at different relative angles.
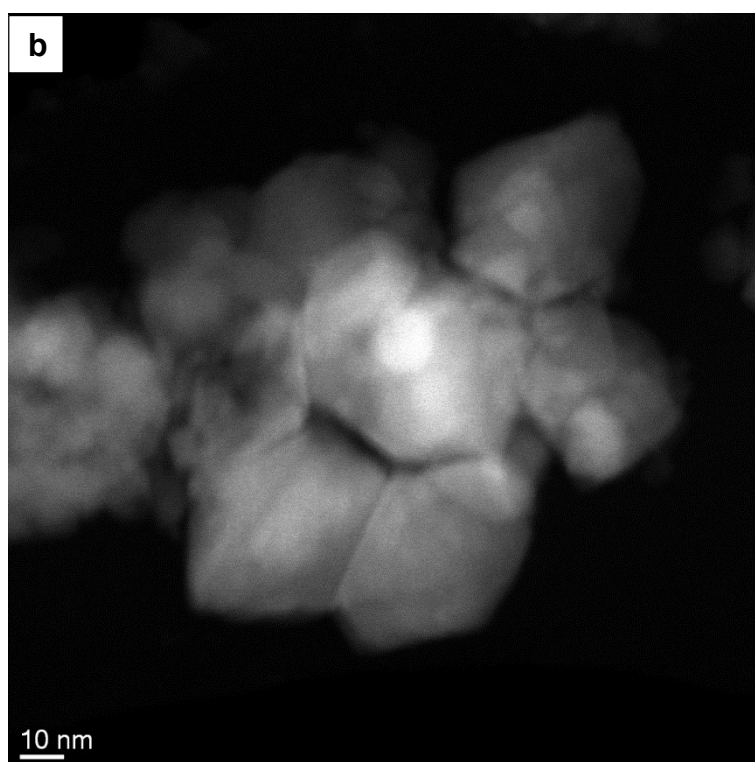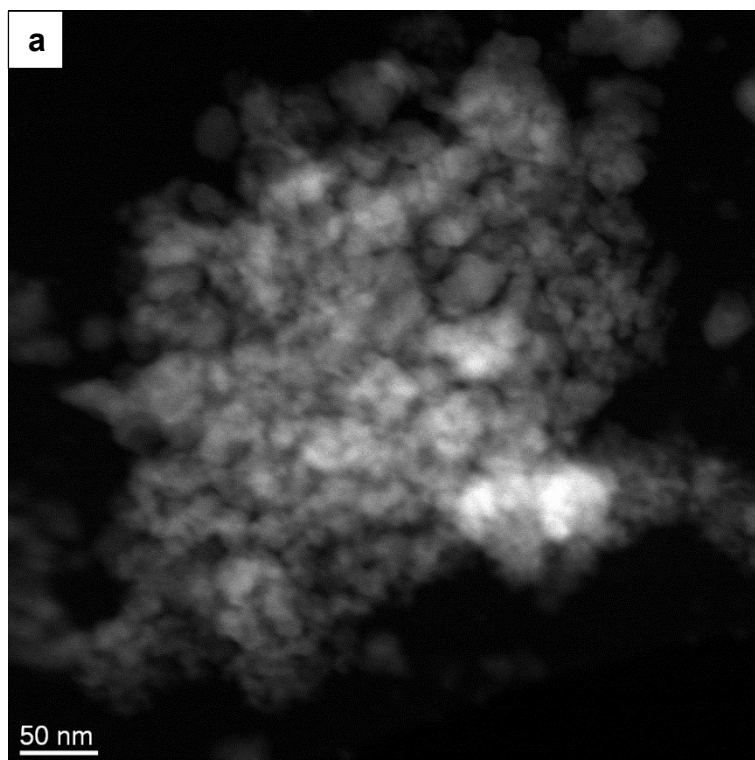
Figure 24 - STEM images of the fresh catalyst sample subjected to reduction and passivation: general view (a) and magnification (b).
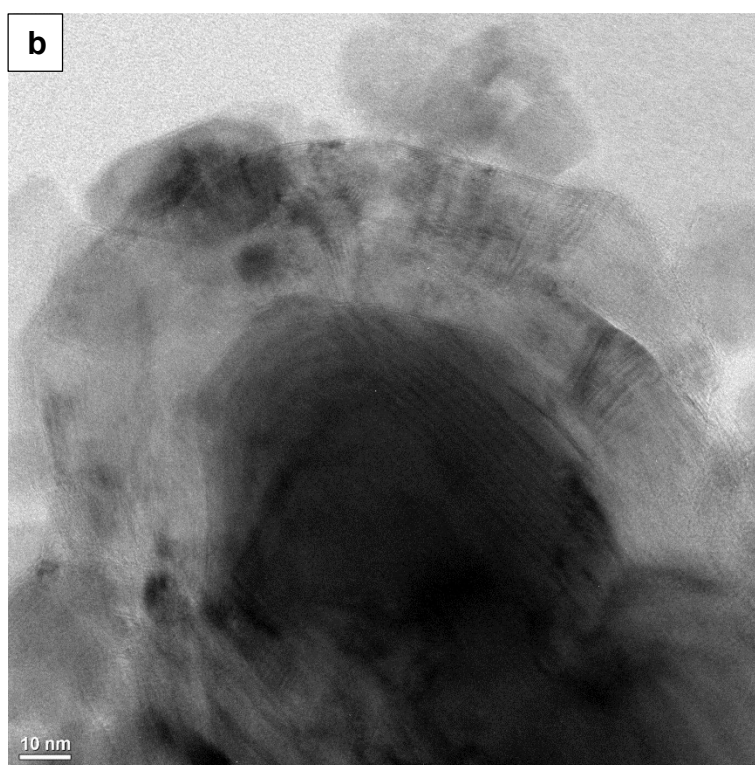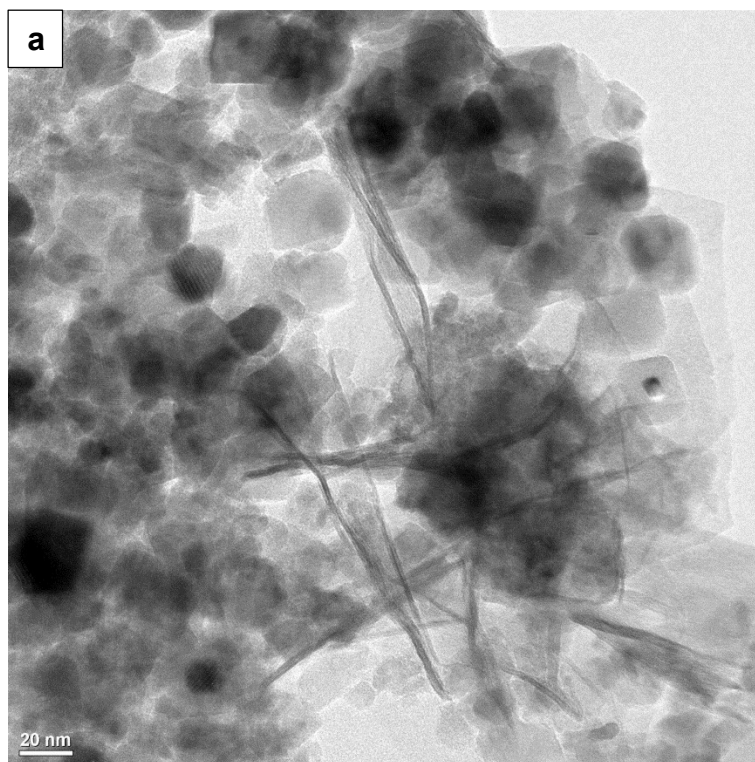
Figure 25 - TEM images of the spent catalyst after reaction: general view (a) and magnification (b).
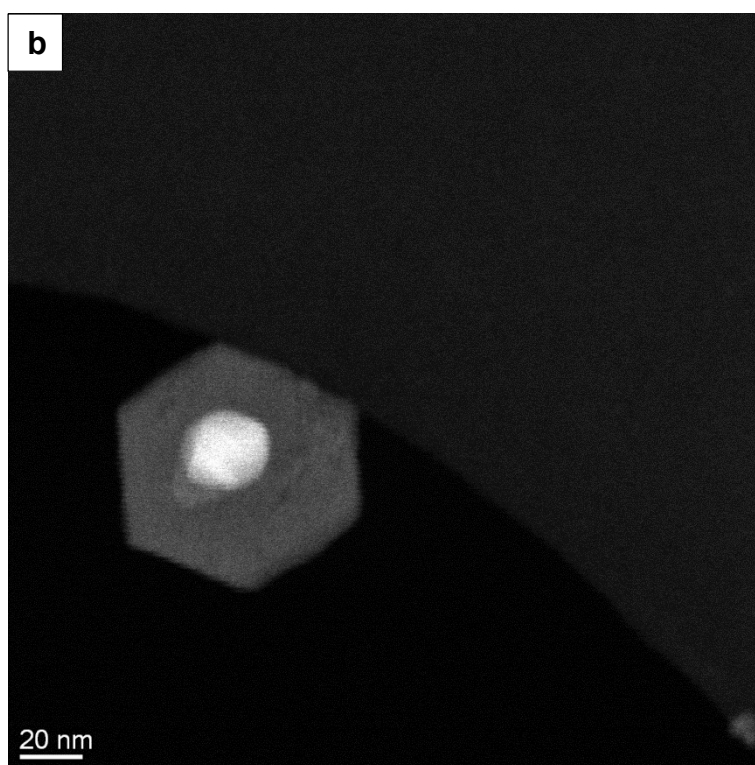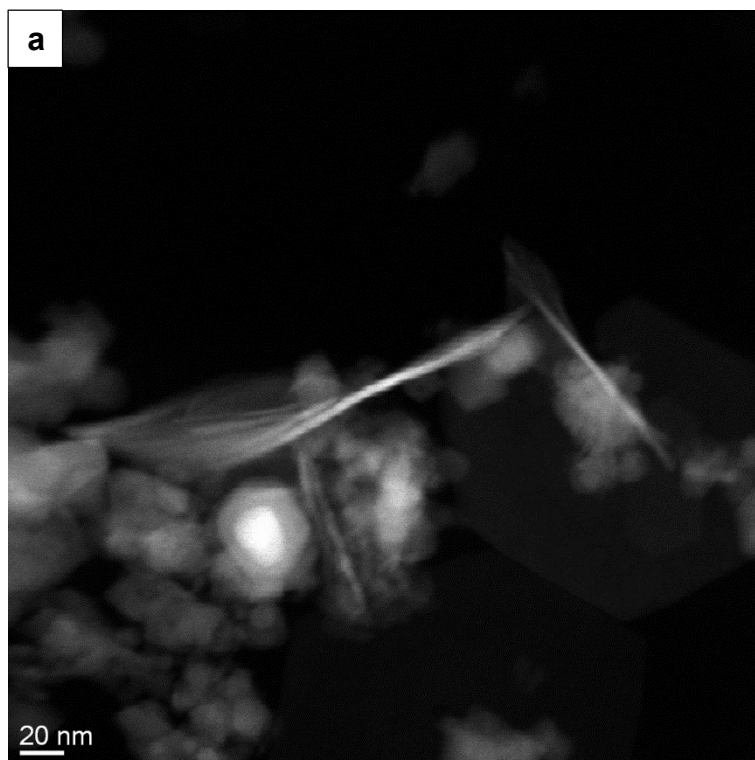
Figure 26 - STEM images of the spent catalyst after reaction: general view (a) and magnification (b).
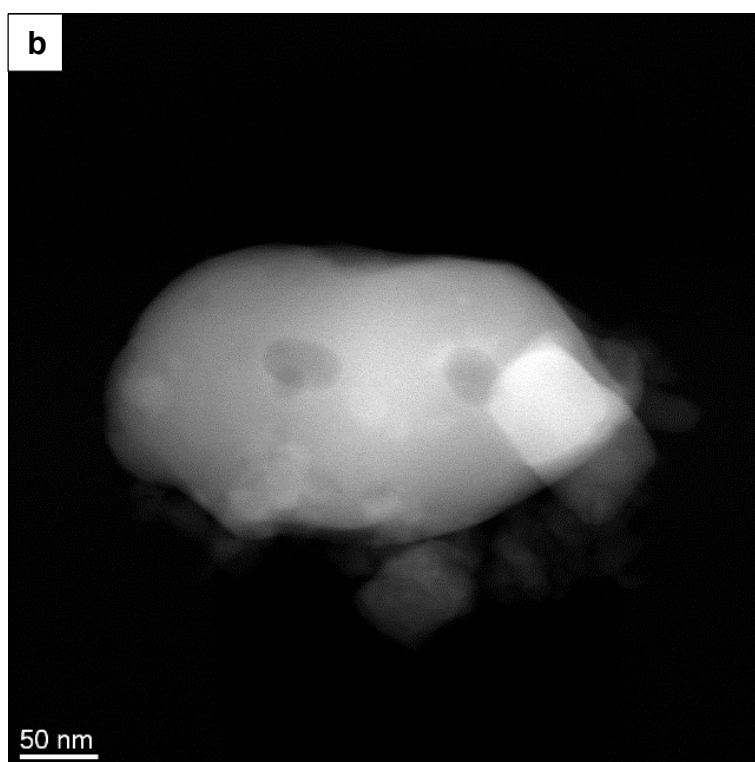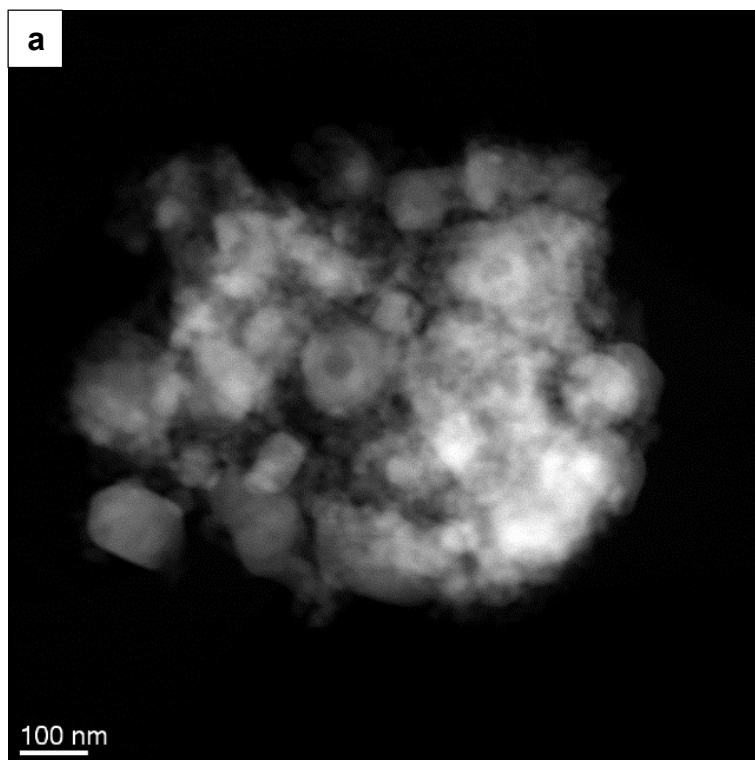
Figure 27 - STEM images of the catalyst sample after 4 cycles of reaction and regeneration: general view (a) and magnification (b).

Finally, the STEM images corresponding to the regenerated catalyst after four reaction/regeneration cycles (five consecutive uses) are shown in Figure 27. The STEM

images were taken after the last regeneration of the sample with 6 vol.% O_2 in N_2. Firstly, it could be observed how the structure of the catalyst drastically changed in relation to the catalyst used after reaction (without regeneration in Figure 26). Very agglomerated particles could be observed of which brighter regions on the surface that could be attributed to Co-rich areas, presumably in the form of Co_3O_4 according to the information provided by the EDS analyses. It can be thus concluded that after the regeneration, the carbon deposits disappeared completely.

In fact, heterogeneous clusters of cobalt-rich oxides having a wide range of sizes (15-350 nm) could be observed in Figure 27, in contrast to what was observed for the non-regenerated catalyst. It could thus be concluded that upon the regeneration of the catalyst by oxidation, Co-rich species migrated from the core of the deactivated particles to the surface and became partially agglomerated. Likewise, darker areas were observed in the core of the particles after the regeneration stage (Figure 27b), that could correspond to cobalt aluminate species. Thus, after reaction and subsequent regeneration in 6 vol.% O_2 in N_2, the core-shell structures were completely transformed. It can be concluded that Co species migrated to the surface over the Co/Al spinel structure, thus acting like a Co reservoir and hence explaining the activity recovery once the catalysts were regenerated and subsequently activated before the next reforming reaction cycle. These results are promising in terms of the applicability of these Co/Al spinel catalysts in further proofs of concept.

5.2.8. Overall considerations

Comparison of results against the literature may present some challenge due to the different ways of reporting data (operational conditions and experimental results). For the sake of completeness, an effort was made in this work to at least undertake global comparisons. For that, the results obtained in this work and those found in literature regarding the oxidative steam reforming of glycerin is presented in Table 10. The conversion presented in this work may seem slightly lower when compared to other works. However, it must be pointed out they are here reported in terms of carbon conversion into to gas, not in terms of glycerol conversion because condensates were not chemically characterized. Anyhow, the results obtained in this work were very promising in terms of H_2 and CO yields, and so in terms of syngas which was the major target of this research.

Table 10 – Summary of the studies in literature on oxidative reforming of glycerol

T (ºC)	O ratio	S ratio	Catalyst	WHSV	GHSV	X_G (%)	H_2 (Y or S)	CO (Y or S)	H_2/CO	H_2 (content)	CO (content)	Ref.
550-850	O/C=0.3	S/C=3	Pd-Cu/K-Al$_2$O$_3$	-	-	-	Y=3-58%	-		50-60%	-	[225]
770-810	O$_2$/C=0.4-0.7	S/C=2.0-2.7	Ni commercial	-	-		Y=1.3-3.5 mol/mol G	Y=0.5-1.2 mol/mol G	-	-		[226]
300-700	O$_2$/C=0.1-0.3	S/C=0.4-1.5	Pt/cordite monolith and Pt-Rh/cordite monolith	-	-	45-98	Y=26-88%	Y=59-70%	0.75-1.9	18-55	22-71	[227]
550-650	O$_2$/G=0.25-0.75	S/G=3-9	Ni/CeO$_2$-ZrO$_2$/Al$_2$O$_3$ and Ni/Al$_2$O$_3$	-	1.6×10^4 h^{-1}	45-99	Y=25.0-80.9%	Y=25.9-49.0%	-	-	-	[223]
500-700	O$_2$/G=0-0.3	S/G=3-9	Ni/CeO$_2$/Al$_2$O$_3$ catalyst and Pd/Ag membrane	5 h^{-1}	-	59.6-99.6	Y=19-85.3	S=23-80	-	-	-	[228]
500-650	O/C=0.2-0.8	S/C=1.6-3.6	Ni/Ce$_{0.5}$Zr$_{0.33}$M$_{0.17}$O$_{2-\delta}$ (M = Mg, Ca or Gd)	-	-	53-95	Y=0.58-1.42 mol/mol G	-	-	-	-	[229]
500-600	C/O=0.75-2.25	S/C=3-6	Ni/Al$_2$O$_3$/FeCrAl plate	2.9×10^5 Nml/g cat.·h	1×10^5 h^{-1}	2-72	Y=0.03-1.09 mol/mol G	Y=0.05-1.67 mol/mol G	-	-	-	[230]
550-700	C/O=0.75-1.125	S/C=3-5	Rh/Al$_2$O$_3$/FeCrAl plate	4.8×10^3 Nml/min·g cat.	-	93-100	Y=0.2-2.2 mol/mol G	Y=1.2-2.1 mol/mol G	0.2-1.5	-	-	[93]
650	O$_2$/G=0.5	S/C=3.7	Ni(12wt.%)-La$_2$(Ce$_{1-x}$Zr$_x$)$_2$O$_7$ (x=0, 0.5, 1)	3 h^{-1}	20 L/g cat·h	>99.7	Y=70-89%	-	-	59.7-60.3	2.8-3.1	[231]
550-750	O/C=0.51	S/C=4	CoAl$_2$O$_4$ disperser in SiC, SiO$_2$ and γ-Al$_2$O$_3$	3.5 g cat. min/g G	1.1×10^5 h^{-1}	83-94%	Y=11-90 mg/g G Y=0.50-4.14 mol/mol G	Y=83-559 mg/g G Y=0.27-1.84 mol/mol G	0.3-2.5	18-61	4-60	This work

5.3. Fractionation of *Pinus pinaster* wood

The cellulose, hemicellulose, lignin and ash contents of the *Pinus pinaster* wood (PPW) used in this study were as follows: 39.6 ±0.1%, 26.3 ±0.1%, 32.4 ±0.4% and 0.8 ±0.0%, respectively. Such distribution of these wood components was within the ranges of those reported by other authors regarding the characterization of PPW [130,132,232–235], *Pinus radiata* [133,236] and *Pinus sylvestris* [134].

5.3.1. Autohydrolysis (AH)

The solid and liquor dry yields of AH experiments are presented in Figure 28 (in kg of each component per 100 kg of dry PPW), while the composition in terms of hemicellulose, cellulose and lignin contents (wt.% of dry product) of AH liquors and AH solids are presented in Figure 29-Figure 30.
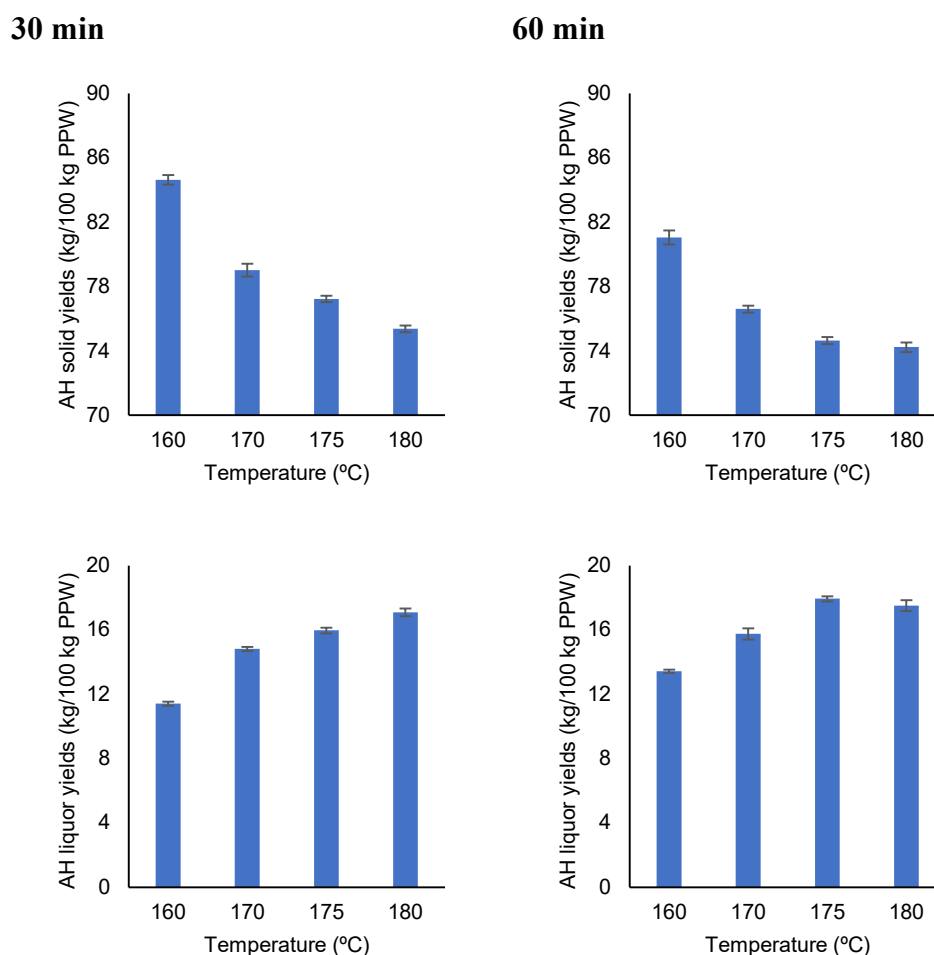
Figure 28 – Yields of autohydrolysis solids (top) and liquors (bottom) upon 30 min (left side) and 60 min (right side) of reaction (dry weights).
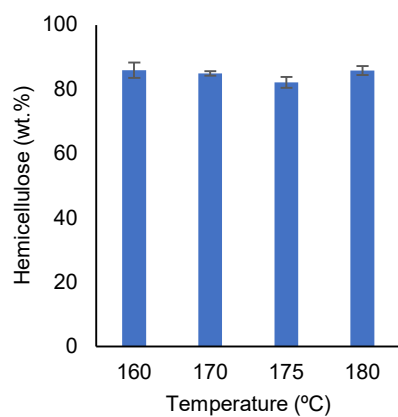
30 min   **60 min**
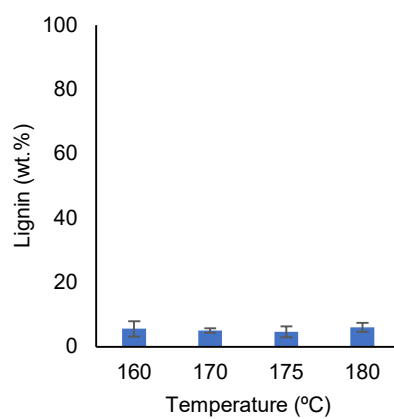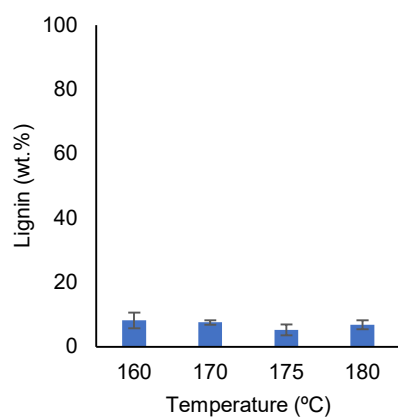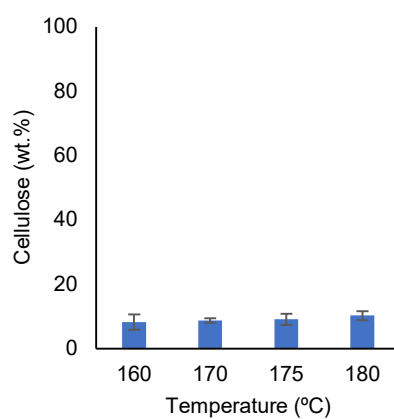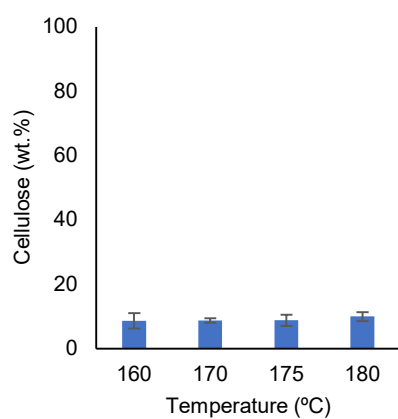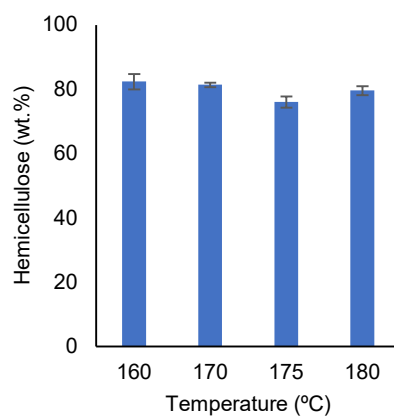
Figure 29 – Composition of AH liquors in terms of hemicellulose, cellulose and lignin contents upon 30 min (left side) and 60 min (right side) of reaction.
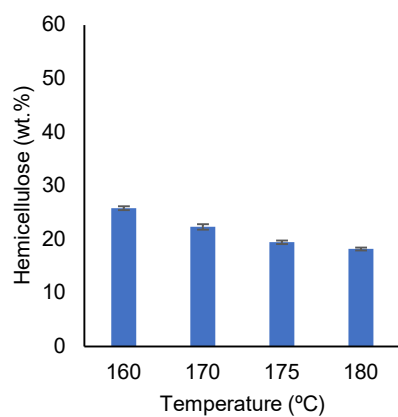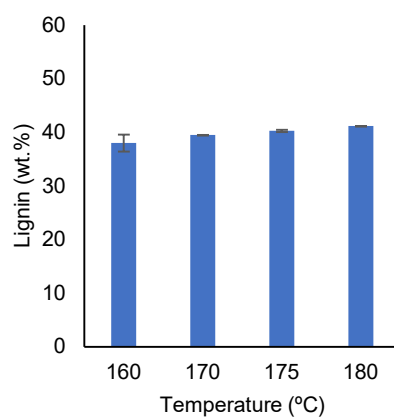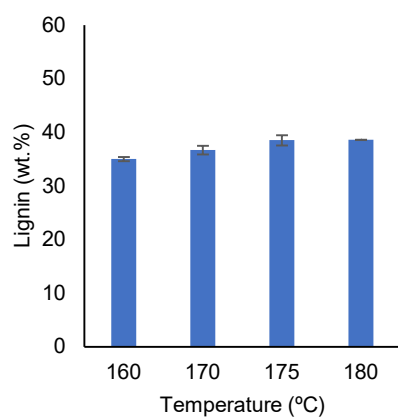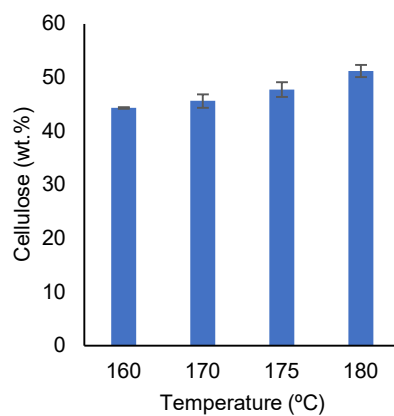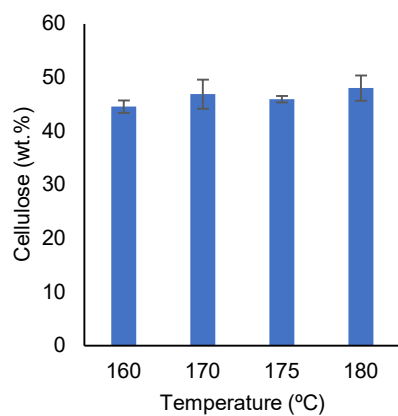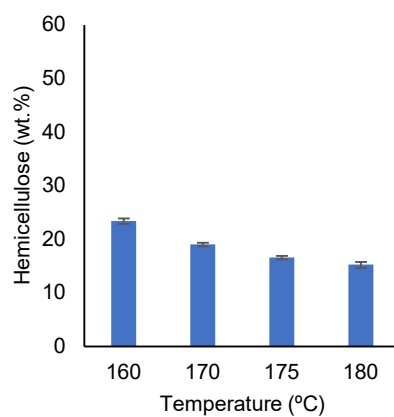
Figure 30 – Composition of AH solids in terms of hemicellulose, cellulose and lignin upon 30 min (left side) and 60 min (right side) of reaction.

As expected, upon AH the solid yields decreased with the increase in reaction temperature, as well as with the reaction time (Figure 28). Accordingly, the amount of solubilized wood components increased, as evidenced by the yield of dry product recovered from AH liquors. Adding the yield of AH solids with the yield of AH liquors, it can be seen that more than 91 wt.% of individual compounds initially present in the parental PPW were identified and quantified in the AH liquors and AH solids by the used analytical techniques. Upon 30 min of reaction 34-60 wt.% of hemicelluloses remained in AH solids, and 24-52 wt.% in 60 min experiments, meaning that the results of hemicellulose removal were in general agreement with those reported in literature regarding AH of pinewoods (Table 11).

Table 11 – Comparison of results of autohydrolysis of pinewoods (Y=yield, H=hemicellulose).

Biomass	T (°C)	tr (min)	Y solid (wt.%)	H Removal (wt.%)	Reference
Pinus radiata	150-190	30-90	64.6-89.9	19-91	[133]
Pinus radiata	150-200	30-60	91.7-66.6	-	[236]
Pinus pinaster	175	26	72.9	-	[132]
Pinewood	180	15	79.8	60	[153]
Pinus pinaster	160-180	30-60	75.4-84.6	34-76	This work

The carbohydrate content of AH liquors (Figure 29) increased with reaction harshness (temperature and time), reflecting the solubilization of non-glucan saccharides (related to hemicellulose content), in agreement with the literature [118,131]. Thus, hemicelluloses were solubilized into the reaction media, leaving a solid mainly constituted by cellulose and lignin (Figure 30) [129]. In fact, between 90-92 wt.% of lignin and 90-95 wt.% of glucose present in PPW remained in AH solids in experiments performed for 30 min, while in experiments performed for 60 min 93-95 wt.% of lignin and 88-96 wt.% of glucose were recovered in the solids. Delignification upon 30 min of AH was in the range of 8-11 wt.%, while in 60 min experiments delignification was in the range of 5-7 wt.%. These results showed that the solubilization of glucan carbohydrates (related to cellulose content) and lignin were both low, as evidenced by the comparable yields of these wood components upon all the tested reaction conditions, in agreement with the literature [118,131]. The apparent lower delignification in experiments performed for 60 min could

be possibly related with some repolymerization of solubilized lignin in acidic reaction medium as the reaction harshness was increased, as previously described by Pielhop e*t al.* [134]. They reported that lignin repolymerization upon AH was more intense in softwoods (such as spruce and pine) than in hardwoods (such as beech and poplar) [134]. Globally, the results evidenced the increase of cellulose content in AH solids with both reaction time and temperature, while hemicellulose carbohydrates decreased, in agreement with the literature [118,129,131]. Besides other possible applications in the production of chemicals included in the C5/C6 platforms [119], the AH liquors seem to have potential for the production of furfural and 5-hydroxymethylfurfural as recently demonstrated by Cornejo *et al.* [237] while using pinewood hydrolysates.

Due to characteristics of the autoclave reactor used in the present study (having an internal coil and a double six-blade propeller), the particle size of the PPW biomass required to operate it had to be small, possibly contributing for higher dilaceration of the material, especially in experiments performed for 60 min. The formation of degradation products increased substantially when AH was performed at 180 ºC and 60 min, indicating that these experimental conditions were too harsh for selective removal of hemicellulose from PPW with such particle size. For such reasons, autohydrolysis temperatures of 175 ºC and 180 ºC for 30 min were selected to precede organosolv delignification in experiments aiming the fractionation of PPW in three sequential steps (AH, SEOS and LP). This way, two different AH solids (AHS) were used, namely, AHS175 produced by AH at 175 ºC for 30 min and AHS180 produced by AH at 180 ºC for 30 min.

5.3.2. Soda ethanol organosolv (SEOS)

Figure 31 shows the yields of pulps on wood dry basis (kg of pulp/100 kg of PPW) produced by SEOS of PPW and autohydrolyzed solids (AH175 and AHS180).

The yields of the pulps obtained by direct SEOS of PPW (two-step procedure, Figure 31a) were much higher than those obtained from autohydrolyzed solids (three-step route, Figure 31 b and c). The lower yields of three-step pulps were expected since the purpose of applying AH to the PPW was to dissolve hemicelluloses in AH liquor, and to obtain pulps having low hemicellulose content upon the pulping of autohydrolyzed solids. The results in Figure 31 show that the increase in ethanol concentration on the cooking solvent did not have a significant advantage in terms of pulp yields.
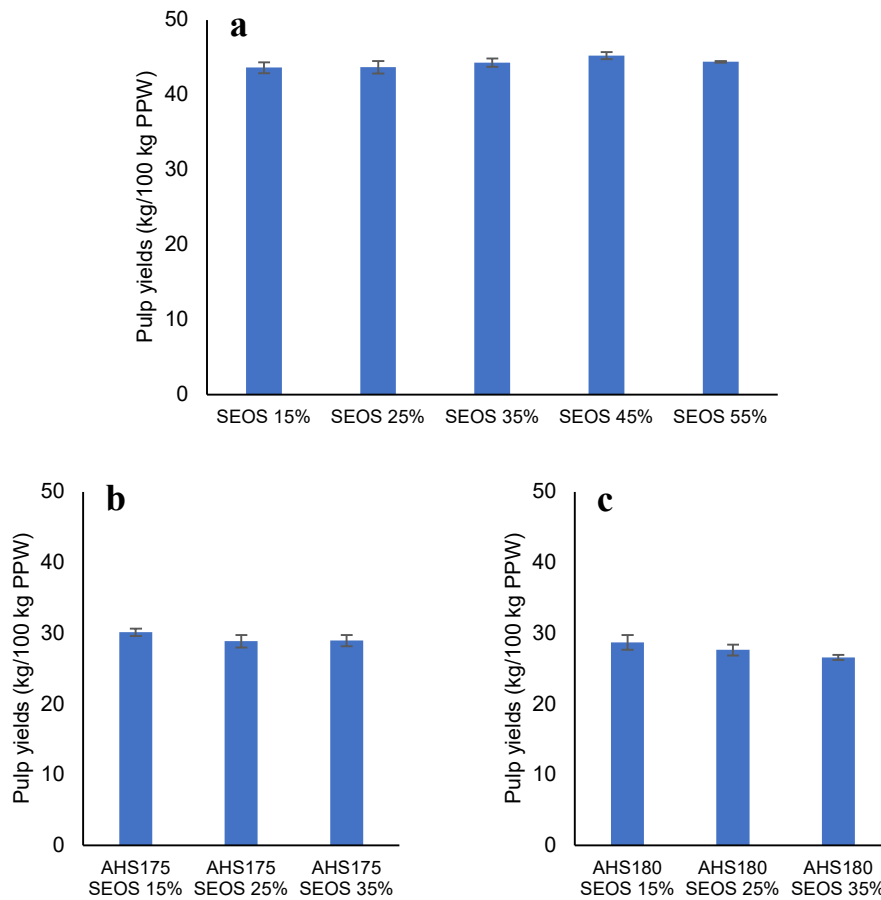
Figure 31 – Pulp yields (in kg of each component per 100 kg of dry PPW) upon SEOS of PPW (a) and AH solids obtained upon autohydrolysis at 175 ºC (b) and 180 ºC (c).

Figure 32-Figure 34 show the cellulose, hemicellulose and lignin contents (in wt.%) of the pulps produced by direct SEOS of PPW, as well as those of pulps produced from autohydrolyzed solids (AHS175 and AHS180).

As expected and desired, the cellulose contents of the pulps were higher when the AH pretreatment was performed at 175 ºC (Figure 32b) as compared to 180 ºC AH pretreatment (Figure 32c). In spite that some trends seem to emerge from Figure 32, when considering the experimental error (presented as standard deviations at the top of each column) the cellulose contents of the pulps seem to be independent from the concentration of ethanol used in the cooking solvent within the same fractionation procedure. Still, the pulps produced from autohydrolyzed solids (AHS175 and AHS180) were much purer, in some cases having cellulose contents over 90 wt.%.
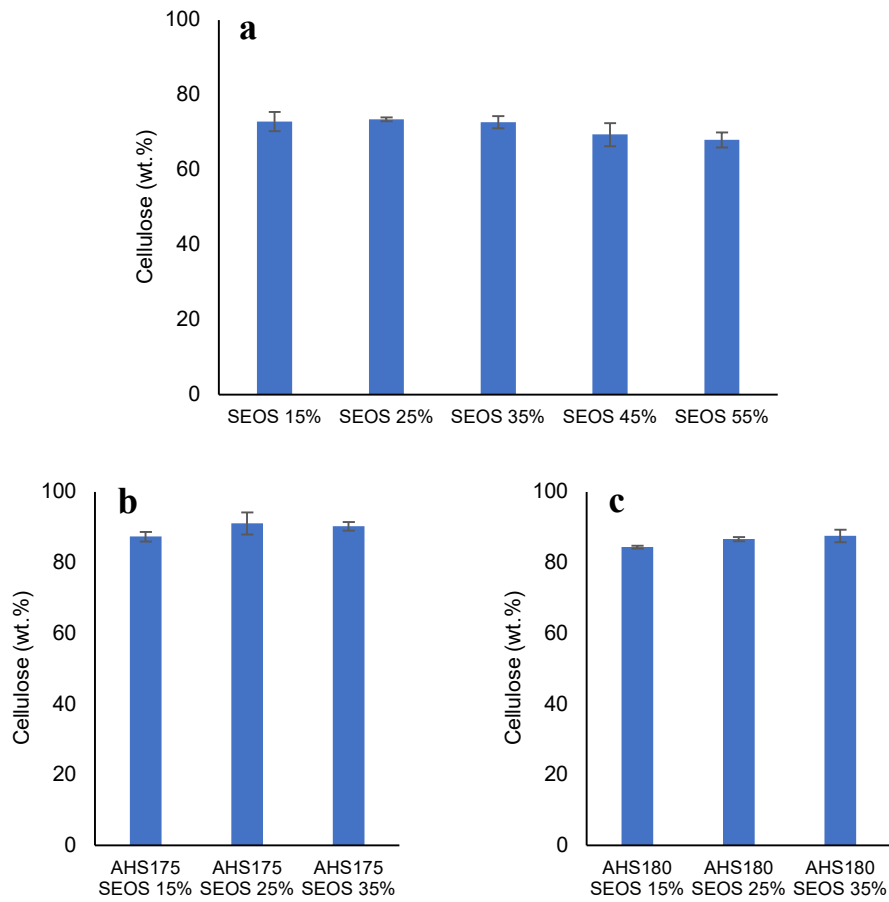
Figure 32 – Cellulose content of pulps upon SEOS of PPW (a) and AH solids obtained upon autohydrolysis at 175 ºC (b) and 180 ºC (c).

As expected, the hemicellulose content of the pulps produced from autohydrolyzed solids (Figure 33 b and c) were much lower than those directly produced from PPW (Figure 33a), especially in the case of pulps produced from AHS180 (Figure 33c).
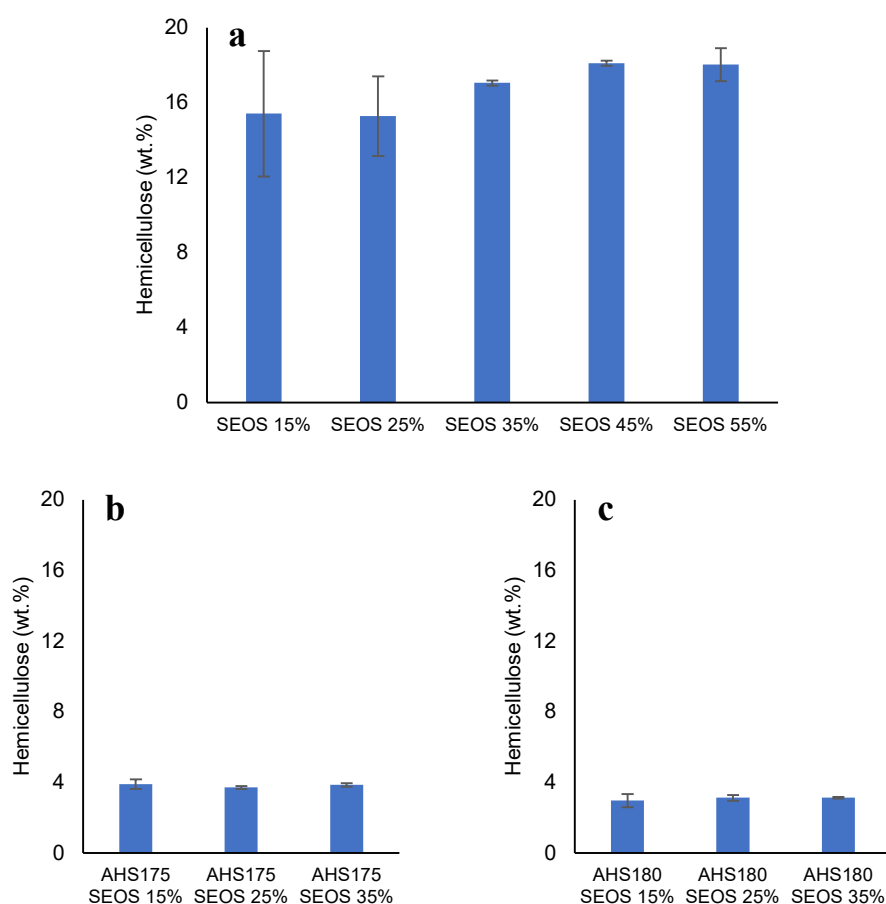
Figure 33 – Hemicellulose content of pulps upon SEOS of PPW (a) and AH solids obtained upon autohydrolysis at 175 ºC (b) and 180 ºC (c).

Upon SEOS, the overall delignification was in the range of 90-91 wt.% in the two-step fractionation, and 93-95 wt.% when SEOS was preceded by AH.

Some variations in lignin contents with the increase in ethanol concentration in the cooking solvent were observed (Figure 34). In pulps produced from autohydrolyzed solids (Figure 34 b and c), there seems to exist a decreasing tendency in pulp lignin contents with the increase in ethanol concentration, especially in the case of pulps obtained from AH solids at 180 ºC. This tendency seems more evident by comparing the lignin contents obtained by using the lowest ethanol concentration (15 wt.%) against those obtained with the highest ethanol concentration (35 wt.%) (Figure 34). In the case of pulps produced by direct SEOS of PPW (Figure 34a), a minimum lignin content seems to emerge at 35 wt.% ethanol concentration (in the cooking liquor). However, such observations should be taken with precaution because such small differences in pulp lignin contents almost disappear when considering the experimental errors.

86
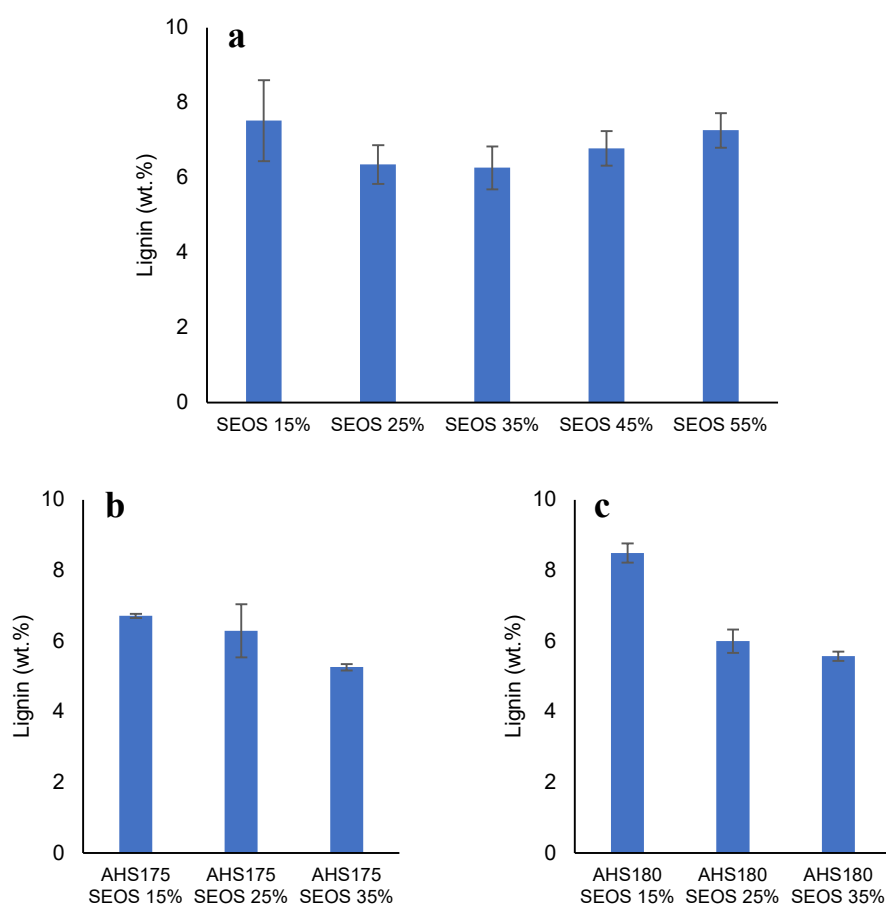
Figure 34 – Lignin content of pulps upon SEOS of PPW (a) and AH solids obtained upon autohydrolysis at 175 ºC (b) and 180 ºC (c).

Globally, the results are consistent with the literature because AH is meant to remove hemicelluloses, while organosolv targets the delignification of lignocellulosic materials [140]. Moreover, these results seem to illustrate the selectivity of the AH and SEOS in the removal of hemicelluloses and lignin (respectively) from lignocellulosic materials.

It should be noted that unbleached softwood Kraft pulps contain an amount of lignin in the range of 3-6 wt.% [238]. Interestingly, the pulps produced by SEOS of autohydrolyzed solids (AH175 and AH180) using an ethanol concentration of 35 wt.% fulfil that requirement. Furthermore, the three-step fractionation procedure may have potential for the manufacturing of dissolving pulps, because the cellulose content of the pulps obtained by this route were higher or close to 90 wt.% before bleaching and simultaneously their hemicellulose contents were low (<4 wt.%) [239,240]. Due to their high purities, the three-step pulps may have other possible added-value applications in the fabrication of C6 platform chemicals [119].

Higher cellulose recovery was achieved upon SEOS of PPW (Figure 35a) than upon SEOS of autohydrolyzed solids. In the last case, the recovery of cellulose was slightly higher when AHS175 (Figure 35b) were used as feedstock when compared to AHS180 (Figure 35c).
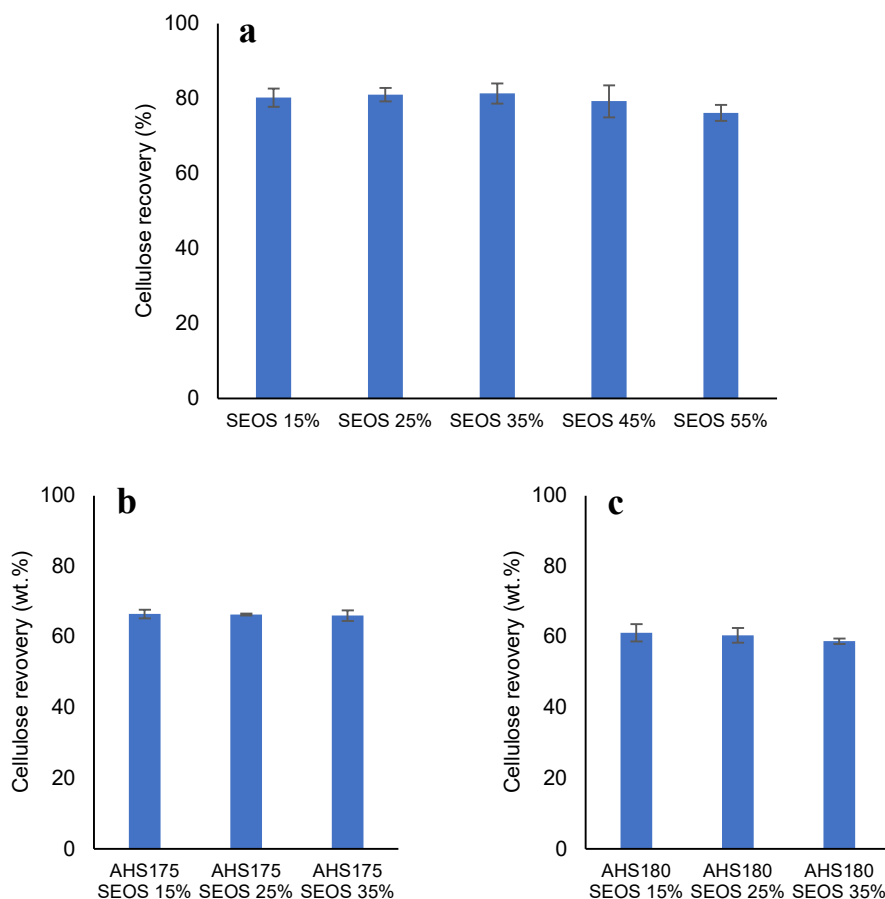
Figure 35 – Cellulose recovery upon SEOS of PPW (a) and AH solids obtained upon autohydrolysis at 175 ºC (b) and 180 ºC (c).

The reason for such differences may have been caused by some degradation and solubilization of cellulose upon two sequential hydrothermal treatments (AH and SEOS), being this effect more evident when higher AH temperature was used. In fact, the differences found in the recovered fractions between non-autohydrolyzed and autohydrolyzed experiments were close to the amount of cellulose removed by AH (9-11 wt.%) considering small allowances for some degradation caused by the consecutive hydrothermal treatments.

The pulp yields achieved in this work by direct SEOS of PPW were close to those reported by Hochegger et al. [241] (47.5-44.5 wt.%) upon acid catalyzed organosolv (at 167-172

ºC) of European larch sawdust (softwood), but their lignin contents (18.2-16.5 wt.%, respectively) were much higher. Similar observations can be made by comparing the two-step pulps obtained in this work with the results achieved by Pan et al. [145] upon acidic organosolv of lodgepole pine (killed by mountain pine beetle). The cellulose recovery (up to 81 wt.%) was also higher in this work upon direct SEOS of PPW as compared to the cellulose recovery achieved by Pan et al. [145] (up to 75 wt.%). Such results seem to show that alkaline organosolv is more effective in the removal of lignin and in the preserving of cellulose, in agreement with the literature [143,144].

Table 12 shows the intrinsic viscosities (η) and kappa numbers (#K) of the pulps obtained by both fractionation procedures, as well as the degree of polymerization and molecular mass.

Table 12 – Viscosities (η), degree of polymerization (DP), molecular mass (M_w) and Kappa number (#K) of produced pulps.

Sample	η (mL/g)	DP [a]	M_w [b] (g/mol)	#K
SEOS 15%	491±15	1,705	276,220	35.4 ±0.5
SEOS 25%	450 ±12	1,548	250,710	30.2 ±0.3
SEOS 35%	398 ±18	1,350	218,740	30.6 ±0.2
SEOS 45%	334 ±6	1,111	180,020	33.9 ±0.4
SEOS 55%	250 ±12	805	130,480	39.6 ±2.1
AH175 SEOS 15%	385 ±6	1,301	210,810	37.3 ±1.7
AH175 SEOS 25%	355 ±6	1,189	192,640	25.9 ±0.5
AH175 SEOS 35%	318 ±5	1,052	170,470	22.2 ±0.8
AH180 SEOS 15%	340 ±25	1,133	183,620	42.3 ±2.2
AH180 SEOS 25%	315 ±14	1,041	168,680	30.0 ±1.1
AH180 SEOS 35%	272 ±6	885	143,300	25.7 ±0.9

[a] $DP = (1.65 \times \eta)^{(1/0.9)}$; [b] $M_w = 162 \times DP$

Pulp viscosity is an important predictor of cellulose polymerization caused by different pulping methods, as well as of fiber mechanical resistance [240,242]. The viscosities of the pulps decreased as the ethanol concentration in the cooking solvent was increased, independently of the fractionation system used (two-step or three-step). Consequently, the degree of polymerization and molecular mass decreased in the same direction. Differently from this work, Akgul and Tozluogu [147] observed that viscosities of pulps prepared by SEOS of cotton stalks increased (from 881 to 948 mL/g) when ethanol concentration was increased (from 20 to 50 wt.%, respectively). The pulp viscosities in

this work were much lower than those presented by Akgul and Tozluogu [147], most likely due to differences in raw materials and SEOS operating conditions (such as catalyst load, reaction time and temperature). Nevertheless, pulps produced by the three-step route presented lower viscosities than those obtained by the two-step system, in agreement with the literature [131].

The degree of polymerization (DP) and molecular mass (M_w) of cellulose were calculated from pulp intrinsic viscosity. The values presented in Table 12 indicate that the size of cellulose molecules decreased with the increase of ethanol concentration in the cooking solvent. This might have been caused by alkaline hydrolysis of glycosidic bonds resulting in cellulose depolymerization [242]. It should be mentioned that the presence of lignin in the samples may affect the viscosity measurement and thus the DP values [243]. As earlier mentioned, the autoclave reactor used in this work has an internal coil and a six-blade propeller, which impeded the use of wood chips of sizes identical to those used in the pulp and paper industry. However, the use of bigger wood particles (for example in a basket reactor) may allow to produce pulps having longer fibers and having characteristics compatible with other value-added applications, which is a possible research line that could be addressed in future works.

The kappa numbers of the pulps produced directly from PPW decreased when the ethanol concentration in the direct SEOS solvent was increased from 15 wt.% to 25 wt.% and increased when the ethanol concentration was increased above 35 wt.% (Table 12). In the case of pretreated substrates (AHS175 and AHS180), kappa numbers decreased consistently with the increase in ethanol concentration. The pulps produced from AHS175 had lower kappa numbers than the pulps produced from AHS180. These results (Table 12) are generally consistent with the literature on SEOS, because pulps with lower residual lignin had lower kappa numbers [135,147].

5.3.3. Lignin precipitation (LP)

As above mentioned, the cooking liquors originated from SEOS were acidified (to pH=5) with sulfuric acid to recover the dissolved lignin. Figure 36 shows the precipitate yields obtained from both two-step (direct SEOS of PPW) and three-step (SEOS of AH solids) fractionation procedures.
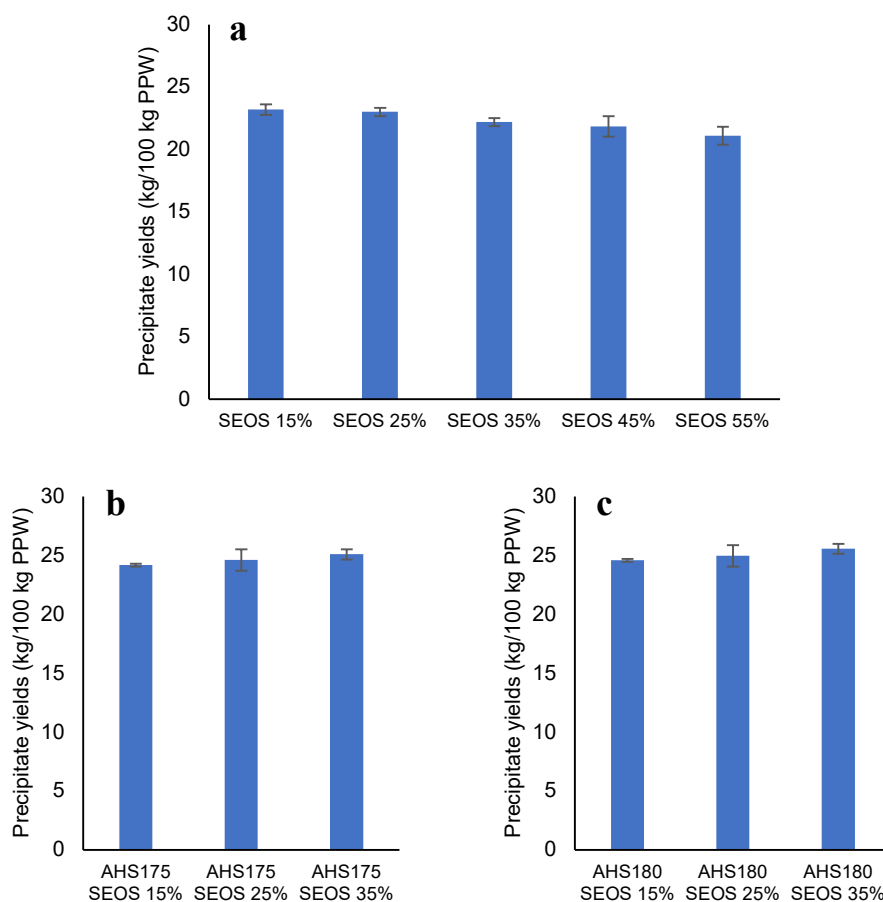
Figure 36 – Precipitate yields (in kg of each component per 100 kg of dry PPW) upon acid precipitation of liquors from SEOS of PPW (a) and AH solids obtained upon autohydrolysis at 175 ºC (b) and 180 ºC (c).

The precipitate yields achieved by the three-step procedure were higher than those obtained by the two-step fractionation. When the two-step procedure was used to fractionate the PPW, the precipitate yields showed a slight decreasing tendency with the increase in ethanol concentration in the cooking solvent (Figure 36a). Contrarily, the precipitate yields showed slight increasing tendencies with the increase in ethanol concentration in the cooking solvent when the three-step route was used (Figure 36 b and c). However consistent, these tendencies should be interpreted with caution because the small differences in yields within the same fractionation procedure (two-step or three-step) were close to the experimental error.

The precipitates obtained from direct SEOS of PPW had small contaminations of cellulose (<1 wt.%) and hemicellulose (2-4 wt.%), with lignin purities varying in the range of 91-94 wt.% (Figure 37).
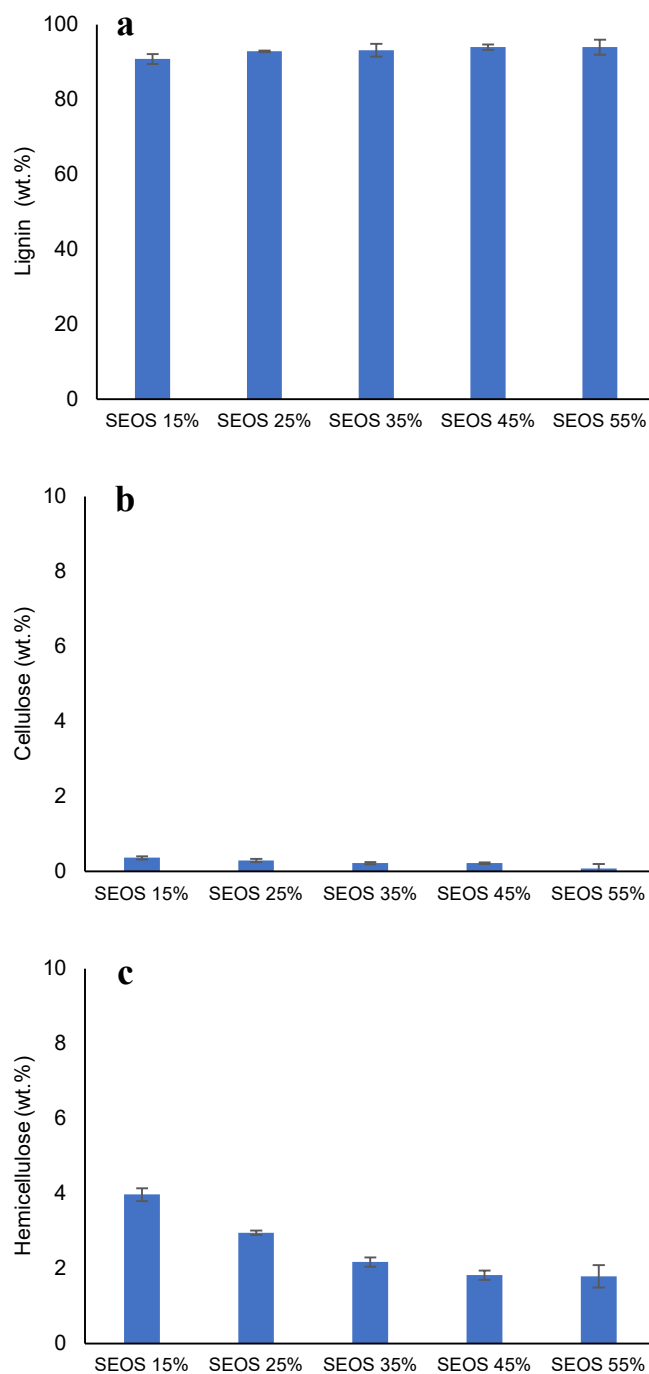
Figure 37 – Lignin (a), cellulose (b) and hemicellulose (c) contents of precipitates produced by SEOS of PPW).

On the other hand, no cellulose or hemicellulose contamination was detected in the precipitates obtained from AHS175 and AHS180, meaning that the purities of the lignins derived from autohydrolyzed solids were generally higher (>97 wt.%) (Figure 38), having ash as the sole contamination source.
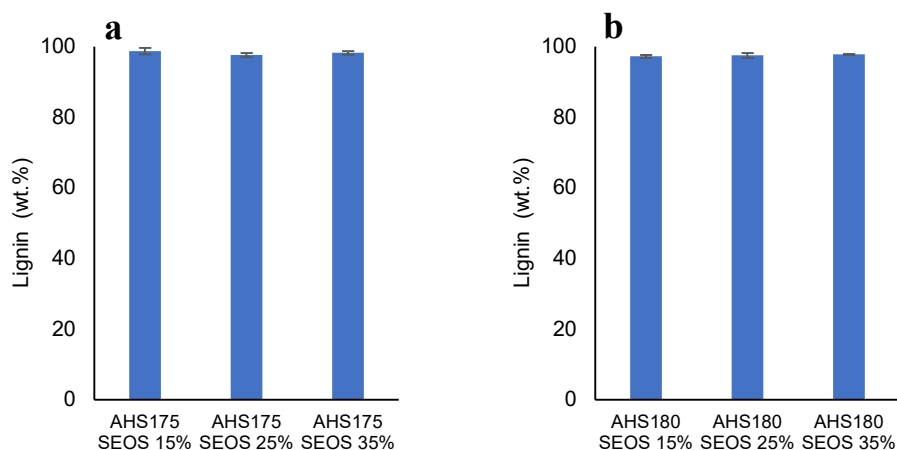
Figure 38 – Lignin contents of precipitates produced by SEOS of AHS175 (a) and AHS180 (b).
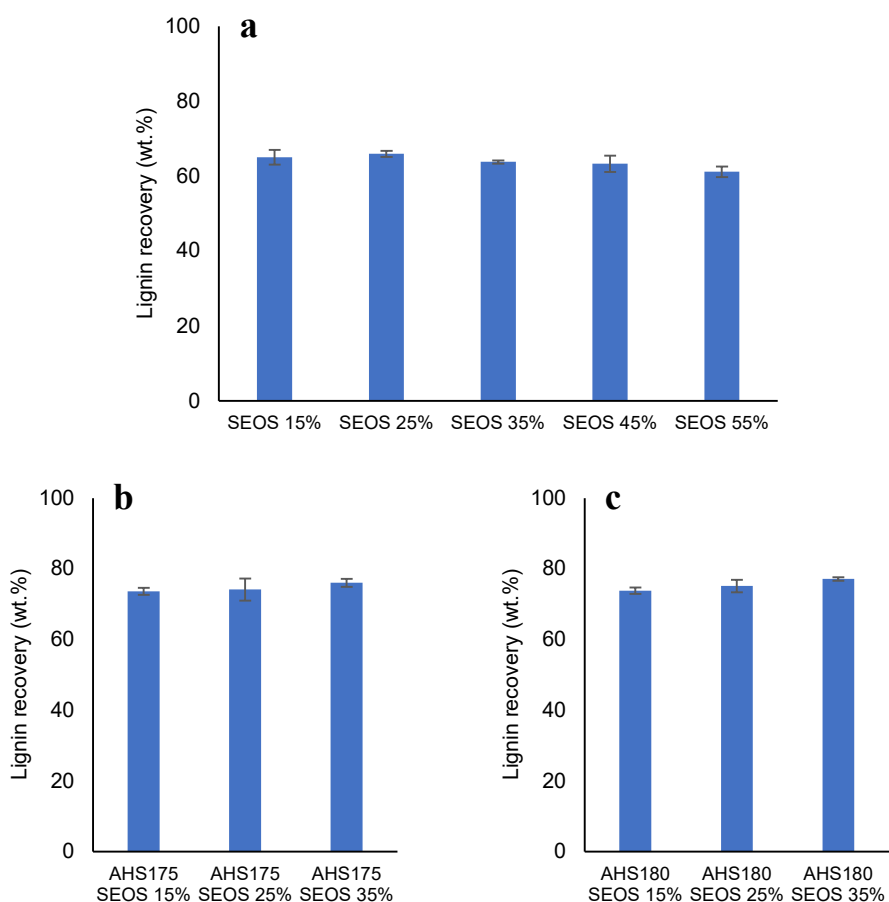
Figure 39 – Lignin recovery upon SEOS of PPW (a) and AH solids obtained upon autohydrolysis at 175 ºC (b) and 180 ºC (c).

The lignin recoveries (Figure 39) achieved by the three-step procedure were much higher than those obtained by the two-step system, with no major differences between the

precipitates derived from AHS175 and AHS180. However, no clear improvements were observed from the increasing o ethanol concentration in the cooking solvent.

Table 13 shows the elemental composition of all the precipitates, as well as the corresponding calculated higher heating value.

Table 13 – Elemental composition and higher heating value (HHV) of precipitates (in ash free dry basis).

Sample	Elemental analysis (wt.%)					HHV
	Carbon	Hydrogen	Oxygen	Nitrogen	Sulfur	(MJ/kg)
Pine wood	47.7 ±0.3	6.3 ±0.1	45.6 ±0.3	0.4 ±0.0	0.0 ±0.0	19.6 ±0.1
SEOS 15%	63.1 ±0.2	6.4 ±0.0	30.1 ±0.2	0.4 ±0.0	0.0 ±0.0	26.5 ±0.1
SEOS 25%	64.0 ±0.1	6.5 ±0.0	29.1 ±0.0	0.4 ±0.1	0.0 ±0.0	27.0 ±0.0
SEOS 35%	64.4 ±0.1	6.5 ±0.1	28.8 ±0.1	0.5 ±0.0	0.0 ±0.0	27.1 ±0.0
SEOS 45%	64.9 ±0.2	6.6 ±0.0	28.1 ±0.2	0.4 ±0.0	0.0 ±0.0	27.5 ±0.1
SEOS 55%	64.6 ±0.2	6.6 ±0.0	28.4 ±0.2	0.4 ±0.0	0.0 ±0.0	27.4 ±0.1
AH175 SEOS 15%	66.1 ±0.2	6.3 ±0.1	27.1 ±0.1	0.5 ±0.0	0.0 ±0.0	27.7 ±0.0
AH175 SEOS 25%	65.6 ±0.1	6.3 ±0.2	27.6 ±0.1	0.5 ±0.0	0.0 ±0.0	27.4 ±0.2
AH175 SEOS 35%	66.1 ±0.1	6.4 ±0.2	27.1 ±0.1	0.5 ±0.0	0.0 ±0.0	27.8 ±0.2
AH180 SEOS 15%	65.9 ±0.1	6.4 ±0.1	27.4 ±0.2	0.3 ±0.0	0.0 ±0.0	27.7 ±0.1
AH180 SEOS 25%	65.8 ±0.2	6.5 ±0.1	27.5 ±0.1	0.3 ±0.0	0.0 ±0.0	27.8 ±0.1
AH180 SEOS 35%	67.0 ±0.3	6.5 ±0.0	26.1 ±0.3	0.4 ±0.0	0.0 ±0.0	29.3 ±0.2

The heating values of the precipitates obtained by the two-step process showed a slight increasing tendency when the ethanol concentration in the organosolv solvent was increased, mostly caused by the increase in carbon contents and the decrease in the oxygen contents of the precipitates. However, the HHV of three-step precipitates were almost identical, no matter the AH reaction temperature or the SEOS ethanol concentration. An exception to this behavior was observed only in the precipitates obtained from AHS180 using an ethanol concentration of 35 wt.% in SEOS, attributed to a slightly higher carbon contents, as well as to the lower oxygen content. In any case, the HHV of the precipitates were similar and substantially higher than the HHV of the parental PPW. In general, these results were consistent with the results regarding the chemical composition in terms of structural wood components (Figure 37-Figure 38) because precipitates with lower carbohydrate contents and higher lignin contents (and consequently less oxygen content) presented higher HHV. The sulfur contents of the precipitates were all below the detection limit (<0.01 wt.%) of the EA equipment.

Globally, the two-step lignins presented elemental compositions close to those of Kraft lignin reported by Constant et al. [125], while the three-step lignins presented elemental compositions closer to those of acidic organosolv lignins reported by Constant et al. [125] and Park et al. [244] (all softwoods). Calculating the HHV corresponding to these elemental compositions reported by Constant et al. [125] and Park et al. [244] through the same methodology used in this work [194], the corresponding HHV would be 27.7 and 25.8 kJ/kg for acidic organosolv lignin and Kraft lignin, respectively, which encompass the range of those observed in this work.

Figure 40 shows the FTIR-ATR spectra of two-step and the three-step precipitates, and Table 14 shows the assignments of each observed band [137,140,241,245–250].

The FTIR-ATR spectra did not show obvious differences between precipitates obtained by both fractionation routes, in spite of the slightly higher carbohydrate contamination (determined by HPLC-RID) of the two-step precipitates as compared to the three-step ones. However, it should be noted that cellulose and hemicellulose present IR bands that could have been overlapped by lignin bands [251,252]. Such results indicated that the functional groups present in both two-step and three-step lignins were similar and were mostly related to the lignin structure. The absence in all spectra of a band at 1330 cm^{-1} and 1120 cm^{-1} characteristic of syringyl units, as well as the lack of bands at 1168 cm^{-1} and 833 cm^{-1} characteristic of coumaryl units, demonstrate that PPW derived precipitates were in fact majorly constituted by guaiacyl type lignin [241,244]. The sulfur band observed at 624 cm^{-1} in all precipitate spectra was in apparent disagreement with elemental analysis (Table 13). This apparent contradiction was attributed to the detection limit for sulfur of elemental analysis equipment (<0.01 wt.%). The presence of sulfur in all precipitates was attributed to the sulfuric acid used to precipitate the lignin dissolved in SEOS cooking liquors, as previously reported by other authors [245,246]. Similar to SEOS, Kraft pulping is an alkaline process so the precipitation of derived lignin is usually performed by acidification of black liquor [125,150]. Interestingly, the softwood Kraft lignins obtained by Constant et al. [125] presented an ash content of 2.6 wt.%, very close to those observed in this work. Furthermore, they analyzed the ashes of their softwood Kraft lignins by ICP-AES and found that sodium and sulfur were the most abundant elements, enlightening this way the effect of lignin acidic precipitation from alkaline liquors.
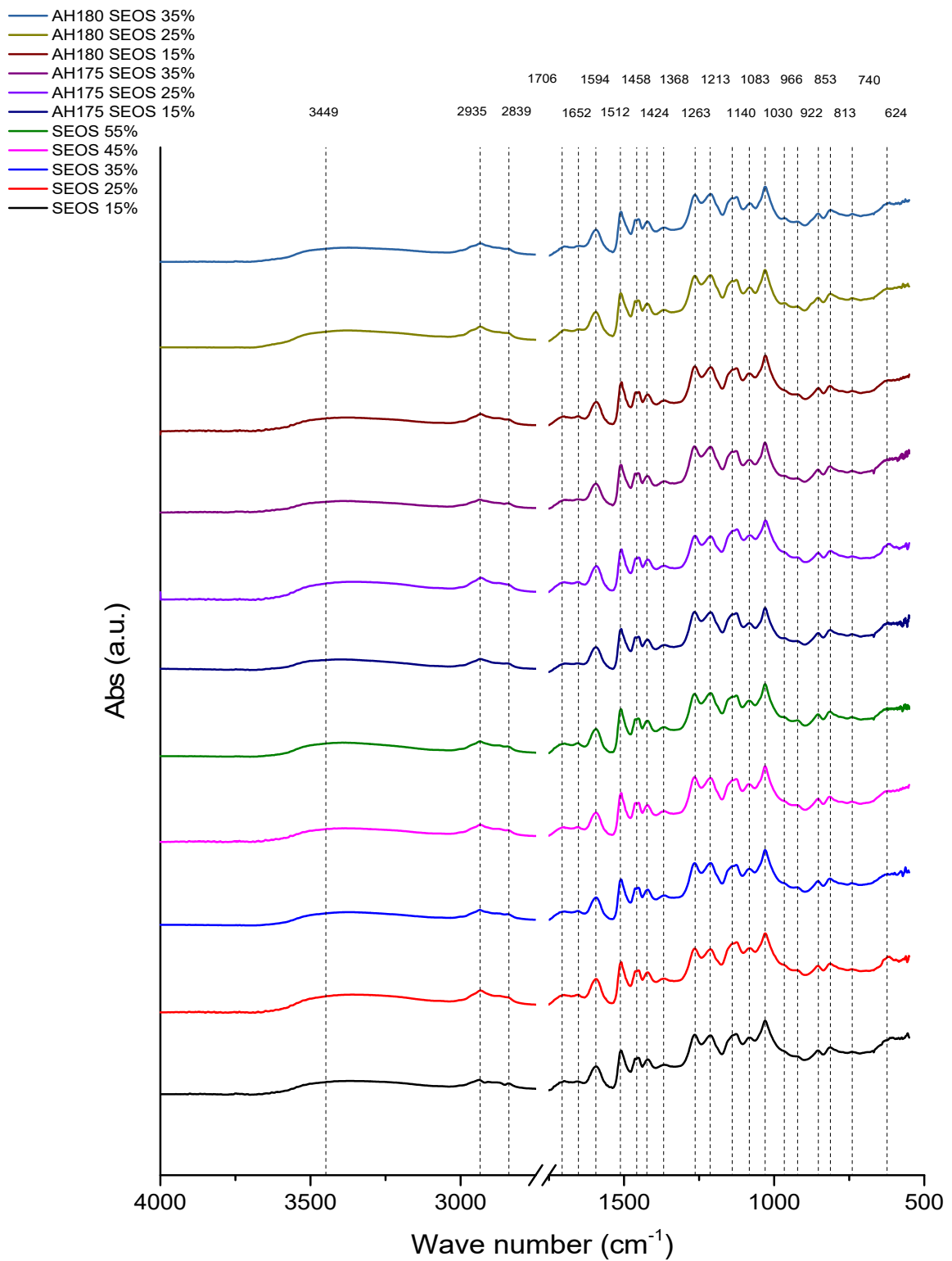
Figure 40– FTIR-ATR spectra of the two-step and three-step precipitates

Table 14 – Assignments of the bands detected in ATR-FTIR spectra of two-step and three-step precipitates shown in Figure 39 [137,140,241,245–250].

Wavelength (cm^{-1})	Assignments
3449	O-H stretching
2935	C-H stretching in methyl and methylene groups
2839	C-H stretching in methyl and methylene groups
1706	C=O stretching in unconjugated ketone, carbonyl and ester groups
1652	C=O stretching in p-substituted aryl ketones
1594	Aromatic skeletal vibrations
1512	Aromatic skeletal vibrations
1458	Asymmetric deformation of methyl and methylene groups
1424	Aromatic skeletal vibrations with C-H in-plane deformation
1368	Phenolic hydroxyl vibrations
1263	Guaiacyl skeletal vibrations with C-O stretching
1213	C-C plus C-O stretching
1140	Guaiacyl C-H in-plane deformation plus C-O stretching secondary alcohols
1083	C-O deformation in secondary alcohols and aliphatic ethers
1030	Guaiacyl C-H in-plane deformation plus C-O deformation in primary alcohols
966	C-H out-of-plane deformation in aromatic rings
922	C-H out-of-plane deformation in aromatic rings
853	C-H out-of-plane deformation in guaiacyl rings
813	C-H out-of-plane deformation in guaiacyl rings
740	C-H deformation in aromatic rings
624	C-S stretching vibrations

5.3.4. Overall considerations

Table 15 shows a comparison of results regarding pulp yields, pulp lignin contents lignin recovery and operational condition of organosolv of several softwoods reported in literature.

Table 15 – Comparison of pulp yields, pulp lignin contents lignin recovery and operational condition of organons of several softwoods reported in literature.

Biomass	T (ºC)	Catalyst	Ethanol	tr (min)	Y pulp	Pulp lignin content	Y lignin (recovery)	Reference
European larch	167-187 ºC	0.75-1.65 wt.% H_2SO_4	75 vol.%	30	22.42-47.49 wt.%	14.14-29.24 wt.%	16.36-21.82 wt.%	[241]
Spruce and pine	185-198		40-60 vol.%	30-60		18.4-27.4		[136]
Pinus cordata (killed by M. Pine Beetle)	152-180	0.76-2.50 wt.% H_2SO_4	48-75 vol.%	40-120	7.15-42.55 wt.%	4.98-27.42 wt.%	17.10-22.00 wt.%	[145]
Pinus cordata (killed by M. Pine Beetle)	170, 170	1 wt.% H_2SO_4, 2 wt.%NaOH	65 vol.%	60	43.5, 45.3	17.59 wt.%, 10.93 wt%	-	[143]
Pinus rigida	160-180	1 wt.% H_2SO_4, 2 wt.% NaOH	50 vol.%	0-20	50.87-61.48 wt.% ca. 34.5 wt.% (NaOH)	ca.24.0 wt.%, ca. 11.5 wt.%	23.78 wt.% 11.72 wt.%	[144]
Pinus sylvestris	180	15-22 wt.% NaOH and 0.1 mol/L Na_2CO_3	4 vol.%	180-300	42.9-45.9 wt.%,	5.4-3.4 wt.% (calc from #K)	-	[253]
Pinus brutia	170	Na_2SO_3 15-25 wt.%, NaOH 3.75-6.25 wt.% and anthraquinone 0.1 wt.%	30-60 vol.%	120-180	46.5-53.9	-	-	[254]
Spruce wood	190	H_2SO_4 (10 mM	60 wt.%	60				[125]
Pinewood	180	1 wt.% H_2SO_4	75 vol.%	180	51.9 ±3.2	25.0 ±0.3	(51.7 wt.%)	[153]
Pinus pinaster	170	30 wt.% NaOH	25-55 wt.%	90	26.6-45.2	5.3-8.5	21.1-25.6 (61.2-77.2 wt.%)	This work

Schenck et al. [253] worked on the fractionation of *Pinus sylvestris* wood using the conventional soda process, against the soda process with the addition of very low ethanol concentrations (4 vol.%) and anthraquinone (0.1 wt.%). These authors [253] worked at 180 ºC with catalyst loads in the range of 15-22 wt.% NaOH and 0.1 mol/L Na_2CO_3, and reaction times in the range of 180-300 min. On a wood basis, the pulp yields oscillated between 42.9-45.9 wt.%, corresponding to carbohydrate yields between 41.3-43.4 wt.% (both values extracted from a figure), respectively. The authors obtained pulps containing approximately 5.4-3.4 wt.% of lignin (values extracted from a figure) using a catalyst load in the range of 19-22 wt.%, respectively, after 240 min of reaction. When the reaction time was increased from 180 to 300 min while using a catalyst load of 21 wt.%, the pulp lignin contents varied in the range of 4.8-3.2 wt.% (values extracted from a figure), respectively [253]. However, the pulp lignin contents where not determined experimentally by Schenck et al. [253], but instead calculated from experimentally determined kappa numbers using a factor of 6.545. Adopting the same calculation methodology based on the values of kappa number presented in Table 12, the lignin contents of the two-step pulps would be in the range of 4.61-6.05 wt.%, while in the case of three-step pulps the lignin contents would be in the range of 3.40-5.70 wt.% for those derived from AHS175 and in the range of 3.93-6.55 wt.% for those derived from AHS180. This way, the lignin contents calculated from the values on Table 12 are close to those presented by Schenck et al. [253], especially in the case of pulps produced from autohydrolyzed wood. Such comparison indicates that similar results may be achieved by using very low concentrations of ethanol (4 vol.%), moderate catalyst loads (19-22 wt.%), high reaction temperature (180 ºC), long reaction time (240 min) and anthraquinone (0.1 wt.%), or as in this work by using shorter reaction times (90 min), lower reaction temperature (170 ºC), higher catalyst loads (30 wt.%) and higher ethanol concentrations (15-35 wt.%) without anthraquinone.

Kirçi et al. [254] processed *Pinus brutia* wood chips by an alkaline organosolv process (15-25 wt.% Na_2SO_3, 3.75-6.25 wt.% NaOH, 0.1 wt.% anthraquinone, 30-60 vol.% ethanol, at 120-180 ºC for 120-180 min), which they named as Alkali-Sulfite-Antraquinone-Ethanol (ASAE) and compared the results against the sulfate (or Kraft) process. The pulp yield of the sulphate process was 45.4 wt.% having a kappa number of 60.9 and a viscosity of 883 mL/g [254]. On the other hand, the yields of the ASAE process at optimized conditions (20 wt.% Na_2SO_3, 5 wt.% NaOH, 0.1 wt.% anthraquinone, 50 vol.% ethanol, at 150 ºC for 150 min) was 50.3 wt.% having a kappa number of 35 and a

viscosity of 1,364 mL/g [254]. The pulp yields and the pulp viscosities observed in this work were lower than those observed by Kirçi et al. [254]. On the other hand, the kappa numbers were lower in the majority of experimental conditions tested in this contribution, meaning that the pulps obtained in this work had lower lignin contents.

An interesting comparison that could be made was to equate the results of the three-step route against those achieved by Amiri and Karimi [153] upon the sequential autohydrolysis (180 ºC for 60 min) and acidic organosolv (75 vol.% ethanol, 1 wt.% H_2SO_4 at 180 ºC for 60 min) of pinewood. They obtained a pulp yield of 51.9 wt.% having cellulose, hemicellulose and lignin contents of 73.9 wt.%, 9.1 wt.% and 25.0 wt.%, respectively. Comparing these values against those in Figure 31-Figure 34 regarding the three-step procedure, it can be said that the pulp yields and cellulose contents achieved by Amiri and Karimi [153] were higher, while the lignin contents of the pulps were almost five-fold lower in this work. The hemicellulose contents of the pulps produced in that work [153] were similar to those produced in this work by direct SEOS of PPW (two-step procedure), but the three-step pulps had hemicellulose contents four-fold lower. These observations were in agreement with those of Del Rio et al. [143], Park et al. [144] and Pan et al. [145], meaning that the pulps obtained in this work were much purer and may possibly have higher value-added applications.

5.4. Depolymerization of organosolv lignin

Because the AH175 SEOS35 precipitate was the one having the highest purity and yield (Figure 36-Figure 39), the same experimental conditions were used to perform 32 batches to generate enough material to be used in lignin depolymerization studies.

5.4.1. Lignin preparation

The characterization of *Pinus pinaster* wood (PPW) and products obtained upon the three-step fractionation procedure are presented in Table 16.

Table 16 – Yields (on wood basis) and composition of products obtained by the separation strategy adopted (ND=not detected).

Sample	Yield (wt.%)	Composition (wt.%)			
		Ash	Lignin	Cellulose	Hemicellulose
PPW	-	0.8 ±0.0	32.3 ±0.4	39.6 ±0.1	26.3 ±0.1
AH liquors	16.1 ±0.5	0.0 ±0.0	5.4 ±0.1	9.2 ±0.1	85.4 ±0.3
AH solids	78.1 ±1.7	0.2 ±0.0	38.5 ±0.9	46.0 ±0.6	12.7 ±0.3
SEOS pulp	31.1 ±2.0	0.8 ±0.1	4.1 ±0.8	89.7 ±1.2	4.4 ±0.1
SEOS lignin	24.3 ±0.3	2.7 ±0.1	97.0 ±0.4	ND	ND

The results showed that ca. 53 wt.% of hemicelluloses were removed from PPW upon AH, and that ca. 70 wt.% of cellulose was recovered as SEOS pulp and 73 wt.% of lignin was recovered by LP. Globally, ca. 72 wt.% of the parental PPW were recovered as products at the end of the selected fractionation system. AH liquors and SEOS pulps were used in parallel studies regarding the production of ethanol by simultaneous saccharification and fermentation [255]. These results were in accordance with those achieved in a previews work in which PPW was fractionated using the same methodology [256].

The ^{1}H-^{13}C HSQC NMR spectra of the so prepared lignin is shown in Figure 41. In the aromatic region (Figure 41a) the C_2-H_2, C_5-H_5 and C_6-H_6 bonds characteristic of guaiacyl subunits could be observed. In the aliphatic region (Figure 41b) methoxy groups characteristic of guaiacyl subunits were detected, as well as $C\gamma$-$H\gamma$ and $C\alpha$-$H\alpha$ in β-O-4 bonds and $C\gamma$-$H\gamma$ in coumaran motifs. Still in the aliphatic region, alkyl side chains could be observed (Figure 41c). All these motifs detected by HSQC were characteristic of softwood lignins which are mainly formed by G subunits [199].
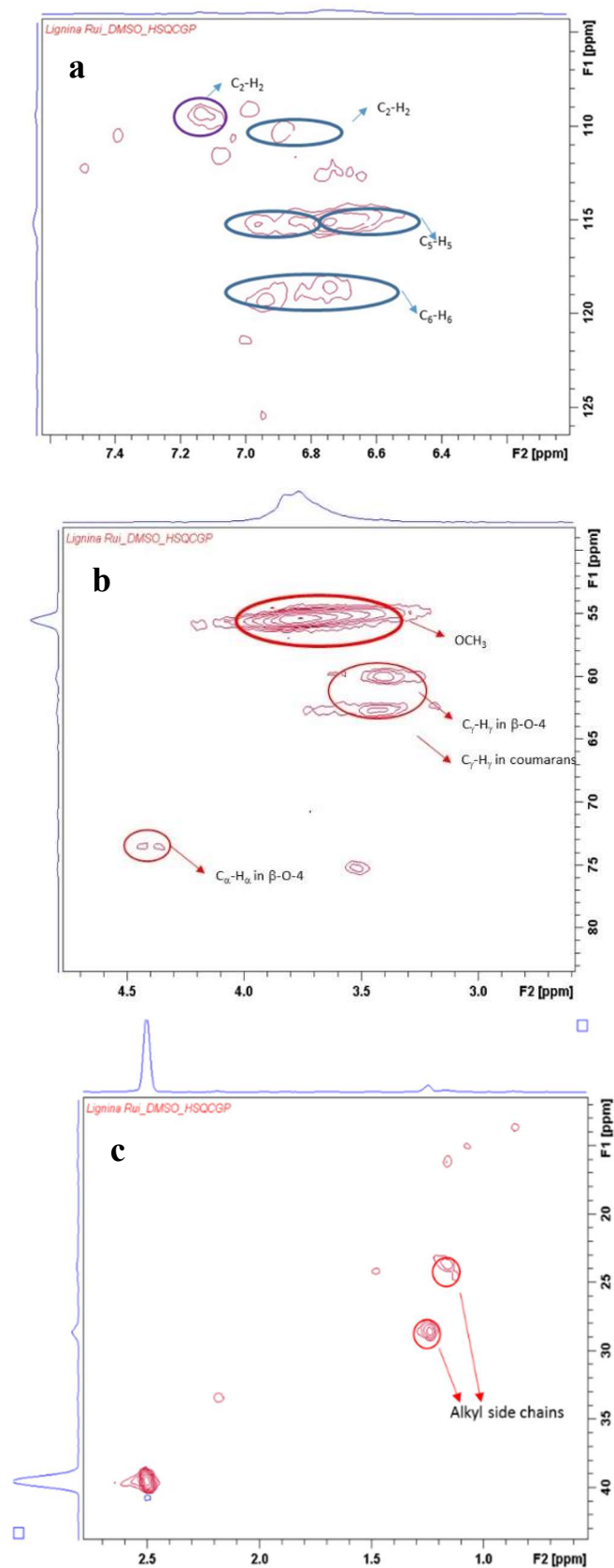
Figure 41 – Aromatic (a) an aliphatic (b and c) regions in ^{1}H-^{13}C HSQC spectra of the produced lignin.

5.4.2. Direct depolymerization of lignin

The reductive catalytic depolymerization (or hydrogenolysis) of the prepared lignin precipitates was attempted over different catalysts. Depolymerization of SEOS lignin using immobilized Ni and/or Cu on HTC and ZSM5 as well as Mo_2C/AC (in ethanol at 200-250 ºC and 20 of bar of H_2) proved to be unsuccessful, because monomer yields were in all cases under 2.5 wt.%. In any case, almost 85% of the monomers under these reaction conditions were compounds not having methoxy substitutions (85%, grouped as phenols) and syringyl monomers (15%), meaning that considerable demethoxylation occurred (data not shown). Direct depolymerization of lignin over commercial Pd/C, Pt/Al_2O_3 and Ni/Al_2O_3 in ethanol at 200-250 ºC and 20 bar of H_2 was also attempted, but again monomer yields were below 2.0 wt.% in all cases (data not shown).

Reductive catalytic depolymerization over Ru/C in supercritical ethanol (scEtOH) at 250 ºC and 20 bar of H_2 (HYD30 in Figure 42, see below) performed slightly better (Table 17, see below), yielding ca. 3.5 wt.% monomers, being guaiacyl derivatives (86%, 9-16 in Table 17, see below) the major monomers followed by phenols (3.4%, 1-8). Among the guaiacyl derived compounds, 4-ethylguaiacol (11) was the most abundant monomer (50.7%) followed by 4-propylguaiacol (14.8%, 12). Small amounts of gigantol (19) were also detected (6%) by GC-MS.

5.4.3. Depolymerization of lignin with NaOH and Ru/C

Due to the low solubility of SEOS lignin in H_2O, the homogeneous base catalyzed depolymerization (BCD) using NaOH in $EtOH/H_2O$ was attempted at 220 ºC and 250 ºC to obtain BCD220 and BCD250 (respectively), as depicted in Figure 42.
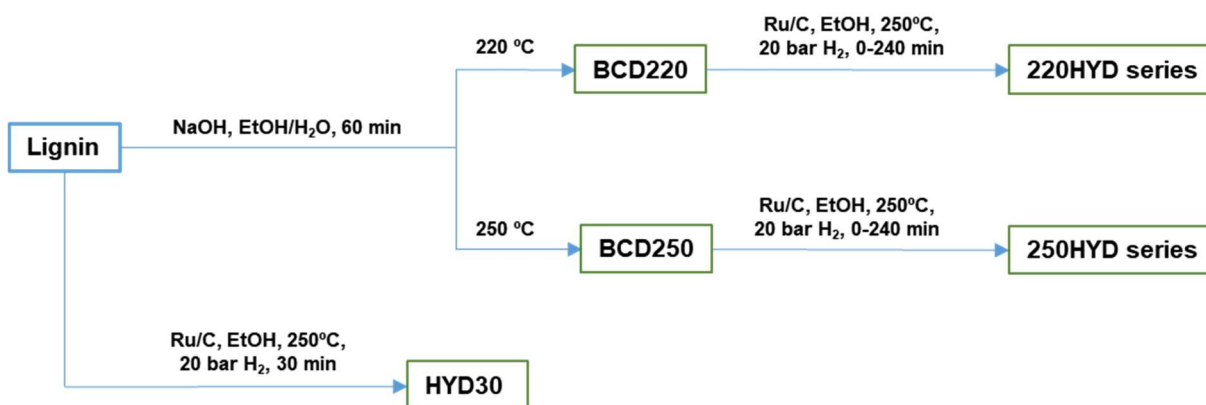
Figure 42 – Scheme of homogeneous base catalyzed depolymerization using NaOH in $EtOH/H_2O$ and heterogenous catalyzed depolymerization using Ru/C in EtOH.

The BDC220 gravimetric yield (91.9 ±4.9%) obtained at 220 ℃ was similar to the BCD250 yield (89.8 ±2.3%) achieved at 250 ℃, considering the experimental error upon seven replicates (at each temperature). Since no solid residue was detected upon filtration of BCD220 and BCD250 products, full conversion of lignin was assumed, and the small differences observed in the yields were attributed to a slightly higher formation of reaction products soluble in water that were not be efficiently separated by the liquid-liquid extraction performed with ethyl acetate.

Low monomer yields were obtained under BCD conditions (0.6 wt.% and 1.0 wt.%, respectively), and distribution showed that major monomers were guaiacyl (80.7% and 90.7%, respectively) followed by syringyl monomers (9.9% and 4.7% respectively). It is generally accepted that syringyl monomers are not present in softwood lignins. However, it has been reported that small amounts of syringyl can be found in pine barks [257] and that syringyl units up to 1 wt.% can be found in softwood lignins [159]. Son et al. [258] detected the presence of syringyl motifs in depolymerization products of acid ethanosolv pinewood lignins over Ru/H-zeolite-β in 65 vol.% ethanol in water identified by gas chromatography, ^{31}P NMR, 2D-(^{1}H-^{13}C)-HSQC NMR and FTIR. Van den Bosch et al. [182] also reported the presence of syringyl monomers (identified by GC-MS) in the product pool upon direct depolymerization of softwoods over Ru/C in methanol. In this work, ^{31}P NMR analysis of derivatized lignin presented a shoulder at 143 ppm suggesting the presence of small amounts of S units, which were not detected in the FTIR-ATR spectrum of this lignin (see above AH175 SEOS35 in Figure 40 and Table 14).

The apparent high relative yield of syringyl units as compared to guaiacyl units (which constitute over 95% of softwood lignins) was possibly related to the fact that syringyl units are more easily detached from lignin due to the stereochemistry provided by the two methoxy groups attached to the phenylpropane backbone, which difficult the formation of C-C bonds (by repolymerization) during delignification/fractionation of lignocellulosic biomass, as well as during lignin depolymerization reactions [15,159,162]. Nevertheless, both DOSY and SEC analysis (see below Figure 44) evidenced that, despite the monomer yields were relatively low, molecular masses of BCD220 and BCD250 products were much lower than those of the parental lignin (see below Table 18)**,** showing that some depolymerization had occurred.

Table 17 – Monomer yields ($Y_{monomers}$) with corresponding structures presented in Figure 42.

Reaction product	Original material	Catalyst	Solvent	T (°C)	t (min)	$Y_{monomers}$ (wt.%)	1-8	9	10	11	12	13	14	15	16	17	18	19
HYD30	Lignin	Ru/C	EtOH	250	30	3.5 ±1.5	3.4 ± 2.0	7.1 ±5.6	8.2 ±2.9	50.7 ±18.9	14.8 ±14.9	0.7 ±1.3	0.0 ±0.0	0.0 ±0.0	4.5 ±4.5	0.0 ±0.0	0.0 ±0.0	6.2 ±3.2
BCD220	Lignin	NaOH	EtOH/H₂O	220	60	0.6 ±0.2	0.1 ±0.1	17.6 ±6.6	3.3 ±1.1	18.4 ±5.4	0.1 ±0.1	1.2 ±1.3	12.9 ±3.6	12.9 ±3.6	14.3 ±2.3	5.1 ±8.8	4.8 ±3.8	0.5
BCD250	Lignin	NaOH	EtOH/H₂O	250	60	1.0 ±0.2	0.8 ±0.8	45.0 ±5.9	8.4 ±0.8	29.4 ±3.2	2.5 ±0.5	0.0 ±0.7	0.0 ±0.0	0.0 ±0.0	5.4 ±1.9	0.0 ±0.0	4.7 ±3.1	2.3 ±3.6
220HYD0	BCD220	Ru/C	EtOH	250	0	2.4	0.0	11.8	10.0	53.5	4.7	0.0	0.0	0.0	7.1	4.2	0.0	5.4
220HYD 30	BCD220	Ru/C	EtOH	250	30	2.2 ±0.4	3.5 ±0.1	9.1 ±3.2	10.4 ±1.0	41.9 ±6.3	4.2 ±0.3	1.7 ±3.1	0.0 ±0.0	0.0 ±0.0	10.5 ±0.2	7.0 ±2.1	1.9 ±4.3	5.9 ±2.9
220HYD 60	BCD220	Ru/C	EtOH	250	60	3.7 ±0.4	0.0 ±0.0	17.3 ±6.1	10.8 ±1.0	45.9 ± 3.9	5.2 ±1.2	0.0 ±0.0	0.0 ±0.0	0.0 ± 0.0	7.0 ±4.4	4.0 ±1.1	0.0 ±0.0	6.1 ±0.6
220HYD 120	BCD220	Ru/C	EtOH	250	120	4.2 ±1.2	1.6 ±0.3	19.3 ±0.1	10.6 ±4.4	35.9 ± 9.7	3.2 ±1.8	2.5 ±3.6	0.0 ±0.0	0.0 ±0.0	8.7 ±3.5	3.0 ±0.6	0.0 ±0.0	9.5 ±6.5
220HYD 240	BCD220	Ru/C	EtOH	250	240	4.2 ±0.3	0.3 ±0.4	20.2 ±6.2	10.5 ±1.4	42.5 ±1.4	3.4 ±2.0	1.3 ±2.1	0.0 ±0.0	0.0 ±0.0	6.2 ±1.1	1.0 ±1.6	1.9 ±3.0	7.9 ±1.6
250HYD0	BCD250	Ru/C	EtOH	250	0	4.9	0.0	29.8	11.9	46.0	4.2	0.0	0.0	0.0	2.2	0.0	0.0	3.7
250HYD30	BCD250	Ru/C	EtOH	250	30	7.3 ±1.6	2.9 ±4.6	30.9 ±4.2	8.1 ±6.2	43.1 ±12.5	4.1 ±1.1	0.0 ±0.0	0.0 ±0.0	0.0 ±0.0	2.4 ±2.4	0.0 ±0.0	4.2 ±6.1	2.3 ±3.1
250HYD60	BCD250	Ru/C	EtOH	250	60	5.1	0.0	32.3	11.3	44.1	3.9	2.1	0.0	0.0	0.0	0.0	0.0	0.0
250HYD120	BCD250	Ru/C	EtOH	250	120	6.7	0.0	33.4	10.6	42.0	3.9	0.0	0.0	0.0	3.0	0.0	0.0	4.4
250HYD240	BCD250	Ru/C	EtOH	250	240	6.6 ±0.5	0.0	31.9 ±12.5	11.7 ±2.2	43.5 ±12.9	4.0 ±1.9	0.0 ±0.0	0.0 ±0.0	0.0 ±0.0	2.1 ± 3.3	0.0 ± 0.0	0.0 ±0.0	4.2 ±0.7

(1) phenol; (2) 2-ethylphenol; (3) o-cresol; (4-5) m-cresol/p-cresol; (6) catechol; (7) 4-methylcatechol; (8) 4-ethylcatechol; (9) guaiacol; (10) 4-methylguaiacol; (11) 4-ethylguaiacol; (12) 4-propylguaiacol; (13) guaiacylketone (4-Hydroxy-3-methoxyphenylacetone); (14) homovanillic alcohol; (15) homovanillic acid; (16) acetovanillone; (17) syringaldehyde; (18) acetosyringone; (19) gigantol.

1 phenol 2 2-ethylphenol 3 o-cresol 4 m-cresol

5 p-cresol 6 Catechol 7 4-methylcatechol 8 4-ethylcatechol

9 guaiacol 10 4-methylguaiacol 11 4-ethylguaiacol

12 4-propylguaiacol 13 4-hydroxy-3-methoxyphenylacetone

14 homovanillic acid 15 homovanillic alcohol

16 acetovanillone 17 acetosyringone 18 syringaldehyde

19 gigantol
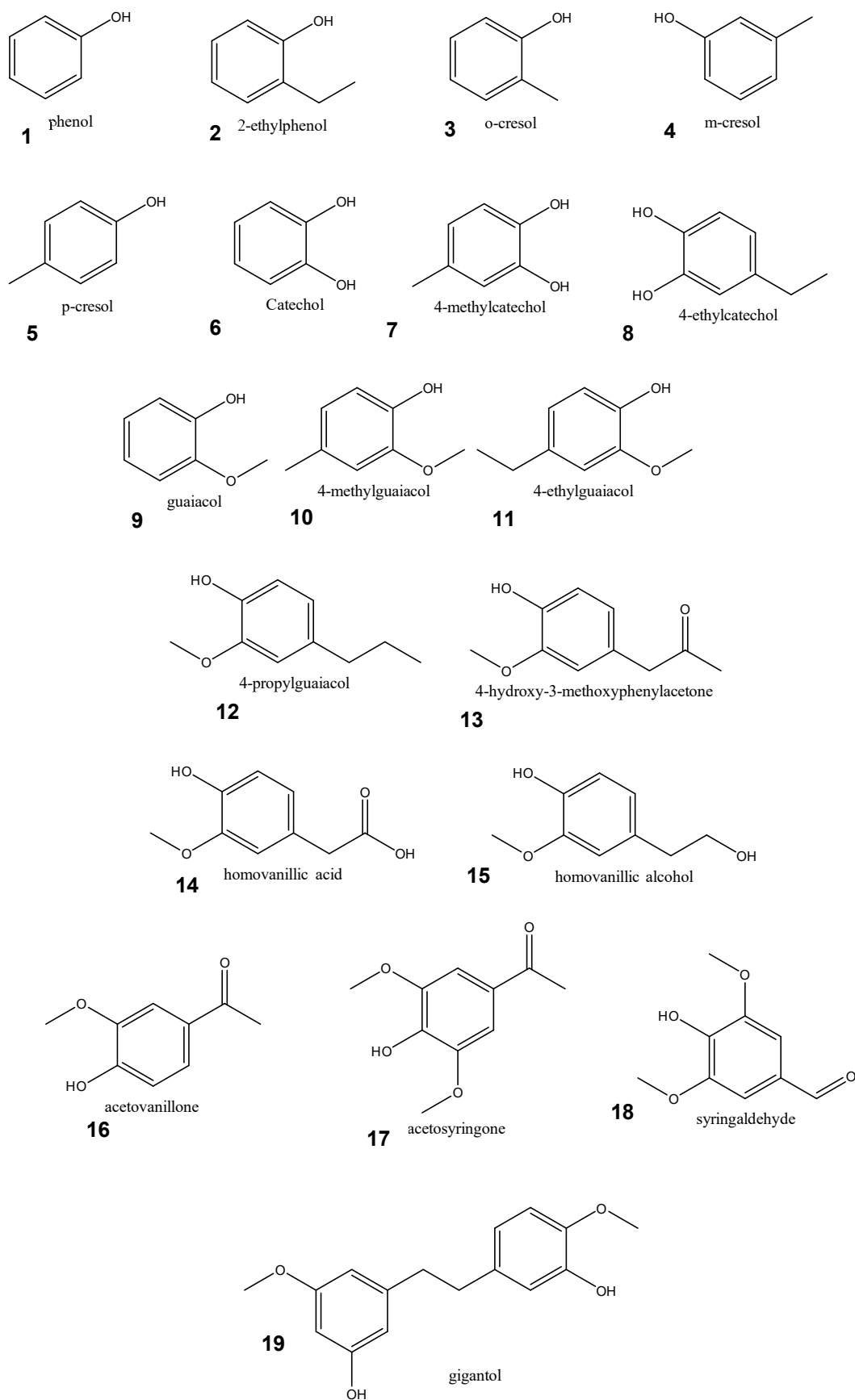
Figure 43 – Structure of monomers identified in Table 17.

Aiming to increase the monomer yields, BCD220 and BCD250 products were subjected to reductive catalytic depolymerization with Ru/C in scEtOH at 250 ºC and 20 bar of H_2, yielding the 220HYD series (220HYD0-220HYD240 corresponding to 0-240 min of reaction) and the 250HYD series (250HYD0-250HYD240 corresponding to 0-240 min of reaction). For the sake of clearness, reaction times of zero minutes (0 min) correspond to experiments stopped immediately after the setpoint temperature has been reached (220HYD0 and 250HYD0), this way not allowing the reaction to proceed and at the same time having an estimate of the chemical transformations occurred upon heating.

As shown in Table 17, monomer yields in 220HYD series steadily increased with reaction time from 2.2 wt.% to 4.2 wt.% (from 0 to 120 min) and remained constant thereafter. Guaiacyl monomers were again the most abundant (80.2% at 120 min and 84.1 at 240 min) and amongst them 4-ethylguaiacol (11). However, its content decreased from 53.5% to 42.5% with reaction time (0 to 240 min) with a concomitant increase in guaiacol (9), whose content raised from 12% to 20%, whereas the proportions of 4-methylguaiacol (10) and acetovanillone (16) remained almost constant with reaction time (ca. 10% and ca. 7% respectively). This suggests that an increase in reaction time caused an increase in guaiacol (9) formation by alkyl side-chain cleavage of 4-ethylguaiacol (11).

A noticeable increase in monomer yields was observed when BCD250 was subjected to hydrogenolysis to produce 250HYD series under the same conditions. Thus, the monomer yield increased from 4.9 wt.% at 0 min to 7.3 wt.% after 30 min and remained almost constant ($\simeq$6.7 wt.%) at longer reaction times (120-240 min). The proportion of guaiacyl monomers grew beyond 90% in all cases, being 4-ethylguaiacol (11) the most abundant amongst them (*ca*. 45%) followed by guaiacol (9, *ca.* 31%). Noteworthy, any change in the monomer distribution in the product pool could be observed regardless the reaction time, meaning that general trends could not be perceived. The relative amounts of 4-methylguaiacol (10) and 4-ethylguaiacol (11) were very similar in 220HYD and 250HYD series. However, the guaiacol content (9) was much higher in the 250HYD series (32% *vs* 20%), while the acetovanillone (16, 7% *vs* 2%) and gigantol (19, 8% *vs* 3%) contents were higher in the case of 220HYD series. Curiously, the syringyl monomers were almost absent in the 250HYD series as well as in HYD obtained by direct hydrogenolysis of SEOS lignin, contrary to the case of 220HYD series. This indicates that higher reaction temperature favored the demethoxylation of syringyl monomers.

Long chain ethyl esters (such as ethyl palmitate or ethyl stearate) were detected by GC-MS in the product pool, possibly derived esterification of tall-oils (containing palmitic

and stearic acids) trapped during lignin isolation. Additionally, other aliphatic compounds such as octanol, hexanol or 4-methyltetrahydro-2H-pyran-2-one were also detected by GC-MS, which suggested that hydrogenolysis proceeded *via* hydrogen transfer from ethanol (which yields acetaldehyde that may undergoes consecutive condensation reaction) as previously reported over Mo_2C catalysts [259] and Cu/HTC catalysts [260]. Indeed, when the reaction was performed using the same operating conditions (temperature, time and pressure) under nitrogen atmosphere (data not shown) no significant differences were found in comparison with reactions performed under hydrogen atmosphere, which indicated that the main reaction mechanism was the hydrogen transfer from ethanol to the lignin materials catalyzed by Ru/C.

Figure 44 shows the profiles of SEC chromatograms and DOSY-NMR spectra of lignin as compared to homogeneous base catalyzed depolymerization products (BCD220 and BCD250) and hydrogenolysis products (220HYD30 and 250HYD30).
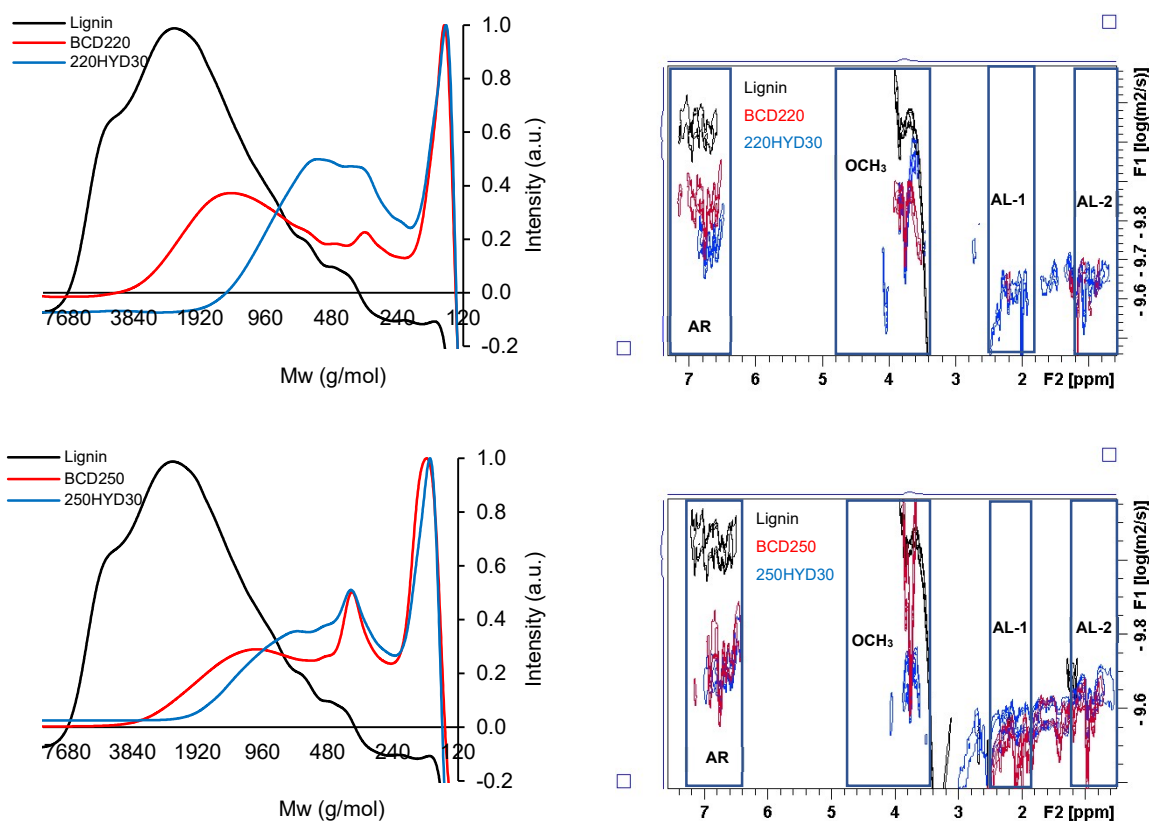
Figure 44 – SEC chromatograms (left) and NMR-DOSY (right) of SEOS lignin, BCD220, 220HYD30, BCD250 and 250HYD30.

The SEC chromatogram of lignin showed that the molecular mass distribution of this material was centered at ca. 2400 g/mol (Figure 44). Upon BCD at 220 ºC (BCD220) molecular mass distribution shifted, and a broad peak at ca. 1400 g/mol, a smaller peak at ca. 330 g/mol and a major peak at ca. 140 g/mol were detected. After treating this sample with Ru/C for 30 min (220HYD30), the molecular mass distribution formed a major peak centered at ca. 440 g/mol having two shoulders at 560 and 330 g/mol, as well as another major peak at ca. 150 g/mol coinciding with that of BCD220. On the other hand, upon BCD at 250 ºC (BCD250) the molecular mass distribution shifted to lower molecular masses as evidenced by the broad peak centered at ca. 1200 g/mol. Again, a major peak appeared at ca. 150 g/mol, and a prominent shoulder at ca. 360 g/mol was observed.

Treating this sample with Ru/C for 30 min (250HYD30), the mass distribution shifted again to lower molecular mass, presenting a shoulder centered at 670 g/mol together with an increase in the peak at ca. 330 g/mol, and a major peak at ca. 150 g/mol. These results globally indicated that the sequential treatments of lignin by BCD (BCD220 and BCD250) and Ru/C (220HYD30 and 250HYD30) caused consecutive decreases in the molecular masses of the reaction products in comparison with the parental materials (i.e., lignin or BCD products).

Diffusion-ordered spectroscopy (DOSY) in pseudo-bidimensional (2D) NMR technique that correlates the chemical shifts with the diffusion coefficient (D) at a given temperature [199,261]. Therefore, this technique allows to correlate the chemical shifts with the molecular mass (through the Stokes-Einstein equation), providing this way information complementary to Size Exclusion Chromatography (SEC) [199,261]. Four zones of the DOSY-NMR spectra can be seen in Figure 44 (right side), corresponding to the aromatic (AR), methoxy groups (OCH$_3$), aliphatic 1 (AL-1) and aliphatic 2 (AL-2) zones. The separate observation of these different zones in DOSY is a major advantage of this NMR technique because the molecular mass of the aromatic fraction can be independently evaluated. Indeed, it can be assumed that the aromatic region corresponds exclusively to lignin and poly-(hydroxy)aromatic ethers, so, the extent of the depolymerization can be evaluated by comparing the diffusion coefficients [199,261–263]. Accordingly, the evolution of the diffusion coefficient for the aromatic zone region in DOSY spectra, it can be seen that the shift of the aromatic fraction was more evident from BCD220 to 220HYD30 (almost no overlap in AR zone, top right) than from BCD250 to 250HYD30 (strong overlap in AR zone). Moreover, when lignin was treated by BCD at 250 ºC

followed by hydrogenolysis it can be also seen that the NMR signal in the AL zones was much stronger indicating the formation of aliphatic compounds.

The results of molecular masses (M_w and M_n) determined by SEC, the molecular masses (M_{AR}, M_{AL-1} and M_{AL-2}) determined by NMR-DOSY, and the hydroxyl group content determined by ^{31}P NMR for lignin, BCD products (BCD220 and BCD250) and hydrogenolysis products (220HYD30 and 250HYD30) are presented in Table 18.

Table 18 - Molecular masses estimated by SEC (M_w and M_n), molecular masses estimated and DOSY NMR (M_{AR}, M_{AL-1} and M_{AL-2}) and OH content estimated by ^{31}P NMR.

Sample	SEC (g/mol)		DOSY NMR (g/mol)			^{31}P-NMR
	Mw	Mn	M_{AR}	M_{AL-1}	M_{AL-2}	(mmol OH/g)
Lignin	3005 ±423	2296 ±244	2200	279	553	4.6
HYD30	956 ±59	752 ±45	746	562	509	2.8
BCD220	1798 ±334	891 ±49	1039	285	463	3.6
BCD250	1250 ±141	587 ±86	660	322	401	4.5
220HYD30	856 ±97	553 ±52	691	441	502	3.0
250HYD30	818 ±122	468 ±74	665	433	540	3.7

It can be seen on Table 18 that M_n (most frequent molecular mass measured by SEC) and M_{AR} (molecular mass of the aromatic fraction measured by DOSY) had similar tendencies. It should be noted that the M_n values measured by SEC include the whole pool of compounds present in the sample, while in DOSY the molecular sizes of aliphatic compounds could be isolated from the aromatic fraction. Therefore, it can be inferred from the values in Table 18 that the differences between M_n and M_{AR} were mainly due to the agglomerated measurement of the three fractions (M_{AR}, M_{AL-1} and M_{AL-2}) by SEC, as previously reported by Cornejo et al. [199].

From Table 17-Table 18 and Figure 44, it can be seen that in spite of the low monomer yields in BCD220 (0.6 wt.%) and BCD250 (1.0 wt.%), SEC and DOSY showed that depolymerization of lignin was more extensive in the case of BCD250 than in BCD220, because the molecular masses of BCD250 measured by both these analytical techniques (M_n and M_{AR}, respectively) were lower than those of BCD220. Upon hydrogenolysis of BCD220 and BCD250 over Ru/C for 30 min, the monomer yields were higher in 250HYD30 (7.3 wt.%) than in 220HYD30 (2.2 wt.%). However, the molecular masses determined by SEC (M_n) and DOSY (M_{AR}) of 220HYD30 were similar to those of 250HYD30. These results indicated a more noticeable effect of the Ru/C treatment on

BCD220 as compared to BCD250. Interestingly, both M_n and M_{AR} were only slightly higher when lignin was directly treated with Ru/C at 250 ºC in ethanol (HYD30). Globally, both SEC and DOSY evidenced the same tendencies in the evolution of molecular masses, despite that each technique in fact measured different values of this variable in the same sample.

The data provided by DOSY spectroscopy helped to understand the profiles of SEC results. The molecular masses of samples determined by DOSY did not seem to match with the most prominent peaks determined by SEC. In fact, the peak at around 150 g/mol present in all SEC chromatograms of the reaction products seemed consistent with the detection by gas chromatography of reaction products arising from the formation of aliphatic compounds by condensation reactions of ethanol (such as the Guerbert reaction) [264]. The formation of aliphatic compounds by alkylation under reaction conditions with scEtOH has been previously reported in the literature [260,265,266]. Moreover, a peak ca. 330 g/mol could be distinguished in SEC chromatograms, possibly consistent with the presence of two-unit aromatic compounds (dimers such as gigantol) whose presence can be also observed in DOSY spectra. Additionally, diffusion coefficients for AL-1 and AL-2 were significantly lower than those of the AR zone, denoting that these diffusion traces were not part of the same molecule.

^{31}P NMR of lignin and reaction mixtures provided the millimoles of aromatic hydroxy groups per gram of sample. It can be observed that the OH content decreased from BCD220 to 220HYD30 as well as from BCD250 to 250HYD30, possibly due to deoxygenation reaction with hydrogen (hydrodeoxygenation) to form water or due to the side reactions promoted by the presence of ethanol. However, the highest decrease was observed upon direct hydrogenolysis of SEOS lignin to HYD30.

5.4.4. Overall considerations

Table 19 shows a comparison of results reported in literature and those obtained in this thesis regarding the depolymerization of softwoods.

Table 19 - Comparison of results of softwood lignin depolymerization.

Sample origin	Temperature (ºC)	Reaction time (min)	Pressure (H$_2$ bar)	Solvent	Catalyst	Monomer yield (%)	Phenols (%)	Guaiacyl (%)	Syringyl (%)	M$_w$ (g/mol)	M$_n$ (g/mol)	Reference
Pinus radiata [a]	225-300	60-1200	-	H$_2$O	NaOH	2.5-8.2	1.6-4.8	0.4-3.9	0.0-2.4	1173	720	[199]
Pinewood [b]	210-280	-	20	EtOH/H$_2$O	Ru/Hβ	11.9-23.6	0.3-1.2	9.8-23.4	2.8-9.2	533-540	202-234	[258]
Softwood [c]	320	480	35	MeOH	NiW/AC,	28.5	20.3	5.5	-	500	-	[267]
					NiW/ZSM-5,	18.0	11.7	4.5	-	280	-	
					NiW/MgO–La$_2$O$_3$,	26.5	17.8	7.0	-	430	-	
					NiW/MgO–CeO$_2$,	22.5	14.9	5.0	-	400	-	
					NiW/MgO–ZrO$_2$,	16.5	7.7	5.5	-	470	-	
					NiMo/AC,	14.5	10.0	2.5	-	-	-	
					CoMo/AC	9.0	5.7	2.5	-	-	-	
Softwood [d]	300-330	45	-	H$_2$O	NaOH	5.5-10.0	0.3-5.3	4.2-4.5	0.4-0.9	-	-	[268]
Pinewood [e]	260	360	40	MeOH	NaOH	7.56	-	-	-	1881	1028	[269]
					Ru/C	6.1	-	-	-	1614	869	
					NaOH+Ru/C	12.7	-	-	-	1537	1342	
					KOH+Ru/C	12.5	-	-	-	-	-	
					Na2CO3+Ru/C	8.7	-	-	-	-	-	
					NaOH+Pd/C	12.4	-	-	-	-	-	
Pinus pinaster [g]	250	0-240	20	EtOH/H$_2$O	NaOH,	0.6-7.3	0.0-0.1	0.5-0.9	0.0-0.1	1250-1798	587-891	This work
				EtOH	Ru/C	3.5	0.1	3.0	0.0	956	752	
				EtOH	NaOH, Ru/C	2.4-7.3	0.0-0.2	1.7-6.5	0.0-0.3	818-856	468-553	

[a] Enzymatic hydrolysis lignin; [b] Acidic organosolv (at 170 and 200 ºC) lignin; [c] Kraft lignin Sigma Aldrich; [d] FIRSST process lignin; [e] Acidic ionic liquid organosolv; [f] Autohydrolysis (at 175 ºC) followed by soda alkaline ethanosolv (at 170 ºC).

From Table 19 it can be assumed that the monomer yields achieved in this work were inferior to others reported in the literature. On the other hand, the molecular masses of depolymerization products obtained in this work can fairly compare with others previously reported in the literature [199,269]. A possible explanation for such results may have been related with the extraction process used in this work to obtain the lignin feedstock (AH followed by SEOS), which seems to have resulted in a highly condensed non-reactive lignin material. In fact, Schutyser et al. [162] stated in their extensive literature review that isolation methods that achieve high lignin yields usually results in highly degraded lignins having low reactivity upon depolymerization processes. Moreover, the authors also evidenced that in spite organosolv processes are usually assumed to be relatively mild isolation procedures that preserve lignin reactivity, in fact traditional processes (such as Kraft and soda) have been often found to produce lignins having higher reactivity than organosolv ones [162].

In this Doctoral Thesis a three-step procedure was used to fractionate *Pinus pinaster* wood, to obtain three different fractions: a hemicellulose-rich liquor, a cellulose-rich pulp and a lignin-rich precipitate. The fractionation procedure used in this thesis encompassed first the autohydrolysis of lignocellulosic biomass (at 175 ºC form 30 min, an acidic environment derived from the formation of organic acids and hydronium ions), followed by a strong alkaline organosolv (35wt.% ethanol, 30 wt.% NaOH at 170 ºC for 90 min) and acidification (to pH=5) for precipitation of lignin having high purity (>97%). The results from the depolymerization study seem to show the high purity lignin precipitate may be formed by very condensed material that could not be depolymerized under the mild conditions used in this work. It could be anticipated that harsher conditions (temperature and pressure) should be tested to clarify this hypothesis. However, the experimental setup available for the experimental work regarding lignin depolymerization did not allow to use harsher operating conditions, therefore the exploration of that research topic had to be left to future works.

5.5. Liquid-phase hydrodeoxygenation of guaiacol

Due to the fact that the guaiacyl monomers were the major ones obtained in the previous study of lignin depolymerization (Table 17), a study of the upgrading of guaiacol (model compound of guaiacyl) was attempted using a Mo_2C/CNF catalyst.

5.5.1. Characterization of carbon nanofibers and fresh catalyst

The results of the characterization of the as-received (CNF_o) and pretreated (CNF) carbon nanofibers by N_2-physisorption and TPD are presented in Table 20, as well as those regarding characterization of the Mo_2C/CNF catalyst by N_2-physisorption.

Table 20 – Results of N_2-physisorption and TPD of the bare CNFs supports (CNF_o=as received carbon nanofibers; CNF=pretreated carbon nanofibers; n.d.=not determined).

Sample	Surface area (m^2/g)	Pore volume (cm^3/g)	Pore size (nm)	CO (mmol/g)	CO_2 (mmol/g)	Oxygen content (wt.%)
CNF_o	39.6	0.156	15.5	0.256	0.079	0.7
CNF	37.8	0.110	13.7	0.410	0.398	1.9
Mo_2C/CNF	44.2	0.147	13.3	n.d.	n.d.	n.d.

Comparing the CNF_o with the CNF N_2-physisorption results (Table 20), the HNO_3 pretreatment slightly reduced the surface area, the pore volume and the pore size of the carbon nanofibers. The evolution of CO_2 during TPD has been assigned to the existence of acid groups over carbonaceous supports caused by the decomposition of carboxylic acids, carboxylic anhydrides and lactones upon heating, while the evolution of CO has been assigned to the presence of basic and neutral groups over such support materials caused by the decomposition of phenols, ethers, quinones and carbonyls [270–272]. These oxygen groups can be created over carbonaceous supports by functionalization with acid or alkali pretreatments [270–272]. The HNO_3 pretreatment substantially increased the number of oxygen groups over the as received CNF, as shown by the production of CO and CO_2 during the TPD experiments and by the (almost three-fold) increase in the support oxygen content (Table 20), in agreement with previous works [201,202]. The increase in the number of acid sites was two times higher than the increase in basic and neutral sites, in agreement with the results of other researchers [270]. The production of CO and CO_2 during the TPD experiments indicate that the majority of the oxygen groups existent over the CNF_o were mainly neutral and basic, whereas over the CNF an almost even distribution between acid and basic/neutral groups was observed.

As shown in Figure 45, XRD patterns of as received and functionalized nanofibers showed a prominent reflexion at ca. 26º and a weak peak at ca. 43-45º assigned to graphitic carbon.
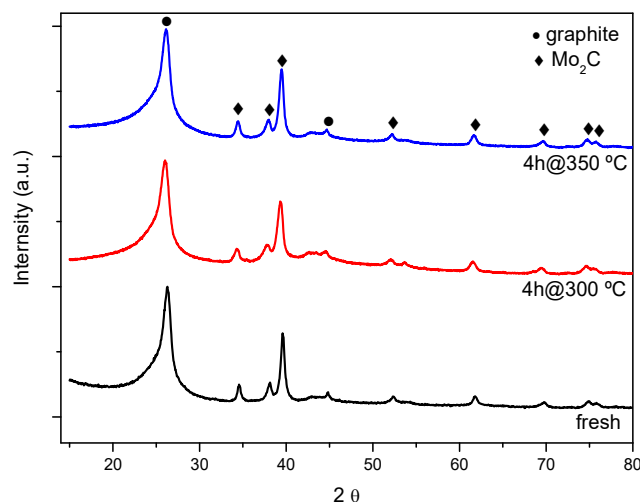
Figure 45 – X-Ray diffraction patterns of the nanofibers and catalyst.

No significative changes in reflexions assigned to carbon were observed after the functionalization treatment with nitric acid. Mo_2C/CNF catalyst also showed a major reflexion intensity at 26º and a minor peak at 45º, both assigned to the graphitic carbon phase. The same diffractograms also revealed seven small peaks assigned to the molybdenum carbide phase (Mo_2C), with reflexions detected at 2θ angles of 34º, 38º, 40º, 52º, 61º, 69º, 75º and 76º, assigned to orthorhombic Mo_2C (lattice parameters a=0.4724 nm, b=0.6002 nm, c=0.5215 nm) [169,273–277]. The size of the crystallites estimated by XRD was ca. 11.2 nm. The molybdenum carbide crystallites in the Mo_2C/CNF catalyst were of the same order of magnitude of those presented in other studies on similar catalysts, having in consideration that values as lower than 3 nm [278] and as high 11.3-12.6 nm [177] have been reported. Moreover, Guil-López et al. [273] synthetized Mo_2C catalysts supported on activated carbon (AC) using similar preparation methodology and obtained particle sizes of comparable magnitude (9-12 nm) to those observed in this work. No other molybdenum phases were detected by XRD in the synthetized catalyst, indicating that the solid phase carburization of the molybdenum oxide used as metal precursor was fully accomplished.

Figure 46 shows the TEM micrographs of the CNF (a and b) and Mo_2C/CNF (c and d).
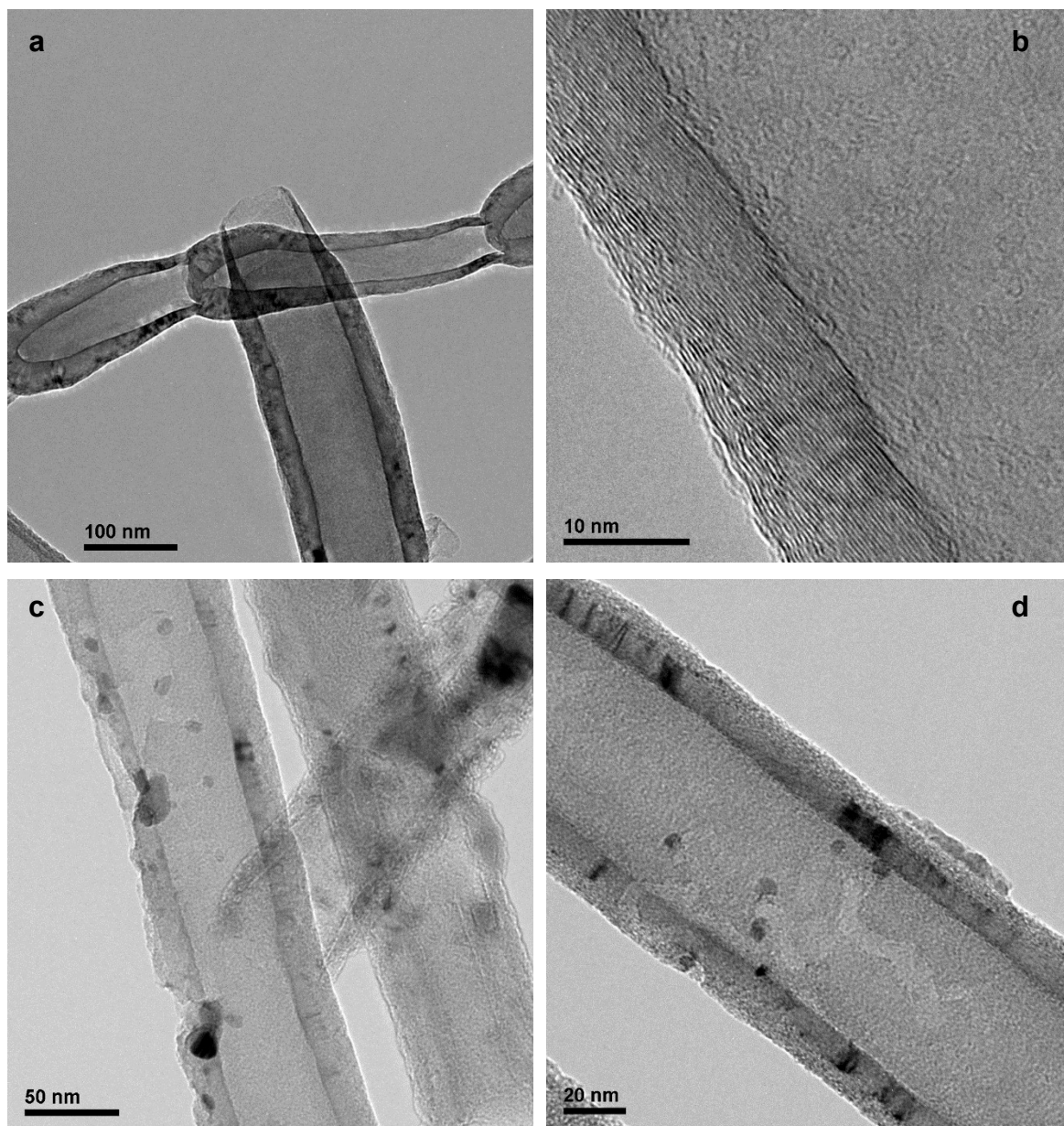
Figure 46 – TEM micrographs of the CNF (a and b) and β-Mo$_2$C/CNF catalyst (c and d).

The CNF had an average diameter of 100 nm with hollow core accounting for almost the entire width (Figure 46 a and b). The Mo$_2$C/CNF catalyst evidenced the presence of Mo$_2$C particles with a relatively narrow distribution between 5 and 12 nm, in agreement with XRD measurements.

Noteworthy, most of the catalytic particles were positioned at inner face of the CNF support (Figure 46 c and d). Apparently, some particles initially deposited at the external walls penetrated the CNF by etching channels from the surface inwards. This phenomenon has been earlier reported by other authors working on several metal-graphene composites [279–286]. It was previously reported in the literature that iron

oxide particles can in fact gasify graphene supports, opening irregular channels throughout the graphene layers during heat treatments at 500 ºC under a reductive hydrogen atmosphere for 2 hours [280–282]. Considering this literature information, the etching of the CNF support in the present study could have been caused by a similar phenomenon. Having in consideration that, in this work, the heat treatment was undertaken at higher temperature (750 ºC) for an equal period of time (2 hours), the molybdenum oxides formed upon the thermal decomposition of the molybdate ions deposited on the CNF surface by incipient wetness impregnation may have gasified the graphene layers during the carburization procedure.

An alternative pathway for the etching of the CNF would be the catalytic hydrogenation of the graphene layers during the carbothermal reduction [282–284]. By this route graphene may have been etched by deposited metal particles at temperatures above 600 ºC in a hydrogen atmosphere. This etching mechanism would involve the dissociation of molecular hydrogen on the metal surface, followed by the reaction of such dissociated hydrogen with the graphene carbon to produce methane [282–284,287].

The high average internal diameter of the CNF used in this work might have contributed for the appearance of the catalytic particles on the inner surface of the support. Xiong et al. [288] prepared cobalt catalysts supported on CNTs and CNFs with internal diameters of 60 and 20 nm (respectively) by incipient wetness impregnation, in which more than 80% of the particles were located at the inner surface of the support materials. Chen et al. [289] impregnated CNT with internal diameters up to 20 nm using aqueous solutions of $Fe(NO_3)_3$ and obtained catalysts in which the Fe^0 and Fe_2C phases were deposited inside the support material. Abbaslou et al. [290] prepared Fe/CNF catalysts and obtained similar results using CNT with internal diameters up to 25 nm. As so, a plausible explanation for the location of the catalytic particles at the inner surface of the CNF could also be the high average internal diameter (up to 100 nm) of the CNF used in this work. This way, the high inner diameter may have allowed the penetration of the impregnation solution through the extremities of the fibers (by capillarity), and the deposition of the precursors over the CNF inner surface, resulting in the formation of inner Mo_2C particles.

5.5.2. Catalytic activity

5.5.2.1 Catalyst performance at 300 ºC

A set of experiments was undertaken for 2 h at 300 ºC over the bare CNF support (pre-treated with HNO_3) and over the Mo_2C/CNF catalyst for 2 and 4 h of reaction. The results of those experiments are presented in Figure 47 in terms of hydrocarbons (toluene, benzene and cyclohexane), anisole, phenol, cresols (*o*-cresol and *p*-cresol) xylenols (2,4-dimethyl-phenol and 2,6-dimethyl-phenol) and catechols (catechol and 3-methyl-catechol).
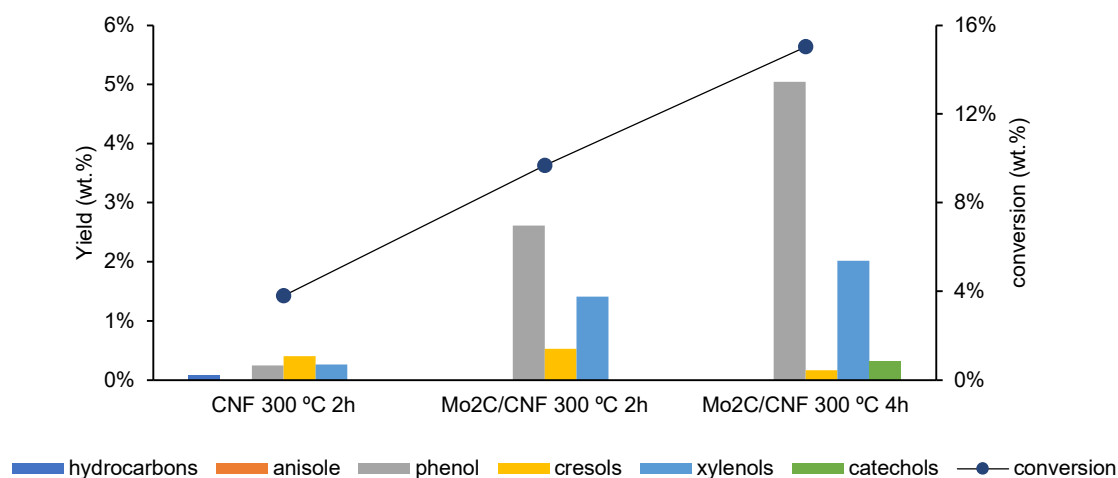
Figure 47 – Conversion and product yields of the main reaction products during the hydrodeoxygenation of guaiacol at 300 ºC over the bare CNF support and the Mo_2C/CNF catalysts upon 2 hours and 4 hours of reaction.

The conversion attained using the Mo_2C/CNF catalyst upon 2 h of reaction was low (9.7%), even though this corresponded to a more than 2.5-fold increase in comparison with conversion achieved over the bare support (3.8%) upon 2 h of reaction. The characterization by gas chromatography allowed the identification and quantification of the 92.5-97.2% of the product pool. The product yields were also significantly different in both runs. In the reaction over the bare support, cresols (*o*-cresol and *p*-cresol) were the main reaction products, followed by phenol and xylenols (2,4-dimethyl-phenol and 2,6-dimethyl-phenol), and a small production toluene was observed. Upon 2 h of reaction over the Mo_2C/CNF, the same main reaction products were detected. The yields of phenol, xylenols and cresols were much higher than over the bare support, and their relative production drastically changed as phenol was the major reaction product followed

by xylenols and cresols, and no toluene production was observed (Figure 47). These observations seem to indicate that the catalyst (having Mo_2C crystallites) favored the reaction pathway of guaiacol conversion into phenol and xylenols, having cresols as intermediate compounds. That is to say, the Mo_2C/CNF catalyst used in this study was more active in disrupting aromatic ether bonds (A-O-CH_3) than in dehydroxylation reactions, because none of the reaction products presented methoxy (OCH_3) groups attached to the phenolic component. Aiming to get a better insight on those aspects, an additional run was performed for 4 hours (Figure 47). The results show that the higher reaction time allowed to increase the conversion (from 9.7 to 15.0%) and the yield of phenol and xylenols increased, while the yield of cresols dropped abruptly. These results confirmed that the increase in phenol yield mainly occurred by demethoxylation of guaiacol, while the increase in the yields of xylenols occurred by methylation of cresols. Catechols also formed upon 4 h of reaction by demethylation of guaiacol, in agreement with the results of other authors while working with similar catalysts [15,177].

Transalkylation reactions are known to be catalyzed by acids [159]. Wandas et al. [291] worked on the HDO of (meta, para and ortho) cresols over Co-Mo/Al_2O_3 catalysts at 360 ºC and 70 bar of H_2, and studied the transformation of these compounds into xylenols and phenol. They concluded that demethylation and methylation reactions comprise elimination-addition reactions involving methyl carbocations adsorbed on acid sites over the catalyst surface. In the case of methylation, cresols adsorb on catalyst acid sites at the hydroxyl group, while the carbocations attack the aromatic rings in the nearest accessible positions [291]. In the case of demethylation, cresols are converted to phenol leaving carbocations derived from their methyl groups on the catalyst surface, which can latter participate in the methylation of other adsorbed molecules [291]. Since the high bonding energy of C-C disfavor its cleavage, in this work the most probable source of methyl carbocations over the catalyst surface would be the demethylation of guaiacol to catechol and/or the demethoxylation of guaiacol into phenol [15,291,292].

5.5.2.2. Catalyst performance at 350 ºC

To study the evolution of product yields over the Mo_2C/CNF catalyst at higher guaiacol conversions, the reaction temperature was increased to 350 ºC. The increase in temperature was accompanied by an increase in the operating pressure since the autoclave reactor was initially charged with the same 20 bar of H_2 (corresponding to a maximum operating pressure of 48 bar at 350 ºC). The contribution of the support material (CNF)

and the catalyst (Mo$_2$C/CNF) to the overall HDO activity may be decoupled by determining the activity the support alone and that of the catalyst containing active metals on the same support, while the contribution of thermal effect (blank) can be determined by not adding any of those materials [293]. The results of those experiments are presented in Figure 48.
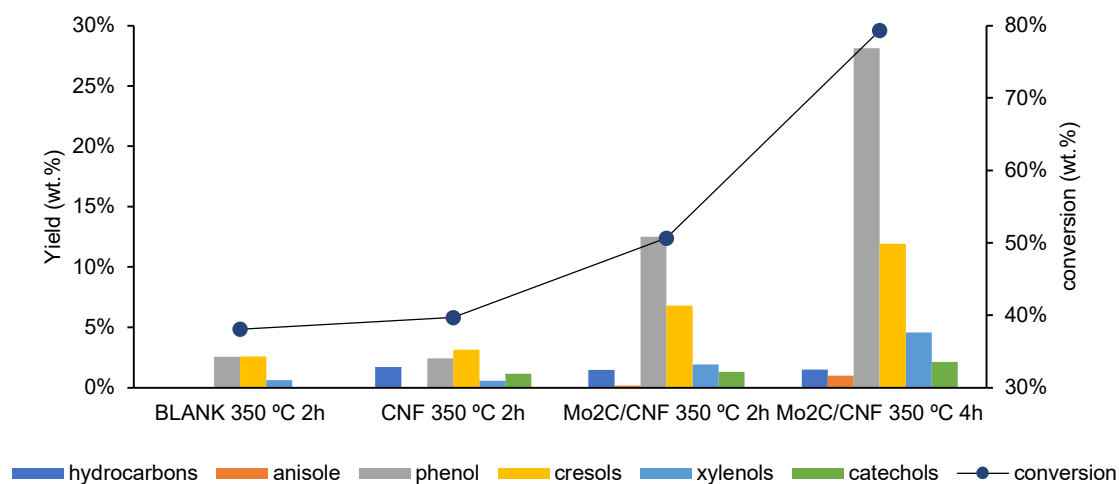

Figure 48 – Conversions and product yields of the main reaction products during the hydrodeoxygenation of guaiacol at 350 ºC, over the bare CNF support the Mo$_2$C/CNF catalyst after 2 and 4 hours of reaction.

When the bare CNF support was used, phenol, cresols, xylenols and toluene were produced, in agreement with the results obtained at 300 ºC. However, a small amount of catechols were also formed by demethylation of guaiacol. It seems that the CNF catalyzed the formation of toluene and catechols at 350 ºC, since that both compounds were not detected in the blank run. These results indicated that the CNF exerted a certain catalytic effect on the hydrodeoxygenation of guaiacol, evidenced by the change in product yields, possibly related to the oxygen sites created by the acid treatment applied to the commercial CNF (Table 20). The catalytic effect towards the production of toluene has been previously reported and attributed to the acid sites created on the surface of the nanofibers by the HNO$_3$ pretreatment [183].

By comparing the experiments in which the bare CNF support was used against those with the Mo$_2$C/CNF catalyst, the conversion increased from 39.7% up to 50.7%. The yields of phenol, cresols, xylenols and catechols were also higher when the catalyst was used, while the yield of hydrocarbons did not change in the presence of catalyst.

Moreover, anisole (which had not been detected the previous experiments) was formed by dehydroxylation of guaiacol in very low quantities at 350 ºC. No hydrogenation products were detected at 350 ºC, in accordance with the experiments performed under milder conditions (300 ºC). However, the yield of cresols was significatntly higher than the yield of xylenols, contrarily to the experiments performed at 300 ºC. Catechols were also produced over the Mo$_2$C/CNF catalysts at 350 ºC as a result of the demethylation of guaiacol, which did not happen upon 2 h of reaction at 300 ºC.

When the reaction time was incresed to 4 h at 350 ºC, the conversion increased from 50.7% to 79.1%. By far, the major reaction products were phenol and cresols followed by xylenols and catechols, as shown in Figure 48. Although the yields of all the other identified compounds increased, the yield of toluene decreased and was accompanied by small productions of benzene and cyclohexane (all aggregated as hydrocarbons in Figure 48) which were possibly formed by demethylation of toluene and hydrogenation of benzene, respectively. Alternative routes for the formation of benzene may have been the demethoxylation of anisole or the dehydroxylation of phenol.

Jongerius et al. [178] worked with Mo$_2$C/CNF catalysts and reported that the formation of phenol during HDO of guaiacol did not involve its demethylation into catechol, but by direct demethoxylation of the guaiacol. However, the formation of phenol having catechol as an intermediate compound has been previously described over Mo$_2$C/AC catalysts [294]. In fact, Santillan-Jimenez et al. [177] reported that the formation of catechols over Mo$_2$C/CNF catalysts occurred by demethylation of guaiacol, and anticipated the possibility of the coexistence of the two reaction pathways, in accordance with the results of this work. The low yields of catechols obtained in this work seem to be supported by the results of other researchers working using transition metal (Ni, Co, Fe, W, Mo) phosphides supported on silica [295] and palladium catalyst supported on zeolites [296], who stated that catechol can only be detected in HDO products when the reaction rate is low, because its conversion is almost immediate. This may help to understand why different reaction pathways have been reported in the literature.

On the other hand, the results obtained at 300 ºC and 350 ºC (Figure 47-Figure 48) indicated that the more severe operating conditions caused a diversification of the HDO reaction pathways, expressed by the formation of catechol as well as by the formation of anisole by demethoxylation and dehydroxylation of guaiacol, respectively [15,293]. In the case of the reactions over the Mo$_2$C/CNF catalysts, the use of harsher operating conditions also led to the formation of toluene most likely by dehydroxylation of cresols.

Apparently, with the increase in the reaction temperature, the activity of the Mo_2C/CNF catalyst was still higher for demethoxylation than for dehydroxylation, while keeping a low hydrogenation activity. Supporting this reasoning was the fact that the yields of cresols and phenol were both high, while the yield of toluene was much higher than the summed yields for benzene and cyclohexane. These results seem to corroborate the hypothesis that the Mo_2C/CNF catalyst used in this study had higher activity in disrupting aromatic ether bonds ($A-O-CH_3$) towards de production of phenol and hydroxyl substituted phenols [15]. However, it should be noted that the compounds identified by gas chromatography accounted only for 79.1% and 69.9% of the HDO products in runs carried out for 2 and 4 hours, respectively. This clearly indicates that a substantial part of the products pool was constituted by nonvolatile compounds impossible to identify by GC-MS, being this effect more evident at larger reaction times and in agreement with the results reported by other authors [178].

Catalysts after HDO test were analyzed by XRD, and the diffractograms and the calculated Mo_2C crystallite size is presented in Figure 49 and Table 21.
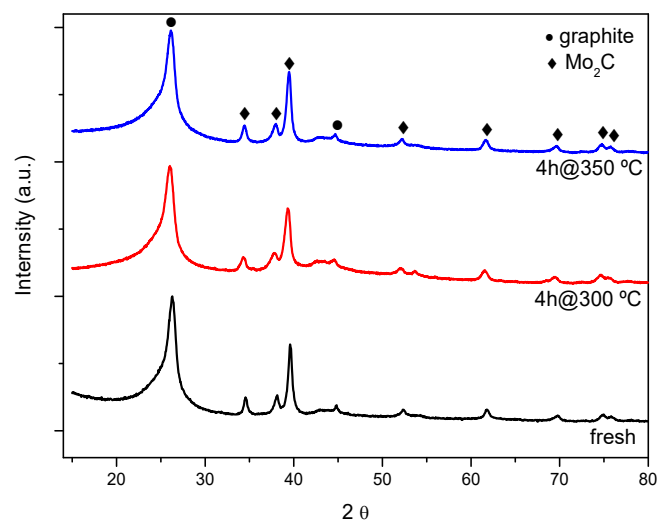
Figure 49 – X-Ray diffraction patterns of fresh and spent catalysts after 4 h reaction tests at 30 ºC and 350 ºC.

Table 21 - Mo₂C crystallite size of the fresh and spent catalysts determined by XRD.

Temperature (ºC)	Reaction time (h)	Pressure (bar)	Mo₂C crystallite size (nm)
fresh catalyst	-	-	11.2
300	2	20	9.7
300	4	20	10.2
350	2	20	7.8
350	4	20	8.6

No noticeable changes were observed by XRD in the catalyst structure after the catalytic tests, given that the only phases detected were Mo_2C and no MoO_x were observed. Besides this, Mo_2C crystallite size presented slightly lower values than in the fresh catalysts, more accentuated at higher temperature, which evidenced that no sintering took place during the HDO reactions.

For the sake of completeness, and aiming to have an estimation of the effect of H_2 pressure in the reaction with the Mo_2C/CNF catalyst, a catalytic test was performed using an initial pressure of 30 bar of H_2 while the temperature was kept at 350 ºC and the reaction time at 2 hours, and the results are compared with the run performed at 20 bar of H_2 in Figure 50.
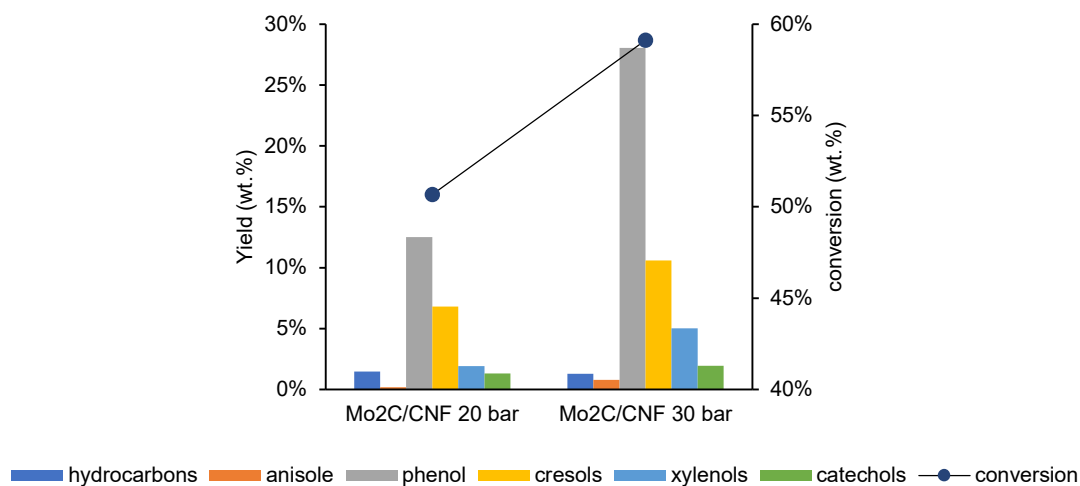
Figure 50 – Conversion and product yields of the main reaction products during the hydrodeoxygenation of guaiacol over the Mo_2C/CNF catalyst at 350 ºC, 2 h reaction time and 20 bar and 30 bar H_2 initial pressure.

The conversion increased when the H_2 pressure was increased, as did the yields of all identified products. These results can be explained by the fact that a higher pressure improves the solubility of hydrogen in the reaction media, this way increasing its availability in the vicinity as well as on the surface of the catalyst, which in turn accelerates the reaction rates while hindering the formation of higher molecular mass products that cannot be analyzed by GC [15,28]. In fact, when the pressure was increased, the conversion of guaiacol increased from 50.7% to 59.1% and the identification of the compounds in the reaction pool increased from 79.1% to 88.6%, indicating that an increase in H_2 pressure inhibited the formation of heavier condensation products, in agreement with the literature [296,297].

During HDO, condensation, polymerization and oligomerization reactions can occur, leading to the formation macromolecules that cannot be analyzed by gas chromatography [15,298]. On the other hand, those macromolecules can undergo cracking, depolymerization and fragmentation reactions leading to the formation of smaller compounds as well as gases [298]. Both macromolecules and gases were not evaluated in this work. Nevertheless, in their recent study Remón et al. [298] reported that the formation of such macromolecules was 81.4 wt.% of the HDO products over bare (acid treated) CNF while operating for 2 h at 300 ºC, 20 bar of H_2 (initial pressure) and 0.15 g of CNF/g of guaiacol. When Mo_2C/CNF (having 12.9 wt.% Mo) was used, the formation of macromolecules decreased to 47.4 wt.% of the HDO products (keeping the other operating conditions constant), while by increasing the H_2 initial pressure to 30 bar that value decreased to 43.5 wt.%. Such results seem to corroborate the results presented in this work.

5.5.3. Overall considerations

The reaction pathways of the guaiacol hydrodeoxygenation over Mo_2C/CNF catalyst comprise dehydroxylation, demethylation, methylation, transalkylation and hydrogenation reactions, and have been thoroughly detailed in the literature [15,28,300,301,29,171,181,291,292,295,296,299]. Based on earlier contributions and all the compounds identified by gas chromatography in this work, the possible reaction routes that support experimental results at 300 ºC are depicted in dashed lines in Figure 51, while those that support the results obtained at 350 ºC are illustrated in both solid and dashed lines.

124
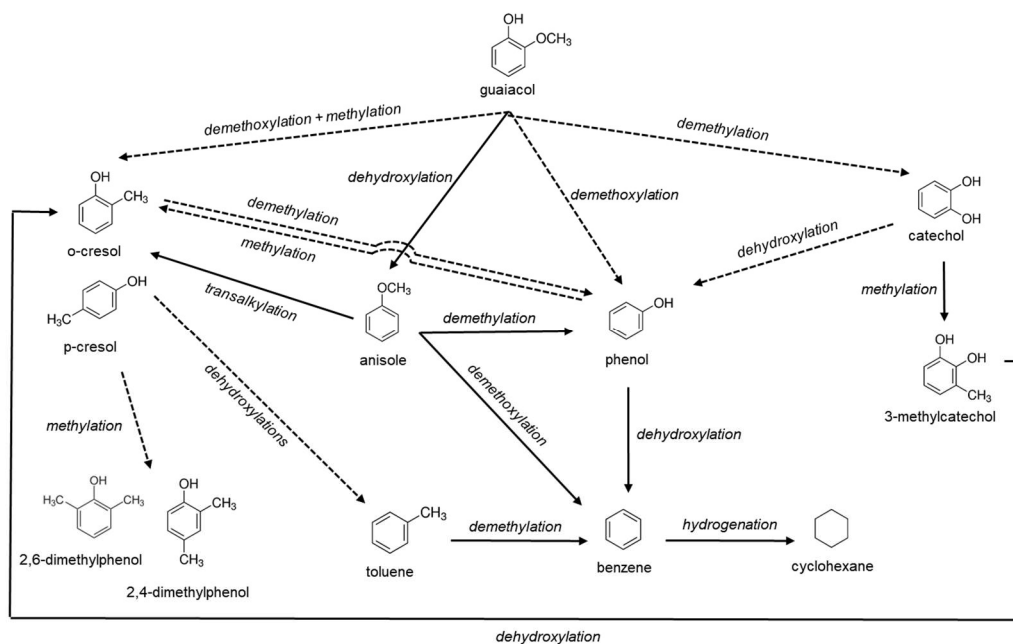
Figure 51 – Scheme of the possible reaction pathways during the hydrodeoxygenation of guaiacol over the Mo₂C/CNF catalysts at 300 ºC (dashed lines) and at 350 ºC (dashed and solid lines) (adapted from [15,28,300,301,29,171,181,291,292,295,296,299]).

Table 22 shows the results found in literature regarding the HDO of guaiacol over Mo₂C/CNF catalysts with those achieved in this work. Globally, the results presented in this work were within the range of others reported in literature regarding the HDO of guaiacol over Mo₂C/CNF catalysts [177,178,183,298,302]. In this work, the major products of guaiacol HDO were phenol and substituted phenols (cresols, xylenols and catechols) while low selectivities for other products where observed (anisole and hydrocarbons), meaning that the chosen approach deserves further investigation in order to improve the conversion of guaiacol into those valuable chemicals.

Table 22 - Comparison of results of hydrodeoxygenation of guaiacol over Mo_2C/CNF catalysts (X_G=guaiacol conversion; Y=mass yield, S=selectivity).

Temperature (°C)	Reaction time (min)	Pressure (H_2 bar)	Mo load (wt.%)	X_G (%)	Y (S) % phenol	Y (S) % anisole	Y (S) % cresols	Y (S) % catechols	Y (S) % xylenols	Y (S) % hydrocarbons	Reference
300-375	0-4	55 [a]	7.5	58.8-99.8	(21.2-56.2)	(5.5-8.5) [b]	(4.3-17.2)	-	-	(0.6-10.1) [c]	[178]
300-350	240	40 [a]	7.5-20	6-99	0.2-48 (3-49)	-	-	0-5.8 (0-19)	-	-	[177]
300	120	20	10	10-67	8-29	0-3	2-4	2-11	1-2	0-7	[183]
300	120	20	10	34.5-80.0	4.3-18.2	2.0-11.2	0.6-3.0	0.4-43.3	0-1.1	4.0-24.5	[302]
270-330	0-180	20-60	12.9	0.4-90.0	1.45-44.7	0.1-4.7	0.2-8.7	0.7-8.9	2.2-48.1	0-34.0	[298]
300-350	120-240	20-30	10	3.8-79.4	0.2-28.1 (6.5-47.4) [d]	0-0.8 (0-1.3) [d]	0.2-11.9 (1.1-17.9) [d]	0-2.1 (0-3.3) [d]	0.3-5.0 (1.4-14.6) [d]	0-1.7 (0-4.3) [d]	This work

[a] operating pressure; [b] including methylated anisole and dimethoxybenzene; [c] including cyclohexanone; [d] S(%)=(Y)/(X_G)×100

126

6. Conclusions and future works

The research carried out in this Doctoral Thesis was devoted to the concept of obtaining biorefinery commodities that could be used as feedstock for the chemical industry. The main objective was to contribute to the development of the syngas and lignin platforms, since syngas can be converted to chemical commodities identical to those that are nowadays derived from petroleum, while lignin is expected to be a source of new aromatic commodities for the industries of the future. The production of syngas was studied by two different routes: (1) the gasification of lignocellulosic charcoal and (2) the oxidative steam reforming (OSR) of glycerol. Then, the production of new aromatic commodities was studied by (1) fractionation of pinewood, (2) depolymerization of a derived lignin precipitate and (3) hydrodeoxygenation (HDO) of a lignin depolymerization product (guaiacol).

1. The gasification of charcoal was experimentally studied in a laboratory scale fluidized bed reactor, varying both steam to carbon (S/C) and equivalence (ER) ratios. The charcoal carbon fraction converted into gas increased when the steam partial pressure was increased in the gasifying mixture up to a S/C=0.625 g/g, while the use of a higher S/C ratio caused negative effects on the properties of the produced gas as well as on the process energy efficiency. The experimental results also showed that carbon conversion into gas increased when ER was increased from 0.25 to 0.35, while the heating value of the gas decreased due to the increase of combustion reactions. Accordingly, both the highest producer gas yield (1.3 Nm^3/kg of charcoal) and the maximum carbon conversion (66.5 wt.%) were achieved using an ER=0.35 and a S/C=0.625 g/g, while the highest H_2 concentration (35 vol.%) was achieved using an ER=0.25 and a S/C=0.625 g/g. The highest H_2 yield (0.412 Nm^3/kg of charcoal or 36.6 g H_2/kg of charcoal), the highest syngas yield (0.8 Nm^3/kg charcoal) and the highest AEE (33.4%) were reached by using S/C=0.625 g/g and ER=0.3. The lowest producer gas tar content (290 mg/Nm^3) was achieved using an ER=0.3 and S/C=0.5 g/g, coinciding with a syngas yield of approximately 0.65 Nm^3/kg of charcoal. Overall, it can be concluded that syngas production from charcoal gasification using O_2/steam mixtures has potential for production of renewable syngas. The main drawback found is the low carbon conversion to gas, that should be further increased. Future

works should consider de use of different reactor configurations (such as entrained flow gasifiers) and higher reaction temperatures.

2. The oxidative steam reforming of glycerol was studied under atmospheric pressure in a laboratory scale tubular quartz reactor setup having a fixed bed configuration. A cobalt aluminate coprecipitated catalyst having a spinel structure was tested in combination with three different bed material fillers, namely alumina, silica and silicon carbide. The heterogeneous thermal decomposition of glycerol and subsequent carbon conversion to gas could be attained (over 83%) using any of the three inexpensive fillers. While using those bulk materials, the best overall results in terms of total gas production, H_2 production and syngas ratio were obtained using γ-Al_2O_3 (266 mg/g feed, 31 mg/g of glycerol H_2/CO=0.94, respectively). The production of CH_4 was noticeable in all three cases, especially in the case of SiC. Regarding the experiments carried out with the Co/Al spinel coprecipitated catalyst, the use of three different activation temperatures within the range of 750-850 ºC did not result in significant differences in the catalyst behavior at a reaction temperature of 750ºC. When compared to the runs in which the catalyst was not dispersed in the bed filler, the use of the catalyst did not result in a significant increase in carbon conversion to gas, but the product gas distribution was significantly affected, thus proving the role exerted by the catalyst. The use of silica as bed filler in catalytic experiments allowed for the highest hydrogen production and syngas ratio (63 mg H_2/g glycerol, H_2/CO=2.53) as compared to alumina (54 mg H_2/g glycerol, H_2/CO=2.15) and silicon carbide (39 mg H_2/g glycerol, H_2/CO=1.08). In any case, all bed fillers allowed for carbon conversion to gases higher than 91% in the catalytic experiments. The overall product gas formation during 4 h time on stream of the catalytic oxidative steam reforming of glycerol conducted at 550 ºC, 650 ºC and 750 ºC decreased with the temperature increase. Conversely, the carbon conversion to gas increased slightly with increased temperatures. As a result of these two different patterns the lowest tested temperature (550 ºC) allowed for the highest hydrogen production (90 mg H_2/g glycerol) and H_2/CO (15.3) due to the better catalyst stability. By microscopy techniques, it was observed that the structure of the catalyst after reaction drastically changed in relation to that of the fresh catalyst. A single run using the Co/Al spinel catalyst in the oxidative steam reforming of glycerol resulted in

carbon encapsulation covering of the catalyst particles, which had a very clearly defined hexagonal shape conformed over the surface of the catalyst particles. Upon four reuse and regeneration cycles, the catalyst could effectively maintain its activity in the oxidative steam reforming of glycerol for a combined total time of 20 h on stream. Upon the regeneration of the catalyst by oxidation (with a 6 vol.% O_2 in N_2 gas mixture), the core-shell structures were completely transformed and Co species migrated to the surface over the Co spinel structure, thus acting like a Co reservoir and hence explaining the complete recovery of activity once the catalysts were regenerated and subsequently activated before the next reforming reaction cycle. These results were promising in terms of the applicability of these Co/Al spinel catalysts. Future works should consider the use of more concentrated glycerol/water mixtures, as well as the use of crude glycerol.

3. The fractionation of *Pinus pinaster* wood (PPW) was studied by two different routes: (1) a two-step system by soda ethanol organosolv (SEOS) followed by lignin precipitation (LP) and (2) a three-step procedure encompassing autohydrolysis (AH) followed by SEOS and LP. The results showed that AH was selective in the removal of hemicellulose from lignocellulosic materials, while SEOS was selective in the removal of lignin. When the three-step fractionation was applied, up to 17 wt.% of the original biomass was dissolved in AH liquors. Pulps having hemicellulose contents as low as 3 wt.% and lignin contents as low as 5 wt.% were produced by sequential AH and SEOS, while LP products had lignin contents higher than 98 wt.%. This route allowed to recover up to 59 wt.% of the hemicelluloses, 66 wt.% of the cellulose and 77 wt.% of the lignin in AH liquors, pulps and precipitates, respectively. The produced AH liquors have potential for the production of furfural and HMF by acidic dehydration through the C5/C6 biorefinery platforms. On the other hand, the pulps produced from autohydrolyzed solids have potential for the direct use in the manufacturing of dissolving pulps, besides their possible use in the production of C6 platform chemicals. The lignins obtained by the three-step process had a very high purity ($\simeq$97%) and no carbohydrate contamination, but the ash contents may hamper their use in heterogeneous catalyzed reactions, so different lignin separation approaches should be considered in future works in other to address this issue. The results evidenced that sodium hydroxide is more effective in the fractionation

of softwoods than sulfuric acid if cellulose and lignin purities are equally desired targets. These results show the potential of the three-step fractionation towards a biorefinery-based bioeconomy. Future works should consider the use of the 3-step fractionation with hardwoods.

4. The depolymerization of the lignin produced in highest yield during the fractionation study of pinewood (AH at 175 ºC followed by SEOS with 35% ethanol) was attempted using different catalytic strategies. A two-step procedure was used, encompassing the base catalyzed depolymerization with NaOH (at 220 and 250 ºC) followed by hydrogenolysis over Ru/C catalyst (at 250 ºC). The maximum monomer yield (7.3 wt.%) was achieved over Ru/C at 250 ºC for 30 min having corresponding weight (M_w) and number (M_n) average molecular masses 818 and 468 g/mol. A possible explanation for such results may have been related with the extraction process used to obtain the lignin used in this work (AH followed by SEOS), which seems to have resulted in a highly condensed non-reactive lignin material. It was anticipated that harsher conditions (temperature and pressure) could eventually be used to improve the monomers yields, which should be addressed in future works.

5. The hydrodeoxygenation (HDO) of guaiacol was studied over a molybdenum carbide catalyst supported on commercial carbon nanofibers (Mo_2C/CNF) under different reaction conditions. The effects of temperature, pressure and reaction time on the guaiacol conversion and product yields were studied. The increase in the reaction temperature from 300 ºC to 350 ºC caused a diversification of the reaction pathways and consequently in the number of products and their yields. The highest guaiacol conversion (79 wt.%) was achieved upon 4 h of reaction at 350 ºC and 20 bar of H_2 (initial pressure). With the increase in H_2 initial pressure (from 20 to 30 bar), the conversion of guaiacol increased from 50.7% to 59.1% upon 2 h reactions at 350 ºC, and the identification of the compounds in the reaction pool increased from 79.1% to 88.6%, indicating that the increase in H_2 pressure inhibited the formation of heavier condensation products. Etching of carbonaceous materials involving molybdenum was observed, which was possibly related with the formation of molybdenum carbides by carburization in hydrogen atmosphere. The Mo_2C/CNF catalyst showed higher selectivity for

demethoxylation products than to dehydroxylation products. The XRD analysis of spent catalysts did not reveal any significant changes as compared to the fresh catalyst. The main reaction products were phenol (0.2-28.1 wt.%), cresols (0.2-11.9 wt.%), xylenols (0-5.0 wt.%) and catechols (0-2.1 wt.%), meaning that the chosen approach deserves further investigation in order to improve the conversion of guaiacol into those valuable chemicals.

References

[1] European Commission, Innovating for Sustainable Growth: A Bioeconomy for Europe, 2012. https://doi.org/10.2777/6462.

[2] J.H. Clark, R. Luque, A.S. Matharu, Green Chemistry, Biofuels, and Biorefinery, Annu. Rev. Chem. Biomol. Eng. 3 (2012) 183–207. https://doi.org/10.1146/annurev-chembioeng-062011-081014.

[3] F. Trippe, M. Fröhling, F. Schultmann, R. Stahl, E. Henrich, Techno-economic assessment of gasification as a process step within biomass-to-liquid (BtL) fuel and chemicals production, Fuel Process. Technol. 92 (2011) 2169–2184. https://doi.org/10.1016/j.fuproc.2011.06.026.

[4] World Commission on Environment and Development, Our common future, Oxford University Press, New York, 1989. https://doi.org/10.1002/jid.3380010208.

[5] European Commission, Closing the loop – An EU action plan for the circular economy, (2015) 1–21. http://eur-lex.europa.eu/legal-content/EN/TXT/?uri=CELEX:52015DC0614 (accessed September 24, 2020).

[6] M. Carus, L. Dammer, The Circular Bioeconomy—Concepts, Opportunities, and Limitations, Ind. Biotechnol. 14 (2018) 83–91. https://doi.org/10.1089/ind.2018.29121.mca.

[7] European Commission, A sustainable Bioeconomy for Europe: strengthening the connection between economy, society and the environment, 2018. https://doi.org/10.2777/478385.

[8] M. Fantini, Biomass Availability, Potential and Characteristics, in: M. Rabaçal, A.F. Ferreira, C.A.M. Silva, M. Costa (Eds.), Biorefineries Target. Energy, High Value Prod. Waste Valoris., Springer International Publishing, Cham, 2017: pp. 21–54. https://doi.org/10.1007/978-3-319-48288-0_2.

[9] European Parliament; European Council, Directive 2009/28/EC on the promotion of the use of energy from renewable sources, Off. J. Eur. Union. 140 (2009) 16–62. https://doi.org/10.3000/17252555.L_2009.140.eng.

[10] J. Ren, J.P. Cao, X.Y. Zhao, F.L. Yang, X.Y. Wei, Recent advances in syngas production from biomass catalytic gasification: A critical review on reactors, catalysts, catalytic mechanisms and mathematical models, Renew. Sustain. Energy Rev. 116 (2019) 109426. https://doi.org/10.1016/j.rser.2019.109426.

[11] V. Claude, C. Courson, M. Köhler, S.D. Lambert, Overview and Essentials of

Biomass Gasification Technologies and Their Catalytic Cleaning Methods, Energy and Fuels. 30 (2016) 8791–8814. https://doi.org/10.1021/acs.energyfuels.6b01642.

[12] J. Barber, Biological solar energy, Philos. Trans. R. Soc. A Math. Phys. Eng. Sci. 365 (2007) 1007–1023. https://doi.org/10.1098/rsta.2006.1962.

[13] F. Cherubini, The biorefinery concept: Using biomass instead of oil for producing energy and chemicals, Energy Convers. Manag. 51 (2010) 1412–1421. https://doi.org/10.1016/j.enconman.2010.01.015.

[14] E. de Jong, A. Higson, P. Walsh, M. Wellisch, Task 42 Biobased Chemicals - Value Added Products from Biorefineries, 2011.

[15] J. Zakzeski, P.C.A. Bruijnincx, A.L. Jongerius, B.M. Weckhuysen, The catalytic valorization of lignin for the production of renewable chemicals, Chem. Rev. 110 (2010) 3552–3599. https://doi.org/10.1021/cr900354u.

[16] S.H. Krishna, K. Huang, K.J. Barnett, J. He, C.T. Maravelias, J.A. Dumesic, G.W. Huber, M. De bruyn, B.M. Weckhuysen, Oxygenated commodity chemicals from chemo-catalytic conversion of biomass derived heterocycles, AIChE J. 64 (2018) 1910–1922. https://doi.org/10.1002/aic.16172.

[17] F. Cherubini, G. Jungmeier, M. Wellisch, T. Willke, I. Skiadas, R. Van Ree, E. de Jong, Toward a common classification approach for biorefinery systems, 2009. https://doi.org/10.1002/bbb.172.

[18] S. Takkellapati, T. Li, M.A. Gonzalez, An overview of biorefinery-derived platform chemicals from a cellulose and hemicellulose biorefinery, Clean Technol. Environ. Policy. 20 (2018) 1615–1630. https://doi.org/10.1007/s10098-018-1568-5.

[19] A. V. Bridgwater, Review of fast pyrolysis of biomass and product upgrading, Biomass and Bioenergy. 38 (2012) 68–94. https://doi.org/10.1016/j.biombioe.2011.01.048.

[20] E. Butler, G. Devlin, D. Meier, K. McDonnell, A review of recent laboratory research and commercial developments in fast pyrolysis and upgrading, Renew. Sustain. Energy Rev. 15 (2011) 4171–4186. https://doi.org/10.1016/j.rser.2011.07.035.

[21] F. Trippe, M. Fröhling, F. Schultmann, R. Stahl, E. Henrich, Techno-economic analysis of fast pyrolysis as a process step within biomass-to-liquid fuel production, Waste and Biomass Valorization. 1 (2010) 415–430.
133

https://doi.org/10.1007/s12649-010-9039-1.

[22] Q. Lu, W.Z. Li, X.F. Zhu, Overview of fuel properties of biomass fast pyrolysis oils, Energy Convers. Manag. 50 (2009) 1376–1383. https://doi.org/10.1016/j.enconman.2009.01.001.

[23] K.H. Kim, T.S. Kim, S.M. Lee, D. Choi, H. Yeo, I.G. Choi, J.W. Choi, Comparison of physicochemical features of biooils and biochars produced from various woody biomasses by fast pyrolysis, Renew. Energy. 50 (2013) 188–195. https://doi.org/10.1016/j.renene.2012.06.030.

[24] A. Dimitriadis, S. Bezergianni, Hydrothermal liquefaction of various biomass and waste feedstocks for biocrude production: A state of the art review, Renew. Sustain. Energy Rev. 68 (2017) 113–125. https://doi.org/10.1016/j.rser.2016.09.120.

[25] M.K. Hrnčič, G. Kravanja, Ž. Knez, Hydrothermal treatment of biomass for energy and chemicals, Energy. 116 (2016) 1312–1322. https://doi.org/10.1016/j.energy.2016.06.148.

[26] K. Tekin, S. Karagöz, S. Bektaş, A review of hydrothermal biomass processing, Renew. Sustain. Energy Rev. 40 (2014) 673–687. https://doi.org/10.1016/j.rser.2014.07.216.

[27] D.C. Elliott, P. Biller, A.B. Ross, A.J. Schmidt, S.B. Jones, Hydrothermal liquefaction of biomass: Developments from batch to continuous process, Bioresour. Technol. 178 (2015) 147–156. https://doi.org/10.1016/j.biortech.2014.09.132.

[28] P.M. Mortensen, J.D. Grunwaldt, P.A. Jensen, K.G. Knudsen, A.D. Jensen, A review of catalytic upgrading of bio-oil to engine fuels, Appl. Catal. A Gen. 407 (2011) 1–19. https://doi.org/10.1016/j.apcata.2011.08.046.

[29] E. Furimsky, Catalytic hydrodeoxygenation, Appl. Catal. A Gen. 199 (2000) 147–190. https://doi.org/10.1016/S0926-860X(99)00555-4.

[30] Y. Zhu, M.J. Biddy, S.B. Jones, D.C. Elliott, A.J. Schmidt, Techno-economic analysis of liquid fuel production from woody biomass via hydrothermal liquefaction (HTL) and upgrading, Appl. Energy. 129 (2014) 384–394. https://doi.org/10.1016/j.apenergy.2014.03.053.

[31] J.A. Ramirez, R.J. Brown, T.J. Rainey, A review of hydrothermal liquefaction bio-crude properties and prospects for upgrading to transportation fuels, Energies. 8 (2015) 6765–6794. https://doi.org/10.3390/en8076765.

[32] F. Bimbela, M. Oliva, J. Ruiz, L. García, J. Arauzo, Hydrogen production by catalytic steam reforming of acetic acid, a model compound of biomass pyrolysis liquids, J. Anal. Appl. Pyrolysis. 79 (2007) 112–120. https://doi.org/10.1016/j.jaap.2006.11.006.

[33] F. Bimbela, J. Ábrego, R. Puerta, L. García, J. Arauzo, Catalytic steam reforming of the aqueous fraction of bio-oil using Ni-Ce/Mg-Al catalysts, Appl. Catal. B Environ. 209 (2017) 346–357. https://doi.org/10.1016/j.apcatb.2017.03.009.

[34] S. Sarker, F. Bimbela, J.L. Sánchez, H.K. Nielsen, Characterization and pilot scale fluidized bed gasification of herbaceous biomass: A case study on alfalfa pellets, Energy Convers. Manag. 91 (2015) 451–458. https://doi.org/10.1016/j.enconman.2014.12.034.

[35] L. García, M.L. Salvador, J. Arauzo, R. Bilbao, Catalytic steam gasification of pine sawdust. Effect of catalyst weight/biomass flow rate and steam/biomass ratios on gas production and composition, Energy and Fuels. 13 (1999) 851–859. https://doi.org/10.1021/ef980250p.

[36] L. García, M.L. Salvador, J. Arauzo, R. Bilbao, Influence of catalyst weight/biomass flow rate ratio on gas production in the catalytic pyrolysis of pine sawdust at low temperatures, Ind. Eng. Chem. Res. 37 (1998) 3812–3819. https://doi.org/10.1021/ie9801960.

[37] J. Gil, P. Aznar, M.A. Caballero, E. Francés, with Steam - Oxygen Mixtures . Product Distribution for, Energy & Fuels Fuels. 11 (1997) 1109–1118.

[38] T. Li, M. Virginie, A.Y. Khodakov, Effect of potassium promotion on the structure and performance of alumina supported carburized molybdenum catalysts for Fischer-Tropsch synthesis, Appl. Catal. A Gen. 542 (2017) 154–162. https://doi.org/10.1016/j.apcata.2017.05.018.

[39] D.V.N. Vo, T.H. Nguyen, E.M. Kennedy, B.Z. Dlugogorski, A.A. Adesina, Fischer-Tropsch synthesis: Effect of promoter type on alumina-supported Mo carbide catalysts, Catal. Today. 175 (2011) 450–459. https://doi.org/10.1016/j.cattod.2011.04.045.

[40] B.M. F. Bustamante, R. Enick, K. Rothenberger, B. Howard, A. Cugini, M. Ciocco, Kinetic study of the reverse water gas-shift reaction in high-temperature, high pressure homogeneous systems, Fuel Chem. Div. Prepr. 47 (2002) 663–664.

[41] J. Sánchez-Hervás; M. Maroño; A. Cabanillas, State of the Art Review on Separation of Hydrogen by Membranes and Water Gas Shift Reaction Catalysts,

Madrid, Spain, 2011.

[42] E.M. Grieco, G. Baldi, Effects of tar model compounds on commercial water gas shift catalysts, Chem. Eng. Res. Des. 90 (2012) 1997–2001. https://doi.org/10.1016/j.cherd.2012.04.004.

[43] D. Lima; F. Zanella; M. Lenzi; P. Ndiaye, Modeling and Simulation of Water Gas Shift Reactor: An Industrial Case, in: V. Patel (Ed.), Petrochemicals, InTech, Rijeka, Croatia, 2012: pp. 53–74.

[44] P. Haro, F. Trippe, R. Stahl, E. Henrich, Bio-syngas to gasoline and olefins via DME - A comprehensive techno-economic assessment, Appl. Energy. 108 (2013) 54–65. https://doi.org/10.1016/j.apenergy.2013.03.015.

[45] S. Ilias, A. Bhan, Mechanism of the catalytic conversion of methanol to hydrocarbons, ACS Catal. 3 (2013) 18–31. https://doi.org/10.1021/cs3006583.

[46] T. Mokrani, M. Scurrell, Gas Conversion to Liquid Fuels and Chemicals: The Methanol Route-Catalysis and Processes Development, Catal. Rev. 51 (2009) 1–145. https://doi.org/10.1080/01614940802477524.

[47] I.L. Motta, N.T. Miranda, R. Maciel Filho, M.R. Wolf Maciel, Biomass gasification in fluidized beds: A review of biomass moisture content and operating pressure effects, Renew. Sustain. Energy Rev. 94 (2018) 998–1023. https://doi.org/10.1016/j.rser.2018.06.042.

[48] P. Basu, Tar Production and Destruction, in: Biomass Gasif. Des. Handb., Elsevier, Oxford, UK, 2010: pp. 97–116. https://doi.org/10.1016/B978-0-12-374988-8.00004-0.

[49] M.L. Valderrama Rios, A.M. González, E.E.S. Lora, O.A. Almazán del Olmo, Reduction of tar generated during biomass gasification: A review, Biomass and Bioenergy. 108 (2018) 345–370. https://doi.org/10.1016/j.biombioe.2017.12.002.

[50] G. García, E. Campos, I. Fonts, J.L. Sánchez, J. Herguido, Gas catalytic upgrading in a two-zone fluidized bed reactor coupled to a cogasification plant, Energy and Fuels. 27 (2013) 2835–2845. https://doi.org/10.1021/ef400227z.

[51] G. Taralas, Catalytic steam cracking of n-heptane with special reference to the effect of calcined dolomite, Ind. Eng. Chem. Res. 35 (1996) 2121–2126. https://doi.org/10.1021/ie950705n.

[52] M.P. Aznar, J. Corella, J. Delgado, J. Lahoz, Improved Steam Gasification of Lignocellulosic Residues in a Fluidized Bed with Commercial Steam Reforming Catalysts, Ind. Eng. Chem. Res. 32 (1993) 1–10.

136

https://doi.org/10.1021/ie00013a001.

[53] L. Devi, K.J. Ptasinski, F.J.J.G. Janssen, Pretreated olivine as tar removal catalyst for biomass gasifiers: Investigation using naphthalene as model biomass tar, Fuel Process. Technol. 86 (2005) 707–730. https://doi.org/10.1016/j.fuproc.2004.07.001.

[54] J. Arauzo, D. Radlein, J. Piskorz, D.S. Scott, A New Catalyst for the Catalytic Gasification of Biomass, Energy and Fuels. 8 (1994) 1192–1196. https://doi.org/10.1021/ef00048a005.

[55] M. Garg, J. Piskorz, D.S. Scott, D. Radlein, The hydrogasification of wood, Ind. Eng. Chem. Res. 27 (1988) 256–264. https://doi.org/10.1021/ie00074a009.

[56] P.J. Woolcock, R.C. Brown, A review of cleaning technologies for biomass-derived syngas, Biomass and Bioenergy. 52 (2013) 54–84. https://doi.org/10.1016/j.biombioe.2013.02.036.

[57] J. Corella, J.M. Toledo, G. Molina, A review on dual fluidized-bed biomass gasifiers, Ind. Eng. Chem. Res. 46 (2007) 6831–6839. https://doi.org/10.1021/ie0705507.

[58] G. Van Rossum, S.R.A. Kersten, W.P.M. Van Swaaij, Staged catalytic gasification/steam reforming of pyrolysis oil, Ind. Eng. Chem. Res. 48 (2009) 5857–5866. https://doi.org/10.1021/ie900194j.

[59] G. García, A. Monzón, F. Bimbela, J.L. Sánchez, J. Ábrego, Desulfurization and catalytic gas cleaning in fluidized-bed co-gasification of sewage sludge-coal blends, Energy and Fuels. 27 (2013) 2846–2856. https://doi.org/10.1021/ef400259g.

[60] T. Rodrigues, A. Braghini Junior, Charcoal: A discussion on carbonization kilns, J. Anal. Appl. Pyrolysis. 143 (2019). https://doi.org/10.1016/j.jaap.2019.104670.

[61] H. den Uil, CASST: A New and Advanced Process for Biomass Gasification, in: A. V. Bridgwater (Ed.), Prog. Thermochem. Biomass Convers., Blackwell Science Ltd, Oxford, UK, 2001: pp. 287–297. https://doi.org/10.1002/9780470694954.ch21.

[62] A. Nzihou, B. Stanmore, P. Sharrock, A review of catalysts for the gasification of biomass char, with some reference to coal, Energy. 58 (2013) 305–317. https://doi.org/10.1016/j.energy.2013.05.057.

[63] L. Wang, J. Sandquist, G. Varhegyi, B. Matas Güell, CO2 gasification of chars prepared from wood and forest residue: A kinetic study, Energy and Fuels. 27

(2013) 6098–6107. https://doi.org/10.1021/ef401118f.

[64]   M. Kajita, T. Kimura, K. Norinaga, C.Z. Li, J.I. Hayashi, Catalytic and noncatalytic mechanisms in steam gasification of char from the pyrolysis of biomass, Energy and Fuels. 24 (2010) 108–116. https://doi.org/10.1021/ef900513a.

[65]   M.M. Wright, J.A. Satrio, R.C. Brown, D.E. Daugaard, D.D. Hsu, Techno-economic analysis of biomass fast pyrolysis to liquid fuels, Golden, Colorado, USA, 2010.

[66]   H. Abdullah, H. Wu, Biochar as a Fuel: 1. Properties and Grindability of Biochars Produced from the Pyrolysis of Mallee Wood under Slow-Heating Conditions, Energy & Fuels. 23 (2009) 4174–4181. https://doi.org/10.1021/ef900494t.

[67]   R.C. de Miranda, R. Bailis, A. de O. Vilela, Cogenerating electricity from charcoaling: A promising new advanced technology, Energy Sustain. Dev. 17 (2013) 171–176. https://doi.org/10.1016/j.esd.2012.11.003.

[68]   H. Haykiri-Acma, S. Yaman, S. Kucukbayrak, Gasification of biomass chars in steam–nitrogen mixture, Energy Convers. Manag. 47 (2006) 1004–1013. https://doi.org/10.1016/j.enconman.2005.06.003.

[69]   P. Nanou, H.E. Gutiérrez Murillo, W.P.M. Van Swaaij, G. Van Rossum, S.R.A. Kersten, Intrinsic reactivity of biomass-derived char under steam gasification conditions-potential of wood ash as catalyst, Chem. Eng. J. 217 (2013) 289–299. https://doi.org/10.1016/j.cej.2012.12.012.

[70]   F. Mermoud, S. Salvador, L. Van de Steene, F. Golfier, Influence of the pyrolysis heating rate on the steam gasification rate of large wood char particles, Fuel. 85 (2006) 1473–1482. https://doi.org/10.1016/j.fuel.2005.12.004.

[71]   S.T. Chaudhari, A.K. Dalai, N.N. Bakhshi, Production of Hydrogen and/or Syngas ($H_2 + CO$) via Steam Gasification of Biomass-Derived Chars, Energy & Fuels. 17 (2003) 1062–1067. https://doi.org/10.1021/ef030017d.

[72]   S.T. Chaudhari, S.K. Bej, N.N. Bakhshi, A.K. Dalai, Steam Gasification of Biomass-Derived Char for the Production of Carbon Monoxide-Rich Synthesis Gas, Energy & Fuels. 15 (2001) 736–742. https://doi.org/10.1021/ef000278c.

[73]   F. Yan, S. yi Luo, Z. quan Hu, B. Xiao, G. Cheng, Hydrogen-rich gas production by steam gasification of char from biomass fast pyrolysis in a fixed-bed reactor: Influence of temperature and steam on hydrogen yield and syngas composition, Bioresour. Technol. 101 (2010) 5633–5637.

138

https://doi.org/10.1016/j.biortech.2010.02.025.

[74]   S. Nilsson, A. Gómez-Barea, D. Fuentes-Cano, M. Campoy, Gasification kinetics of char from olive tree pruning in fluidized bed, Fuel. 125 (2014) 192–199. https://doi.org/10.1016/j.fuel.2014.02.006.

[75]   M. Klaas, C. Greenhalf, L. Ferrante, C. Briens, F. Berruti, Optimisation of hydrogen production by steam reforming of chars derived from lumber and agricultural residues, Int. J. Hydrogen Energy. 40 (2015) 3642–3647. https://doi.org/10.1016/j.ijhydene.2014.12.086.

[76]   Z. Ma, S. Zhang, D. Xie, Y. Yan, Z. Ren, Hydrogen Production from Bio-Char via Steam Gasification in a Fluidized-Bed Reactor, Chem. Eng. Technol. 36 (2013) 1599–1602. https://doi.org/10.1002/ceat.201300057.

[77]   H. De Lasa, E. Salaices, J. Mazumder, R. Lucky, Catalytic steam gasification of biomass: Catalysts, thermodynamics and kinetics, Chem. Rev. 111 (2011) 5404–5433. https://doi.org/10.1021/cr200024w.

[78]   N. Gil-Lalaguna, J.L. Sánchez, M.B. Murillo, E. Rodríguez, G. Gea, Air-steam gasification of sewage sludge in a fluidized bed. Influence of some operating conditions, Chem. Eng. J. 248 (2014) 373–382. https://doi.org/10.1016/j.cej.2014.03.055.

[79]   N. Gil-Lalaguna, J.L. Sánchez, M.B. Murillo, V. Ruiz, G. Gea, Air-steam gasification of char derived from sewage sludge pyrolysis. Comparison with the gasification of sewage sludge, Fuel. 129 (2014) 147–155. https://doi.org/10.1016/j.fuel.2014.03.059.

[80]   R. Moreira; A. Portugal; N. Gil-Lalaguna; F. Bimbela; J.L. Sánchez, Preliminary study on pyrolysis char gasification using bubbling fluidized bed gasifier, in: 23th Eur. Biomass Conf., Götenborg, Netherlands, 2015: pp. 660–663.

[81]   European Parliament, Directive 2009/30/EC - amending Directive 98/70/EC as regards the specification of petrol, diesel and gas-oil and introducing a mechanism to monitor and reduce greenhouse gas emissions, Off. J. Eur. Union. (2009) 88–113. https://eur-lex.europa.eu/legal-content/EN/TXT/PDF/?uri=CELEX:32009L0030&from=EN.

[82]   European Parliament, Directive 98/70/EC of the European Parliamente and of the Council of 13 October 1998 relating to the quality of petrol and diesel fuels and amending Council Directive 93/12/EEC [1998] OJ L 350, Off. J. Eur. Union. (2011) 1–41. http://eur-lex.europa.eu/legal-

content/EN/TXT/HTML/?uri=CELEX:01998L0070-20110622&rid=1.

[83]   European Parliament, Directive 2015/1513 of the European Parliament and of the Council, Off. J. Eur. Union. L239 (2015) 1–29. https://doi.org/http://eur-lex.europa.eu/pri/en/oj/dat/2003/l_285/l_28520031101en00330037.pdf.

[84]   Fuels Europe, Refining Products for our everyday life, Statistical Report 2016, Belgium, 2016.

[85]   P.D. Vaidya, A.E. Rodrigues, Glycerol reforming for hydrogen production: A review, Chem. Eng. Technol. 32 (2009) 1463–1469. https://doi.org/10.1002/ceat.200900120.

[86]   B. Dou, Y. Song, C. Wang, H. Chen, Y. Xu, Hydrogen production from catalytic steam reforming of biodiesel byproduct glycerol: Issues and challenges, Renew. Sustain. Energy Rev. 30 (2014) 950–960. https://doi.org/10.1016/j.rser.2013.11.029.

[87]   G. Bagnato, A. Iulianelli, A. Sanna, A. Basile, Glycerol Production and Transformation: A Critical Review with Particular Emphasis on Glycerol Reforming Reaction for Producing Hydrogen in Conventional and Membrane Reactors, Membranes (Basel). 7 (2017) 17. https://doi.org/10.3390/membranes7020017.

[88]   J.M. Silva, M.A. Soria, L.M. Madeira, Challenges and strategies for optimization of glycerol steam reforming process, Renew. Sustain. Energy Rev. 42 (2015) 1187–1213. https://doi.org/10.1016/j.rser.2014.10.084.

[89]   N.D. Charisiou, K. Polychronopoulou, A. Asif, M.A. Goula, The potential of glycerol and phenol towards H2 production using steam reforming reaction: A review, Surf. Coatings Technol. 352 (2018) 92–111. https://doi.org/10.1016/j.surfcoat.2018.08.008.

[90]   F. Bimbela, M. Oliva, J. Ruiz, L. García, J. Arauzo, Hydrogen production via catalytic steam reforming of the aqueous fraction of bio-oil using nickel-based coprecipitated catalysts, Int. J. Hydrogen Energy. 38 (2013) 14476–14487. https://doi.org/10.1016/j.ijhydene.2013.09.038.

[91]   A. Gallo, C. Pirovano, P. Ferrini, M. Marelli, R. Psaro, S. Santangelo, G. Faggio, V. Dal Santo, Influence of reaction parameters on the activity of ruthenium based catalysts for glycerol steam reforming, Appl. Catal. B Environ. 121–122 (2012) 40–49. https://doi.org/10.1016/j.apcatb.2012.03.013.

[92]   A. Moral, I. Reyero, C. Alfaro, F. Bimbela, L.M. Gandía, Syngas production by

means of biogas catalytic partial oxidation and dry reforming using Rh-based catalysts, Catal. Today. 299 (2018) 280–288. https://doi.org/10.1016/j.cattod.2017.03.049.

[93] A. Delparish, S. Koc, B.S. Caglayan, A.K. Avci, Oxidative steam reforming of glycerol to synthesis gas in a microchannel reactor, Catal. Today. 323 (2019) 200–208. https://doi.org/10.1016/j.cattod.2018.03.047.

[94] D.C. Rennard, J.S. Kruger, L.D. Schmidt, Autothermal catalytic partial oxidation of glycerol to syngas and to non-equilibrium products, ChemSusChem. 2 (2009) 89–98. https://doi.org/10.1002/cssc.200800200.

[95] A. Ebshish, Z. Yaakob, Y.H. Taufiq-Yap, A. Bshish, S.M. Tasirin, Review of hydrogen production via glycerol reforming, Proc. Inst. Mech. Eng. Part A J. Power Energy. 226 (2012) 1060–1075. https://doi.org/10.1177/0957650912464624.

[96] B. Zhang, X. Tang, Y. Li, Y. Xu, W. Shen, Hydrogen production from steam reforming of ethanol and glycerol over ceria-supported metal catalysts, Int. J. Hydrogen Energy. 32 (2007) 2367–2373. https://doi.org/10.1016/j.ijhydene.2006.11.003.

[97] Y.C. Lin, Catalytic valorization of glycerol to hydrogen and syngas, Int. J. Hydrogen Energy. 38 (2013) 2678–2700. https://doi.org/10.1016/j.ijhydene.2012.12.079.

[98] K.H. Lin, A.C.C. Chang, W.H. Lin, S.H. Chen, C.Y. Chang, H.F. Chang, Autothermal steam reforming of glycerol for hydrogen production over packed-bed and Pd/Ag alloy membrane reactors, Int. J. Hydrogen Energy. 38 (2013) 12946–12952. https://doi.org/10.1016/j.ijhydene.2013.04.134.

[99] D. Aman, D. Radwan, M. Ebaid, S. Mikhail, E. van Steen, Comparing nickel and cobalt perovskites for steam reforming of glycerol, Mol. Catal. 452 (2018) 60–67. https://doi.org/10.1016/j.mcat.2018.03.022.

[100] V. Nichele, M. Signoretto, F. Menegazzo, A. Gallo, V. Dal Santo, G. Cruciani, G. Cerrato, Glycerol steam reforming for hydrogen production: Design of Ni supported catalysts, Appl. Catal. B Environ. 111–112 (2012) 225–232. https://doi.org/10.1016/j.apcatb.2011.10.003.

[101] N.D. Charisiou, K.N. Papageridis, G. Siakavelas, V. Sebastian, S.J. Hinder, M.A. Baker, K. Polychronopoulou, M.A. Goula, The influence of SiO2 doping on the Ni/ZrO2 supported catalyst for hydrogen production through the glycerol steam

reforming reaction, Catal. Today. 319 (2019) 206–219. https://doi.org/10.1016/j.cattod.2018.04.052.

[102] Å. Slagtern, H.M. Swaan, U. Olsbye, I.M. Dahl, C. Mirodatos, Catalytic partial oxidation of methane over Ni-, Co- and Fe-based catalysts, Catal. Today. 46 (1998) 107–115. https://doi.org/10.1016/S0920-5861(98)00332-0.

[103] K.N. Papageridis, G. Siakavelas, N.D. Charisiou, D.G. Avraam, L. Tzounis, K. Kousi, M.A. Goula, Comparative study of Ni, Co, Cu supported on γ-alumina catalysts for hydrogen production via the glycerol steam reforming reaction, Fuel Process. Technol. 152 (2016) 156–175. https://doi.org/10.1016/j.fuproc.2016.06.024.

[104] C.K. Cheng, S.Y. Foo, A.A. Adesina, H2-rich synthesis gas production over Co/Al2O 3 catalyst via glycerol steam reforming, Catal. Commun. 12 (2010) 292–298. https://doi.org/10.1016/j.catcom.2010.09.018.

[105] K.N. Papageridis, G.I. Siakavelas, N.D. Charisiou, M.A. Goula, Hydrogen production through glycerol steam reforming using transition metals on alumina catalysts, in: 14th Int. Conf. Environ. Sci. Technol., Rhodes, Greece, 2015.

[106] M. Surendar; K. Upendar; B. Haribabu; T. Sagar; N. Lingaiah; S. Prasad, Glycerol steam reforming on Co/ZrO2 catalysts, in: CHEMCON-2014, IICHE, Istanbul, Turkey, 2014: pp. 1–2.

[107] C.K. Cheng, S.Y. Foo, A.A. Adesina, Glycerol steam reforming over bimetallic Co-Ni/Al2O3, Ind. Eng. Chem. Res. 49 (2010) 10804–10817. https://doi.org/10.1021/ie100462t.

[108] E.A. Sanchez, R.A. Comelli, Hydrogen production by glycerol steam-reforming over nickel and nickel-cobalt impregnated on alumina, Int. J. Hydrogen Energy. 39 (2014) 8650–8655. https://doi.org/10.1016/j.ijhydene.2013.12.067.

[109] C.K. Cheng, S.Y. Foo, A.A. Adesina, Carbon deposition on bimetallic Co-Ni/Al2O3 catalyst during steam reforming of glycerol, Catal. Today. 164 (2011) 268–274. https://doi.org/10.1016/j.cattod.2010.10.040.

[110] M. Araque, L.M. Martínez T, J.C. Vargas, A.C. Roger, Hydrogen production by glycerol steam reforming over CeZrCo fluorite type oxides, Catal. Today. 176 (2011) 352–356. https://doi.org/10.1016/j.cattod.2010.11.066.

[111] M. Araque, L.M. Martínez T, J.C. Vargas, M.A. Centeno, A.C. Roger, Effect of the active metals on the selective H2 production in glycerol steam reforming, Appl. Catal. B Environ. 125 (2012) 556–566.

https://doi.org/10.1016/j.apcatb.2012.06.028.

[112] L.M. Martínez T, M. Araque, J.C. Vargas, A.C. Roger, Effect of Ce/Zr ratio in CeZr-CoRh catalysts on the hydrogen production by glycerol steam reforming, Appl. Catal. B Environ. 132–133 (2013) 499–510. https://doi.org/10.1016/j.apcatb.2012.12.027.

[113] J. Dobosz, M. Cichy, M. Zawadzki, T. Borowiecki, Glycerol steam reforming over calcium hydroxyapatite supported cobalt and cobalt-cerium catalysts, J. Energy Chem. 27 (2018) 404–412. https://doi.org/10.1016/j.jechem.2017.12.004.

[114] M. Surendar, T. V. Sagar, B.H. Babu, N. Lingaiah, K.S.R. Rao, P.S.S. Prasad, Glycerol steam reforming over La–Ce–Co mixed oxide-derived cobalt catalysts, RSC Adv. 5 (2015) 45184–45193. https://doi.org/10.1039/C5RA02837J.

[115] E.B. Pereira, P. Ramírez de la Piscina, N. Homs, Efficient hydrogen production from ethanol and glycerol by vapour-phase reforming processes with new cobalt-based catalysts, Bioresour. Technol. 102 (2011) 3419–3423. https://doi.org/10.1016/j.biortech.2010.10.021.

[116] J. De Vrieze, K. Verbeeck, I. Pikaar, J. Boere, A. Van Wijk, K. Rabaey, W. Verstraete, The hydrogen gas bio-based economy and the production of renewable building block chemicals, food and energy, N. Biotechnol. 55 (2020) 12–18. https://doi.org/10.1016/j.nbt.2019.09.004.

[117] S.I. Mussatto, G.M. Dragone, Biomass Pretreatment, Biorefineries, and Potential Products for a Bioeconomy Development, in: S.I. Mussatto (Ed.), Biomass Fractionation Technol. a Lignocellul. Feed. Based Biorefinery, Elsevier, Amsterdam, Netherlands, 2016: pp. 1–22. https://doi.org/10.1016/B978-0-12-802323-5.00001-3.

[118] N.S. Kapu, H.L. Trajano, Review of hemicellulose hydrolysis in softwoods and bamboo, Biofuels, Bioprod. Biorefining. 8 (2014) 857–870. https://doi.org/10.1002/bbb.1517.

[119] A. Corma, S. Iborra, A. Velty, Chemical routes for the transformation of biomass into chemicals, Chem. Rev. 107 (2007) 2411–2502. https://doi.org/10.1021/cr050989d.

[120] M.J. Cocero, Á. Cabeza, N. Abad, T. Adamovic, L. Vaquerizo, C.M. Martínez, M.V. Pazo-Cepeda, Understanding biomass fractionation in subcritical & supercritical water, J. Supercrit. Fluids. 133 (2018) 550–565. https://doi.org/10.1016/j.supflu.2017.08.012.

[121] C. Huang, X. Wang, C. Liang, X. Jiang, G. Yang, J. Xu, Q. Yong, A sustainable process for procuring biologically active fractions of high-purity xylooligosaccharides and water-soluble lignin from Moso bamboo prehydrolyzate, Biotechnol. Biofuels. 12 (2019) 1–13. https://doi.org/10.1186/s13068-019-1527-3.

[122] D. Lavanya, P. Kulkarni, M. Dixit, P. Raavi, L. Krishna, Sources of Cellulose and Their Applications–a Review, Int J Drug Formul Res. 2 (2011) 2.

[123] Suhas, V.K. Gupta, P.J.M. Carrott, R. Singh, M. Chaudhary, S. Kushwaha, Cellulose: A review as natural, modified and activated carbon adsorbent, Bioresour. Technol. 216 (2016) 1066–1076. https://doi.org/10.1016/j.biortech.2016.05.106.

[124] C.A.E. Costa, P.C.R. Pinto, A.E. Rodrigues, Evaluation of chemical processing impact on E. globulus wood lignin and comparison with bark lignin, Ind. Crops Prod. 61 (2014) 479–491. https://doi.org/10.1016/j.indcrop.2014.07.045.

[125] S. Constant, H.L.J. Wienk, A.E. Frissen, P. De Peinder, R. Boelens, D.S. Van Es, R.J.H. Grisel, B.M. Weckhuysen, W.J.J. Huijgen, R.J.A. Gosselink, P.C.A. Bruijnincx, New insights into the structure and composition of technical lignins: A comparative characterisation study, Green Chem. 18 (2016) 2651–2665. https://doi.org/10.1039/c5gc03043a.

[126] H. Dong, L. Zheng, P. Yu, Q. Jiang, Y. Wu, C. Huang, B. Yin, Characterization and Application of Lignin-Carbohydrate Complexes from Lignocellulosic Materials as Antioxidants for Scavenging in Vitro and in Vivo Reactive Oxygen Species, ACS Sustain. Chem. Eng. 8 (2020) 256–266. https://doi.org/10.1021/acssuschemeng.9b05290.

[127] J.M. Lavoie, T. Ghislain, E. Bahl, J. Arauzo, A. Gonzalo, N. Gil-Lalaguna, J.L. Sánchez, Renewable antioxidant additive for biodiesel obtained from black liquor, Fuel. 254 (2019) 115689. https://doi.org/10.1016/j.fuel.2019.115689.

[128] D. Amendola, D.M. De Faveri, I. Egües, L. Serrano, J. Labidi, G. Spigno, Autohydrolysis and organosolv process for recovery of hemicelluloses, phenolic compounds and lignin from grape stalks, Bioresour. Technol. 107 (2012) 267–274. https://doi.org/10.1016/j.biortech.2011.12.108.

[129] F.M. Gírio, C. Fonseca, F. Carvalheiro, L.C. Duarte, S. Marques, R. Bogel-Łukasik, Hemicelluloses for fuel ethanol: A review, Bioresour. Technol. 101 (2010) 4775–4800. https://doi.org/10.1016/j.biortech.2010.01.088.

[130] G. Garrote, H. Domínguez, J.C. Parajó, Hydrothermal processing of lignocellulosic materials, Holz Als Roh - Und Werkst. 57 (1999) 191–202. https://doi.org/10.1007/s001070050039.

[131] M.J. González-Muñoz, R. Alvarez, V. Santos, J.C. Parajó, Production of hemicellulosic sugars from Pinus pinaster wood by sequential steps of aqueous extraction and acid hydrolysis, Wood Sci. Technol. 46 (2012) 271–285. https://doi.org/10.1007/s00226-011-0408-0.

[132] S. Rivas, A.M. Raspolli-Galletti, C. Antonetti, V. Santos, J.C. Parajó, Sustainable conversion of Pinus pinaster wood into biofuel precursors: A biorefinery approach, Fuel. 164 (2016) 51–58. https://doi.org/10.1016/j.fuel.2015.09.085.

[133] T.M. Santos, M.V. Alonso, M. Oliet, J.C. Domínguez, V. Rigual, F. Rodriguez, Effect of autohydrolysis on Pinus radiata wood for hemicellulose extraction, Carbohydr. Polym. 194 (2018) 285–293. https://doi.org/10.1016/j.carbpol.2018.04.010.

[134] T. Pielhop, C. Reinhard, C. Hecht, L. Del Bene, M.H. Studer, P. Rudolf von Rohr, Application potential of a carbocation scavenger in autohydrolysis and dilute acid pretreatment to overcome high softwood recalcitrance, Biomass and Bioenergy. 105 (2017) 164–173. https://doi.org/10.1016/j.biombioe.2017.07.005.

[135] M. Hundt, K. Schnitzlein, M.G. Schnitzlein, Alkaline polyol pulping and enzymatic hydrolysis of hardwood: Effect of pulping severity and pulp composition on cellulase activity and overall sugar yield, Bioresour. Technol. 136 (2013) 672–679. https://doi.org/10.1016/j.biortech.2013.02.084.

[136] X. Pan, C. Arato, N. Gilkes, D. Gregg, W. Mabee, K. Pye, Z. Xiao, X. Zhang, J. Saddler, Biorefining of softwoods using ethanol organosolv pulping: Preliminary evaluation of process streams for manufacture of fuel-grade ethanol and co-products, Biotechnol. Bioeng. 90 (2005) 473–481. https://doi.org/10.1002/bit.20453.

[137] X. Erdocia, R. Prado, M.Á. Corcuera, J. Labidi, Base catalyzed depolymerization of lignin: Influence of organosolv lignin nature, Biomass and Bioenergy. 66 (2014) 379–386. https://doi.org/10.1016/j.biombioe.2014.03.021.

[138] C. Tang, Y. Chen, J. Liu, T. Shen, Z. Cao, J. Shan, C. Zhu, H. Ying, Sustainable biobutanol production using alkali-catalyzed organosolv pretreated cornstalks, Ind. Crops Prod. 95 (2017) 383–392. https://doi.org/10.1016/j.indcrop.2016.10.048.

[139] Z. Zhang, M.D. Harrison, D.W. Rackemann, W.O.S. Doherty, I.M. O'Hara,

Organosolv pretreatment of plant biomass for enhanced enzymatic saccharification, Green Chem. 18 (2016) 360–381. https://doi.org/10.1039/c5gc02034d.

[140] J. Fernández-Rodríguez, X. Erdocia, C. Sánchez, M. González Alriols, J. Labidi, Lignin depolymerization for phenolic monomers production by sustainable processes, J. Energy Chem. 26 (2017) 622–631. https://doi.org/10.1016/j.jechem.2017.02.007.

[141] H.T. Sahin, Base-catalyzed organosolv pulping of jute, J. Chem. Technol. Biotechnol. 78 (2003) 1267–1273. https://doi.org/10.1002/jctb.931.

[142] C. Nitsos, U. Rova, P. Christakopoulos, Organosolv fractionation of softwood biomass for biofuel and biorefinery applications, Energies. 11 (2018) 50. https://doi.org/10.3390/en11010050.

[143] L.F. Del Rio, R.P. Chandra, J.N. Saddler, The effect of varying organosolv pretreatment chemicals on the physicochemical properties and cellulolytic hydrolysis of mountain pine beetle-killed lodgepole pine, Appl. Biochem. Biotechnol. 161 (2010) 1–21. https://doi.org/10.1007/s12010-009-8786-6.

[144] N. Park, H.Y. Kim, B.W. Koo, H. Yeo, I.G. Choi, Organosolv pretreatment with various catalysts for enhancing enzymatic hydrolysis of pitch pine (Pinus rigida), Bioresour. Technol. 101 (2010) 7046–7053. https://doi.org/10.1016/j.biortech.2010.04.020.

[145] X. Pan, D. Xie, R.W. Yu, D. Lam, J.N. Saddler, Pretreatment of lodgepole pine killed by mountain pine beetle using the ethanol organosolv process: Fractionation and process optimization, Ind. Eng. Chem. Res. 46 (2007) 2609–2617. https://doi.org/10.1021/ie061576l.

[146] R. Valenzuela, X. Priebe, E. Troncoso, I. Ortega, C. Parra, J. Freer, Fiber modifications by organosolv catalyzed with H2SO4 improves the SSF of Pinus radiata, Ind. Crops Prod. 86 (2016) 79–86. https://doi.org/10.1016/j.indcrop.2016.03.037.

[147] M. Akgul, A. Tozluogu, Alkaline-ethanol pulping of cotton stalks, Sci. Res. Essays. 5 (2010) 1068–1074.

[148] A.A. Shatalov, H. Pereira, Kinetics of organosolv delignification of fibre crop Arundo donax L., Ind. Crops Prod. 21 (2005) 203–210. https://doi.org/10.1016/j.indcrop.2004.04.010.

[149] A. Johansson, O. Aaltonen, P. Ylinen, Organosolv pulping - methods and pulp

properties, Biomass. 13 (1987) 45–65. https://doi.org/10.1016/0144-4565(87)90071-0.

[150] C. Huang, J. He, R. Narron, Y. Wang, Q. Yong, Characterization of Kraft Lignin Fractions Obtained by Sequential Ultrafiltration and Their Potential Application as a Biobased Component in Blends with Polyethylene, ACS Sustain. Chem. Eng. 5 (2017) 11770–11779. https://doi.org/10.1021/acssuschemeng.7b03415.

[151] M.E. Vallejos, M.D. Zambon, M.C. Area, A.A. da S. Curvelo, Low liquid-solid ratio fractionation of sugarcane bagasse by hot water autohydrolysis and organosolv delignification, Ind. Crops Prod. 65 (2015) 349–353. https://doi.org/10.1016/j.indcrop.2014.11.018.

[152] A. Romaní, G. Garrote, F. López, J.C. Parajó, Eucalyptus globulus wood fractionation by autohydrolysis and organosolv delignification, Bioresour. Technol. 102 (2011) 5896–5904. https://doi.org/10.1016/j.biortech.2011.02.070.

[153] H. Amiri, K. Karimi, Integration of autohydrolysis and organosolv delignification for efficient acetone, butanol, and ethanol production and lignin recovery, Ind. Eng. Chem. Res. 55 (2016) 4836–4845. https://doi.org/10.1021/acs.iecr.6b00110.

[154] H. Wang, M. Tucker, Y. Ji, Recent Development in Chemical Depolymerization of Lignin: A Review, J. Appl. Chem. 2013 (2013) 1–9. https://doi.org/10.1155/2013/838645.

[155] H. Wang, Y. Pu, A. Ragauskas, B. Yang, From lignin to valuable products–strategies, challenges, and prospects, Bioresour. Technol. 271 (2019) 449–461. https://doi.org/10.1016/j.biortech.2018.09.072.

[156] I.F. Demuner, J.L. Colodette, A.J. Demuner, C.M. Jardim, Biorefinery review: Wide-reaching products through kraft lignin, BioResources. 14 (2019) 7543–7581. https://doi.org/10.15376/biores.l4.3.Deuiiuier.

[157] A.J. Ragauskas, G.T. Beckham, M.J. Biddy, R. Chandra, F. Chen, M.F. Davis, B.H. Davison, R.A. Dixon, P. Gilna, M. Keller, P. Langan, A.K. Naskar, J.N. Saddler, T.J. Tschaplinski, G.A. Tuskan, C.E. Wyman, Lignin Valorization: Improving Lignin Processing in the Biorefinery, Science (80-.). 344 (2014) 1246843–1246843. https://doi.org/10.1126/science.1246843.

[158] J. Zhu, C. Yan, X. Zhang, C. Yang, M. Jiang, X. Zhang, A sustainable platform of lignin: From bioresources to materials and their applications in rechargeable batteries and supercapacitors, Prog. Energy Combust. Sci. 76 (2020) 100788. https://doi.org/10.1016/j.pecs.2019.100788.

[159] C. Li, X. Zhao, A. Wang, G.W. Huber, T. Zhang, Catalytic Transformation of Lignin for the Production of Chemicals and Fuels, Chem. Rev. 115 (2015) 11559–11624. https://doi.org/10.1021/acs.chemrev.5b00155.

[160] S. Laurichesse, L. Avérous, Chemical modification of lignins: Towards biobased polymers, Prog. Polym. Sci. 39 (2014) 1266–1290. https://doi.org/10.1016/j.progpolymsci.2013.11.004.

[161] C. Chio, M. Sain, W. Qin, Lignin utilization: A review of lignin depolymerization from various aspects, Renew. Sustain. Energy Rev. 107 (2019) 232–249. https://doi.org/10.1016/j.rser.2019.03.008.

[162] W. Schutyser, T. Renders, S. Van Den Bosch, S.F. Koelewijn, G.T. Beckham, B.F. Sels, Chemicals from lignin: An interplay of lignocellulose fractionation, depolymerisation, and upgrading, Chem. Soc. Rev. 47 (2018) 852–908. https://doi.org/10.1039/c7cs00566k.

[163] S. Gillet, M. Aguedo, L. Petitjean, A.R.C. Morais, A.M. Da Costa Lopes, R.M. Łukasik, P.T. Anastas, Lignin transformations for high value applications: Towards targeted modifications using green chemistry, Green Chem. 19 (2017) 4200–4233. https://doi.org/10.1039/c7gc01479a.

[164] Z. He, X. Wang, Hydrodeoxygenation of model compounds and catalytic systems for pyrolysis bio-oils upgrading, Catal. Sustain. Energy. 1 (2013) 28–52. https://doi.org/10.2478/cse-2012-0004.

[165] J.S. Choi, G. Bugli, G. Djéga-Mariadassou, Influence of the degree of carburization on the density of sites and hydrogenating activity of molybdenum carbides, J. Catal. 193 (2000) 238–247. https://doi.org/10.1006/jcat.2000.2894.

[166] T.H. Nguyen, T.V. Nguyen, Y.J. Lee, T. Safinski, A.A. Adesina, Structural evolution of alumina supported Mo-W carbide nanoparticles synthesized by precipitation from homogeneous solution, Mater. Res. Bull. 40 (2005) 149–157. https://doi.org/10.1016/j.materresbull.2004.09.007.

[167] E. Furimsky, Metal carbides and nitrides as potential catalysts for hydroprocessing, Appl. Catal. A Gen. 240 (2003) 1–28. https://doi.org/10.1016/S0926-860X(02)00428-3.

[168] S. Boullosa-Eiras, R. Lødeng, H. Bergem, M. Stöcker, L. Hannevold, E.A. Blekkan, Catalytic hydrodeoxygenation (HDO) of phenol over supported molybdenum carbide, nitride, phosphide and oxide catalysts, Catal. Today. 223 (2014) 44–53. https://doi.org/10.1016/j.cattod.2013.09.044.

[169] J.R.D.S. Politi, F. Viñes, J.A. Rodriguez, F. Illas, Atomic and electronic structure of molybdenum carbide phases: Bulk and low Miller-index surfaces, Phys. Chem. Chem. Phys. 15 (2013) 12617–12625. https://doi.org/10.1039/c3cp51389k.

[170] S. Posada-Pérez, F. Viñes, R. Valero, J.A. Rodriguez, F. Illas, Adsorption and dissociation of molecular hydrogen on orthorhombic β-Mo2C and cubic δ-MoC (001) surfaces, Surf. Sci. 656 (2017) 24–32. https://doi.org/10.1016/j.susc.2016.10.001.

[171] A.B. Dongil, I.T. Ghampson, R. García, J.L.G. Fierro, N. Escalona, Hydrodeoxygenation of guaiacol over Ni/carbon catalysts: Effect of the support and Ni loading, RSC Adv. 6 (2016) 2611–2623. https://doi.org/10.1039/c5ra22540j.

[172] P. Serp, M. Corrias, P. Kalck, Carbon nanotubes and nanofibers in catalysis, Appl. Catal. A Gen. 253 (2003) 337–358. https://doi.org/10.1016/S0926-860X(03)00549-0.

[173] R. Vieira, Carbon Nanofibers as Macro-Structured Catalytic Support, in: Nanofibers, InTech, Croatia, 2010: pp. 1–12. https://doi.org/10.5772/8145.

[174] K.P. De Jong, J.W. Geus, Carbon Nanofibers: Catalytic Synthesis and Applications, Catal. Rev. - Sci. Eng. 42 (2000) 481–510. https://doi.org/10.1081/CR-100101954.

[175] C. Park, P.E. Anderson, A. Chambers, C.D. Tan, R. Hidalgo, N.M. Rodriguez, Further Studies of the Interaction of Hydrogen with Graphite Nanofibers, J. Phys. Chem. B. 103 (1999) 10572–10581. https://doi.org/10.1021/jp990500i.

[176] F. Rodríguez-reinoso, The role of carbon materials in heterogeneous catalysis, Carbon N. Y. 36 (1998) 159–175. https://doi.org/10.1016/S0008-6223(97)00173-5.

[177] E. Santillan-Jimenez, M. Perdu, R. Pace, T. Morgan, M. Crocker, Activated carbon, carbon nanofiber and carbon nanotube supported molybdenum carbide catalysts for the hydrodeoxygenation of guaiacol, Catalysts. 5 (2015) 424–441. https://doi.org/10.3390/catal5010424.

[178] A.L. Jongerius, R.W. Gosselink, J. Dijkstra, J.H. Bitter, P.C.A. Bruijnincx, B.M. Weckhuysen, Carbon nanofiber supported transition-metal carbide catalysts for the hydrodeoxygenation of guaiacol, ChemCatChem. 5 (2013) 2964–2972. https://doi.org/10.1002/cctc.201300280.

[179] D. Mordenti, D. Brodzki, G. Djéga-Mariadassou, New Synthesis of Mo2C 14 nm

in Average Size Supported on a High Specific Surface Area Carbon Material, J. Solid State Chem. 141 (1998) 114–120. https://doi.org/10.1006/jssc.1998.7925.

[180] S. Chaudhury, S.K. Mukerjee, V.N. Vaidya, V. Venugopal, Kinetics and mechanism of carbothermic reduction of MoO3 to Mo2C, J. Alloys Compd. 261 (1997) 105–113. https://doi.org/10.1016/S0925-8388(97)00212-0.

[181] K.L. Deutsch, B.H. Shanks, Hydrodeoxygenation of lignin model compounds over a copper chromite catalyst, Appl. Catal. A Gen. 447–448 (2012) 144–150. https://doi.org/10.1016/j.apcata.2012.09.047.

[182] S. Van Den Bosch, W. Schutyser, R. Vanholme, T. Driessen, S.F. Koelewijn, T. Renders, B. De Meester, W.J.J. Huijgen, W. Dehaen, C.M. Courtin, B. Lagrain, W. Boerjan, B.F. Sels, Reductive lignocellulose fractionation into soluble lignin-derived phenolic monomers and dimers and processable carbohydrate pulps, Energy Environ. Sci. 8 (2015) 1748–1763. https://doi.org/10.1039/c5ee00204d.

[183] E. Ochoa, D. Torres, R. Moreira, J.L. Pinilla, I. Suelves, Carbon nanofiber supported Mo2C catalysts for hydrodeoxygenation of guaiacol: The importance of the carburization process, Appl. Catal. B Environ. 239 (2018) 463–474. https://doi.org/10.1016/j.apcatb.2018.08.043.

[184] H. Fiege, Cresols and Xylenols, in: Ullmann's Encycl. Ind. Chem., Wiley-VCH Verlag GmbH & Co. KGaA, Weinheim, Germany, 2000. https://doi.org/10.1002/14356007.a08_025.

[185] M. Weber, M. Weber, M. Kleine-Boymann, Phenol, in: Ullmann's Encycl. Ind. Chem., Wiley-VCH Verlag GmbH & Co. KGaA, Weinheim, Germany, 2004: pp. 1–17. https://doi.org/10.1002/14356007.a19_299.pub2.

[186] P. Basu, Gasification Theory and Modeling of Gasifiers, in: Biomass Gasif. Des. Handb., Elsevier, Oxford, UK, 2010: pp. 117–165. https://doi.org/10.1016/B978-0-12-374988-8.00005-2.

[187] A. Moral, F. Bimbela, G. Arzamendi, Oxidación parcial de metano para la producción de gas de síntesis con catalizadores Co/Al coprecipitados, in: Catálisis, Confluencia Interdiscip. Model. Catalizadores y React. SECAT'15, Barcelona, Spain, 2015: pp. 2–3.

[188] F. Bimbela, D. Chen, J. Ruiz, L. García, J. Arauzo, Ni/Al coprecipitated catalysts modified with magnesium and copper for the catalytic steam reforming of model compounds from biomass pyrolysis liquids, Appl. Catal. B Environ. 119–120 (2012) 1–12. https://doi.org/10.1016/j.apcatb.2012.02.007.

[189] D. Hames, B.; Ruiz, R.; Scarlata, C.; Sluiter, A.; Sluiter, J.; Templeton, Preparation of Samples for Compositional Analysis: Laboratory Analytical Procedure (LAP), NREL/TP-510-42620 Revised, Golden, Colorado, USA, 2008.

[190] D. Sluiter, A.; Hames, V; Ruiz, R.; Scarlata, C.; Sluiter, J.; Templeton, D.; Crocker, Determination of Structural Carbohydrates and Lignin in Biomass, Laboratory Analytical Procedure (LAP), NREL/TP-510-42618, Golden, Colorado, USA, 2008.

[191] Tappi T236, TAPPI Test Methods: Kappa number of pulp, 1999.

[192] ISO 5361:2010(E), Pulps — Determination of limiting viscosity number in cupri-ethylenediamine (CED) solution, 2010.

[193] K. Wang, H. Yang, S. Guo, Y. Tang, J. Jiang, F. Xu, R.-C. Sun, Organosolv fractionation process with various catalysts for improving bioconversion of triploid poplar, Process Biochem. 47 (2012) 1503–1509. https://doi.org/10.1016/j.procbio.2012.06.002.

[194] F. Hardi, M. Mäkelä, K. Yoshikawa, Non-catalytic hydrothermal liquefaction of pine sawdust using experimental design: Material balances and products analysis, Appl. Energy. 204 (2017) 1026–1034. https://doi.org/10.1016/j.apenergy.2017.04.033.

[195] J.S. Kruger, N.S. Cleveland, S. Zhang, R. Katahira, B.A. Black, G.M. Chupka, T. Lammens, P.G. Hamilton, M.J. Biddy, G.T. Beckham, Lignin Depolymerization with Nitrate-Intercalated Hydrotalcite Catalysts, ACS Catal. 6 (2016) 1316–1328. https://doi.org/10.1021/acscatal.5b02062.

[196] R. Moreira, E. Ochoa, J. Pinilla, A. Portugal, I. Suelves, Liquid-Phase Hydrodeoxygenation of Guaiacol over Mo2C Supported on Commercial CNF. Effects of Operating Conditions on Conversion and Product Selectivity, Catalysts. 8 (2018) 127. https://doi.org/10.3390/catal8040127.

[197] L. Serrano, J.A. Cecilia, C. García-Sancho, A. García, Lignin Depolymerization to BTXs, Top. Curr. Chem. 377 (2019) 1–28. https://doi.org/10.1007/s41061-019-0251-6.

[198] Y. Pu, S. Cao, A.J. Ragauskas, Application of quantitative 31P NMR in biomass lignin and biofuel precursors characterization, Energy Environ. Sci. 4 (2011) 3154. https://doi.org/10.1039/c1ee01201k.

[199] A. Cornejo, Í. García-Yoldi, I. Alegria-Dallo, R. Galilea-Gonzalo, K. Hablich, D. Sánchez, E. Otazu, I. Funcia, M.J. Gil, V. Martínez-Merino, Systematic Diffusion-

Ordered Spectroscopy for the Selective Determination of Molecular Weight in Real Lignins and Fractions Arising from Base-Catalyzed Depolymerization Reaction Mixtures, ACS Sustain. Chem. Eng. 8 (2020) 8638–8647. https://doi.org/10.1021/acssuschemeng.0c01375.

[200] A. Cornejo, F. Bimbela, R. Moreira, K. Hablich, Í. García-Yoldi, M. Maisterra, A. Portugal, L.M. Gandía, V. Martínez-Merino, Production of aromatic compounds by catalytic depolymerization of technical and downstream biorefinery lignins, Biomolecules. 10 (2020) 1–30. https://doi.org/10.3390/biom10091338.

[201] J.L. Pinilla, H. Purón, D. Torres, S. de Llobet, R. Moliner, I. Suelves, M. Millan, Carbon nanofibres coated with Ni decorated MoS2 nanosheets as catalyst for vacuum residue hydroprocessing, Appl. Catal. B Environ. 148–149 (2014) 357–365. https://doi.org/10.1016/j.apcatb.2013.11.019.

[202] J.L. Pinilla, H. Purón, D. Torres, I. Suelves, M. Millan, Ni-MoS2 supported on carbon nanofibers as hydrogenation catalysts: Effect of support functionalisation, Carbon N. Y. 81 (2015) 574–586. https://doi.org/10.1016/j.carbon.2014.09.092.

[203] M. Amutio, G. Lopez, J. Alvarez, R. Moreira, G. Duarte, J. Nunes, M. Olazar, J. Bilbao, Flash pyrolysis of forestry residues from the Portuguese Central Inland Region within the framework of the BioREFINA-Ter project, Bioresour. Technol. 129 (2013) 512–518. https://doi.org/10.1016/j.biortech.2012.11.114.

[204] M. Amutio, G. Lopez, M. Artetxe, G. Elordi, M. Olazar, J. Bilbao, Influence of temperature on biomass pyrolysis in a conical spouted bed reactor, Resour. Conserv. Recycl. 59 (2012) 23–31. https://doi.org/10.1016/j.resconrec.2011.04.002.

[205] P.W. He, S.Y. Luo, G. Cheng, B. Xiao, L. Cai, J.B. Wang, Gasification of biomass char with air-steam in a cyclone furnace, Renew. Energy. 37 (2012) 398–402. https://doi.org/10.1016/j.renene.2011.07.001.

[206] K. Yip, F. Tian, J. Hayashi, H. Wu, Effect of Alkali and Alkaline Earth Metallic Species on Biochar Reactivity and Syngas Compositions during Steam Gasification, Energy & Fuels. 24 (2010) 173–181. https://doi.org/10.1021/ef900534n.

[207] N. Xiao, H. Luo, W. Wei, Z. Tang, B. Hu, L. Kong, Y. Sun, Microwave-assisted gasification of rice straw pyrolytic biochar promoted by alkali and alkaline earth metals, J. Anal. Appl. Pyrolysis. 112 (2015) 173–179. https://doi.org/10.1016/j.jaap.2015.02.001.

[208] A. Gómez-Barea, P. Ollero, B. Leckner, Optimization of char and tar conversion in fluidized bed biomass gasifiers, Fuel. 103 (2013) 42–52. https://doi.org/10.1016/j.fuel.2011.04.042.

[209] U. Henriksen, J. Ahrenfeldt, T.K. Jensen, B. Gøbel, J.D. Bentzen, C. Hindsgaul, L.H. Sørensen, The design, construction and operation of a 75 kW two-stage gasifier, Energy. 31 (2006) 1542–1553. https://doi.org/10.1016/j.energy.2005.05.031.

[210] R.Ø. Gadsbøll, Z. Sárossy, L. Jørgensen, J. Ahrenfeldt, U.B. Henriksen, Oxygen-blown operation of the TwoStage Viking gasifier, Energy. 158 (2018) 495–503. https://doi.org/10.1016/j.energy.2018.06.071.

[211] A.D. Lewis, E.G. Fletcher, T.H. Fletcher, CO2 Char Gasification Rates of Sawdust, Switchgrass, and Corn Stover in a Pressurized Entrained-Flow Reactor, Energy & Fuels. 28 (2014) 5812–5825. https://doi.org/10.1021/ef500903c.

[212] L. Van De Steene, J.P. Tagutchou, F. Mermoud, E. Martin, S. Salvador, A new experimental Continuous Fixed Bed Reactor to characterise wood char gasification, Fuel. 89 (2010) 3320–3329. https://doi.org/10.1016/j.fuel.2010.03.035.

[213] P.A. Salam, S.C. Bhattacharya, A comparative study of charcoal gasification in two types of spouted bed reactors, Energy. 31 (2006) 228–243. https://doi.org/10.1016/j.energy.2005.01.004.

[214] R. Lødeng, E. Bjørgum, B.C. Enger, J.L. Eilertsen, A. Holmen, B. Krogh, M. Rønnekleiv, E. Rytter, Catalytic partial oxidation of CH4 to H2 over cobalt catalysts at moderate temperatures, Appl. Catal. A Gen. 333 (2007) 11–23. https://doi.org/10.1016/j.apcata.2007.08.038.

[215] G. Jacobs, T.K. Das, Y. Zhang, J. Li, G. Racoillet, B.H. Davis, Fischer-Tropsch synthesis: Support, loading, and promoter effects on the reducibility of cobalt catalysts, Appl. Catal. A Gen. 233 (2002) 263–281. https://doi.org/10.1016/S0926-860X(02)00195-3.

[216] H.Y. Wang, E. Ruckenstein, Conversions of methane to synthesis gas over Co/γ-Al2O3 by CO2 and/or O2, Catal. Letters. 75 (2001) 13–18. https://doi.org/10.1023/A:1016719703118.

[217] R. Moreira; R.Vaz; A. Portugal; N. Gil-Lalaguna; F. Bimbela; J.L. Sánchez, Oxygen/steam charcoal gasification in a fluidized alumina bed, in: 5th Int. Congr. Green Process Eng., Mont Tremblant, Québec, Canada, 2016.

[218] R. Moreira, R. Vaz, A. Portugal, N. Gil-Lalaguna, J.L. Sánchez, F. Bimbela, Gasification of Charcoal in Air, Oxygen, and Steam Mixtures over a γ-Al2O3 Fluidized Bed, Energy & Fuels. 32 (2018) 406–415. https://doi.org/10.1021/acs.energyfuels.7b02257.

[219] B. Valle, A. Remiro, A.T. Aguayo, J. Bilbao, A.G. Gayubo, Catalysts of Ni/α-Al2O3 and Ni/La 2O3-αAl2O3 for hydrogen production by steam reforming of bio-oil aqueous fraction with pyrolytic lignin retention, Int. J. Hydrogen Energy. 38 (2013) 1307–1318. https://doi.org/10.1016/j.ijhydene.2012.11.014.

[220] L. García; J. Ábrego; F. Bimbela; J.L. Sánchez, Hydrogen production from catalytic biomass pyrolysis, in: X.Q. Z. Fang, Zhen, J. Smith Richard (Ed.), Biofuels and Biorefineries, Springer Netherlands, Netherlands, Dordrecht, 2015: pp. 119–147.

[221] A. Moral, I. Reyero, J. Llorca, F. Bimbela, L.M. Gandía, Partial oxidation of methane to syngas using Co/Mg and Co/Mg-Al oxide supported catalysts, Catal. Today. 333 (2019) 259–267. https://doi.org/10.1016/j.cattod.2018.04.003.

[222] S. Wang, Q. Wang, X. Song, J. Chen, Dry autothermal reforming of glycerol with in situ hydrogen separation via thermodynamic evaluation, Int. J. Hydrogen Energy. 42 (2017) 838–847. https://doi.org/10.1016/j.ijhydene.2016.09.103.

[223] K. Kamonsuangkasem, S. Therdthianwong, A. Therdthianwong, Hydrogen production from yellow glycerol via catalytic oxidative steam reforming, Fuel Process. Technol. 106 (2013) 695–703. https://doi.org/10.1016/j.fuproc.2012.10.003.

[224] C.H. Bartholomew, Mechanisms of catalyst deactivation, Appl. Catal. A Gen. 212 (2001) 17–60. https://doi.org/10.1016/S0926-860X(00)00843-7.

[225] S.M. Swami, M.A. Abraham, Integrated catalytic process for conversion of biomass to hydrogen, Energy and Fuels. 20 (2006) 2616–2622. https://doi.org/10.1021/ef060054f.

[226] A.M.D. Douette, S.Q. Turn, W. Wang, V.I. Keffer, Experimental investigation of hydrogen production from glycerin reforming, Energy and Fuels. 21 (2007) 3499–3504. https://doi.org/10.1021/ef060379w.

[227] Y. Liu, R. Farrauto, A. Lawal, Autothermal reforming of glycerol in a dual layer monolith catalyst, Chem. Eng. Sci. 89 (2013) 31–39. https://doi.org/10.1016/j.ces.2012.11.030.

[228] K.H. Lin, A.C.C. Chang, W.H. Lin, S.H. Chen, C.Y. Chang, H.F. Chang,

Autothermal steam reforming of glycerol for hydrogen production over packed-bed and Pd/Ag alloy membrane reactors, Int. J. Hydrogen Energy. 38 (2013) 12946–12952. https://doi.org/10.1016/j.ijhydene.2013.04.134.

[229] A. Abdul Ghani, F. Torabi, H. Ibrahim, Autothermal reforming process for efficient hydrogen production from crude glycerol using nickel supported catalyst: Parametric and statistical analyses, Energy. 144 (2018) 129–145. https://doi.org/10.1016/j.energy.2017.11.132.

[230] S. Koc, A.K. Avci, Reforming of glycerol to hydrogen over Ni-based catalysts in a microchannel reactor, Fuel Process. Technol. 156 (2017) 357–365. https://doi.org/10.1016/j.fuproc.2016.09.019.

[231] S. Veiga, M. Romero, R. Faccio, D. Segobia, H. Duarte, C. Apesteguía, J. Bussi, Hydrogen-rich gas production by steam and oxidative steam reforming of crude glycerol over Ni-La-Me mixed oxide catalysts (Me= Ce and/or Zr), Catal. Today. 344 (2020) 190–198. https://doi.org/10.1016/j.cattod.2019.02.008.

[232] S. Rivas, M.J. González-Muñoz, V. Santos, J.C. Parajó, Acidic processing of hemicellulosic saccharides from pine wood: Product distribution and kinetic modeling, Bioresour. Technol. 162 (2014) 192–199. https://doi.org/10.1016/j.biortech.2014.03.150.

[233] M.J. González-Muñoz, S. Rivas, V. Santos, J.C. Parajó, Aqueous processing of Pinus pinaster wood: Kinetics of polysaccharide breakdown, Chem. Eng. J. 231 (2013) 380–387. https://doi.org/10.1016/j.cej.2013.07.041.

[234] I. Ballesteros, J.M. Oliva, A.A. Navarro, A. González, J. Carrasco, M. Ballesteros, Effect of chip size on steam explosion pretreatment of softwood, Appl. Biochem. Biotechnol. - Part A Enzym. Eng. Biotechnol. 84–86 (2000) 97–110. https://doi.org/10.1385/ABAB:84-86:1-9:97.

[235] S. Rivas, A.M. Raspolli-Galletti, C. Antonetti, V. Santos, J.C. Parajó, Sustainable production of levulinic acid from the cellulosic fraction of pinus pinaster wood: Operation in aqueous media under microwave irradiation, J. Wood Chem. Technol. 35 (2015) 315–324. https://doi.org/10.1080/02773813.2014.962152.

[236] V. Rigual, T.M. Santos, J.C. Domínguez, M.V. Alonso, M. Oliet, F. Rodriguez, Evaluation of hardwood and softwood fractionation using autohydrolysis and ionic liquid microwave pretreatment, Biomass and Bioenergy. 117 (2018) 190–197. https://doi.org/10.1016/j.biombioe.2018.07.014.

[237] A. Cornejo, I. Alegría-Dallo, Í. García-Yoldi, Í. Sarobe, D. Sánchez, E. Otazu, I.

Funcia, M.J. Gil, V. Martínez-Merino, Pretreatment and enzymatic hydrolysis for the efficient production of glucose and furfural from wheat straw, pine and poplar chips, Bioresour. Technol. 288 (2019) 121583. https://doi.org/10.1016/j.biortech.2019.121583.

[238] H. Sixta, Pulp Bleaching, in: H. Sixta (Ed.), Handb. Pulp, Wiley-VCH Verlag GmbH, Weinheim, Germany, 2008: pp. 609–932. https://doi.org/10.1002/9783527619887.ch1.

[239] H. Sixta, Pulp Purification, in: H.Sixta (Ed.), Handb. Pulp, Wiley-VCH Verlag GmbH, Weinheim, Germany, 2008: pp. 933–965. https://doi.org/10.1002/9783527619887.ch8.

[240] C. Huang, R. Sun, H.M. Chang, Q. Yong, H. Jameel, R. Phillips, Production of dissolving grade pulp from tobacco stalk through SO2-ethanol-water fractionation, alkaline extraction, and bleaching processes, BioResources. 14 (2019) 5544–5558. https://doi.org/10.15376/biores.14.3.5544-5558.

[241] M. Hochegger, B. Cottyn-Boitte, L. Cézard, S. Schober, M. Mittelbach, Influence of Ethanol Organosolv Pulping Conditions on Physicochemical Lignin Properties of European Larch, Int. J. Chem. Eng. 2019 (2019) 1–10. https://doi.org/10.1155/2019/1734507.

[242] M.G. Carvalho, P.J. Ferreira, M.M. Figueiredo, Cellulose depolymerisation and paper properties in E. Globulus kraft pulps, Cellulose. 7 (2000) 359–368. https://doi.org/10.1023/A:1009293924205.

[243] B.B. Hallac, A.J. Ragauskas, Analyzing cellulose degree of polymerization and its relevancy to cellulosic ethanol, Biofuels, Bioprod. Biorefining. 5 (2011) 215–225. https://doi.org/10.1002/bbb.269.

[244] J. Park, A. Riaz, R. Insyani, J. Kim, Understanding the relationship between the structure and depolymerization behavior of lignin, Fuel. 217 (2018) 202–210. https://doi.org/10.1016/j.fuel.2017.12.079.

[245] J. Domínguez-Robles, T. Tamminen, T. Liitiä, M.S. Peresin, A. Rodríguez, A.S. Jääskeläinen, Aqueous acetone fractionation of kraft, organosolv and soda lignins, Int. J. Biol. Macromol. 106 (2018) 979–987. https://doi.org/10.1016/j.ijbiomac.2017.08.102.

[246] J. Domínguez-Robles, E. Espinosa, D. Savy, A. Rosal, A. Rodríguez, Biorefinery process combining Specel® process and selective lignin precipitation using mineral acids, BioResources. 11 (2016) 7061–7077.

https://doi.org/10.15376/biores.11.3.7061-7077.

[247] T. V. Lourençon, F.A. Hansel, T.A. Da Silva, L.P. Ramos, G.I.B. De Muniz, W.L.E. Magalhães, Hardwood and softwood kraft lignins fractionation by simple sequential acid precipitation, Sep. Purif. Technol. 154 (2015) 82–88. https://doi.org/10.1016/j.seppur.2015.09.015.

[248] J. Coates, Interpretation of Infrared Spectra, A Practical Approach, in: R.A. Meyers (Ed.), Encycl. Anal. Chem., John Wiley & Sons Ltd, New York, USA, 2004: pp. 1–23. http://www3.uma.pt/jrodrigues/disciplinas/QINO-II/Teorica/IR.pdf.

[249] H. Li, A.G. McDonald, Fractionation and characterization of industrial lignins, Ind. Crops Prod. 62 (2014) 67–76. https://doi.org/10.1016/j.indcrop.2014.08.013.

[250] O. Faix, Fourier Transform Infrared Spectroscopy, in: C.W.D. S. Y. Lin (Ed.), Spectrosc. Methods Nanomater. Charact., Springer-Verlag, Berlin, Germany, 1992: pp. 83–109. https://doi.org/10.1016/B978-0-323-46140-5.00004-2.

[251] X. Li, C. Sun, B. Zhou, Y. He, Determination of Hemicellulose, Cellulose and Lignin in Moso Bamboo by Near Infrared Spectroscopy, Sci. Rep. 5 (2015) 17210. https://doi.org/10.1038/srep17210.

[252] A.M. Raspolli Galletti, A. D'Alessio, D. Licursi, C. Antonetti, G. Valentini, A. Galia, N. Nassi O Di Nasso, Midinfrared FT-IR as a tool for monitoring herbaceous biomass composition and its conversion to furfural, J. Spectrosc. 2015 (2015) 1–12. https://doi.org/10.1155/2015/719042.

[253] A. von Schenck, N. Berglin, J. Uusitalo, Ethanol from Nordic wood raw material by simplified alkaline soda cooking pre-treatment, Appl. Energy. 102 (2013) 229–240. https://doi.org/10.1016/j.apenergy.2012.10.003.

[254] H. Kirçi, S. Bostançi, M.K. Yalinkiliç, A new modified pulping process alternative to sulphate method "Alkali-Sulfite-Antraquinone-Ethanol (ASAE)," Wood Sci. Technol. 28 (1994) 89–99. https://doi.org/10.1007/BF00192688.

[255] C. Mendes, R. Moreira, A. Portugal, M.G. Carvalho, Production of ethanol from Pinus pinaster stump wood extracted pulp and lignin recovery, in: CHEMPOR 2018, Aveiro, Portugal, 2018: pp. 57–58.

[256] R. Moreira, C.V.T. Mendes, M.B.F. Banaco, M.G.V.S. Carvalho, A. Portugal, New insights in the fractionation of Pinus pinaster wood: sequential autohydrolysis, soda ethanol organosolv and acidic precipitation, Ind. Crops Prod. 152 (2020) 112499. https://doi.org/10.1016/j.indcrop.2020.112499.

[257] A. Lourenço, H. Pereira, Compositional Variability of Lignin in Biomass, in: M. Poletto (Ed.), Lignin - Trends Appl., InTech, Rijeka, 2018: pp. 65–99. https://doi.org/10.5772/intechopen.71208.

[258] D. Son, S. Gu, J.W. Choi, D.J. Suh, J. Jae, J. Choi, J.M. Ha, Production of phenolic hydrocarbons from organosolv lignin and lignocellulose feedstocks of hardwood, softwood, grass and agricultural waste, J. Ind. Eng. Chem. 69 (2019) 304–314. https://doi.org/10.1016/j.jiec.2018.09.009.

[259] R. Ma, W. Hao, X. Ma, Y. Tian, Y. Li, Catalytic Ethanolysis of Kraft Lignin into High-Value Small-Molecular Chemicals over a Nanostructured α-Molybdenum Carbide Catalyst, Angew. Chemie Int. Ed. 53 (2014) 7310–7315. https://doi.org/10.1002/anie.201402752.

[260] X. Huang, C. Atay, T.I. Korányi, M.D. Boot, E.J.M. Hensen, Role of Cu–Mg–Al Mixed Oxide Catalysts in Lignin Depolymerization in Supercritical Ethanol, ACS Catal. 5 (2015) 7359–7370. https://doi.org/10.1021/acscatal.5b02230.

[261] J. Rönnols, A. Jacobs, F. Aldaeus, Consecutive determination of softwood kraft lignin structure and molar mass from NMR measurements, Holzforschung. 71 (2017) 563–570. https://doi.org/10.1515/hf-2016-0182.

[262] D. Li, G. Kagan, R. Hopson, P.G. Williard, Formula Weight Prediction by Internal Reference Diffusion-Ordered NMR Spectroscopy (DOSY), J. Am. Chem. Soc. 131 (2009) 5627–5634. https://doi.org/10.1021/ja810154u.

[263] W. Ge, J.H. Zhang, C.M. Pedersen, T. Zhao, F. Yue, C. Chen, P. Wang, Y. Wang, Y. Qiao, DOSY NMR: A Versatile Analytical Chromatographic Tool for Lignocellulosic Biomass Conversion, ACS Sustain. Chem. Eng. 4 (2016) 1193–1200. https://doi.org/10.1021/acssuschemeng.5b01259.

[264] S. Veibel, J.I. Nielsen, On the mechanism of the Guerbet reaction, Tetrahedron. 23 (1967) 1723–1733. https://doi.org/10.1016/S0040-4020(01)82571-0.

[265] X. Huang, T.I. Korányi, M.D. Boot, E.J.M. Hensen, Ethanol as capping agent and formaldehyde scavenger for efficient depolymerization of lignin to aromatics, Green Chem. 17 (2015) 4941–4950. https://doi.org/10.1039/C5GC01120E.

[266] B.N. Kuznetsov, N.V. Chesnokov, I.G. Sudakova, N.V. Garyntseva, S.A. Kuznetsova, Y.N. Malyar, V.A. Yakovlev, L. Djakovitch, Green catalytic processing of native and organosolv lignins, Catal. Today. 309 (2018) 18–30. https://doi.org/10.1016/j.cattod.2017.11.036.

[267] A. Narani, R.K. Chowdari, C. Cannilla, G. Bonura, F. Frusteri, H.J. Heeres, K.

Barta, Efficient catalytic hydrotreatment of Kraft lignin to alkylphenolics using supported NiW and NiMo catalysts in supercritical methanol, Green Chem. 17 (2015) 5046–5057. https://doi.org/10.1039/c5gc01643f.

[268] J.-M. Lavoie, W. Baré, M. Bilodeau, Depolymerization of steam-treated lignin for the production of green chemicals, Bioresour. Technol. 102 (2011) 4917–4920. https://doi.org/10.1016/j.biortech.2011.01.010.

[269] J. Long, Y. Xu, T. Wang, Z. Yuan, R. Shu, Q. Zhang, L. Ma, Efficient base-catalyzed decomposition and in situ hydrogenolysis process for lignin depolymerization and char elimination, Appl. Energy. 141 (2015) 70–79. https://doi.org/10.1016/j.apenergy.2014.12.025.

[270] J.H. Zhou, Z.J. Sui, J. Zhu, P. Li, D. Chen, Y.C. Dai, W.K. Yuan, Characterization of surface oxygen complexes on carbon nanofibers by TPD, XPS and FT-IR, Carbon N. Y. 45 (2007) 785–796. https://doi.org/10.1016/j.carbon.2006.11.019.

[271] Q.L. Zhuang, T. Kyotani, A. Tomita, DRIFT and TK/TPD Analyses of Surface Oxygen Complexes Formed during Carbon Gasification, Energy and Fuels. 8 (1994) 714–718. https://doi.org/10.1021/ef00045a028.

[272] H.. Boehm, Surface oxides on carbon and their analysis: a critical assessment, Carbon N. Y. 40 (2002) 145–149. https://doi.org/10.1016/S0008-6223(01)00165-8.

[273] R. Guil-López, E. Nieto, J.A. Botas, J.L.G. Fierro, On the genesis of molybdenum carbide phases during reduction-carburization reactions, J. Solid State Chem. 190 (2012) 285–295. https://doi.org/10.1016/j.jssc.2012.02.021.

[274] K.M. Reddy, T.N. Rao, J. Revathi, J. Joardar, Structural stability of α/β-Mo2C during thermochemical processing, J. Alloys Compd. 494 (2010) 386–391. https://doi.org/10.1016/j.jallcom.2010.01.055.

[275] J. Dubois, T. Epicier, C. Esnouf, G. Fantozzi, P. Convert, Neutron powder diffraction studies of transition metal hemicarbides M2C1-x-I. Motivation for a study on W2C and Mo2C and experimental background for an in situ investigation at elevated temperature, Acta Metall. 36 (1988) 1891–1901. https://doi.org/10.1016/0001-6160(88)90292-1.

[276] T. Epicier, J. Dubois, C. Esnouf, G. Fantozzi, P. Convert, Neutron powder diffraction studies of transition metal hemicarbides M2C1-x-II. In situ high temperature study on W2C1-x and Mo2C1-x, Acta Metall. 36 (1988) 1903–1921. https://doi.org/10.1016/0001-6160(88)90293-3.

[277] C.P.B. Araujo, C.P. De Souza, L.M.D. Maia, M.V.M. Souto, C.M. Barbosa, On the synthesis of molybdenum carbide with cobalt addition via gas-solid reactions in a CH4/H2 atmosphere, Brazilian J. Chem. Eng. 33 (2016) 577–588. https://doi.org/10.1590/0104-6632.20160333s20150107.

[278] D.R. Stellwagen, J.H. Bitter, Structure-performance relations of molybdenumand tungsten carbide catalysts for deoxygenation, Green Chem. 17 (2015) 582–593. https://doi.org/10.1039/c4gc01831a.

[279] W. Baaziz, G. Melinte, O. Ersen, C. Pham-Huu, I. Janowska, Effect of nitriding/nanostructuration of few layer graphene supported iron-based particles; catalyst in graphene etching and carbon nanofilament growth, Phys. Chem. Chem. Phys. 16 (2014) 15988–15993. https://doi.org/10.1039/c4cp01887g.

[280] V. Papaefthimiou, I. Florea, W. Baaziz, I. Janowska, W.H. Doh, D. Begin, R. Blume, A. Knop-Gericke, O. Ersen, C. Pham-Huu, S. Zafeiratos, Effect of the specific surface sites on the reducibility of α-Fe2O3/graphene composites by hydrogen, J. Phys. Chem. C. 117 (2013) 20313–20319. https://doi.org/10.1021/jp4067718.

[281] S.S. Datta, D.R. Strachan, S.M. Khamis, A.T.C. Johnson, Crystallographic etching of few-layer graphene, Nano Lett. 8 (2008) 1912–1915. https://doi.org/10.1021/nl080583r.

[282] Q.M. Ramasse, R. Zan, U. Bangert, D.W. Boukhvalov, Y. Son, K.S. Novoselov, Direct Experimental Evidence of Metal-Mediated Etching of Suspended Graphene, ACS Nano. 6 (2012) 4063–4071. https://doi.org/10.1021/nn300452y.

[283] F. Schäffel, J.H. Warner, A. Bachmatiuk, B. Rellinghaus, B. Büchner, L. Schultz, M.H. Rümmeli, Shedding light on the crystallographic etching of multi-layer graphene at the atomic scale, Nano Res. 2 (2009) 695–705. https://doi.org/10.1007/s12274-009-9073-0.

[284] F. Schäffel, J.H. Warner, A. Bachmatiuk, B. Rellinghaus, B. Büchner, L. Schultz, M.H. Rümmeli, On the catalytic hydrogenation of graphite for graphene nanoribbon fabrication, Phys. Status Solidi Basic Res. 246 (2009) 2540–2544. https://doi.org/10.1002/pssb.200982293.

[285] R. Wang, J. Wang, H. Gong, Z. Luo, D. Zhan, Z. Shen, J.T.L. Thong, Cobalt-mediated crystallographic etching of graphite from defects, Small. 8 (2012) 2515–2523. https://doi.org/10.1002/smll.201102747.

[286] L.C. Campos, V.R. Manfrinato, J.D. Sanchez-Yamagishi, J. Kong, P. Jarillo-

Herrero, Anisotropic etching and nanoribbon formation in single-layer graphene, Nano Lett. 9 (2009) 2600–2604. https://doi.org/10.1021/nl900811r.

[287] C. Liang, P. Ying, C. Li, Nanostructured β-Mo2C prepared by carbothermal hydrogen reduction on ultrahigh surface area carbon material, Chem. Mater. 14 (2002) 3148–3151. https://doi.org/10.1021/cm020202p.

[288] H. Xiong, M.A.M. Motchelaho, M. Moyo, L.L. Jewell, N.J. Coville, Cobalt catalysts supported on a micro-coil carbon in Fischer-Tropsch synthesis: A comparison with CNTs and CNFs, Catal. Today. 214 (2013) 50–60. https://doi.org/10.1016/j.cattod.2012.10.018.

[289] W. Chen, Z. Fan, X. Pan, X. Bao, Effect of confinement in carbon nanotubes on the activity of Fischer-Tropsch iron catalyst, J. Am. Chem. Soc. 130 (2008) 9414–9419. https://doi.org/10.1021/ja8008192.

[290] R.M.M. Abbaslou, A. Tavassoli, J. Soltan, A.K. Dalai, Iron catalysts supported on carbon nanotubes for Fischer-Tropsch synthesis: Effect of catalytic site position, Appl. Catal. A Gen. 367 (2009) 47–52. https://doi.org/10.1016/j.apcata.2009.07.025.

[291] R. Wandas, J. Surygała, E. Śliwka, Conversion of cresols and naphthalene in the hydroprocessing of three-component model mixtures simulating fast pyrolysis tars, Fuel. 75 (1996) 687–694. https://doi.org/10.1016/0016-2361(96)00011-7.

[292] M. Saidi, F. Samimi, D. Karimipourfard, T. Nimmanwudipong, B.C. Gates, M.R. Rahimpour, Upgrading of lignin-derived bio-oils by catalytic hydrodeoxygenation, Energy Environ. Sci. 7 (2014) 103–129. https://doi.org/10.1039/c3ee43081b.

[293] E. Furimsky, Catalytic Activity of Carbons, in: J.J. Spivey (Ed.), Carbons Carbon-Supported Catal. Hydroprocessing, Royal Society of Chemistry, Cambridge, UK, 2008: pp. 40–47.

[294] R. Ma, K. Cui, L. Yang, X. Ma, Y. Li, Selective catalytic conversion of guaiacol to phenols over a molybdenum carbide catalyst, Chem. Commun. 51 (2015) 10299–10301. https://doi.org/10.1039/c5cc01900a.

[295] H.Y. Zhao, D. Li, P. Bui, S.T. Oyama, Hydrodeoxygenation of guaiacol as model compound for pyrolysis oil on transition metal phosphide hydroprocessing catalysts, Appl. Catal. A Gen. 391 (2011) 305–310. https://doi.org/10.1016/j.apcata.2010.07.039.

[296] H. Lee, H. Kim, M.J. Yu, C.H. Ko, J.K. Jeon, J. Jae, S.H. Park, S.C. Jung, Y.K. Park, Catalytic Hydrodeoxygenation of Bio-oil Model Compounds over Pt/HY

Catalyst, Sci. Rep. 6 (2016) 28765. https://doi.org/10.1038/srep28765.

[297] R.H. Venderbosch, A.R. Ardiyanti, J. Wildschut, A. Oasmaa, H.J. Heeres, Stabilization of biomass-derived pyrolysis oils, J. Chem. Technol. Biotechnol. 85 (2010) 674–686. https://doi.org/10.1002/jctb.2354.

[298] J. Remón, E. Ochoa, C. Foguet, J.L. Pinilla, I. Suelves, Towards a sustainable bio-fuels production from lignocellulosic bio-oils: Influence of operating conditions on the hydrodeoxygenation of guaiacol over a Mo2C/CNF catalyst, Fuel Process. Technol. 191 (2019) 111–120. https://doi.org/10.1016/j.fuproc.2019.04.008.

[299] T. Nimmanwudipong, C. Aydin, J. Lu, R.C. Runnebaum, K.C. Brodwater, N.D. Browning, D.E. Block, B.C. Gates, Selective hydrodeoxygenation of guaiacol catalyzed by platinum supported on magnesium oxide, Catal. Letters. 142 (2012) 1190–1196. https://doi.org/10.1007/s10562-012-0884-3.

[300] C. Zhao, J. He, A.A. Lemonidou, X. Li, J.A. Lercher, Aqueous-phase hydrodeoxygenation of bio-derived phenols to cycloalkanes, J. Catal. 280 (2011) 8–16. https://doi.org/10.1016/j.jcat.2011.02.001.

[301] C. Zhao, D.M. Camaioni, J.A. Lercher, Selective catalytic hydroalkylation and deoxygenation of substituted phenols to bicycloalkanes, J. Catal. 288 (2012) 92–103. https://doi.org/10.1016/j.jcat.2012.01.005.

[302] E. Ochoa, D. Torres, J.L. Pinilla, I. Suelves, Influence of carburization time on the activity of Mo2C/CNF catalysts for the HDO of guaiacol, Catal. Today. (2019). https://doi.org/10.1016/j.cattod.2019.03.030.